Escherichia coli K1 interactions with human brain microvascular endothelial cells, a primary step in the development of neonatal meningitis

Lip Nam Loh

This thesis is submitted for the degree of Doctor of Philosophy, University of London

Department of Immunology and Infection

Faculty of Infectious and Tropical Diseases

London School of Hygiene and Tropical Medicine

University of London

December 2011

PAGE NUMBERS CUT OFF IN ORIGINAL

Declaration by candidate

I have read and understood the School's definition of plagiarism and cheating given in the Research Degree Handbook. I declare that this thesis is my own work, and that I have acknowledged all results and quotations from the published or unpublished work of other people.

I have read and understood the School's definition and policy on the use of third parties (either paid or unpaid) who have contributed to the preparation of this thesis by providing copy editing and, or, proof reading service. I declare that no changes to the intellectual content or substance of this thesis were made as a result of this advice, and, that I have fully acknowledged all such contributions.

Signed: Date:

Full name: Lip Nam Loh

Abstract

Escherichia coli (*E. coli*) K1 is one of the commonest Gram negative bacteria causing neonatal bacterial meningitis in both developed and developing countries. Haematogenous spread is a key step in *E. coli* K1 meningitis; however, it is not clear how bacteria cross the brain endothelium to gain entry into the central nervous system. Previous studies have focussed mainly on the identification of bacterial virulence factors, as well as the signalling pathways that are activated for the recruitment of actin cytoskeleton to the bacterial adhesion site on the apical surface of human brain microvascular endothelial cells (HBMEC) and finally lead to bacterial uptake. However, the cellular requirements and mechanisms of post-invasion events are poorly understood.

This study aims to further characterize *E. coli* K1 entry, intracellular trafficking and the associated molecular mechanisms. To achieve this, a virulent fluorescent protein-expressing *E. coli* K1 strain was constructed. In a previous study, caveolin-1, a lipid raft marker associated with clathrin-independent endocytosis, was found associated with invading and intracellular bacteria in HBMEC. To further study the effect of caveolin-1 on the bacterial entry, different caveolin-1 mutants were applied here. Overexpression of caveolin-1 Y14A mutant and caveolin-1β, which is non-phosphorylatable, did not block *E. coli* K1 invasion of HBMEC. Furthermore, *E. coli* K1 invasion of caveolin-1 knockout mouse lung endothelial cells (MLEC) was not blocked, which suggested that caveolin-1 was not required for *E. coli* K1 invasion of endothelial cells. The role of dynamin, a large GTPase that has been implicated in the membrane fission of caveolae buds, was also investigated. Based on quantitative microscopy scoring, no evidence of any inhibitory effect on the bacterial invasion was observed in cells overexpressing green fluorescent protein- (GFP) tagged dominant negative dynamin 2 [Dyn2(aa)K44A] and dominant negative dynamin 1 (Dyn1K44A). The experimental evidence from this study therefore

2

suggests that *E. coli* K1 might invade HBMEC via a caveolae- and dynamin-independent endocytic pathway.

To further explore the endocytosis pathway that the bacteria use to invade HBMEC, immunofluorescence staining of *E. coli* K1 infected HBMEC revealed co-localization of the bacteria with flotillin 1, another lipid raft marker associated with clathrin-independent endocytosis. However, *E. coli* K1 infection of flotillin 1 knockout MLEC demonstrated a significantly increased bacterial uptake. This observation suggests that *E. coli* K1 uptake does not require flotillin 1. In parallel, the number of intracellular non-pathogenic *E. coli* K-12 recovered from the lysates of flotillin 1 knockout MLEC was also significantly higher than that recovered from the lysates of wild type MLEC. Further, overexpression of GFP-tagged flotillin 1 and flotillin 2 in HBMEC inhibited *E. coli* K1 invasion, which suggest flotillin might have a role as a regulatory cell barrier in host defence.

Acknowledgements

I would like to express my deep gratitude to the following individuals whose unwavering support and faith were critical to the completion of this research.

First, I would like to thank Dr. Theresa Ward and Dr. Naveed Khan for giving me the opportunity to work on this project. I appreciate their guidance, feedbacks and supports. It is an honour to have them as supervisors.

A special thank you to Dr. Elizabeth McCarthy, Dr. John Raynes, Dr. Bianca Schneider, Dr. Anna Cogen, Dr. Greg Bancroft, Dr. Dominic Mills, Dr. Sam Willcocks, Dr. Andrea Zelmer, Dr. Bjoern Corleis, and Mr. Emmanuel Patin for their valuable suggestions, and scientific discussions.

I would also like to thank all the great people I met in LSHTM and Birbeck College for the past 3 years, Mr. Abid Sunderji, Dr. Parisa Mortazavi, Ms. Jia Li Lim, Dr. Eiko Matsuo, Ms. Rachel Gregory, Dr. Maria Podinovskaia, Dr. Nuha Mansour, Dr. Ozan Gundogdu, Mr. Abdi Elmi, Dr. Graham Clark, Professor John Kelly, Dr. Mark Boyce, and others. Your direct and indirect (probably just a brief chat in the lift or corridor, or brief discussion during departmental poster day, etc.) assistance enable my research to progress smoothly and also give me the momentum to move on.

Not forgetting to thank my best friends, Swee Tin, Michelle, Eddie, and Senthil. They have taught me a lot in performing scientific research in resource scarcity environment during my previous job, which I greatly benefited for surviving throughout this study.

I want to thank my family in Malaysia, especially to both my lovely old parents, for standing by me every step of the way. Thank you so much for your endless love and support at every stage of my life, although you do not really understand what I am doing, the reasons I enjoy so much in spending days and nights working with microbes even

though all the hard works do not guarantee a successful career. Both of you do not only raise me up, but also shaped my life. I am very sorry for being selfish while continuously chasing after my dreams. I won't be as successful as Professor David Ho (the only biomedical scientist that my father knows of), because there is only one Professor Ho, but I will be myself and I will carve my own career path.

Table of contents

7

8

•

List of figures

List of tables

List of abbreviations

AEE	Apical early endosomes
APS	Ammonium persulphate
ARE	Apical recycling endosomes
ATP	Adenosine triphosphate
BBB	Blood-brain barrier
BCSFB	Blood-cerebrospinal fluid barrier
BEE	Basolateral early endosomes
BMEC	Brain microvascular endothelial cells
bp	Base pairs
BSA	Bovine serum albumin
$CaCl_2$	Calcium chloride
Cav1	Caveolin-1
$^\circ$C	Celsius
CβG	Cyclic β-1,2-glucan
CCD	Charge-coupled device
CCV	*Coxiella*-containing vacuoles
Cdc42	Cell division cycle 42
cDNA	Complementary DNA
CFP	Cyan fluorescent protein
cfu	Colony-forming unit
CLIC	Clathrin-independent carrier
cm	Centimetre
cm^2	Centimetre squared
Cm^R	Chloramphenicol resistance gene

CNF1	Cytotoxic necrotizing factor-1
CNS	Central nervous system
CO_2	Carbon dioxide
CPAF	Chlamydial protease-like activity factor
CRE	Common recycling endosome
CSF	Cerebrospinal fluid
DAPI	4',6-diamidino-2-phenylindole
dATP	Deoxyadenosine triphosphate
DAEC	Diffusely adherent *E. coli*
dCTP	Deoxycytidine triphosphate
dGTP	Deoxyguanosine triphosphate
DMEM	Dulbecco's Modified Eagles Medium
DMSO	Dimethyl sulfoxide
DNA	Deoxyribonucleic acid
dNTP	Deoxyribonucleoside triphosphate
Drp1	Dynamin-related protein 1
dTTP	Deoxythymidine triphosphate
Dyn1	Dynamin 1
Dyn2	Dynamin 2
Dyn3	Dynamin 3
E. coli	*Escherichia coli*
EAEC	Enteroaggregative *E. coli*
EB	Elution buffer
ECL	Enhanced chemiluminescent
ECV	*E. coli* K1 containing vacuoles
EDTA	Ethylenediamine tetraacetic acid

EE	Early endosomes
EEA1	Early endosomal antigen-1
EGFP	Enhanced green fluorescent protein
EHEC	Enterohaemorrhagic *E. coli*
EIEC	Enteroinvasive *E. coli*
endoE	Endosialidase
EPEC	Enteropathogenic *E. coli*
ER	Endoplasmic reticulum
ETEC	Enterotoxigenic *E. coli*
FAK	Focal adhesion kinase
FBS	Fetal bovine serum
FimH	Type 1 fimbriae
FITC	Fluorescein isothiocyanate
Flot1	Flotillin 1
FRAP	Fluorescence recovery after photobleaching
GBS	Group B *Streptococci*
GDP	Guanosine diphosphate
GEEC	GPI-enriched early endosomal compartment
GFP	Green fluorescent protein
GPI	Glycosyl-phosphatidylinositol
GSP	General secretory pathway
GTP	Guanosine triphosphate
h	Hours
H_2O	Water molecule
HBMEC	Human brain microvascular endothelial cells
HDMEC	Human dermal microvascular endothelial cells

HEPES	4-(2-hydroxyethyl)-1-piperazineethanesulfonic acid
HIV	Human immunodeficiency virus
HRP	Horseradish peroxidase
IAP	Intrapartum antibiotic prophylaxis
K1	*Escherichia coli* K1 strain
K-12	*Escherichia coli* K-12 (HB101) strain
KAc	Potassium acetate
kb	Kilobases
KCl	Potassium chloride
kDa	Kilo Dalton
KH_2PO_4	Potassium dihydrogen phosphate
K/O	Knockout
kV	Kilovolt
LAMP1	Lysosomal-associated membrane protein-1
LB	Luria-Bertani
LDLR	Low-density lipoprotein receptor
LE	Late endosomes
LPS	Lipopolysaccharides
Lys	Lysosomes
MCD	Medullary collecting duct
$MgCl_2$	Magnesium chloride
μg	Microgramme
μl	Microlitre
μm	Micrometre
μM	Micromolar
mins	Minutes

ml	Millilitre
MLEC	Mouse lung endothelial cells
mM	Millimolar
MnCl$_2$	Manganese chloride
MOI	Multiplicity of infection
N.B.	Note
n.s.	Not statistically significant
NA	Numerical aperture
Na$_2$CO$_3$	Sodium carbonate
Na$_2$HPO$_4$	Disodium hydrogen phosphate
NaCl	Sodium chloride
NBM	Neonatal bacterial meningitis
NCAM	Neural cell adhesion molecule
NH$_4$Cl	Ammonium chloride
NHS	*N*-Hydroxysuccinimide
NLS	Nuclear localization signal
NMEC	Neonatal meningitis *E. coli*
NPC1L1	Niemann-Pick C1-like 1
OD	Optical density
OmpA	Outer membrane protein A
OriM	Origin of replication
p.i.	Post infection
PAK	p21-activated protein kinase
palm	Palmitoylation
PBS	Phosphate buffered saline
PBSA	Dulbecco's phosphate buffered saline

PCR	Polymerase chain reaction
Pfu	*Pyrococcus furiosus*
pH	Hydrogen potential
PI3K	Phosphatidylinositol-3-kinase
PK1A-GFP	Endosialidase–GFP fusion protein
PKCα	Protein Kinase Cα
pmol	Picomol
PolySia	Polysialic acid
PtdIns(3)P	Phosphatidylinositol-3-phosphate
PtdIns(3,5)P_2	Phosphatidylinositol-3,5-biphosphate
PTFE	Polytetrafluoroethylene
PYG	Proteose peptone, yeast extract, and glucose media
RhoA	Ras homolog gene family, member A
RILP	Rab7-interacting lysosomal protein
RNA	Ribonucleic acid
ROS	Reactive oxygen species
rpm	Revolutions per minute
SCV	*Salmonella*-containing vacuoles
SD	Standard deviation
SDS	Sodium dodecyl sulfate
SDS-PAGE	Sodium dodecyl sulfate polyacrylamide gel electrophoresis
secs	Seconds
SEM	Standard error of mean
siRNA	Small interfering RNA
sp.	Species
SPI	*Salmonella* pathogenicity island

Stat3	Signal transducer and activator of transcription 3
SV40	Simian virus 40
T3SS	Type 3 secretion system
TBE	Tris-borate EDTA
TEER	Transendothelial electrical resistance
TEM	Transmission electron microscope
tet^R	Tetracycline resistance gene
TfR	Transferrin receptor
TGN	Trans-Golgi network
TJ	Tight junction
TLR4	Toll-like receptor 4
Tris	Tris(hydroxymethyl)aminomethane
Tyr	Tyrosine
U	Unit
UPEC	Uropathogenic *E. coli*
UTI	Urinary tract infections
UV	Ultraviolet
VF	Virulence factors
WT	Wild type
YFP	Yellow fluorescent protein

1. Introduction

1.1 Neonatal bacterial meningitis (NBM)

Neonatal bacterial meningitis (NBM) is caused by inflammation of the meninges, a result of bacterial infection during the first month of life. In developing countries, of 125000 diagnosed cases about 50000 newborns die of meningitis annually (mortality rate of 40%) (Mulholland, 1998). Comparatively, in developed countries, the NBM mortality rate has declined from about 50% in the 1970s to about 10% in the late 1990s, although the morbidity (0.22 per 1000 births) remains very similar in the past two decades (Holt et al., 2001; Gaschignard et al., 2011). A better understanding of the disease pathogenesis and pathophysiology would improve the morbidity and mortality of the disease, despite the advances in chemotherapy and supportive care (Polin and Harris, 2001; Bonacorsi and Bingen, 2005).

The clinical presentation of NBM is non-specific, including apnea, temperature instability, hypotension, bradycardia, tachycardia, lethargy or irritability, and abdominal distention or feeding intolerance (de Louvois, 1994; Wynn and Levy, 2010). The prevalence of the causative organisms isolated from early- (occurring between day 0 and day 4 of life) and late-onset (occurring between day 5 and day 28 of life) NBM is different, and it varies in different countries (Osrin et al., 2004; Wu et al., 2009; Zaidi et al., 2009; Talbert et al., 2010; Gaschignard et al., 2011). E. coli and group B Streptococci (GBS) are the commonest bacteria isolated from NBM cases; however, the mortality rate of E. coli associated cases is relatively higher than GBS infection in some countries (Holt et al., 2001; Stoll et al., 2002; May et al., 2005; Wu et al., 2009), and about half of the E. coli-associated NBM survivors develop neurological disability (Unhanand et al., 1993; Harvey et al., 1999; Dellagrammaticas et al., 2000).

Following the implementation of intrapartum antibiotic prophylaxis (IAP) treatment in mothers who carry GBS from screening at 35 to 37 weeks of gestation since the mid-1990s in developed countries, the number of GBS-associated NBM cases have declined significantly, while non-GBS NBM cases are either stable (Baltimore *et al.*, 2001) or on the increase (Levine *et al.*, 1999). Notably, increased ampicillin resistance has been found in *E. coli* strains isolated from *E. coli*-NBM in the current IAP era (Levine *et al.*, 1999; Baltimore *et al.*, 2001; Stoll *et al.*, 2002; Alarcon *et al.*, 2004; Cordero *et al.*, 2004; Bizzarro *et al.*, 2008).

1.2 *Escherichia coli* (*E. coli*)

E. coli is a member of *Enterobacteriaceae*. It is a facultative anaerobic Gram negative bacillus, which colonizes the human neonatal gastrointestinal tract within hours of birth, remains as a commensal and provides a lifetime of benefits to the host from intruding pathogens, including competition for space or binding sites, competition for nutrients, and regulate immune homeostasis (Kaper *et al.*, 2004; Willing *et al.*, 2011). However, some *E. coli* strains have acquired specific virulence factors, and are major community and hospital-acquired pathogens, and veterinary pathogens. The resultant diseases can be categorized into enteric/diarrhoeal disease, urinary tract infections (UTI), and sepsis/meningitis (Kaper *et al.*, 2004; Bonacorsi and Bingen, 2005). There are eight main pathogenic *E. coli* pathovars, with six diarrhoeagenic: enteropathogenic *E. coli* (EPEC), enterohaemorrhagic *E. coli* (EHEC), enterotoxigenic *E. coli* (ETEC), enteroaggregative *E. coli* (EAEC), enteroinvasive *E. coli* (EIEC) and diffusely adherent *E. coli* (DAEC); two extraintestinal infections: uropathogenic *E. coli* (UPEC) and neonatal meningitis *E. coli* (NMEC). In addition to the major pathovars, other pathovars have also been identified (Kaper *et al.*, 2004; Croxen and Finlay, 2010).

The *E. coli* species has 170 O lipopolysaccharides antigens or LPS, 103 capsular or K antigens, and 56 flagellar or H antigens, and strains are categorised on the basis of their antigen configuration (Robbins *et al.*, 1974; Kaper *et al.*, 2004).

Strains possessing the K1 capsular polysaccharide predominate the majority of NBM cases (Robbins *et al.*, 1974). Interestingly, only a few O antigens (e.g. O18, O7, O1, O16) are associated with most of the K1 strains isolated from the cerebrospinal fluid (CSF) (Sarff *et al.*, 1975; Pluschke *et al.*, 1983).

1.3 Pathogenesis of *E. coli* K1 neonatal meningitis

In most cases of *E. coli* neonatal meningitis, the infants are believed to acquire the pathogen from the mother's delivery canal or from the environment, leading to colonization of the infant's intestinal tract (Robbins *et al.*, 1974; Sarff *et al.*, 1975; Headings and Overall, 1977; Raymond *et al.*, 2008). The bacteria are normally confined to the intestinal tract by the gut mucosal barrier, where they form part of the normal commensal flora. The gut barrier is formed of epithelial cells held closely together by tight junctions, and has major roles in regulating the movement of ions and molecules between cellular spaces, as well as in protecting the host from invading pathogens (Daneman and Rescigno, 2009). In *E. coli* K1 meningitis, the bacteria are able to traverse the gut barrier and enter the bloodstream. The interaction of *E. coli* K1 with gut barrier has not been studied extensively; however, an *in vitro* study with human intestinal epithelial cell lines, Caco-2 and T84, showed that *E. coli* K1 breached the epithelial barrier by disrupting tight junctions, evidenced by a decrease in the transendothelial electrical resistance (TEER) value and the increased passage of non-invasive *E. coli* strain through the monolayer on Transwell® insert in co-infection experiments (Burns *et al.*, 2001).

Once the bacteria have crossed gut mucosal barrier, the bacteria gain access to the bloodstream and must overcome the host defense mechanisms to survive intravascularly.

The bacterial polysaccharide K1 capsule has been shown to possess anti-phagocytic properties (Bortolussi *et al.*, 1979; Mushtaq *et al.*, 2005) and provides resistance to classic complement-mediated bactericidal activity (Cross *et al.*, 1986; Mushtaq *et al.*, 2004). In addition, the neonatal host defense mechanism is less able to deal with an intravascular infection when compared to an adult's immune system. Neonatal macrophages and neutrophils have been found to be inefficient in phagocytosis (Filias *et al.*, 2011), as well as in the production and secretion of reactive oxygen species (ROS) (Levy, 2007; Wynn and Levy, 2010). Neonatal leukocytes also expresses low levels of surface CR3, which functions as a pathogen sensor and recruits complement (Wynn and Levy, 2010). Moreover, neonates are found to express low levels of C9 and other components of the complement system (C1, C3, C4, C5) (Wilfert, 1978; Lassiter *et al.*, 1992). Bacterial intravascular survival might be further aided by the deficiency of pro-inflammatory and T_H1-polarizing cytokines production by neonatal antigen-presenting cells, which aim to avoid triggering excessive inflammation during colonization of gut commensal flora (Wynn and Levy, 2010). As a consequence of the deficiencies in neonatal immunity, the bacterial bloodstream survival is promoted; hence, the bacteria are able to multiply to a high level of bacteraemia, and finally invade into the cerebraspinal fluid (CSF) (Glode *et al.*, 1977; Pluschke *et al.*, 1983; Kim *et al.*, 1992; Zelmer *et al.*, 2008). It has been documented that patients with bacteraemia of $>10^3$ colony forming units per ml of blood are highly likely to develop meningitis (Dietzman *et al.*, 1974).

The precise sites and mechanisms that *E. coli* K1 and other meningitis-causing extracellular bacterial pathogens, such as *Streptococcus pneumonia*, *Haemophilus influenza*, and *Neisseria meningitidis*, enter into CSF are still unclear and in many cases controversial. *Haemophilus influenza* and *Neisseria meningitidis* are believed to invade CSF via the blood-cerebrospinal fluid barrier (BCSFB) at choroid plexus based on histological examinations of brain tissue, which found the presence of the bacteria in the

endothelium of choroid plexus and meninges (Smith, 1987; Pron *et al.*. 1997). However, if BCSFB is the bacterial portal of entry, meningitis should be theoretically linked to ventriculitis, which has never been observed in post-mortem specimens (Join-Lambert *et al.*, 2010). The cerebral microvascular endothelial cells, which form the BBB, have been proposed as an alternative bacterial entry site (Quagliarello *et al.*, 1986; Parkkinen *et al.*, 1988), but meningitis-causing extracellular bacteria do not cause encephalitis, and there is no evidence that these bacteria are able to multiply in the brain parenchyma (Join-Lambert *et al.*, 2010). Nevertheless, at later stages of the infection, the increased permeability of BBB, resulting from increased pinocytosis, leads to the disruption of the intercellular junctions of the cerebral capillaries in BBB (Quagliarello *et al.*, 1986). Intriguingly, post-mortem examination of a patient who died of fulminant meningococcal meningitis revealed that the bacteria adhered to cerebral capillary (Mairey *et al.*, 2006), suggesting that meningitis-causing extracellular bacteria do interact with BBB during infection. In the case of *E. coli* K1, bacteria have been found in the perivascular area of the subarachnoid space of histological brain sections of subcutaneously-infected 5–day-old rats (Kim *et al.*, 1992). However a decade later, bacteria were observed in the choroid plexus of histological brain sections of *E. coli* K1-infected 2-day-old rats, where the animals were infected orally (Zelmer *et al.*, 2008). Despite the controversies on the bacterial portal of entry into CSF, *in vitro* studies with cerebral microvascular endothelial cells have allowed the identification of bacterial virulence factors that are essential for endothelial cell adherent and invasion, as reviewed in section 1.8.1. Future studies will hopefully elucidate the precise mechanism by which entry into the CSF is achieved by these pathogens.

Once in the subarachnoid space, the bacteria take advantage of the immune privilege of the CNS and replicate and induce inflammatory cytokines production (Simberkoff *et al.*, 1980). In the CSF, the concentrations of immunoglobulin and complement components are low, which leads to inefficient removal of the pathogens

(Tofte *et al.*, 1979; Simberkoff *et al.*, 1980). The bacterial cell wall components, but not the bacterial capsule, have been shown to be potent inducers for tumor necrosis factor (TNF) and interleukin-1 (IL-1) production, which promote the adherence of neutrophils to endothelium, meningeal inflammation, and BBB breakdown (Dinarello, 1989; Waage *et al.*, 1989; Ramilo *et al.*, 1990; Quagliarello *et al.*, 1991). The hallmark of bacterial meningitis is the recruitment of neutrophils into CSF; however, the neutrophils are not efficient killers in the CSF (Ernst *et al.*, 1983). Conversely, neutrophils recruitment appears to have a negative effect and may contribute to the pathogenesis of the disease. When the recruitment of neutrophils was blocked during the infection, brain edema, intracranial pressure, and neuronal apoptosis in the hippocampus of infected animals were reduced (Tuomanen *et al.*, 1989; Braun *et al.*, 1999).

1.4 Blood-brain barrier and blood-cerebrospinal fluid barrier, and *in vitro* models

The BBB separates the circulating blood from the elements of CNS. The capillary BBB, which is localized in cerebral cortex, is formed by endothelial cells that are connected via a network of junctional complexes, and have very few endocytic vesicles (Figure 1.1A) (Rubin and Staddon, 1999). The junctional complexes are composed of adheren junctions and tight junctions, which restrict the movement of hydrophilic macromolecules and small ions between the blood and the brain, and result in high endothelial electric resistance in the brain capillaries (Abbott *et al.*, 2006). The major molecules of the tight junctions present in brain capillary endothelium are occludin, claudin-1, claudin-5, ZO-1, and ZO-2 (Rubin and Staddon, 1999; Abbott *et al.*, 2006). The tight junctional complexes are further stabilized by adheren junctions, which are mainly composed of cadherin, and the cytoplasmic tail of which is associated with catenins (Rubin and Staddon, 1999). The endothelial cells are also in close contact with astrocytes, the paracrine factors produced by these astrocytes might also contribute to the endothelial cells

tight junction complexes formation (Arthur *et al.*, 1987). Other perivascular cell types, including pericytes, microglial cells, and perivascular macrophages, form the CNS perivascular immunological barrier to protect the CNS from invading pathogens (Join-Lambert *et al.*, 2010).

In addition to the intracerebral capillaries, the brain post-capillary venules (Figure 1.1B) are also part of the BBB. These venules have very similar properties as intracerebral capillaries, but they do not form as tight barrier as that of intracerebral capillaries (Abbott *et al.*, 2006; Nachman and Rafii, 2008). Ultrastructural studies showed that these venules have discontinuous and less complex junctional complexes than that of intracerebral capillaries (Nagy *et al.*, 1984; Allt and Lawrenson, 1997). There is no electrophysiological data to demonstrate the resistance of these post-capillary venules, although rat pial venules have been shown to have lower resistance than that of pial arterioles (Butt and Jones, 1992). Furthermore, when the capillaries turn into venules and veins, the contact between endothelial cells and astrocyte processes is gradually reduced as they are separated by the increasing Virchow-Robin perivascular spaces (Join-Lambert *et al.*, 2010).

Primary brain microvascular endothelium (BMEC) of various origins can be isolated and used as a BBB *in vitro* model; however, the application of the primary cells is limited by the costly cell isolation and maintenance, rapid loss of the differentiated cell phenotypes at later passages, and failure to form tight junctions (Arthur *et al.*, 1987; Bourdoulous *et al.*, 2002). Several groups have immortalized the isolated BMEC by transfecting the cells with SV40 large T antigen, and the immortalized BMEC are shown to express specific brain endothelial properties, cell surface adhesion molecules, and junctional markers (Blasig *et al.*, 2001; Stins *et al.*, 2001; Weksler *et al.*, 2005). Importantly, these BMEC lines are able to form integral layer on Transwell® insert with high endothelial electrical resistance when they are cultured in the absence of astrocytes either in static or in flow-based system (Stins *et al.*, 2001; Cucullo *et al.*, 2008). As *in vivo*

studies of *E. coli* K1 interactions with BBB in newborn rats do not allow high resolution imaging at cellular level, thus do not allow studies of the cell biology aspect of the infection, the stable properties and indefinite growth potential of these endothelial lines provide an alternative approach, and allow experiments to be conducted with same cell source. Despite the ambiguity of extracellular bacterial pathogens utilize capillary BBB for invading into CSF, the BMEC lines have benefited studies on the interactions of these pathogens with the endothelial cells (Stins *et al.*, 2001; Doran *et al.*, 2005; Coureuil *et al.*, 2009; Orihuela *et al.*, 2009; Untucht *et al.*, 2011).

Mouse brain endothelioma cell line (bEnd5) is another BBB *in vitro* model. However, this endothelial line is not suitable for studying the interactions of meningitis-causing bacterial pathogens with endothelial cells, as the cells showed defects in tight junctional protein expression, and they fail to form intact monolayer on Transwell® insert (Steiner *et al.*, 2011).

Arachnoid

Arachnoid trabeculae

Virchow-Robin perivascular space

Artery

Capillaries

Subarachnoid space

Pia mater

Vein

Cerebral cortex

A

Astrocyte

Pericyte

Capillary endothelium

Basement membrane

Tight junction

Neuron

Blood

B

Virchow-Robin perivascular space

Astrocyte

Pericyte

Endothelium

Perivascular macrophage

Blood

29
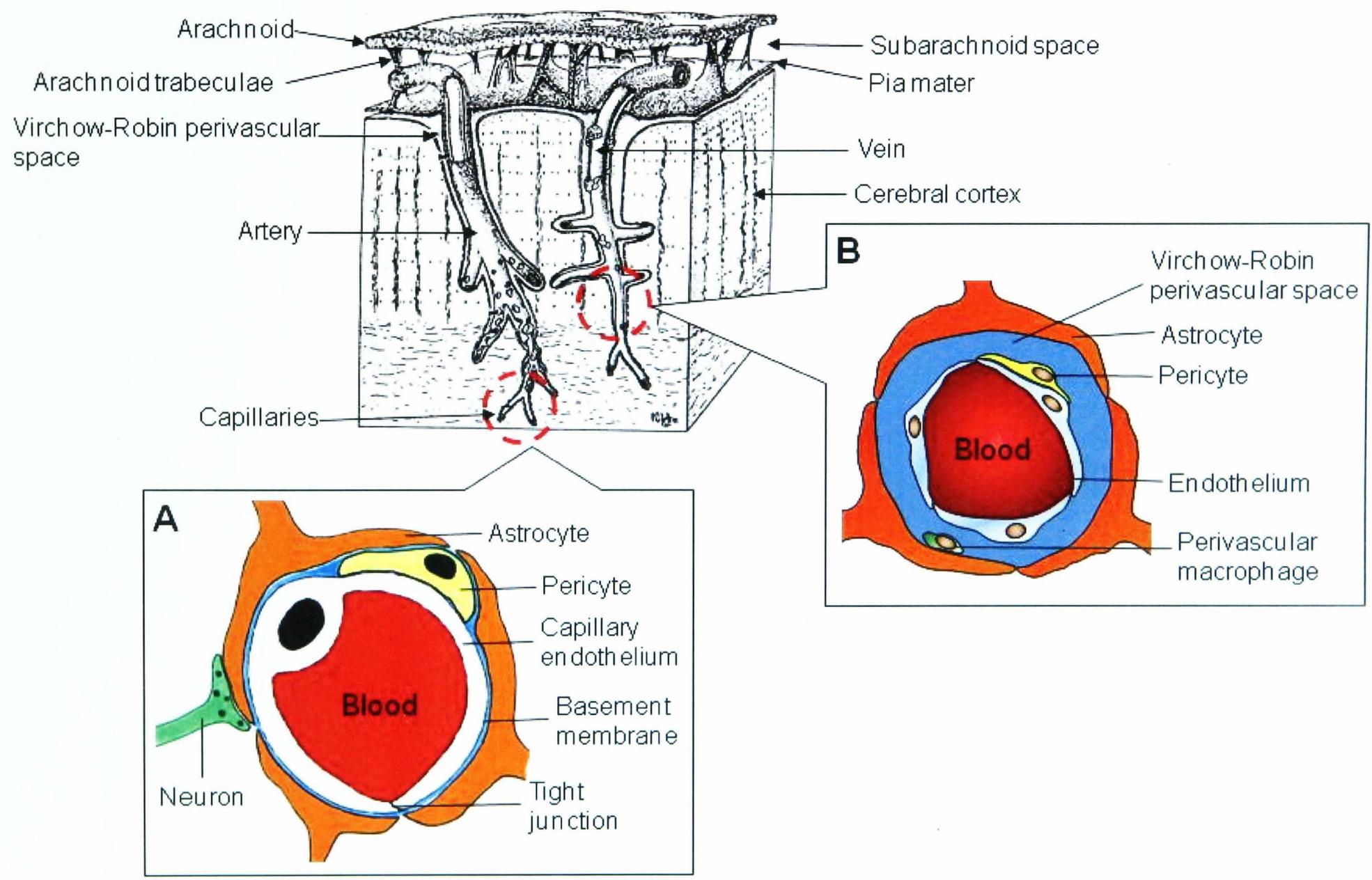
Figure 1.1. Vascular arrangement in the cerebral cortex. The illustration shows the arrangement of intracerebral blood vessels in the brain. The illustration was adapted from (Abbott *et al.*, 1999). (A) The capillary BBB. The intracerebral capillaries are composed of endothelial cells that form tight junctions, and they are in contact with foot processes of astrocytes, and pericytes. A thin basement provides both mechanical support and a barrier function. (B) The brain post-capillary venules. In contrast to the capillary BBB, the brain post-capillary venules, which form the venous BBB, do not form as tight barrier as that of the capillary BBB, although they have very similar properties. The presence of Virchow-Robin perivascular space prevents close contact of the endothelial cells with the foot processes of astrocytes.

BCSFB forms the barrier that separates blood components from CSF. CSF is actively produced by the ependymal cells of choroid plexus in brain ventricles. From the choroid plexus, the CSF is drained into the subarachnoid space over brain and spinal cord, and is reabsorbed into blood through arachnoid villi of the dura mater venous sinuses (Join-Lambert *et al.*, 2010).

In contrast to the blood vessels of BBB, the endothelial cells of BCSFB are fenestrated. The ependymal cells that actively produce CSF are linked together by tight junctions (Figure 1.2). Primary choroidal epithelium is available as a BCSFB *in vitro* model and has been used for studying *Streptococcus suis* infection (Tenenbaum *et al.*, 2009). In addition to the primary choroidal epithelium, several choroid plexus epithelial cell lines are available. Z310 and TR-CSFB3 are immortalized rat choroid plexus epithelial cell lines carrying the simian virus 40 (SV40) large T antigen gene (Kitazawa *et al.*, 2001; Zheng and Zhao, 2002); while the CPC-2 cell line was derived from a human choroid plexus carcinoma (Kumabe *et al.*, 1996). Although all the cell lines provide lower cost and easier maintenance than primary choroidal epithelium, they vary in the expression of junctional proteins, and the protein distribution for some of these junctional proteins are altered after immortalization (Szmydynger-Chodobska *et al.*, 2007).
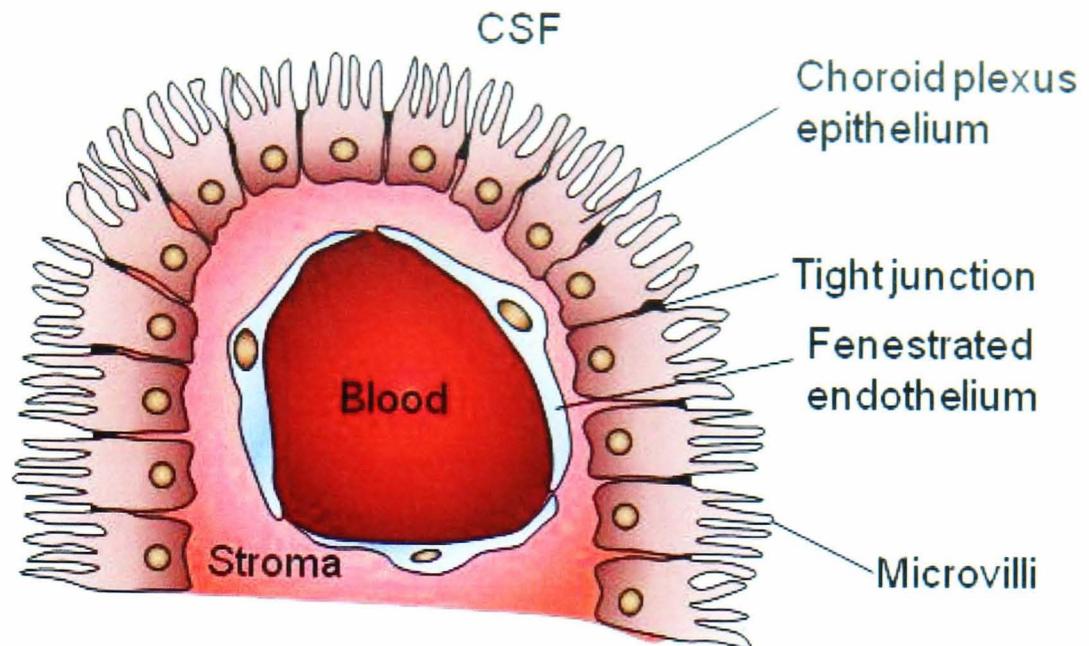
Figure 1.2. Schematic diagrams of BCSFB. The BCSFB is composed of fenestrated capillaries in close contact with ependymal epithelial cells.

Since both BBB and BCSFB are tightly regulated barriers, pathogens need to cross the endothelium (for BBB) or epithelium (for BCSFB) via transcellular (Figure 1.3A), paracellular (Figure 1.3B), or trojan-horse mechanism (Figure 1.3C). For the transcellular traversal route, a pathogen invades the host cell, survives intracellularly, traverses through the cell, and manipulates host cell exocytosis mechanisms for cell egress (Nassif *et al.*, 2002; Kim, 2008). Several pathogens, such as *E. coli* K1 (Stins *et al.*, 2001), UPEC (Chassin *et al.*, 2008), *Streptococcus iniae* (Eyngor *et al.*, 2007), *Streptococcus pneumoniae* (Ring *et al.*, 1998), *Streptococcus suis* (Tenenbaum *et al.*, 2009), and *Neisseria gonorrhoeae* (Wang *et al.*, 1998), have been demonstrated to traverse transcellularly in infected cells. For the paracellular traversal route, the pathogen crosses between host cells, with or without disrupting tight junctions (Nassif *et al.*, 2002; Kim, 2008). *Trypanosoma* sp. have been suggested to cross the BBB via paracellular route (Grab *et al.*, 2004). *Mycobacterium tuberculosis* (Jain *et al.*, 2006), and *Listeria monocytogenes* (Greiffenberg *et al.*, 1998), have been suggested to cross a BBB via trojan-horse mechanism, which involves transmigration of an infected phagocyte across the polarized HBMEC (Kim, 2008).

31
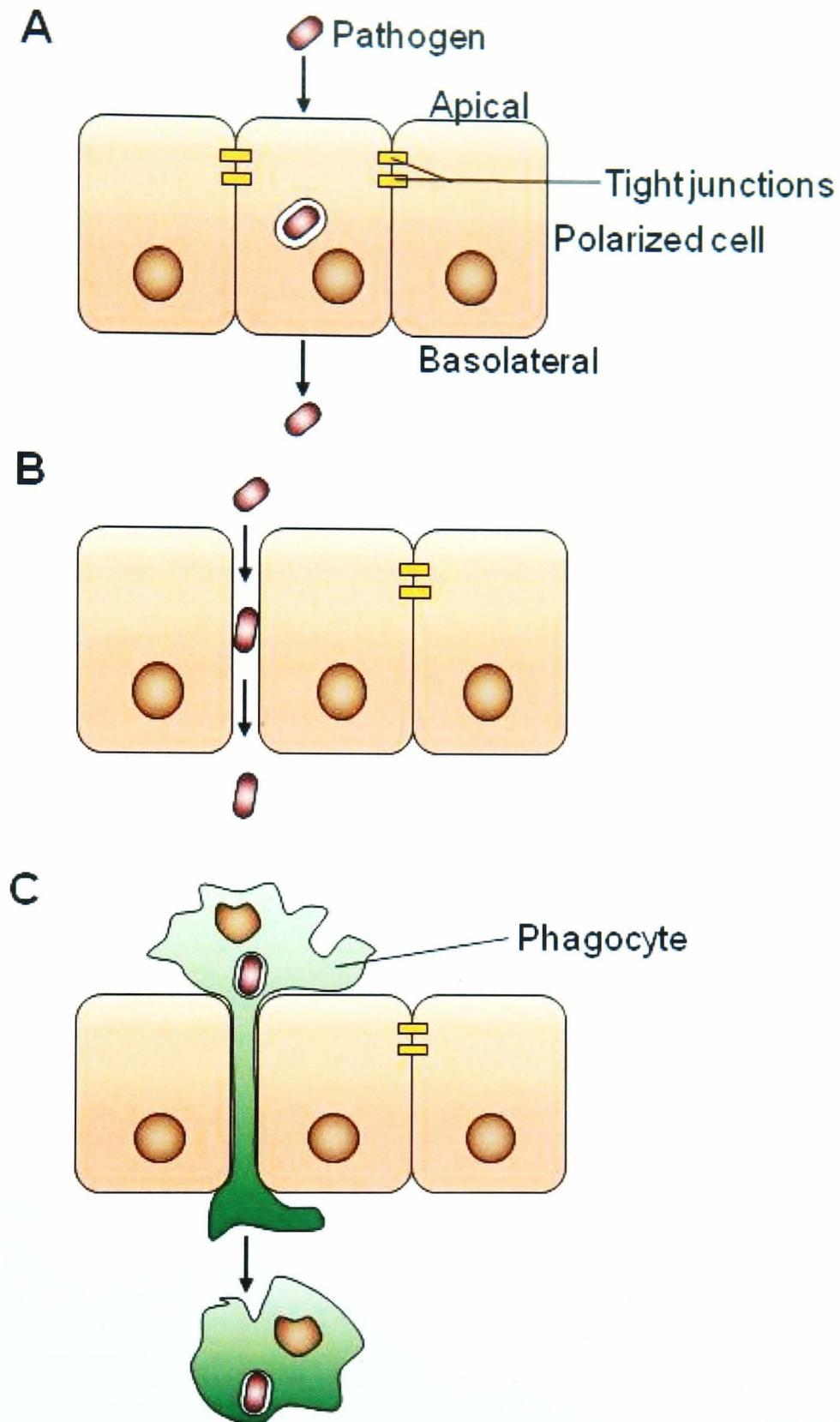
Figure 1.3. Models of pathogen traversal of polarized epithelia or endothelia. (A) Transcellular traversal. (B) Paracellular traversal. (C) Trojan-horse mechanism.

1.5 Plasma membranes structures

Plasma membranes are barriers that protect cell components from external environment. They are composed of dynamic lipid bilayers, which are spanned by or

associated with proteins at either side of the lipid bilayers, and the proteins have roles in membrane trafficking and signalling (Simons and Gerl, 2010; Simons and Sampaio, 2011). The lipid molecules (sphingolipids, and sterols) on the plasma membranes have been proposed to be able to assemble into specialized microdomains, termed lipid rafts, which are usually stabilized by specific proteins (Lingwood and Simons, 2010). They have several significant biological functions, including T cell signalling, viral assembly, ER-to-Golgi trafficking, and endocytosis (Simons and Gerl, 2010).

1.6 Endocytosis

The homeostasis between the cytosol and extracellular environment is maintained by regulating the entry and exit of fluids, solutes, and particles through the membrane lipid bilayer. Small molecules, such as amino acids, sugars, and ions, enter the cell through membrane pumps or ion channels; large molecules enter the non-phagocytic cell by endocytosis (Conner and Schmid, 2003). Various pathogens have also been documented to hijack endocytic pathways for invading non-phagocytic cells (Table 1.1). Endocytic pathways are generally identified by the coat proteins in endocytosis. The major endocytic pathways (Figure 1.4) includes macropinocytosis, clathrin-mediated endocytosis, caveolae-mediated endocytosis, and clathrin- and caveolae-independent endocytosis (Conner and Schmid, 2003).
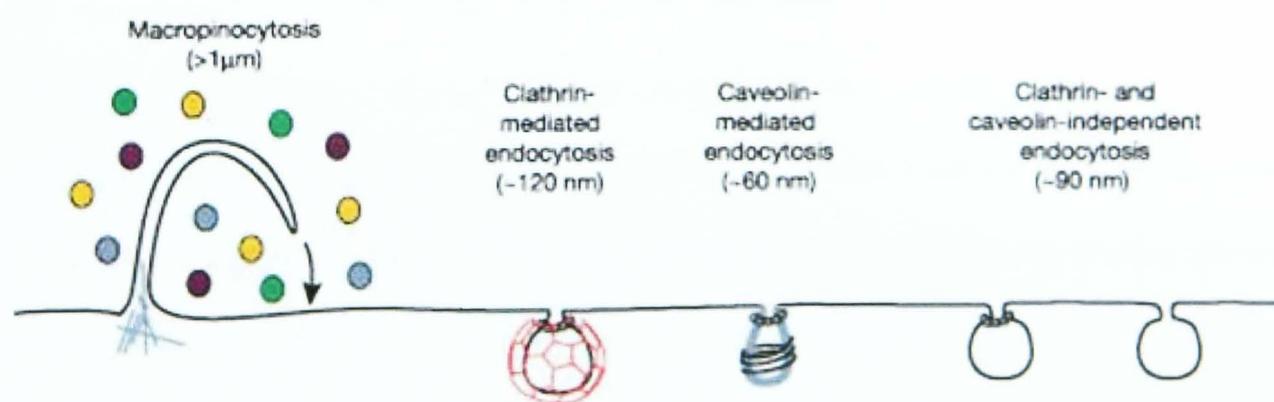
Figure 1.4. Endocytic routes. The illustration shows various endocytic routes in non-phagocytic cell and the size of the endocytic vesicles (Conner and Schmid, 2003).

33

These endocytic routes are classified by their dependence on large GTPase, dynamin (Figure 1.5), which is recruited to the neck of the budding vesicle on plasma membrane for vesicle scission (Iversen *et al.*, 2003), and it is able to assemble into spirals and form helical structures on lipid nanotubes *in vitro* (Stowell *et al.*, 1999). In mammals, there are three dynamin isoforms identified. Dynamin 1 is found specifically in neuronal tissue (Scaife and Margolis, 1990); dynamin 2 is ubiquitously expressed (Nakata *et al.*, 1993; Cook *et al.*, 1994); and dynamin 3 is found in testis, lung, and neurons (Nakata *et al.*, 1993). Despite the GTPase domain, dynamin contains a middle domain, a pleckstrin-homology domain, a GTPase effector domain, and a C-terminal proline-rich domain. In addition to vesicle scission, dynamin also functions in mitochondria and chloroplast division and fusion, and cytokinesis, as reviewed in (Praefcke and McMahon, 2004).
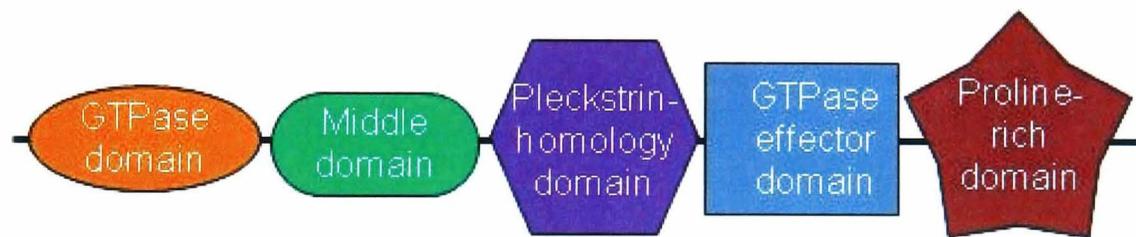
Figure 1.5. Domain structure of a dynamin. Protein domains of a dynamin.

The catalytic mechanism of dynamin is very similar as other Ras-family GTPases, although it has lower affinity for GTP and higher rates of GTP hydrolysis than the other Ras superfamily GTPases (Damke *et al.*, 2001). In general, the conversion between GDP- and GTP-bound forms of Ras GTPase is catalyzed by Ras specific guanine-nucleotide-exchange factors (GEF) (Figure 1.6A), while the conversion from the GTP- to the GDP-bound form occurs through GTP hydrolysis catalyzed by GTPase-activating proteins (GAP) (Stenmark, 2009). In the GTP-bound (active) form, Ras activates or binds with high

affinity to other cytoplasmic targets or effector proteins and lead to activation of signalling cascades.

To elucidate the functions of Ras proteins in cells, dominant negative Ras mutants have been widely applied (Figure 1.6B). The dominant negative Ras mutants function by competing with normal Ras for binding to GEF, and form "dead-end" complexes, which are unable to interact with downstream effectors (Feig, 1999). The dominant negative Ras mutants have also been shown to have higher affinities for GDP than for GTP in NIH3T3 cells overexpressing dominant negative Ras mutant, RasS17N (Feig and Cooper, 1988).
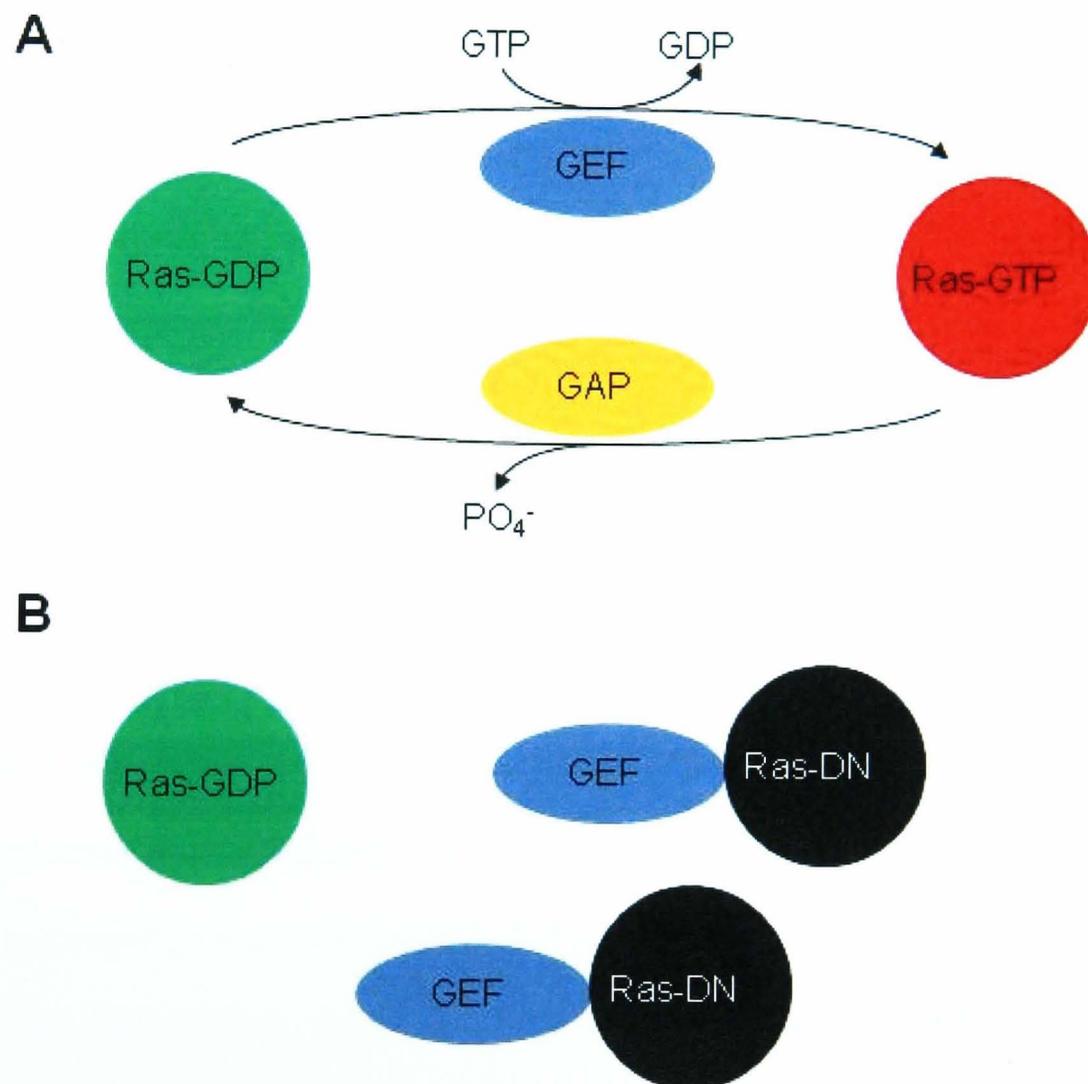
Figure 1.6. The Ras-GTPase cycle. (A) The illustration shows the biochemical conversion of GDP-bound Ras to GTP-bound. GEF, guanine-nucleotide-exchange factors; GAP, GTPase-activating protein; PO_4^-, inorganic phosphate. (B) The illustration shows the mechanism that dominant negative Ras mutants (Ras-DN) compete with normal Ras for GEF in cells expressing the dominant negative Ras.

Based on the understanding of Ras-family GTPases and by referring to the Ras-GTPase structure, dominant negative dynamin mutants have been constructed and the GTPase activities *in vitro* have been studied (Herskovits *et al.*, 1993; Damke *et al.*, 1994; Marks *et al.*, 2001). It was found that overexpression of K44A or S45N dynamin mutant, which demonstrated weak guanosine triphosphate (GTP) affinity *in vitro*, inhibits ligand uptake via dynamin-dependent endocytic routes (Herskovits *et al.*, 1993; Damke *et al.*, 1994; Marks *et al.*, 2001; Pelkmans *et al.*, 2002).

1.6.1 Clathrin-mediated endocytosis

Clathrin was the first discovered coat protein, which it forms a triskelion shape, composed of three clathrin heavy chains and three light chains (Pearse, 1976). Clathrin role in mediating endocytosis has been well-studied, and it is the classical receptor-mediated endocytosis pathway (Pearse, 1976). Clathrin-mediated endocytosis has several physiological functions, including cholesterol, iron internalization, and synaptic vesicle recycling (Anderson *et al.*, 1977; Pearse, 1982; Sato *et al.*, 2009).

After the binding of extracellular cargoes on specific receptors on the plasma membrane with cargo-specific adaptor proteins, such as AP2, clathrin triskelions are recruited to the plasma membrane from the cytosol, which leads to the formation of a polyhedral clathrin cage (Henne *et al.*, 2010). In addition to AP2, other adaptor proteins, such as epidermal growth factor protein substrate 15 (Eps15) and Eps15 interaction protein (epsin), are recruited to the clathrin assembly sites to stabilize the structure on phosphatidylinositol-4,5-bisphosphate (PtdIns(4,5)P$_2$)-rich plasma membrane (Gaidarov *et al.*, 1996; Gaidarov and Keen, 1999; Benmerah and Lamaze, 2007; McMahon and Boucrot, 2011). At the later stage of vesicle formation, dynamin is recruited to the neck of the coated pits by BAR domain-containing proteins, such as amphiphysin, endophilin, and sorting nexin 9 (SNX9), and eventually releases the vesicle from plasma membrane

(Wigge *et al.*, 1997; Ferguson *et al.*, 2009; Sundborger *et al.*, 2011). The requirement of actin polymerization during vesicle scission from the plasma membrane varies with species, and these variations are believed to be due to membrane rigidity, intracellular pressure, and cargo size (McMahon and Boucrot, 2011). In instances where actin is recruited to clathrin vesicles, the role of actin is to contribute energy for vesicle scission and movement (Engqvist-Goldstein and Drubin, 2003; Kaksonen *et al.*, 2005; Aghamohammadzadeh and Ayscough, 2009).

Once the clathrin vesicle is released into the cytosol, clathrin coat is uncoated, and the clathrin triskelia recruited in another cycle of clathrin vesicle assembly. Clathrin uncoating is facilitated by auxilin that binds to the terminal domain and ankle of clathrin triskelia, and then recruits heat shock cognate 70 (HSC70) to uncoat the clathrin coat (Schlossman *et al.*, 1984; Ungewickell *et al.*, 1995).

After the vesicle is released into the cytosol, the endocytosed cargo is sorted in the endosome, and it is either recycled back via recycling endosome to the plasma membrane or targeted to late endosomal compartment, which is increasingly acidified, and eventually degraded in lysosomes. (Figure 1.7) (Idrissi *et al.*, 2008; Kinchen and Ravichandran, 2008). Both early and late endosomes are distinctly different in their protein and lipid composition (Zerial and McBride, 2001; Gruenberg and van der Goot, 2006). The most distinctive markers that distinguish early endosome (EE) are the presence of the small GTPase Rab5, early endosomal antigen-1 (EEA1), and phosphatidylinositol-3-phosphate (PtdIns(3)P) (Clague, 1998; Gruenberg and van der Goot, 2006). Rab7, Rab9, lysosomal-associated membrane protein-1 (Lamp1), lysobisphosphatidic acid (LBPA), phosphatidylinositol-3,5-biphosphate (PtdIns(3,5)P$_2$), are present on late endosomes (LE) (Clague, 1998; Efe *et al.*, 2005; Michell *et al.*, 2006). The presence of Rab7 has been shown to be necessary for trafficking the cargo from late endosome to lysosome (Vanlandingham and Ceresa, 2009), while vesicle transportation from late endosome to

Golgi complex as well as newly synthesized lysosomal enzyme transportation from Golgi to lysosome are mediated by Rab9 (Riederer *et al.*, 1994; Barbero *et al.*, 2002).
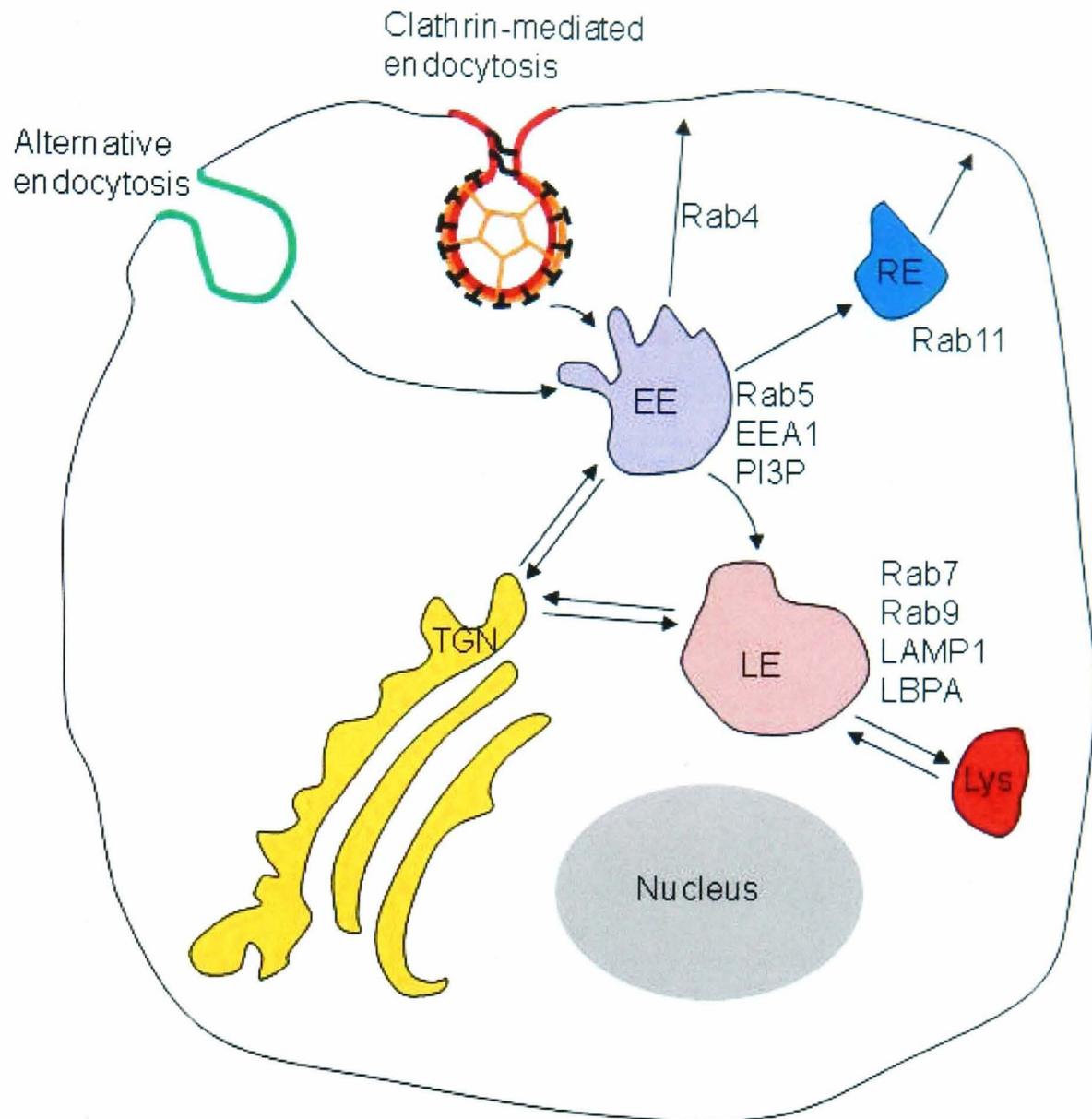
Figure 1.7. Clathrin-mediated endocytic pathway. The illustration shows the clathrin-mediated endocytosis and the endosome trafficking pathway in the mammalian cell. EE, early endosome; LE, late endosome; RE, recycling endosome; Lys, lysosome; TGN, trans golgi network.

1.6.2 Caveolae-mediated endocytosis

Caveolae are membrane microdomains enriched with caveolins, sphingolipid and cholesterol, and act as clathrin-independent sites of endocytosis of a different subset of cargo, such as albumin, and cholera toxin B. Caveolae appear as flask-shaped invaginations of 50 – 80 nm diameter on plasma membrane, and are present in specific

cells types, such as endothelial cells, fibroblasts, type I pneumocytes, and adipocytes (Figure 1.8A) (Pelkmans and Helenius, 2002; Frank *et al.*, 2003; Parton and Simons, 2007).

A Caveolae

B

Caveola

C

Palmitoylation

Cholesterol

Scaffolding
domain
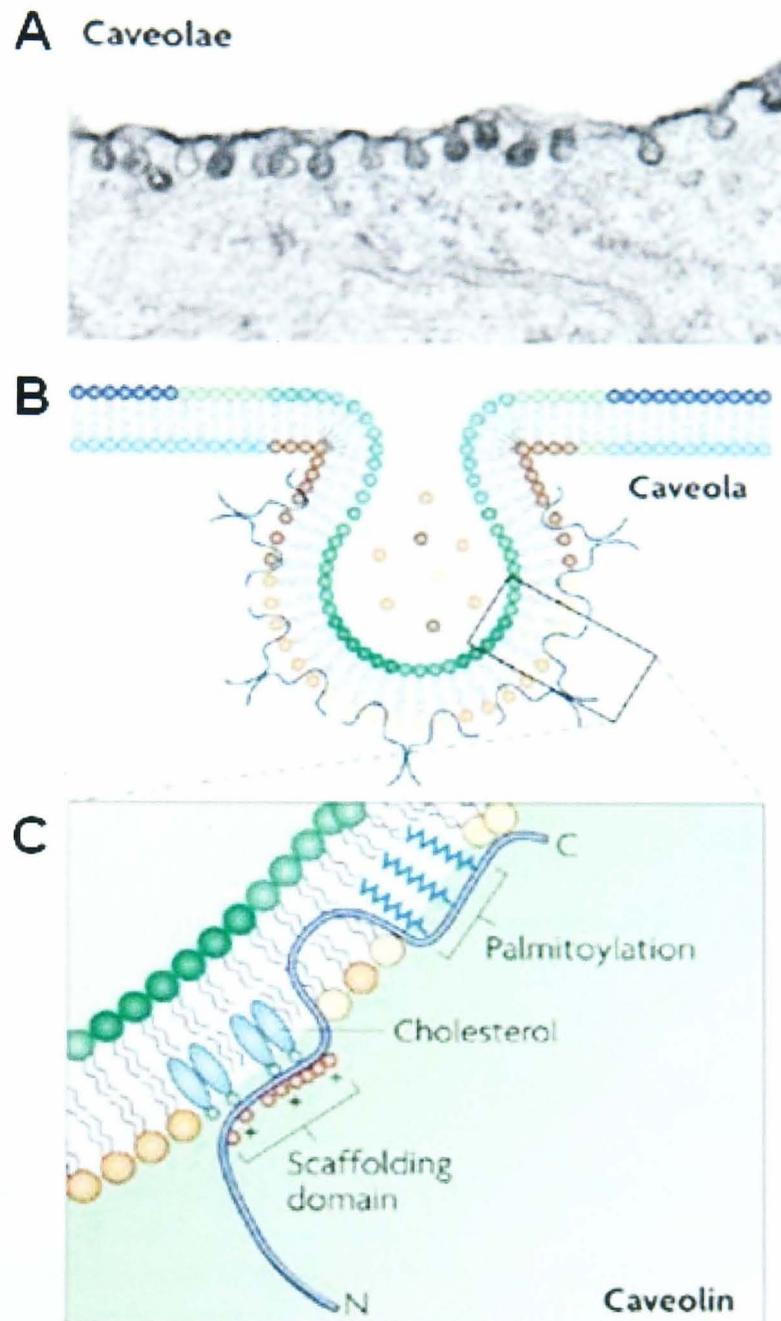
N   Caveolin

Figure 1.8. Caveolae and caveolin structure. (A) The electron micrograph shows caveolae on cell surface. (B) and (C) show the insertion of caveolin into caveolar membrane and its structural domains (Parton and Simons, 2007).

Caveolins are abundant in caveolae, and they consist of three subtypes, caveolin-1, caveolin-2, and caveolin-3. Caveolin-1 and caveolin-2 are expressed in non-skeletal cells, whereas caveolin-3 is found in skeletal muscle and cardiac muscle (Parton, 2003; Kumari *et al.*, 2010). Both caveolin-1 and caveolin-3 have been shown to be essential for the

formation of caveolae on the plasma membrane, while loss of caveolin-2 has no effect on caveolar formation (Parton and Simons, 2007). Furthermore, in the absence of caveolin-1, caveolin-2 forms low molecular weight oligomers and is retained in the Golgi (Parolini *et al.*, 1999).

Caveolin shows an atypical topology in the cell, with the protein N and C termini in the cytoplasm and a hydrophobic hairpin transmembrane domain inserted into lipid bilayers in a wedge-like manner (Figure 1.8B and C) (Parton and Simons, 2007). The protein is palmitoylated at the cysteine residue 133, 143, and 156 at the C terminus (Dietzen *et al.*, 1995). Cysteine palmitoylation is required for cholesterol binding and chaperone complex formation for cholesterol transport to caveolae, but it is not required for the protein's localization to caveolae (Dietzen *et al.*, 1995; Uittenbogaard and Smart, 2000). In addition to palmitoylation, caveolin is also phosphorylated at the tyrosine residue 14 by Src tyrosine kinases, which is essential for caveolar vesiculation (Li *et al.*, 1996).

Caveolae-mediated endocytosis is not very well-characterized. Caveolin-1 is relatively immobile on the plasma membrane *in vivo* (Thomsen *et al.*, 2002); however, caveolae is able to bud off and is responsible for the uptake of various agents and virus, such as albumin (Schnitzer *et al.*, 1994), cholera toxin B (Shogomori and Futerman, 2001), and SV40 (Pelkmans *et al.*, 2001). As in clathrin-mediated endocytosis, the caveolar pathway requires the recruitment of dynamin and actin polymerization to the endocytic site (Henley *et al.*, 1998; Oh *et al.*, 1998; Pelkmans *et al.*, 2001; Pelkmans and Helenius, 2002; Pelkmans *et al.*, 2002; Yao *et al.*, 2005). The released vesicle either fuses with tubular membrane organelles with neutral pH, termed caveosomes (Pelkmans *et al.*, 2001), or is directed to regular trafficking pathways as in clathrin-mediated endocytosis (Mayor and Pagano, 2007). Because of the route to caveosomes, caveolae-mediated endocytosis has been suggested as a safer cellular route of pathogen entry to avoid lysosomal degradation (Pelkmans *et al.*, 2001; Parton and Simons, 2007).

In caveolin-1 knockout mice, caveolae are absent on the plasma membrane, and albumin uptake is abrogated, but transferrin (a ligand for clathrin-mediated endocytosis) uptake is unaffected (Razani *et al.*, 2001). However, SV40 infection of primary embryonic fibroblasts isolated from caveolin-1 knockout mice is unaffected (Damm *et al.*, 2005). There is also some evidence that caveolin-1 might negatively regulate cargo uptake, as, for example, uptake of *Neisseria gonorrhoeae* and *Staphylococcus aureus* into cells overexpressing nonphosphorylatable caveolin-1, or in caveolin-1 knockout cells, is enhanced (Boettcher *et al.*, 2010; Hoffmann *et al.*, 2010). Boettcher *et al.* (2002) showed that inhibition of *Neisseria gonorrhoeae* uptake in caveolin-1 expressing cells is due to activation of Vav2- and RhoA-mediated cytoskeletal rearrangement as a result of caveolin-1 phosphorylation. It is still unclear which pathway is implicated in caveolin-1 knockout cells, as caveolin-1 seems to interact with other signalling molecules. Recently, caveolin-1 was shown to regulate endothelial permeability and endothelial nitric oxide synthase (eNOS) pathway as well as nitric oxide (NO) and peroxynitrite production in cells isolated from caveolin-1 knockout mice (Siddiqui *et al.*, 2011).

1.6.3 Clathrin- and caveolae-independent endocytosis

Several endocytic routes that are clathrin- and caveolae-independent have been described lately, and the understandings of these pathways are still very superficial. Most of these pathways are predominantly dynamin-independent, but it is unclear how vesicle scission occurs at the plasma membrane in the absence of dynamin. The following sections briefly discussed some of the clathrin- and caveolae-independent endocytosis.

1.6.3.1 Flotillin-mediated endocytosis

Flotillins are widely expressed in all tissues (Volonte *et al.*, 1999). The proteins form microdomains distinct from caveolae on the plasma membrane (Glebov *et al.*, 2006;

41

Frick *et al.*, 2007), and have been implicated in a variety of different cellular processes, such as cell adhesion, endocytosis, and cell signalling events (Hoehne *et al.*, 2005; Glebov *et al.*, 2006; Langhorst *et al.*, 2007; Ludwig *et al.*, 2010).

There are two flotillin proteins, flotillin 1 and flotillin 2 (also known as reggie 2 and reggie 1, respectively). Both proteins have an SPFH domain (stomatins, prohibitins, flotillins, HflK/C), also known as prohibitin homology domain (PHB), at the N terminal, which has been shown to interact with F-actin (Figure 1.9) (Langhorst *et al.*, 2007). The C terminal of flotillins contains flotillin repeats that are required for the formation of flotillin homo- and hetero-tetramers on the plasma membrane (Solis *et al.*, 2007). Myristoylation at glycine 2 and palmitoylation at cysteines 4, 19, and 20 are essential for membrane association of flotillin 2 (Neumann-Giesen *et al.*, 2004); whereas flotillin 1 is localized to membrane raft and plasma membrane via the hydrophobic regions at the N terminal (Liu *et al.*, 2005).
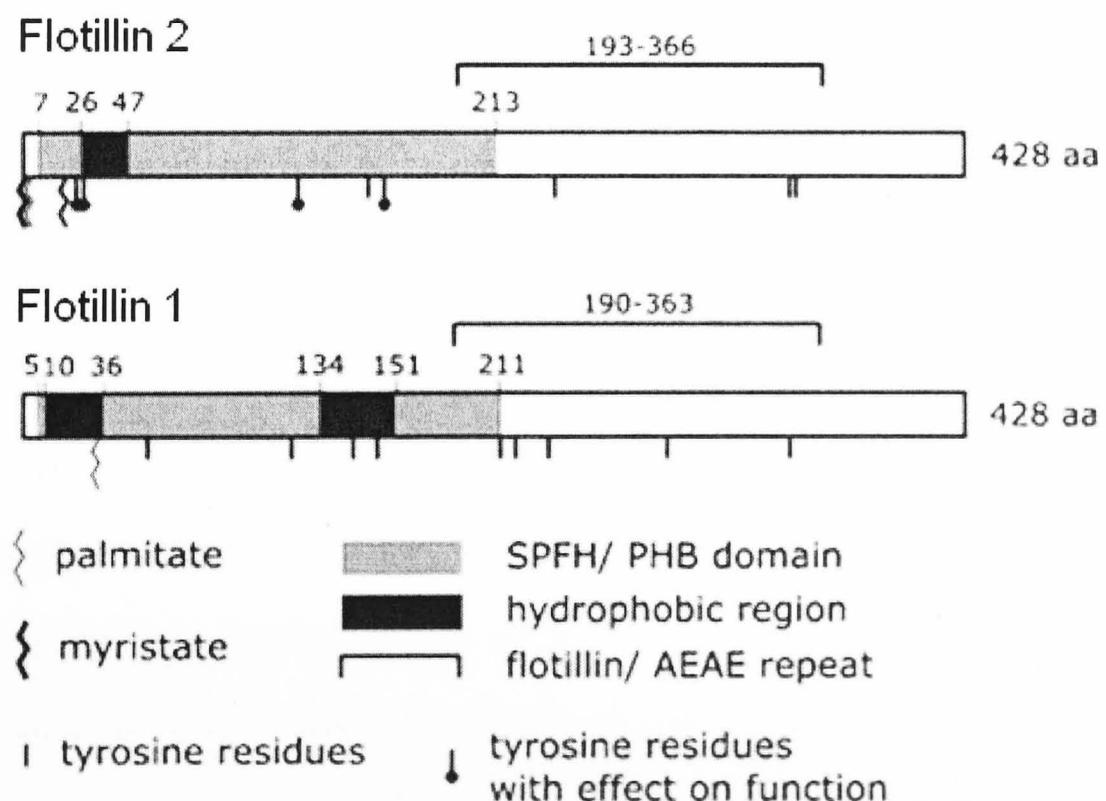
Figure 1.9. Structure of flotillin 1 and flotillin 2. The illustration shows the protein domains of flotillin 1 and 2. Both flotillins have SPFH/PHB domain at the N terminus, and flotillin repeats are found at the C-terminus. Palmitoylation, myristoylation, and tyrosine residues are indicated (Babuke and Tikkanen, 2007).

Flotillin budding from the plasma membrane is rare (Frick *et al.*, 2007). Hence, the role of the flotillin domain as endocytic carriers is still not clear, and the lack of flotillin-specific ligands further hampers the study of this pathway. Cholera toxin B and glycosyl phosphatidylinositol (GPI)-linked proteins are endocytosed into COS-7 and NIH3T3 cells via a flotillin 1 and 2-mediated, but dynamin-independent, pathway initiated by phosphorylation of Fyn kinase (Glebov *et al.*, 2006; Riento *et al.*, 2009); however, another study found that flotillin 2 was not involved in endocytosis of a GPI-anchored protein into HeLa cells (Langhorst *et al.*, 2008b). Flotillin 2 was also shown to promote clustering of amyloid precursor protein (APP) at the cell surface for internalization via a clathrin-mediated-like endocytosis, which is cholesterol and AP-2 dependent but epsin 1-independent (Schneider *et al.*, 2008). Despite being considered an endocytic coat, flotillin has also been found on late endosomal membranes, evidenced by co-localization of the proteins with LAMP1 and Lysotracker (Dermine *et al.*, 2001; Langhorst *et al.*, 2008b).

1.6.3.2 CLIC/GEEC pathway

Some studies have also found that GPI-linked proteins are endocytosed via clathrin-independent carriers (CLIC) into specialized endosomes termed GPI-linked proteins-enriched early endosomal compartments (GEECs), which have a tubulovesicular structure instead of the typical small spherical carriers of clathrin and caveolar pathways (Sabharanjak *et al.*, 2002; Kirkham *et al.*, 2005). The endocytosis process is regulated by the Rho family member Cdc42, as well as Arf1 (an ADP-ribosylation factor family protein) by recruiting a RhoGAP domain-containing protein, ARHGAP10, to the plasma membrane, and it is dynamin-independent (Kumari *et al.*, 2008; Kumari and Mayor, 2008). Recently, it was found that the CLIC/GEEC endocytosis pathway is the key endocytic route for cholera toxin B uptake into fibroblasts (Howes *et al.*, 2010), where previously the toxin had always been regarded as internalized via caveolae- and flotillin-mediated

pathway (Shogomori and Futerman, 2001; Glebov *et al.*, 2006). The post-internalization route of the cargo via CLIC/GEEC pathway is unclear, but study of *Helicobacter pylori* VacA toxin showed that trafficking of GEECs to early endosomes and late endosomes additionally requires polymerized actin (Gauthier *et al.*, 2007).

1.6.3.3 Arf6 mediated pathway

Arf6, a GTPase involved in actin remodelling, has been implicated as a mode of clathrin-, caveolae-, and dynamin-independent endocytosis for several cargo proteins, such as class I major histocompatibility complex (MHCI), and E-cadherin, into tubular endosomes (Mayor and Pagano, 2007; Donaldson *et al.*, 2009; Kumari *et al.*, 2010). Endosomes in this pathway are enriched with Arf6, PIP_2, and cholesterol, and are also coated with actin. At later stages, the endosomes are either directed to late endosomes or recycled back to plasma membrane (Donaldson *et al.*, 2009). Overall, it is not clear whether Arf6 is involved directly in cargo internalization or if it is required for vesicle trafficking to the downstream pathway, since overexpression of GTP-locked Arf6 blocked at a post-internalisation step (Brown *et al.*, 2001).

1.6.4 Macropinocytosis

Macropinocytosis is a non-specific cellular uptake pathway that involves formation of transient membrane protrusions on the plasma membrane for internalization of fluid into a large vacuole, termed macropinosome, $0.2 - 10$ μm in diameter (Mercer and Helenius, 2009; Kumari *et al.*, 2010). The formation of the membrane protrusions is driven by small GTPases (Rac1, Cdc42, Arf6), and kinases, such as p21-activated kinase 1 (PAK1), protein kinase C (PKC), c-Src, which lead to activation of the actin polymerization cascade (Ridley *et al.*, 1992; Dharmawardhane *et al.*, 2000; Garrett *et al.*, 2000; Lundmark *et al.*, 2008; Mercer and Helenius, 2008). Macropinosomes are formed as a result of the collapse

and fusion of the membrane protrusions onto the plasma membrane. The membrane fission machinery for a macropinosome formation is unknown, but some studies suggested the fission is achieved by either C-terminal binding protein 1 (CtBP-1) or dynamin for some instances (Liberali *et al.*, 2008; Mercer and Helenius, 2009).

Macropinocytosis uptake overlaps with several other endocytic pathways, and there is no specific cellular marker for the pathway. Rab34 was found to co-localize with actin at membrane ruffles, and it also facilitated macropinosome formation in platelet-derived growth factor- or phorbol ester-induced macropinocytosis in mouse 10T1/2 fibroblasts (Sun *et al.*, 2003), but not in HeLa cells (Goldenberg *et al.*, 2007). Currently, one of the main experimental criteria for macropinocytosis of a pathogen is the inhibition of the pathogen uptake by amiloride or ethylisopropyl amiloride (EIPA) treatment (Mercer and Helenius, 2009). Both chemical inhibitors are not specific to macropinocytosis, and other signalling pathways might be altered during the treatment.

1.7 Transcytosis

Transcytosis is a diverse mechanism that plays an important role in the continuous exchange of molecules across the cells (Predescu *et al.*, 2007). To date, the knowledge on transcytosis pathways is mainly from studies of immunoglobulins, and macromolecules transportation in polarized epithelial cells (Ghitescu and Bendayan, 1992; Apodaca, 2001; Tzaban *et al.*, 2009). However, it is unknown if similar membrane trafficking pathways exist in flat endothelial cells.

After ligands are internalized from apical or basolateral surfaces, the generic trafficking pathways that they follow are to either first enter into apical (AEE) or basolateral early endosomes (BEE), respectively (Figure 1.10). Cargoes sorted for recycling to the plasma membrane are transported to common recycling endosomes (CRE) and sorted into apical and basolateral recycling routes, facilitated by Rab11a, Rab25 and

their effector myosin Vb (myoVb) (Golachowska *et al.*, 2010). Some cargo may recycle directly from BEE to the basolateral plasma membrane surface (Sheff *et al.*, 1999). Similarly, apically internalized cargo may be transported to Rab11-positive ARE and recycle back to apical plasma membrane (Leung *et al.*, 2000). Study of the transportation of immunoglobulin G (IgG) by Fc receptor (FcRN) revealed that apical to basolateral transcytosis of the complex is regulated by Rab25 and myoVb, but not Rab11a (Tzaban *et al.*, 2009). While Rab11a, Rab11 family interacting proteins (Rab11-FIPs), Rab25, and myoVb are required for IgG-FcRN and polymeric IgA (pIgA) basolateral to apical transcytosis (Ducharme *et al.*, 2007; Tzaban *et al.*, 2009). On the other hand, a transcytosis route that results from LE fusion with either apical or basolateral plasma membrane surface has been proposed (Lakkaraju and Rodriguez-Boulan, 2008), based on the observation of the release of exosomes from apical and basolateral surface by different epithelial cells, but the molecular details are unknown (Hundorfean *et al.*, 2007; Mallegol *et al.*, 2007).

For endothelial cells, albumin and insulin transportation across the cultured endothelium monolayer on Transwell® insert has been proposed to be via caveolae (Schnitzer *et al.*, 1994). The *in vitro* observation has also been demonstrated *in vivo* by employing caveolin-1 knockout mice, where the uptake and transport of radioiodinated albumin from the blood to the interstitium is abolished in the knockout animals (Schubert *et al.*, 2001). Beyond caveolae-mediated transcytosis, the roles of microtubules, cytoskeleton, motor proteins, and GTPases during transcytosis in endothelium are poorly understood.
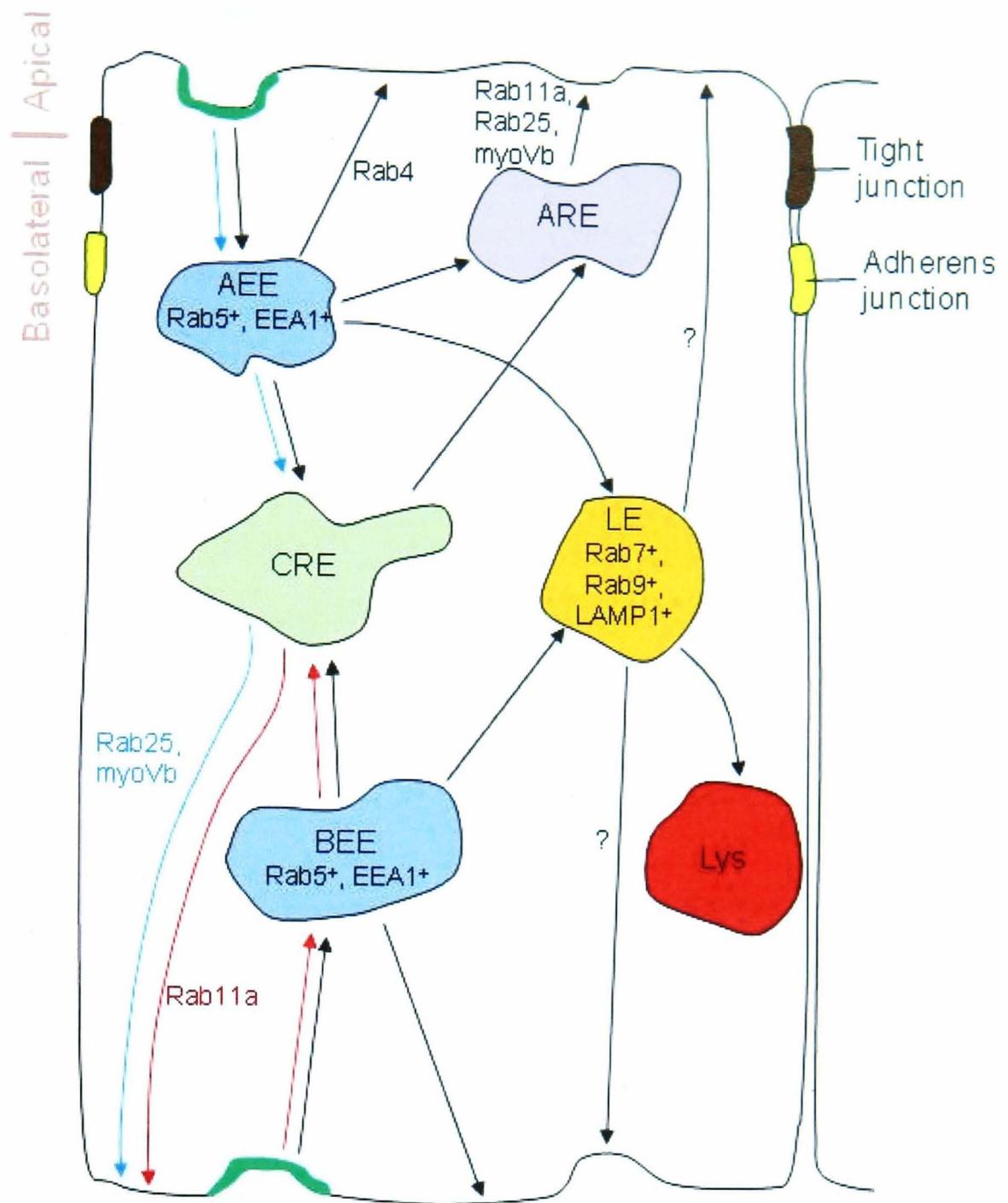
Figure 1.10. Endocytosis and transcytosis pathway in polarized epithelial cells. The illustration shows the transcytosis routes in polarized epithelial cells. The light blue arrows highlight apical to basolateral transcytosis route based on study of IgG-FcRN transportation in Mardin-Darby canine kidney epithelial cell line (MDCK) (Tzaban *et al.*, 2009).

1.8 Endocytosis of pathogens

The main difference between phagocytic and non-phagocytic cells is that the uptake of molecules by phagocytic cells is an active process, and the cells are able to take up relatively large cargo; whereas non-phagocytic cells would only endocytose small molecules in general, and the uptake process is passive. In the past, endocytosis was

thought to occur independently of actin, while phagocytosis is an actin-dependent cellular uptake pathway (Messick and Rikihisa, 1993). Therefore, bacteria were thought to enter non-phagocytic cells via phagocytosis-like pathway, which required actin remodelling (Veiga and Cossart, 2006). Generally, invasive bacterial entry of non-phagocytic cells is classically categorized into the "zipper" and the "trigger" mechanisms (Finlay and Cossart, 1997; Cossart and Sansonetti, 2004; Veiga and Cossart, 2006; Haglund and Welch, 2011). *Listeria monocytogenes* and *Yersinia pseudotuberculosis* are two well-studied bacteria that invade host cells by the zipper mechanism. Upon interaction of bacterial surface proteins and cellular receptors on the plasma membrane, such as *Listeria* InlA and InlB interact with E-cadherin and Met respectively (Cossart and Sansonetti, 2004), a cascade of signalling molecules is activated that results in actin polymerization and minor membrane extensions that engulf a bacterium into the epithelial cell line, Vero (Cossart and Sansonetti, 2004). For trigger mechanism, bacteria such as *Salmonella* and *Shigella*, inject bacterial effectors via secretory apparatus, such as the type 3 secretion system (T3SS), into eukaryotic cells, triggering massive actin polymerization and membrane ruffling that results in bacterial engulfment (Cossart and Sansonetti, 2004).

The classical dogma of bacterial invasion of non-phagocytic cells was challenged when *Listeria*, whose entry requires actin polymerization and which was at least 10-fold larger than a clathrin coat, was found to invade epithelial cells by hijacking clathrin-mediated endocytic machinery (Veiga and Cossart, 2005). Following this discovery, the involvement of an endocytic coat in bacterial invasion of non-phagocytic cells was established. It was shown that "zippering" bacteria, but not "triggering" bacteria, hijack cellular endocytic machinery for non-phagocytic cell entry. Intriguingly, EPEC, which remains extracellular during an infection, injects bacterial factors that recruit clathrin to form actin-rich pedestal at the bacterial attachment site (Veiga *et al.*, 2007). Table 1 shows

a list of endocytic pathways with pathogens or pathogen-derived toxins that have been identified to hijack respective endocytosis pathways for cell entry.

Table 1.1. Endocytosis pathways and pathogens or pathogen derived toxins.

Endocytic mechanism	Dynamin-dependence	Pathogen or toxin	Cell lines/ cells
Clathrin-mediated endocytosis	Yes	*Listeria monocytogenes* (Veiga and Cossart, 2005; Veiga *et al.*, 2007)	HeLa; JEG3, Caco-2.
		Staphylococcus aureus (Veiga *et al.*, 2007)	HeLa, BSC1.
		Chlamydia trachomatis (Hybiske and Stephens, 2007)	HeLa
		Ebola virus (Bhattacharyya *et al.*, 2010)	HEK293T, Vero, HeLa, HOS-CD4, human microvascular endothelial cells.
		Severe acute respiratory syndrome coronavirus (SARS-coV) (Inoue *et al.*, 2007)	Human hepatoma HepG2
		Vesicular stomatitis virus (Cureton *et al.*, 2009)	BSC1.
		Dengue virus (Mosso *et al.*, 2008)	C6/36 HT *Aedes albopictus* cell lines.
		Cholera toxin (Torgersen *et al.*, 2001)	BHK, Caco-2, HeLa.
Caveolae-mediated endocytosis	Yes	SV40 (Pelkmans *et al.*, 2001)	CV-1.
		FimH-expressing *E. coli* K-12 strain [ORN103(pSH2)] (Shin *et al.*, 2000)	Mouse bone marrow-derived mast cells.
		Mouse polyoma virus (Richterova *et al.*, 2001)	NIH 3T6 mouse fibroblasts, normal murine mammary gland (NMuMG) epithelial cells.

		Cholera toxin B (Shogomori and Futerman, 2001)	Hippocampal neuron.
Flotillin-mediated endocytosis	No	Cholera toxin B (Glebov *et al.*, 2006)	COS-7.
Macropinocytosis	Yes (in some instances)	Vaccinia virus (Mercer and Helenius, 2008)	HeLa.
		Human rhinovirus type 8 (HRV8) (Khan *et al.*, 2011)	Rhabdomyosarcoma cells.
		HIV-1 (Liu *et al.*, 2002)	Primary human BMEC.
		Kaposi's sarcoma-associated herpesvirus (KSHV) (Raghu *et al.*, 2009)	Human dermal microvascular endothelial cells, human umbilical vein endothelial cells.
		Afipia felis (Schneider *et al.*, 2007)	Murine macrophage-like cell lines J774E, RAW264.7.
CLIC/GEEC pathway	No?	*Helicobacter pylori* VacA toxin (Gauthier *et al.*, 2005; Gauthier *et al.*, 2007)	HeLa
		Cholera toxin B (Howes *et al.*, 2010)	Fibroblast
Arf6-dependent endocytosis	No	unknown	

1.8.1 *E. coli* K1 virulence factors and invasion of HBMEC

Although a newborn rat model has long been established for *E. coli* K1 infection (Glode *et al.*, 1977; Moxon *et al.*, 1977), compared to animal models for other bacterial infections, this has not led to much understanding of the bacterial pathogenesis. Since the availability of purified human brain microvascular endothelial cells (HBMEC) as an *in vitro* BBB model, bacterial invasion mechanisms and bacterial virulence factors (VF) contributing to the disease pathophysiology have been studied extensively (Stins *et al.*, 1994; Huang *et al.*, 1995).

The K1 capsule of *E. coli* K1 has long been identified as the primary bacterial virulence factor responsible for bacterial intravascular survival and replication (Wilfert, 1978; Kim *et al.*, 1992; Metkar *et al.*, 2007). The capsule is a homopolymer of N-acetylneuraminic acid with poly(α-2,8) linkages, structurally similar to the polysialic acid (PolySia) moiety on mammalian neural cell adhesion molecule (NCAM) found in the neonatal brain as well as kidney (Finne, 1982; Finne *et al.*, 1983a; Roth *et al.*, 1987), which is important for cell migration and neuronal plasticity (Rutishauser, 2008). The capsule is also immunochemically similar to the *Meningococcus* group B polysaccharides (Finne *et al.*, 1983b). It has also been shown to exist as O-acetylated and non-O-acetylated forms in clinical isolates, but the significance of the capsule acetylation in bacterial virulence is not clear (Frasa *et al.*, 1993; Colino and Outschoorn, 1999). Capsule variation results from slipped-strand DNA mispairing of a microsatellite domain located at the 5` of *neuO* gene, an acetylase gene (Deszo *et al.*, 2005; Vimr and Steenbergen, 2006). Zelmer *et al.* (2008) showed that the meningitis-causing K1 strain expresses the non-O-acetylated form of PolySia in the gastrointestinal tract and in the blood compartment, but stops expressing PolySia capsule in the meninges, which might suggest that the bacteria regulate their capsule expression in response to unknown molecules secreted from the host immune cells. It is also believed that structural and immunochemical similarity between *E. coli* K1

capsule and mammalian PolySia glycan made the K1 capsule a poor immunogen for the host, to avoid host autoimmune responses to PolySia glycan (Harvey *et al.*, 2001).

Intriguingly, the K1 capsule also demonstrates anti-phagocytic property (Bortolussi *et al.*, 1979) as *E. coli* K1 with depolymerised capsule (mediated by endosialidase E) show enhanced uptake into peritoneal macrophages isolated from 5 – 10 days old rats (Mushtaq *et al.*, 2005). It has also been shown that the K1 capsule prevents binding of C3 cleavage products and deposition of C9, which is required for the formation of complement membrane attack complex (MAC), on the bacteria (Cross *et al.*, 1986; Mushtaq *et al.*, 2004). Therefore, the PolySia capsule protects the bacterium from the bactericidal action of serum and the host complement system (Cross *et al.*, 1986), which enable the bacteria to survive and replicate intravascularly to high levels of bacteraemia. In addition to the important role for evading host immunity, the PolySia capsule is also important for the bacterial intracellular survival by preventing the bacteria-containing vacuoles from fusing with lysosomes (Hoffman *et al.*, 1999; Kim *et al.*, 2003).

The ability of *E. coli* K1 to replicate to high level of bacteraemia is insufficient to develop meningitis, but the bacteria must have the ability to bind to the target tissue under high blood flow and pressure in the BBB, followed by cell invasion. It is known that pathogenic *E. coli* can form filamentous surface appendages known as pili or fimbriae, which function primarily for cell adhesion at the initial stage of infection (Capitani *et al.*, 2006). *E. coli* is able to express many types of fimbriae, which can be divided according to the structures of specific mammalian cell receptor that they recognise, such as α-D-mannosides (type 1 fimbriae), α-D-Gal-(1,4)-β-D-Gal (P fimbriae), or NeuAcα2,3-galactose (S fimbriae) (Saukkonen *et al.*, 1988; Wang *et al.*, 2004). Fimbrial phase variation has been observed both *in vitro* and *in vivo* (Nowicki *et al.*, 1985; Saukkonen *et al.*, 1988). *E. coli* K1 expressing type S-fimbriae bind to choroid plexus epithelium, the luminal surface of vascular endothelium, and HBMEC *in vitro* (Parkkinen *et al.*, 1988;

Prasadarao *et al.*, 1993; Stins *et al.*, 1994). It was also found that the S-fimbriae-expressing bacteria predominate in all body fluid and CSF after infection, and it is more virulent than *E. coli* K1 expressing type 1-fimbriated form *in vivo* (Saukkonen *et al.*, 1988). Further study with a *pilA-* (*fimA*), the gene that codes for the main fimbriae structure, deleted *E. coli* K1 mutant showed no difference in level of bacteraemia and intestinal colonization, but the bacterial oropharyngeal colonization was impaired (Bloch and Orndorff, 1990). In contrast, by using a different *E. coli* K1 clinical isolate, RS218, and its S fimbriae-deleted mutant, another study found that S fimbriae are not major determinants for bacterial binding to HBMEC and for causing meningitis *in vivo* (Wang *et al.*, 2004). Studies with the RS218 strain further found that the bacteria bind to CD48 on HBMEC via FimH of the bacterial type 1 fimbriae (Teng *et al.*, 2005; Khan *et al.*, 2007), which is a tip component of the fimbriae (Capitani *et al.*, 2006). Interaction of the bacterial FimH with CD48 increases cytosolic free calcium levels and activates RhoA (Khan *et al.*, 2007). In addition to having a major role in bacterial adhesion, purified *E. coli* K1 FimH has also been shown to activate a murine microglial cell line, which results in production of nitric oxide and tumour necrosis factor-α (TNFα) (Lee *et al.*, 2005).

Outer membrane protein A (OmpA) is a 35 kDa bacterial surface transmembrane protein with four extracellular loops. It is highly conserved in many Gram negative bacteria, and is important for efficient binding of *E. coli* K1 to HBMEC (Prasadarao *et al.*, 1996b). The N-terminal loops of the protein interact with N-acetylglucosamine (GlcNAc) epitopes on the gp96 receptor on HBMEC (Prasadarao *et al.*, 1996a; Prasadarao, 2002). gp96 receptor is an endoplasmic reticulum chaperone, which is also expressed on the cell surface of human colonic carcinoma (Caco-2) cell line (Li *et al.*, 2002), and has also been shown to interact with *Listeria* Vip (Cabanes *et al.*, 2005). OmpA-gp96 interaction induces the signal transducer and activator of transcription 3 (stat3) signalling pathway, phosphorylation of the focal adhesion kinase (FAK), activation of phosphatidylinositol-3-

kinase (PI3K), and leads to the phosphorylation of protein kinase Cα (PKCα) (Reddy *et al.*, 2000a; Reddy *et al.*, 2000b; Prasadarao, 2002; Maruvada *et al.*, 2008). The activation of these signalling events results in actin polymerization at the bacterial adhesion site that is necessary for bacterial internalization into HBMEC (Prasadarao *et al.*, 1999).

Several other bacterial determinants have been identified to be crucially important for *E. coli* K1 invasion of HBMEC, namely IbeA, IbeB, YijP, and cytotoxic necrotizing factor 1 (CNF1) (Huang *et al.*, 1995; Huang *et al.*, 1999; Wang *et al.*, 1999; Khan *et al.*, 2002). A specific HBMEC receptor for CNF1 has been identified as a 37 kDa laminin receptor precursor (37LRP) by screening the cDNA library of HBMEC in a yeast two-hybrid system (Chung *et al.*, 2003), whereas vimentin was identified as the specific HBMEC receptor that interacts with IbeA (Chi *et al.*, 2010). It was found that both CNF1 and OmpA use different signalling pathway for recruiting actin to bacterial adhesion site, where the interaction of the bacterial CNF1 with HBMEC leads to RhoA activation, without activating PI3K (Khan *et al.*, 2002; Khan *et al.*, 2003).

The data from previous studies might suggest that *E. coli* K1 invasion of HBMEC involved the activation of several signaling pathways by different bacterial VF, with the primary goal in inducing actin cytoskeleton rearrangement for bacterial entry via zippering mechanism (Prasadarao *et al.*, 1999). However, the specific endocytic pathway hijacked by the bacterial invasion of HBMEC is not well-studied. Clathrin was shown to be absent from the bacterial attachment site (Prasadarao *et al.*, 1999), but the bacteria were reported to invade HBMEC via caveolae-mediated endocytosis (Sukumaran *et al.*, 2002).

Studies performed with the BBB *in vitro* model showed that, following bacterial invasion, *E. coli* K1 do not replicate intracellularly (Prasadarao *et al.*, 1999). The bacteria are localised in compartments positive for early endosomal markers (Rab5, EEA1, and transferrin receptor) at early time point of infection, and are labelled for late endosomal markers (Rab7 and LAMP1) without the presence of cathepsin D, a lysosomal hydrolytic

enzyme (Kim *et al.*, 2003). The intracellular *E. coli* K1 were also reported to co-localize with caveolin-1 (Sukumaran *et al.*, 2002).

The transcytosis route of *E. coli* K1 across BBB is unclear. The bacteria were demonstrated to traverse HBMEC monolayer grown on Transwell insert without affecting monolayer integrity, which suggested the bacteria crossed the monolayer via transcellular route (Stins *et al.*, 2001; Zhang *et al.*, 2002). In contrast, another study reported that OmpA-expressing *E. coli* K1 transcytosed HBMEC via a paracellular route by activating PKCα, which subsequently disrupted HBMEC tight junctions by dissociating β-catenins from vascular endothelial cadherins (Sukumaran and Prasadarao, 2003). Similar to *E. coli* K1, the transcytosis of *Neiserria meningitidis* across brain endothelial cells is unclear and has been debated for a long time (Nassif *et al.*, 2002; Coureuil *et al.*, 2009). Recently, *N. Meningitidis* were shown to recruit junctional proteins, such as VE-cadherin, β-catenin, claudin-5, ZO-1, to the attachment site of the bacterial colonies via β-arrestin-dependent pathway, subsequently depleted junctional proteins, and resulted with the opening of intercellular junctions, which allowed the bacterial to traverse endothelial cells via paracellular route (Coureuil *et al.*, 2009; Coureuil *et al.*, 2010).

Although *E. coli* K1 is known to cause meningitis, the gastrointestinal tract has been shown as the primary site of colonization in neonatal animal model (Saukkonen *et al.*, 1988; Bloch and Orndorff, 1990). Therefore, it is likely that the bacteria have to breach gastrointestinal epithelium into the bloodstream. The application of Caco-2, and human colonic adenocarcinoma (T84) cell lines as *in vitro* gastrointestinal epithelium model showed that *E. coli* K1 infection of these cell lines is dependent on the cell differentiation and the bacterium disrupted the tight junctions during infection for crossing the epithelium via paracellular route (Burns *et al.*, 2001). The difference in the bacterial traversal of HBMEC and gastrointestinal epithelium model might implicate that different transcytosis routes were manipulated by the bacteria for crossing the cell barriers.

1.9 Project aims

E. coli K1 is able to invade HBMEC *in vitro*, and the bacterial entry is receptor-mediated via zippering mechanism. The signalling pathways that lead to actin polymerization to enable the bacterial internalization into HBMEC have been very well-investigated in previous studies, as detailed above. However, the endocytosis pathway that is responsible for the bacterial uptake is not clear. Some studies have shown that bacterial uptake is clathrin-independent (Prasadarao *et al.*, 1999), but caveolae-dependent (Sukumaran *et al.*, 2002). Further, the bacteria have been shown to traverse HBMEC via a transcellular route (Stins *et al.*, 2001), but the transcytosis pathway used by the bacterium has not been described.

The major aim of this study was to further investigate the endocytosis pathway that is responsible for *E. coli* K1 invasion of HBMEC, and to describe the transcytosis pathway that the bacterium manipulates for traversal of HBMEC transcellularly. The hypothesis was that the bacterium invaded HBMEC via caveolae-mediated endocytosis and further traversed to the basolateral surface of HBMEC in a caveolin-1-associated compartment.

The first objective was to make a fluorescent protein-expressing *E. coli* K1 strain that could retain bacterial virulence. The fluorescent *E. coli* K1 strain would allow investigation of bacterium-HBMEC interactions under a confocal microscope. The second objective was to optimize HBMEC transfection efficiency with various transfection methods. High HBMEC transfection efficiency would allow investigation of comparative distributions of cellular markers with intracellular bacteria, and also the effect of a cellular marker and its corresponding mutant on *E. coli* K1 invasion/traversal of HBMEC. The third objective was then to utilise the fluorescent *E. coli* K1 strain and the optimized HBMEC transfection protocol to further investigate *E. coli* K1 invasion via caveolae-mediated endocytosis. The final objective of this project was to study the transcytosis

pathway that the bacterium manipulated for crossing HBMEC monolayer. This would give

a much clearer picture of the infective behaviour of this pathogenic bacterium.

2. Materials and methods

2.1 Materials

Unless otherwise stated, all reagents and biochemicals were purchased from Sigma-Aldrich, Poole, Dorset, UK.

2.1.1 Bacterial culture and reagents

2.1.1.1 Bacterial strains

Strains	Genotype or characteristic(s)
E44 (*E. coli* K1) [A kind gift from Dr. Naveed Khan (University of Nottingham, Sutton Bonington, UK)].	O18:K1:H7. A spontaneous rifampin resistant mutant of RS218 strain, isolated from the CSF of meningitis patient (Silver *et al.*, 1980; Achtman *et al.*, 1983).
HB101 (*E. coli* K-12) (New England Biolabs Inc.,Herts, UK)	F⁻, *thi*-1, *hsd*S20 (r_B–, m_B–), *sup*E44, *rec*A13, *ara*-14, *leu*B6, *pro*A2, *lac*Y1, *gal*K2, *rps*L20 (str^r), *xyl*-5, *mtl*-1
DH5α (Invitrogen, Paisley, UK)	F- Φ80*lacZ*ΔM15 Δ(*lacZYA-argF*)U169 *deo*R *rec*A1 *end*A1 *hsd*R17(r_k^-, m_k^+) *pho*A *sup*E44 *thi*-1 *gyr*A96 *rel*A1 λ⁻
K1-Cherry	E44 transformed with pFPV-mCherry.
K1-GFP	E44 transformed with pFPV25.1.
K1rpsM⁻	E44 transformed with rpsM⁻

2.1.1.2 Bacterial culture media

Media	Contents
Luria-Bertani (LB) broth	1% (w/v) tryptone (Merck, Nottingham, UK), 0.5% (w/v) yeast extract (DIFCO, Surrey, UK), 0.5% (w/v) NaCl

	(VWR BDH Prolabo, West Sussex, UK)
Luria-Bertani (LB) agar	1% (w/v) tryptone, 0.5% (w/v) yeast extract, 0.5% (w/v) NaCl, 1.5% (w/v) bacteriological agar (Oxoid, available via Thermo Fisher Scientific, Loughborough, UK)
MacConkey agar (Code: CM0007) (Oxoid)	Bought as pre-made mix: 2% (w/v) peptone, 1% (w/v) lactose, 0.5% (w/v) bile salts, 0.5% (w/v) NaCl, 0.0075% (w/v) neutral red, 1.2% (w/v) agar

2.1.2 Mammalian cell propagation reagents

2.1.2.1 Mammalian cell

Cell	Descriptions	Source
Human brain microvascular endothelial cells (HBMEC)	Isolated from cerebral cortex specimens obtained from patients (4 – 7-year-old) with seizure disorders or from post-mortem brains. Immortalized with SV40 large T antigen.	Stins *et al.*, 2001. A kind gift from Dr. Naveed Khan.
Primary mouse lung endothelial cells (MLEC)	Isolated from mouse lung.	Purified by Dr. Grant Otto and was a kind gift from Dr. Ben Nichols (MRC LMB, Cambridge).
Primary flotillin 1 knockout MLEC	Isolated from flotillin 1 knockout mouse lung.	Purified by Dr. Grant Otto and was a kind gift from Dr. Ben Nichols.
Primary caveolin 1 knockout MLEC	Isolated from caveolin 1 knockout mouse lung.	Purified by Dr. Grant Otto and was a kind gift from Dr. Ben Nichols.

2.1.2.2 Mammalian cell culture media

Culture media	Contents
HBMEC growth media	RPMI-1640 supplemented with 20% (v/v) fetal bovine serum (FBS) (Biosera, Ringmer, UK), 2 mM L-glutamine, 1 mM sodium pyruvate, 100 µg/ml streptomycin, 100 units/ml penicillin, non-essential amino acids (Gibco, Invitrogen), and vitamins (Gibco, Invitrogen).
MLEC growth media	50 ml low glucose Dulbecco's Modified Eagles Medium (DMEM) and 50 ml Ham's F12 supplemented with 20% (v/v) FBS, 0.00125% (w/v) heparin, 2 mM L-glutamine, 100 µg/ml streptomycin, and 100 units/ml penicillin, 0.1 mg/ml endothelial cell growth supplement (AbD Serotec, Oxford, UK).
Experimental media	RPMI-1640 supplemented with 5% (v/v) FBS, and 2 mM L-glutamine.
Imaging media	RPMI-1640 without phenol red supplemented with 5% (v/v) FBS, 2 mM L-glutamine, 25 mM HEPES (pH 7.4).
Freezing media	Growth media supplemented with 10% (v/v) DMSO, and 20% (v/v) FCS.

2.1.3 Bacterial expression vectors used in this study

Plasmids	Characteristic(s)	Reference or source
pCherry1	Bacterial expression vector containing *Mycobacterium tuberculosis* codon-optimised mCherry gene, hygromycin resistant.	Carroll *et al.* (2010); A kind gift from Dr. Paul Carroll (Queen Mary, University of London, UK).
pCherry3	Bacterial expression vector containing *Mycobacterium tuberculosis* codon-optimised mCherry gene, hygromycin resistant.	Carroll *et al.* (2010); A kind gift from Dr. Paul Carroll.
pEnvy1	Bacterial expression vector containing *Mycobacterium tuberculosis* codon-optimised GFP gene, hygromycin resistant.	A kind gift from Dr. Paul Carroll.
pEnvy2	Bacterial expression vector containing *Mycobacterium tuberculosis* codon-optimised GFP gene, hygromycin resistant.	A kind gift from Dr. Paul Carroll.
pFPV25.1	Bacterial expression vector containing *gfpmut3a* gene downstream of a *Salmonella typhimurium* promoter, *rpsM*, ampicillin resistant.	Valdivia and Falkow (1996); A kind gift from Dr. Olivier Marchés (Queen Mary, University of London, UK).
pRSET-mCherry	Bacterial expression vector containing mCherry, ampicillin resistant.	Shaner *et al.* (2004); A kind gift from Dr. Roger Tsien (University of California, San Diego).
pFPV-mCherry	Bacterial expression vector containing mCherry gene downstream	Constructed in this study.

of a *Salmonella typhimurium* promoter, *rpsM*, ampicillin resistant.

pEGFP	Bacterial expression vector encodes a red-shifted variant of wild type GFP, ampicillin resistant.	Clontech, BD Biosciences, Oxford, UK; A kind gift from Dr. John Raynes (London School of Hygiene and Tropical Medicine).
rpsM⁻	pFPV25.1 with *rpsM* deleted, ampicillin resistant.	Constructed in this study.

2.1.4 Mammalian expression vectors used in this study

Plasmids	Characteristic(s)	Reference or source
pN1-EGFP	Mammalian expression vector encodes a red-shifted variant of wild type GFP, kanamycin resistant.	Clontech, BD Biosciences.
Cav1-GFP	pN1-EGFP vector containing wild type canine caveolin-1 gene, kanamycin resistant.	Pelkmans *et al.* (2001); A kind gift from Dr. Ben Nichols.
Cav1-YFP	Mammalian expression vector carrying EYFP tagged wild type canine caveolin-1 gene, cloned by replacing EGFP gene in Cav1-GFP, kanamycin resistant.	Constructed in this study.

63

GFP-Rab7WT	pC1-EGFP vector containing wild type canine Rab7 gene, kanamycin resistant.	(Bucci *et al.*, 2000); A kind gift from Professor Albert Haas (University of Bonn, Germany) and Dr. Bianca Schneider (Research Center Borstel, Germany).
GFP-Rab7T22N	pC1-EGFP vector containing canine Rab7 T22N mutant gene, kanamycin resistant.	Bucci *et al.* (2000); A kind gift from Professor Albert Haas and Dr. Bianca Schneider.
GFP-Rab7Q67L	pC1-EGFP vector containing canine Rab7 Q67L mutant gene, kanamycin resistant.	Bucci *et al.* (2000); A kind gift from Professor Albert Haas and Dr. Bianca Schneider.
CFP-Rab7WT	Mammalian expression vector carrying ECFP tagged wild type canine Rab7 gene, cloned by replacing EGFP gene in GFP-Rab7, kanamycin resistant.	Constructed in this study.
Dyn2(aa)WT GFP	pN1-EGFP vector containing wild type rat dynamin 2 gene, kanamycin resistant.	Cao *et al.* (1998); A kind gift from Dr. Mark McNiven (Mayo Clinic, Rochester, MN).
Dyn2(aa)K44A GFP	pN1-EGFP vector containing rat dynamin 2 K44A mutant gene, kanamycin resistant.	Cao *et al.* (1998); A kind gift from Dr. Mark McNiven.
Dyn1WT GFP	Unknown EGFP mammalian expression vector containing dynamin 1 gene, ampicillin resistant.	A kind gift from Dr. Emmanuel Boucrot and Dr. Harvey McMahon (MRC LMB, Cambridge, UK).

Dyn1K44A GFP	Unknown EGFP mammalian expression vector containing dynamin 1 K44A mutant gene, ampicillin resistant.	A kind gift from Dr. Emmanuel Boucrot and Dr. Harvey McMahon.
Cav1-palm⁻-GFP	pN1-EGFP vector containing human caveolin-1 palmitoylation mutant gene, kanamycin resistant.	Parat *et al.* (2003); A kind gift from Dr. Marie-Odile Parat (University of Queensland, Australia).
Cav1-Tyr14-GFP	pN1-EGFP vector containing human caveolin-1 T14A mutant gene, kanamycin resistant.	Parat *et al.* (2003); A kind gift from Dr. Marie-Odile Parat.
Cav1β-GFP	pN1-EGFP vector containing human caveolin-1β gene, kanamycin resistant.	Parat *et al.* (2003); A kind gift from Dr. Marie-Odile Parat.
Flotillin 1-GFP	pN1-EGFP vector containing wild type murine flotillin 1 gene, kanamycin resistant.	Glebov *et al.* (2006); A kind gift from Dr. Ben Nichols.
Flotillin 2-GFP	pN1-EGFP vector containing wild type rat flotillin 2 gene, kanamycin resistant.	(Neumann-Giesen *et al.*, 2004); A kind gift from Dr. Ben Nichols.
GFP-Rab5WT	pC1-EGFP vector containing wild type murine Rab5 gene, kanamycin resistant.	Nichols *et al.* (2001); A kind gift from Dr. Ben Nichols.
GFP-Rab5S34N	pC1-EGFP vector containing murine Rab5 S34N mutant gene, kanamycin resistant.	Nichols *et al.* (2001); A kind gift from Dr. Ben Nichols.

GFP-Rab5Q79L	pC1-EGFP vector containing murine Rab5 Q79L mutant gene, kanamycin resistant.	Nichols *et al.* (2001); A kind gift from Dr. Ben Nichols.
GFP-Rab11aWT	pC1-EGFP vector containing wild type human Rab11a gene, kanamycin resistant.	(Knodler *et al.*, 2010); A kind gift from Dr. Wei Guo (University of Pennsylvania, Philadelphia, PA).
GFP-Rab11aS25N	pC1-EGFP vector containing human Rab11a S25N mutant gene, kanamycin resistant.	Knodler *et al.* (2010); A kind gift from Dr. Wei Guo.
GFP-Rab11aQ70L	pC1-EGFP vector containing human Rab11a Q70L mutant gene, kanamycin resistant.	Knodler *et al.* (2010); A kind gift from Dr. Wei Guo.
LDLR-A18-GFP	pN1-EGFP vector containing recycling-deficient mutant of the low-density-lipoprotein receptor gene, kanamycin resistant.	(Kreitzer *et al.*, 2003); A kind gift from Dr. Geri Kreitzer (University of Cornell).
GFP-Rab9WT	pC1-EGFP vector containing wild type murine Rab9 gene, kanamycin resistant.	(Seaman, 2004); A kind gift from Dr. Matthew Seaman (CIMR, Cambridge).
GFP-Rab9Q66L	pC1-EGFP vector containing murine Rab9 Q66L mutant gene, kanamycin resistant.	A kind gift from Dr. Matthew Seaman.
GFP-Rab9S21N	pC1-EGFP vector containing murine Rab9S21N mutant gene,	A kind gift from Dr. Matthew Seaman.

66

kanamycin resistant.

LAMP1-GFP   pN1-EGFP vector containing wild type rat lgp120 gene, kanamycin   (Patterson and Lippincott-Schwartz, 2002); A kind

resistant.   gift from Dr. George Patterson.

2.1.5 Primary antibodies

Name	Species	Monoclonal or polyclonal	Fixation	Concentrations used	Source
Anti-caveolin-1	Rabbit	Polyclonal	Methanol, or formaldehyde	1:200 (IF)	BD Biosciences. A kind gift from Dr. Ben Nichols.
Anti-caveolin-1	Mouse	Monoclonal	Methanol	1:200 (IF)	BD Biosciences. A kind gift from Dr. Ben Nichols.
Anti-flotillin 1	Mouse	Monoclonal	Methanol	1:200 (IF)	BD Biosciences. A kind gift from Dr. Ben Nichols.
Anti-flotillin 2	Mouse	Monoclonal	Methanol	1:200 (IF)	BD Biosciences.
Anti-β-Actin (Clone Ac-15)	Mouse	Monoclonal	-	1:20000 (WB)	Sigma-Aldrich.

Anti- *E. coli* O18	Rabbit	Polyclonal	Methanol, or formaldehyde	1:500 (IF)	Denka-Seiken, Coventry, UK.
Anti-GFP	Rabbit	Polyclonal		1:1000 (WB)	Invitrogen.
Anti-GFP (Clone 3E6)	Mouse	Monoclonal	Formaldehyde	1:500 (IF)	Invitrogen.
Anti-EEA1 (Clone 14/EEA1)	Mouse	Monoclonal	Formaldehyde	1:200 (IF)	BD Biosciences.
Anti-pan cadherin (Clone CH-19)	Mouse	Monoclonal	Methanol, or formaldehyde	1:200 (IF)	Abcam, Cambridge, UK.
Anti-LAMP2 (Clone ABL-93)	Rat	Monoclonal	Methanol, or formaldehyde	1:500 (IF)	Abcam. A kind gift from Dr. Sharon Tooze and Dr. Minoo Razi (Cancer Research UK, Lincoln's Inn Field, London)

2.1.6 Secondary antibodies

Name	Species	Monoclonal or polyclonal	Concentrations used	Source
FluoProbes®-546 anti-rabbit	Donkey	Polyclonal	1:200	Interchim, Cheshire Science Ltd., Chester, UK
FluoProbes®-488 anti-mouse	Donkey	Polyclonal	1:200	Interchim.
FluoProbes®-642 anti-mouse	Donkey	Polyclonal	1:200	Interchim.
FluoProbes®-642 anti-rabbit	Donkey	Polyclonal	1:200	Interchim.
Cy2 anti-rabbit	Goat	Polyclonal	1:200	A kind gift from Professor Ulrich Schaible (Research Center Borstel, Germany).
Cy2 anti-rat	Goat	Polyclonal	1:200	A kind gift from Professor Ulrich Schaible.
ECL anti-rabbit IgG, HRP-linked whole antibody	Donkey	Polyclonal	1:3000	GE Healthcare, Buckinghamshire, UK.
ECL anti-mouse IgG, HRP-linked whole antibody	Sheep	Polyclonal	1:3000	GE Healthcare, Buckinghamshire, UK.

2.1.7 Cell imaging reagents

Reagents	Source
4′,6-diamidino-2-phenylindole, dihydrochloride (DAPI)	Molecular Probes, Invitrogen.
Endosialidase–GFP fusion protein (PK1A-GFP)	Jokilammi *et al.* (2004); A kind gift from Professor Jukka Finne (University of Turku, Finland).
Fluorescein isothiocyanate (FITC)	Sigma-Aldrich.
Phalloidin-TRITC	Sigma-Aldrich.

2.1.8 Reagents used in the transfection of mammalian cells

Reagents	Source
jetPRIME™	Polyplus-transfection SA, Illkirch, France.
jetPEI™	Polyplus-transfection SA.
jetPEI™-HUVEC	Polyplus-transfection SA.
FuGENE® HD	Promega, Southampton, UK.
Lipofectamine™ 2000	Invitrogen.
PLUS™ Reagent	Invitrogen.

2.1.9 Primers for constructing pFPV-mCherry

Oligonucleotides were synthesized by Eurofins MWG Synthesis, Germany. The primers were dissolved to 100 pmol/µl in sterile MilliQ water and stored at -20°C.

1. mCherry-FXba   TGC<u>TCTAGA</u>TTTAAGAAGGAGATATACATATGGTGAGC

              AAGGGCGAGGAG

2. mCherry-RSph   CAT<u>GCATGC</u>TTACTTGTACAGCTCGTCCAT

2.1.10 Buffers and solutions

TBE Buffer, 50x	Dissolve 108 g Tris base (Trizma), 55 g boric acid and 40 ml 0.5 M EDTA [pH8.0]. Make up to 1000 ml with water.
Agarose Loading Dye, 5x	0.25% (w/v) bromophenol blue, 0.25% (w/v) xylene cyanol FF in 40% (w/v) sucrose solution.
Ampicillin (100 mg/ml) (1000x)	Dissolve 1 g ampicillin in 5 ml sterile MilliQ water, and add 5 ml absolute ethanol to the solution. Store at -20°C, protected from light.
Kanamycin (30 mg/ml) (1000x)	Dissolve 0.3 g kanamycin in 10 ml sterile MilliQ water. Store at -20°C.
Chloramphenicol (34 mg/ml) (1000x)	Dissolve 0.34 g chloramphenicol in 10 ml absolute ethanol. Store at -20°C, protected from light.
10% (w/v) sodium dodecyl sulphate (SDS)	Dissolve 10 g SDS in 100 ml MilliQ water.
CCMB buffer [10 mM KAc, 10% (v/v) glycerol, 80 mM $CaCl_2 \cdot 2H_2O$, 10 mM $MgCl_2 \cdot 6H_2O$, 20 mM $MnCl_2 \cdot 4H_2O$, pH6.4]	Dissolve 0.1 g KAc, 10 ml glycerol, 1.18 g $CaCl_2 \cdot 2H_2O$, 0.2g $MgCl_2 \cdot 6H_2O$, 0.4g $MnCl_2 \cdot 4H_2O$ in 50 ml MilliQ water. Adjust pH to 6.4. Top up with MilliQ water to 100 ml, and filter the solution with 0.22 μm syringe filter. Store at 4°C.
10x Tris-Glycine buffer	Dissolve 15 g Tris, and 72 g Glycine in 500 ml MilliQ water. Store at 4°C.
4x resolving buffer [1.5 M Tris, 0.4% (w/v) SDS, pH8.8]	Dissolve 18.17 g Tris and 4 ml 10% (w/v) SDS in 100 ml MilliQ water. Adjust pH to 8.8. Store at 4°C.

4x stacking buffer [0.5 M Tris, 0.4% (w/v) SDS, pH6.8]	Dissolve 6.06 g Tris and 4 ml 10% (w/v) SDS in 100 ml MilliQ water. Adjust pH to 6.8. Store at 4°C.
1x SDS-PAGE running buffer	50 ml 10x Tris-Glycine buffer and 5 ml 10% (w/v) SDS. Top up to 500 ml with MilliQ water.
Blotting buffer	100 ml 10x Tris-Glycine buffer and 200 ml methanol. Top up to 1000 ml with MilliQ water.
10% (w/v) ammonium persulphate (APS)	Dissolve 0.05 g APS in 0.5 ml MilliQ water. Made fresh each time.
6x SDS sample buffer	Dissolve 1 g SDS, 1.2 mg bromophenol blue, 3 ml glycerol in 7 ml 4x resolving buffer. Store at room temperature. Prior to usage, add 6 µl 2-Mercaptoethanol to 94 µl the solution.
1x Dulbecco's phosphate buffered saline (PBSA)	Dissolve 0.2 g KCl, 0.2 g KH$_2$PO$_4$, 8 g NaCl, and 1.74 g Na$_2$HPO$_4$·7H$_2$O in 900 ml MilliQ water. Adjust pH to 7.2. Top up to 1000 ml with MilliQ water. Sterilize by autoclaving.
10x Phosphate buffered saline (PBS)	Dissolve 80 g NaCl, 2 g KCl, 11.5 g Na$_2$HPO$_4$·7H$_2$O, and 2 g KH$_2$PO$_4$ in 900 ml MilliQ water. Adjust pH to 7.2. Top up with MilliQ water to 1000 ml. Sterilize by autoclaving.
0.2 mg/ml hydrocortisone	5 mg/ml hydrocortisone: Dissolve 50 mg hydrocortisone in 10 ml absolute ethanol. Store solution at -20°C protected from light. 0.2 mg/ml hydrocortisone: Add 0.4 ml 5 mg/ml hydrocortisone to 9.6 ml sterile complete growth medium. Aliquot into 1 ml aliquots. Store at -20°C protected from light.

2.2 Methods

2.2.1 PCR amplification of mCherry gene from pRSET-B mCherry

50 µl PCR reactions were carried out using 1x Pfu reaction buffer (Roche, West Sussex, UK), 0.3 µM primers (see section 2.10), 0.2 mM dNTPs (an equimolar mixture of dATP, dCTP, dGTP, and dTTP to an overall concentration of 0.2 mM), 1 U Pfu DNA polymerase (Roche), and 10 ng pRSET-B mCherry plasmid DNA.

200 µl thin-walled reaction tubes were used in a thermal cycler (MJ-Research, Hertfordshire, UK). The reactions were heated to 95°C for 5 mins before 25 cycles of: 94°C for 45 secs (denaturation), 55°C for 1 min (primer-template annealing), and 72°C for 1 min (polymerisation); followed by 72°C for 10 mins and 4°C indefinitely. The resulting products were analysed on a 0.7% (w/v) agarose gel.

2.2.2 DNA analysis by agarose gel electrophoresis

Agarose gel electrophoresis was used to check restriction digested plasmid DNA products, to visualize PCR products, and to isolate specific DNA fragments for vector and insert preparation.

Typically, 0.7% (w/v) agarose gels were casted by dissolving 0.7 g agarose in 100 ml 1x TBE buffer. When it had cooled to a temperature of around 55°C, 1 µl 10 mg/ml ethidium bromide (Invitrogen) was added. The molten agarose was poured into the gel frame and allowed to set before adding enough 1x TBE buffer to cover the gel.

Prior to loading, 2 µl loading dye was added to the DNA sample and carefully pipetted into the wells. The gel was run at a 5V/cm until the bromophenol blue front had migrated at a sufficient distance. Gels were then visualized using a UV trans-illuminator (Syngene Bio imaging, Synoptics Ltd., UK) and then photographed if required.

2.2.3 DNA fragment purification

For PCR reactions that resulted in a single PCR product on an agarose gel. QIAquick PCR Purification kit (Qiagen, West Sussex, UK) was used according to the manufacturer's instructions to purify the PCR product from excess primers, nucleotides, polymerases, and salts, before the PCR product was used for setting up a restriction endonuclease digestion. PCR product was eluted in 30 μl buffer EB (10 mM Tris-Cl, pH8.5).

In this study, DNA from post-enzymatic manipulations for vector and insert preparation was purified from agarose gel by using QIAEX II gel extraction kit (Qiagen) according to manufacturer's instructions. The DNA was eluted by adding 20 μl Tris buffer to the air-dried pellet and incubated at 50°C for 5 mins.

2.2.4 Restriction endonuclease digestion of DNA

Usually, 5 μg DNA was digested in a volume of 50 μl. To this, 5 μl 10x reaction buffer was added, plus enzyme to a concentration of 2 U/μg DNA (typically 1 - 2 μl) and 100 μg/ml BSA. The mixture was mixed and incubated at 37°C for 2 h, or longer if complete digestion was required. At the end of the reaction, the enzyme was inactivated by heating at 65°C for 20 mins or higher temperatures as appropriate.

2.2.5 Ligation of DNA fragments

The reaction that allows for the insertion of the desired gene into a vector is catalyzed by T4 DNA ligase and involves the ATP-dependent formation of a phosphodiester bond between the 3'hydroxyl end of a double-stranded DNA fragment and the 5'phosphate end of the same or another DNA fragment. The reaction conditions for ligation of DNA fragments are shown in Table 2.1.

Table 2.1. Components and conditions used for a ligation reaction.

10x T4 DNA ligase buffer	1.0 µl
Insert DNA	Depending on the ratio of insert DNA to
Vector DNA	vector DNA used. Generally 3:1 molar equivalent insert to vector.
T4 DNA ligase (Fermentas, UK)	1.0 µl
Final Reaction volume	10.0 µl
Ligation condition	Incubated at 4°C for overnight.

The ligation reaction was performed in an autoclaved 0.5 ml centrifuge tube and centrifuged briefly to bring all the contents to the bottom of the tube.

2.2.6 Extraction and purification of plasmid DNA

Plasmids are generally prepared from bacterial cultures grown between 16 - 18 h in the presence of selective agent such as an antibiotic. For routine molecular biology works, small scale plasmid DNA purification was performed with Wizard® Plus SV Minipreps DNA Purification System (Promega); whereas for mammalian cell transfection, medium scale plasmid DNA purification was performed by PureYield™ Plasmid Midiprep System (Promega) according to the manufacturer's instructions.

Both plasmid DNA purification kits uses alkaline conditions to lyse the bacterial cells, which denatures chromosomal and plasmid DNA, as well as proteins. Denatured chromosomal DNA and proteins are precipitated after the addition of acidic buffer for neutralization, while circular plasmid DNA are covalently closed. Plasmid DNA in the solution are bound to an anion-exchange column under appropriate low salt and pH conditions. RNA, proteins and other contaminants are removed by a medium-salt wash. The plasmid DNA was eluted in 10 mM Tris-Cl, pH8.5 buffer and stored at -20 °C.

2.2.7 Determination of DNA concentration and purity definitely in DNA techniques

Determination of DNA concentration was carried out using a spectrophotometer model ND-1000 (NanoDrop®) to measure absorption of DNA solutions at OD_{260} and OD_{280}. A figure of between 1.8-1.9 indicates pure DNA.

2.2.8 Bacterial culture conditions

E. coli were grown at 37°C in Luria-Bertani (LB) broth overnight in a shaker incubator. For transformed bacteria, media was supplemented with ampicillin (100 µg/ml), kanamycin (30 µg/ml) or hygromycin B (50 µg/ml) as appropriate.

2.2.9 Making electroporation competent *E. coli* K1 and transformation of plasmid DNA encoding fluorescent protein into *E. coli* K1 by electroporation

To enable fluorescence visualisation of the bacteria under a confocal microscope, a plasmid DNA encoding fluorescent protein was transformed into the bacteria. The transformation of plasmid DNA into *E. coli* K1 was performed using electroporation according to Seidman *et al.*, 2001, since plasmid DNA transformation using heat shock of chemically-competent cells was very inefficient for this strain.

Briefly, a starter culture of *E. coli* K1 was grown overnight at 37°C in LB broth with shaking. The overnight bacterial culture was inoculated into 500 ml LB broth at 50 times dilution and was grown at 37°C for approximately 1.5 h with shaking, or until the OD_{595nm} reached between 0.5 – 0.7. Bacteria were harvested (4200 rpm in Beckman JS-13.1, at 4°C for 20 mins), washed twice in pre-chilled sterile distilled water and once in 10% (v/v) glycerol, suspended in 0.5 ml 10% (v/v) glycerol, and stored at -80°C in 50 µl aliquots. Plasmid DNA (approximately 1.0 µg in maximum 5 µl volume) was added to competent bacteria, pulsed at 2.5 kV (Biorad Gene Pulser Xcell electroporation system) with an electrode gap of 0.2 cm. 250 µl LB broth was added immediately to the bacteria,

and incubated at 37°C for 1.5 h with shaking. The culture was plated onto an LB agar plate supplemented with the appropriate antibiotic to select for transformed bacteria and was incubated at 37°C overnight. Colonies were picked the following day and grown up.

To screen for transformed bacteria that fluoresced, 5 μl of the overnight bacterial culture was spotted onto a glass slide and a cover slip was laid onto the culture carefully to avoid air bubble formation. The transformed bacteria were checked for fluorescence using a Zeiss Axioplan 2 fluorescence microscope with CCD or a Zeiss LSM510 confocal microscope.

2.2.10 Making chemical competent *E. coli* cells and transformation of plasmid DNA into *E. coli* by heat shock

To maintain plasmid in bacterial stocks, all plasmid DNA were initially propagated in *E. coli* DH5α strain. This strain, and *E. coli* K-12 (HB101) that was used as a non-pathogenic *E. coli* control in all bacterial assays, are compatible with heat-shock transformation and were prepared by chemical competency (Seidman *et al.*, 2001).

To make competent bacteria, a starter culture of *E. coli* K-12 or DH5α was grown overnight at 37°C in LB broth with shaking. The overnight bacterial culture was inoculated into 500 ml LB broth at 50 times dilution and was grown at 37°C for 3 h with shaking to the OD$_{595nm}$ reached between 0.5 – 0.7. Bacteria were harvested (4200 rpm in Beckman JS-13.1 at 4°C for 15 mins), washed once in pre-chilled CCMB buffer, and incubated on ice for 1 h. The bacterial suspension was harvested as previously described, the bacterial pellet was re-suspended in 5 ml CCMB buffer, and stored at -80°C in 50 μl aliquots. Plasmid DNA (approximately 1.0 μg in maximum 10% bacterial volume) was added to competent bacteria, mixed and incubated on ice for 30 mins. Each transformation reaction was heat-pulsed at 42°C for 30 s and immediately incubated on ice for 2 mins. 250 μl LB broth was added to the bacteria, and incubated at 37°C for 1.5 h with shaking. The culture was plated

onto an LB agar plate supplemented with the appropriate antibiotic to select for transformed bacteria and was incubated at 37°C overnight. Colonies were picked the following day and grown up in LB supplemented with the appropriate antibiotic.

When making fluorescent *E. coli* K-12, the transformed bacteria were checked for fluorescence with a Zeiss Axioplan 2 fluorescence microscope with CCD or a Zeiss LSM510 confocal microscope, as described in section 2.2.9.

2.2.11 Making bacterial frozen stocks

400 μl log phase bacterial culture was added to 600 μl sterile 75% (v/v) glycerol in a sterile microcentrifuge tube. The bacteria-glycerol mixture was vortexed and stored immediately in -80°C. To recover the bacteria, the bacterial stock was retrieved from -80°C on dry ice, and the frozen surface of the culture was scraped with a sterile inoculation loop. The bacteria on the loop were streaked immediately onto LB agar plate containing appropriate antibiotics, if required. The LB agar plate was incubated at 37°C for 16 – 18 h.

2.2.12 Bacterial growth kinetics

A starter culture of the bacteria was grown overnight at 37°C in LB broth with shaking. The overnight culture was inoculated into fresh LB broth at 50 times dilution. The optical density (OD_{595}) of the culture was read using a spectrophotometer (WPA lightware®, Cambridge, UK). The culture was then incubated at 37°C in a shaker incubator with shaking at 200 rpm for 120 mins. At various time points (30, 60, and 120 mins), 1 ml of the culture was sampled and the OD_{595} was read with the spectrophotometer.

2.2.13 HBMEC and primary mouse lung endothelium (MLEC) culture maintenance

2.2.13.1 HBMEC and MLEC propagation

HBMEC, and MLEC cultures were maintained in a 75cm^2 vented tissue culture flasks in growth media at 37°C, 5% CO_2 in a CO_2 incubator. Cells were split at approximately a 1:10 ratio every 5 days using the following protocol. Medium was removed and flasks were rinsed with 2 ml 0.25% trypsin, 0.53 mM EDTA solution. An additional 3 ml trypsin-EDTA was added and the cells were incubated at 37°C for 10 mins. 7 ml growth media was added and re-suspended. 9 ml of the trypsin/cell mixture was removed and growth medium was added to the cells. For *in vitro* infection experiments, 1 x 10^5 cells/ml HBMEC or MLEC are plated in 24-well tissue culture dishes 3 days prior to experiment; for time-lapse live-cell imaging, 5 x 10^4 cells/ml HBMEC are plated in LabTek 8-well glass cover slip chambers (Nalge Nunc, VWR) 3 days prior to experiment.

2.2.13.2 Cryopreservation of HBMEC and MLEC

HBMEC and MLEC were trypsinised as above and centrifuged at 1000 rpm for 10 mins. The supernatant was removed. The cell pellet was then re-suspended in cryopreservation media to cell density of 1 x 10^6 cells/ml and dispensed as 1 ml aliquots into cryotubes. The aliquots were frozen at -80°C in an isopropanol freezing container for 2 – 3 days and then transferred to liquid nitrogen. For recovery from liquid nitrogen the cells were warmed in a water bath for 1 – 2 mins, and then the cells were carefully added dropwise to 10 ml pre-warmed growth media in a 50 ml tube. The cells were centrifuged at 1000 rpm for 5 mins. The media was aspirated and 1 ml fresh pre-warmed growth media was added to the cell pellet and re-suspended gently. The cell suspension was added to 9 ml pre-warmed growth media in a 75 cm^2 vented flask. The cells were allowed to adhere in an incubator at 37°C with 5% CO_2.

2.2.14 HBMEC transfection

For plasmid DNA transfection into HBMEC cells, 1×10^5 cells/ml HBMEC were seeded onto 70% ethanol cleaned microscope glass cover slips (No. 1 13mm diameter) (VWR, Lutterworth, UK) in a 24-well tissue plate 2 days prior to experiment, in order to achieve approximately 80% confluency for transfection. Various cationic polymer and lipid-based transfection reagents as well as Nucleofection kits were tested.

2.2.14.1 Transfection with jetPRIME^{TM} transfection reagent

On the day of transfection, cells were replenished with 0.5 ml fresh HBMEC growth medium. 1.0 μg plasmid DNA was diluted in 50 μl jetPRIME^{TM} buffer, mixed the tube gently by tapping. 2 μl jetPRIME^{TM} transfection reagent was added to the diluted DNA, and mixed by tapping immediately. The DNA-lipid complex mixture was incubated at room temperature for 10 mins. The DNA-lipid complex was added dropwise onto the cells, and repeatedly pipetted up and down with a P200 micropipette. The cells were incubated with the DNA-lipid complex in a tissue culture incubator at 37°C, 5% CO_2. 5 - 6 hours post-incubation, the medium containing DNA-lipid complex was removed, and cells were washed once with pre-warmed unsupplemented RPMI-1640. Cells were replenished with fresh HBMEC growth medium, were further incubated in a tissue culture incubator for 20 – 24 hours.

2.2.14.2 Transfection with Lipofectamine^{TM} 2000 transfection reagent

On the day of transfection, cells were replenished with 0.5 ml fresh HBMEC growth medium. 0.5 μg of plasmid DNA was diluted in 100 μl Opti-MEM® reduced serum medium (Invitrogen), mixed the tube by tapping. 1 μl PLUS^{TM} reagent was added directly to the diluted DNA, and was mixed by tapping. The reaction was incubated for 5 mins at room temperature. 3 μl Lipofectamine^{TM} 2000 transfection reagent was added to

the diluted DNA, and mixed by tapping immediately. The DNA-lipid complex mixture was incubated at room temperature for 30 mins. The DNA-lipid complex was added dropwise onto the cells, and repeatedly pipetted up and down with a P200 micropipette. The cells were incubated with the DNA-lipid complex in a tissue culture incubator at 37°C, 5% CO_2. 5 - 6 hours post-incubation, the medium containing DNA-lipid complex was removed, and cells were washed once with pre-warmed unsupplemented RPMI-1640. Cells were replenished with fresh HBMEC growth medium, were further incubated in a tissue culture incubator for 20 – 24 hours.

2.2.14.3 Transfection with jetPEI™ transfection reagent

On the day of transfection, cells were replenished with 1.0 ml fresh HBMEC growth medium. 1.0 µg plasmid DNA was diluted in 50 µl 150 mM NaCl buffer, mixed the tube gently by tapping. 2 or 4 µl jetPEI™ transfection reagent was diluted in 50 µl 150 mM NaCl buffer in a separate microcentrifuge tube, mixed by tapping. The diluted jetPEI™ solution was added to the diluted DNA, and mixed by tapping immediately. The DNA-lipid complex mixture was incubated at room temperature for 30 mins. 100 µl DNA-lipid complex was added dropwise onto the cells, and repeatedly pipetted up and down with a P200 micropipette. The cells were incubated with the DNA-lipid complex in a tissue culture incubator at 37°C, 5% CO_2 for 20 – 24 hours.

2.2.14.4 Transfection with jetPEI™-HUVEC transfection reagent

On the day of transfection, cells were replenished with 1.0 ml fresh experimental medium. 2.0 µg plasmid DNA was diluted in 50 µl 150 mM NaCl buffer, and the tube mixed gently by tapping. 4 µl jetPEI™-HUVEC transfection reagent was diluted in 50 µl 150 mM NaCl buffer in a separate microcentrifuge tube, and mixed by tapping. The diluted jetPEI™-HUVEC solution was added to the diluted DNA, and mixed by tapping

81

immediately. The DNA-lipid complex mixture was incubated at room temperature for 30 mins. 100 µl the DNA-lipid complex was added dropwise onto the cells, and repeatedly pipetted up and down with a P200 micropipette. The cells were incubated with the DNA-lipid complex in a tissue culture incubator at 37°C, 5% CO_2 for 4 hours, then the medium containing DNA-lipid complex was removed, and cells were washed once with pre-warmed unsupplemented RPMI-1640. Cells were replenished with fresh HBMEC growth medium, were further incubated in a tissue culture incubator for 20 – 24 hours.

2.2.14.5 Transfection with FuGENE® HD transfection reagent

On the day of transfection, cells were replenished with 0.5 ml fresh HBMEC growth medium. Before transfection, FuGENE® HD was warmed to room temperature, and mixed briefly by inverting. 0.5 µg plasmid DNA was diluted in 25 µl Opti-MEM® reduced serum medium (Invitrogen), the tube mixed gently by tapping. 1.5 µl FuGENE® HD transfection reagent was added to the diluted DNA, and mixed immediately by repeatedly pipette up and down ≈15 times. The DNA-lipid complex mixture was incubated at room temperature for 15 mins. The DNA-lipid complex was added dropwise onto the cells, and repeatedly pipetted up and down with a P200 micropipette. The cells were incubated with the DNA-lipid complex in a tissue culture incubator at 37°C, 5% CO_2 for 20 – 24 hours.

2.2.14.6 HBMEC Nucleofection with HUVEC Nucleofector Kit-OLD and Amaxa HUVEC Nucleofector Kit

Prior to experiment, Nucleofector solution was thawed to room temperature. HBMEC growth medium was pre-incubated at 37°C, 5% CO_2. 5 x 10^5 cells/ml HBMEC were prepared and re-suspended in 100 µl Nucleofector solution. 2 µg plasmid DNA was added to the side of the electroporation cuvette and the HBMEC suspension was added

carefully into the cuvette. Cells were electroporated according to the manufacturer's instructions. 500 µl HBMEC growth medium was added immediately to the electroporated cells and transferred to a tissue culture plate. The cells were incubated in a tissue culture incubator at 37°C, 5% CO_2 for 24 or 48 hours.

2.2.15 HBMEC and MLEC infection

On the day of experiment, 95% confluency or confluent HBMEC or MLEC in 24-well tissue culture plates were washed three times with pre-warmed plain RPMI-1640 media, and replenished with pre-warmed experimental medium. HBMEC were incubated with *E. coli* at MOI of 100. After the addition of bacteria, the plate was centrifuged at 500 x g, 15°C for 5 mins. The plate was incubated at 37°C, 5% CO_2 for 120 mins. The monolayers were washed three times with plain RPMI-1640 medium and further incubated in experimental medium containing 100 µg/ml gentamicin for 60 mins, or 5 and 18 hours for 7 and 20 hours time point respectively, to kill off extracellular bacteria. The monolayers were washed three times with plain RPMI-1640 medium or PBS and lysed with 0.3% (w/v) SDS in PBSA. The serial diluted lysates were plated on LB agar plates, and the plates were incubated overnight at 37°C. The number of bacterial colonies were counted and calculated as cfu/ml = (number of counted colonies / volume of culture plated) x dilution factor.

2.2.16 HBMEC transcytosis assay

5 x 10^4 cells/ml HBMEC were seeded onto the apical chamber of a 4.67cm^2 collagen-coated polytetrafluoroethylene (PTFE) Transwell membrane, pore size 0.4 µm (Corning). Transendothelial electrical resistance (TEER) of the HBMEC monolayer on Transwell was measured with a Millicell® ERS volt-ohm meter (Millipore, Watford, UK) according to the manufacturer's instructions. Briefly, the probe was sterilized by

immersing in 70% ethanol for 30 mins and air-dried. The probe was rinsed with plain RPMI-1640. For measuring TEER, the shorter probe was inserted into the Transwell insert carefully without touching the cells at 90°; while the longer probe was inserted into the medium in the lower chamber. The meter was set to Ohms mode and the resistance was recorded. The resistance of the monolayer was calculated by subtracting the resistance reading obtained from sample well to the resistance reading obtained from blank well. To correct for the area covered by the cell monolayer, the calculated resistance value was multiplied by the effective membrane area of the Transwell insert.

When the cells on the Transwell membrane reached complete confluency, the medium was replaced with HBMEC growth media containing 1.0 µg/ml hydrocortisone to induce intercellular tight junctions formation. The medium was changed on alternate days. 5 days after hydrocortisone treatment, the cells were used for transcytosis assay. The Transwell membranes were washed in plain RPMI-1640 medium and replenished with fresh experimental medium. 0.2 ml bacterial suspension, which contained approximately 1 x 10^8 cfu/ml bacteria, was applied to the apical chamber. At each time point (0, 2, 8, and 12 h incubation), 600 µl medium in the lower chamber was sampled for quantitation of cfu and replaced with 600 µl fresh experimental medium. The recovered organisms were differentiated by lactose fermentation on MacConkey agar.

2.2.17 Cell imaging

2.2.17.1 Fluorescein isothiocyanate (FITC) labelling of *E. coli*

Bacteria were grown up as above, then pelleted in a microfuge at 13000 rpm for 2 mins and re-suspended in PBS. FITC was added to a final concentration of 0.5 mg/ml in 50 mM Na_2CO_3-100 mM NaCl buffer, pH8.0. The bacteria were incubated in the dark at room temperature for 10 mins. Free FITC was removed by washing in PBS and centrifugation at 8000 rpm, and the bacteria were used immediately.

2.2.17.2 Cell fixation

HBMEC cells were grown on glass coverslips in a 24-well tissue culture plate until 95% or complete confluent. The cells were incubated with bacteria and were processed for immunofluorescence microscopy. The cells were washed three times with plain RPMI-1640 to remove unbound bacteria prior to fixation. For formaldehyde fixation, cells were fixed with 3% formaldehyde/PBS for 15 mins at room temperature. To quench the autofluorescence signal from formaldehyde, the fixed cells were incubated in 50 mM NH_4Cl for 20 mins at room temperature.

An alternative fixation method to formaldehyde is methanol fixation. Cells on coverslips were incubated with absolute methanol for 10 mins at -20°C. Fixed cells were rehydrated sequentially in the following solutions for 1 min: absolute ethanol, 95% ethanol, 70% ethanol, 50% ethanol, and MilliQ water. After fixation, the cells were washed three times for 5 mins in wash solution (5% FCS/PBS), and immunolabelled as described in section 2.2.19.3.

2.2.17.3 Immunofluorescence staining

For intracellular staining, primary antibody (section 2.1.6) was diluted in wash solution containing 0.2% saponin. 15µl antibody mix was aliquoted onto a piece of Parafilm within a petri dish. The coverslips were inverted onto the antibody drop and incubated for 1 hour at room temperature. The humidity within the petri dish was maintained using a small damp tissue. After 1 hour incubation, the coverslips were washed three times with wash solution. The binding of primary antibodies was visualised with secondary antibodies conjugated to fluorophores (section 2.1.7), by incubating at room temperature in the dark for 1 hour. After washing three times with wash solution, the cells nuclei were stained with 1µg/ml DAPI. The cells were washed once with wash solution

and once with PBS, cells were mounted on the glass slide with Confocal Matrix (Micro-Tech-Lab, Austria).

2.2.17.4 Differential antibody staining

To distinguish intracellular from extracellular bacteria, differential antibody staining was performed. For formaldehyde fixed cells, extracellular bacteria were labelled without permeabilization using anti-*E. coli* O18 and FluoProbes®-642 conjugated donkey anti-rabbit. In methanol fixation, the plasma membrane is permeabilized during fixation. Therefore, for methanol fixation, the above staining procedure was performed on ice prior to fixation.

After staining with secondary antibody, cells were permeabilized with 0.1% TritonX-100/PBS for 10 mins, then intracellular bacterial staining using the same primary antibodies, followed by FluoProbes®-546 conjugated donkey anti-rabbit. This staining procedure yields extracellular bacteria with both 642 and 546 signals, while intracellular bacteria only positive for 546 signal only.

2.2.17.5 K1 capsule staining

5 μl sterile PBS was spotted onto a glass cover slip, and bacterial colonies were picked, smeared onto the glass cover slip. The bacterial smear was air-dried, fixed with 2% (v/v) formaldehyde and stained with 10 μg/ml PK1A-GFP probe in PBS without detergent. To differentiate the GFP signal from the probe and intracellular GFP signal from the K1-GFP, the PK1A-GFP-stained K1-GFP was counterstained with mouse anti-GFP clone 3E6 antibody, and followed by Fluoprobes-642 conjugated donkey anti-mouse antibody in PBS without detergent. The anti-GFP antibody only stained the GFP of PK1A-GFP probe, which bound the bacterial surface. The cover slip was mounted onto a glass slide with Confocal Matrix.

2.2.17.6 Confocal microscopy

Fluorescent images were acquired with an inverted confocal microscope (LSM510; Carl Zeiss MicroImaging, Inc.). Argon laser (excitation 488 nm) and a filter set to detect FITC emission (BP505 – 550) for imaging EGFP, FITC, Cy2, and FluoProbes-488; Argon laser (excitation 458 nm) and a filter set to detect CFP emission (BP470 – 500) for imaging ECFP; HeNe1 laser (excitation 543 nm) and a filter set to detect Rhodamine emission (LP585) for imaging mCherry and FluoProbes-546; HeNe1 laser (excitation 514 nm) and a filter set to detect YFP emission (LP530) for imaging EYFP; HeNe2 laser (excitation 633 nm) and a filter set to detect Cy5 emission (LP630) for imaging FluoProbes-642; Laser Diode (excitation 405 nm) and a filter set to detect DAPI emission (BP390 – 420) for imaging DAPI. Cells were observed using a 63x/NA 1.40 plan-Apochromat oil immersion objective with the confocal pinhole set to one Airy unit. Imaging parameters, such as gain and offset levels, and line averaging, are optimised to avoid oversaturation of pixels and to improve signal:noise ratio. Images were acquired using LSM510 software package (Carl Zeiss MicroImaging, Inc.). Image analyses were performed with ImageJ and Adobe Photoshop Elements 8.0.

2.2.17.7 Live cell imaging

For short-duration imaging experiments, HBMEC cells were grown on glass coverslips in a 24-well tissue culture plate, and were infected with *E. coli* K1 expressing fluorescent protein at 37°C with 5% CO_2. Unless otherwise stated, at the end of infection, cells were incubated in experimental medium containing 100 µg/ml gentamicin at 37°C for 1 hour. Coverslips were washed three times with prewarmed unsupplemented RPMI-1640 medium. Coverslips were lifted from the well and mounted onto a low-tech rubber gasket imaging chamber with approximately 35 µl imaging medium (Ward. 2007).

In order to track the intracellular bacterial activity over time, time lapse imaging was set up. For time lapse imaging experiments, HBMEC cells were grown in a LabTek 8-well glass cover slip chamber (Nalge Nunc) and transfected with fluorescent protein-tagged mammalian expression vector. Infection was performed as described above (section 2.2.17), infected cells were replenished with imaging medium containing 100 μg/ml gentamicin, and imaged immediately.

Prior to imaging, the confocal microscope imaging chamber was preheated to 37°C to avoid focus problems resulting from expanding metal components of the stage. If CO_2 chamber was used, CO_2 control was switched on to zero the CO_2 in the system from previous usage, and CO_2 was then supplied to the system approximately 15 mins before imaging. For acquisition of tile-z stack images, tile dimensions [n(x), n(y)] was set in addition to the z-stack parameters. To avoid focus drift during imaging, autofocus function was set up during timelapse imaging.

2.2.17.8 Tile z-stack imaging

For quantification of the effect of cells overexpressing mutant proteins on *E. coli* K1 invasion, tile z-stack imaging was performed. The rationale to acquire tile images was to avoid potential experimental bias by acquiring neighbouring fields over large areas of the cover slip automatically under software control. Imaging parameters were set up as described in section 2.2.19.5, and saved. Z-stack parameters as well as tile dimensions [n(x), n(y)] was set.

2.2.18 Protein gel electrophoresis and Western blotting

Cells were washed once with PBSA. 50μl 6x SDS sample buffer was added to the cells and the cells were scraped off from the tissue culture dish with a cell scraper (Sarstedt, Leicester, UK). The cell lysates were transferred to a 1.5 ml microcentrifuge

tube, and incubated at 98°C for 10 mins, followed by 1 min incubation on ice. The lysates were centrifuged at 13000 rpm for 5 mins, room temperature and supernatants removed to clean tubes. 20 µl samples were resolved in a 10% SDS gel in a Mini-Protean 3 (BioRad) with 2 µl PageRuler prestained protein ladder (Fermentas) in 1x running buffer. Gels were run for approximately 70 mins at constant current 15mA or until the front dye reached the bottom edge of the gel. The separated proteins were then transferred onto PVDF membranes (Millipore, Sigma-Aldrich) using the Mini-protean 3 transfer apparatus (BioRad). Membranes were immersed in methanol for 15 seconds, followed by soaking in distilled water for 2 mins, and then equilibrated in blotting buffer for 5 mins. Proteins were transferred overnight at 4°C at 30V, 90mA. Non-specific binding sites were blocked using PBS/0.1% Tween-20 containing 5% (w/v) dry skimmed milk for 1 hour with shaking at room temperature. To probe for specific proteins, membranes were incubated for 1 hour at room temperature with primary antibodies. After washing three times in PBS/0.1% Tween-20, membranes were incubated with HRP-conjugated secondary antibody at 1:3000 dilution. Antibody-protein complexes were detected using Enhanced chemiluminescent (ECL) Western blotting substrate (Pierce, Fisher Scientific, Leicestershire, UK) and exposure to film (Kodak, Sigma-Aldrich) in the dark for the appropriate amount of time (1 to 20 minutes) depending on signal strength. Film was developed by automatic x-ray film processor (Xograph, Gloucestershire, UK).

2.2.19 Statistical analysis

All experiments were repeated three times and performed in duplicate or triplicate. Data were analysed with GraphPad Prism Version 4.02. For data from two experimental conditions compared with each other, 2-tailed Student's t test was used to test statistical significance. In instances where multiple experimental conditions were compared with a single control group, statistical significance was tested using one-way ANOVA followed

by Newman-Keuls multiple comparison post-comparison test. A p value less than 0.05 was considered significant.

3. Construction of a fluorescent *E. coli* K1 strain that retains virulence

3.1 Introduction

To date, in published *E. coli* K1 studies involving fluorescence microscopy, the bacteria have either been surface labelled with fluorescent dye or immunolabelled with a bacteria-specific antibody or with an endosialidase-GFP fusion probe (Kim *et al.*, 2003: Sukumaran *et al.*, 2003; Alsam *et al.*, 2005; Zelmer *et al.*, 2008). Whilst these studies have provided great advances in understanding *E. coli* K1 interactions with host cells, the techniques used do have their limitations.

Surface labelling of bacteria with a fluorescent dye, such as fluorescein isothiocyanate (FITC), and NHS Rhodamine, is a rapid and cheap bacterial labelling approach (Hazenbos *et al.*, 1994; Schneider *et al.*, 2000; Steele-Mortimer *et al.*, 2000). However, as the dye only labels the bacterial extracellular surface, the dye will be diluted over each generation during bacterial replication. Furthermore, binding of FITC to the bacterial surface has been demonstrated to interfere with adenylate cyclase toxin activity of *Bordetella pertussis*, which affects bacterial uptake by human neutrophils *in vitro* (Weingart *et al.*, 1999).

Immunolabelling of fixed bacteria with a specific bacterial antibody is another common method widely employed for labelling bacteria in fixed samples. As the sample requires prior fixation, some fixatives, especially aldehydes, generate autofluorescent signal, and some cell structures, such as lipid raft-associated molecules, are not properly preserved by the fixative (Drecktrah *et al.*, 2008; Tanaka *et al.*, 2010). Further, certain bacterial antigens, such as fimbriae (Saukkonen *et al.*, 1988), and *E. coli* K1 capsule (Zelmer *et al.*, 2008), express different forms of their antigens at different stages of infection, therefore selection of antibody requires care. For *E. coli* K1, the endosialidase-GFP probe is an alternative non-antibody probe. It is an engineered noncatalytic *E. coli*

K1-specific bacteriophage-encoded endosialidase tagged with GFP that binds specifically to the K1 capsule in a fixed sample but does not degrade it (Jokilammi *et al.*, 2004).

An alternative bacterial-labelling strategy is cytoplasmic expression of fluorescent proteins in bacterial cells from an introduced plasmid (Weingart *et al.*, 1999; Qazi *et al.*, 2001; Ruthel *et al.*, 2004; Knodler *et al.*, 2005; Drecktrah *et al.*, 2007; Lamberti *et al.*, 2010; Van Engelenburg and Palmer, 2010). This bacterial labelling approach provides stably fluorescent live bacteria for microscopy studies, but some adverse outcomes from the burden of fluorescent protein synthesis to *Salmonella* pathogenicity have been observed in bacterial uptake into macrophages and epithelial cell lines *in vitro* as well as *in vivo* infection (Knodler *et al.*, 2005). In addition to the production of fluorescent proteins, the presence of plasmid, and antibiotic resistance markers, such as tetracycline resistance gene (tet^R), and chloramphenicol resistance gene (Cm^R), on the plasmid has also been shown to affect bacterial virulence traits (Abromaitis *et al.*, 2005; Knodler *et al.*, 2005; Clark *et al.*, 2009). However, it has been further demonstrated that by integrating Cm^R and fluorescent reporter genes into the bacterial chromosome, the fluorescent protein-expressing *Salmonella* retains its virulence (Clark *et al.*, 2009).

The aim of this project was to study the interactions of *E. coli* K1 with various cellular and organellar markers in HBMEC by live-cell imaging. Live-cell imaging allows the study of the dynamic interactions of the pathogen with host factors over time (Schroder *et al.*, 2006; Drecktrah *et al.*, 2008). For example, the application of live-cell imaging revealed that *Salmonella*-induced filaments (Sifs) are highly dynamic and bidirectional, with microtubule-dependent movement (Drecktrah *et al.*, 2008). Therefore, to enable the application of live-cell imaging for studying *E. coli* K1 interaction with HBMEC, a fluorescent *E. coli* K1 strain that retains virulence is required. The virulence of the fluorescent protein-expressing *E. coli* K1 can then be screened with an HBMEC invasion

assay, which has been extensively applied to study *E. coli* K1 pathogenesis. as reviewed in chapter 1.

3.2 Objectives and aims

The aim of this chapter was to construct a fluorescent *E. coli* K1 strain that retained virulence. The specific objectives are:

- To determine the optimal infection conditions for *E. coli* K1 infection of HBMEC by testing different multiplicities of infection (MOI) and varying the incubation time of the cells with the bacteria.

- To transform various bacterial fluorescent reporter constructs into *E. coli* K1 and to screen the virulence of the transformed *E. coli* K1 by the optimised HBMEC invasion assay in comparison to untransformed *E. coli* K1.

3.3 Results

3.3.1 Invasion and intracellular survival of *E. coli* K1 and K-12 in HBMEC

To determine the kinetics of the bacterial invasion of HBMEC, the cells were incubated with the bacteria at MOI of 100 for varying intervals of time (Figure 3.1A). Extracellular bacteria were killed by gentamicin, which is poorly permeable to eukaryotic cell membranes (Barnhart *et al.*, 2002). Therefore, bacteria that have invaded into the host cells are protected from the bactericidal effect of gentamicin. After gentamicin treatment, cells were washed, and the viable intracelluar bacteria were quantified as described in chapter 2.

The percentage of recovered intracellular *E. coli* K1 from HBMEC increased with longer incubation times (Figure 3.1B). An incubation of 120 minutes resulted in a significant increase in the percentage of intracellular *E. coli* K1 recovered compared to a 30 and 60 minutes incubation ($p < 0.05$. using t-test, one-tailed distribution), which might

be resulted from intracellular bacterial replication. As expected, when the non-invasive *E. coli* K-12 were used, no intracellular bacteria were recovered after 30 or 60 minutes incubation, and only a very low percentage of bacteria (0.00018%) had invaded HBMEC after 120 minutes. These results show that more *E. coli* K1 invade HBMEC with longer incubation times; whereas for *E. coli* K-12, which is a non-invasive laboratory *E. coli* strain, extended incubation time of the bacteria with HBMEC results with no or very low number of bacterial invasion.
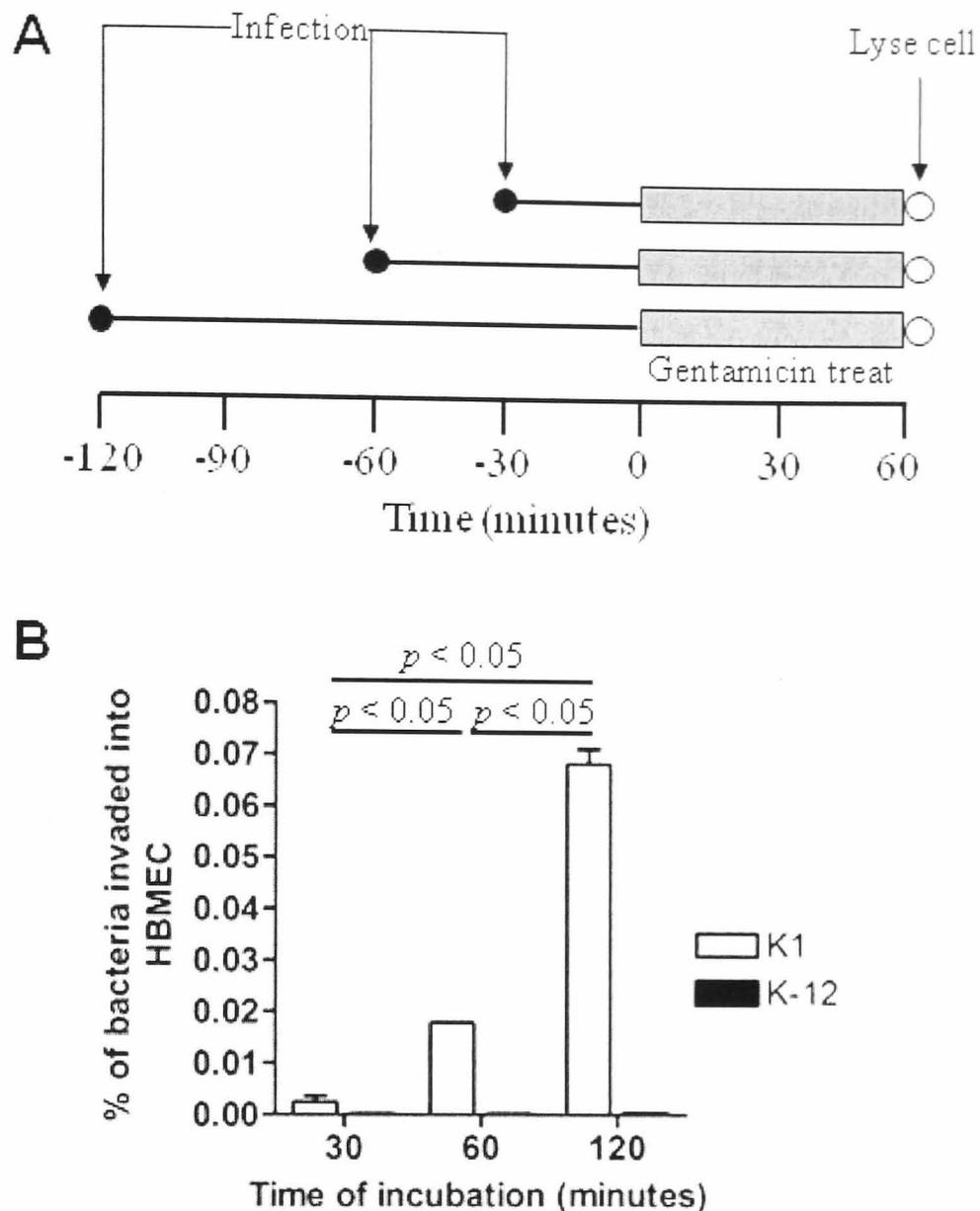
Figure 3.1. Invasion of *E. coli* K1 and K-12 into HBMEC. (A) Schematic of experimental design. To determine the optimal infection time, HBMEC were infected with *E. coli* K1 or K-12 at MOI of 100 for different time intervals. The infected cells were washed and incubated in medium containing 100 µg/ml gentamicin for 60 minutes to kill extracellular bacteria at the end of the infection. Cells were washed and lysed. The cell lysates were plated on LB agar to enumerate the number of bacteria. (B) Quantitation of the number of bacteria invaded HBMEC at various time intervals of incubation as indicated. The result represents the percentage of bacteria invaded into HBMEC. Results are from one representative experiment of two independent repeats performed in triplicate and presented as mean of triplicates ± SD.

E. coli K1 are able to replicate extracellularly in the blood of infected neonates as well as the neonatal rat model (Glode *et al.*, 1977; Pluschke *et al.*, 1983; Kim *et al.*, 1992; Zelmer *et al.*, 2008). However, the ability of the bacteria to survive intracellularly is unclear. To investigate the ability of *E. coli* K1 to survive intracellularly in HBMEC, the cells were incubated with either K1 or K-12 at MOI of 100 for 120 minutes (Figure 3.2A). Following this, the cells were cultured in experimental medium containing gentamicin to

kill extracellular bacteria (Figure 3.2B). The intracellular bacterial load was then assessed at increasing time intervals to determine bacterial persistence. A minor decrease in the percentages of intracellular *E. coli* K1 was observed at 180 minutes, but the percentage of intracellular *E. coli* K1 increased significantly at the end of the 300 minutes incubation in gentamicin ($p < 0.05$, using *t*-test, one-tailed distribution). For intracellular survival assays involving *E. coli* K-12, a very low percentage of intracellular bacteria (0.0003%) were recovered 60 minutes post-gentamicin treatment, and the percentage of recovered bacteria was further decreased to 0.0000635% at 300 minutes post-gentamicin treatment. The results clearly indicate that *E. coli* K1 are able to survive and replicate intracellularly in HBMEC at least up to 5 hours post infection, as very low number of viable intracellular *E. coli* K1 was recovered after 18 hours incubation in media containing gentamicin (data not shown), which might be due to bacterial killing intracellularly or bacterial egress from the infected HBMEC at later time point. Whereas the non-pathogenic *E. coli* K-12 are not able to survive intracellularly in HBMEC. In addition, these results also demonstrated that the gentamicin did not affect the survival of intracellular K1 bacteria.
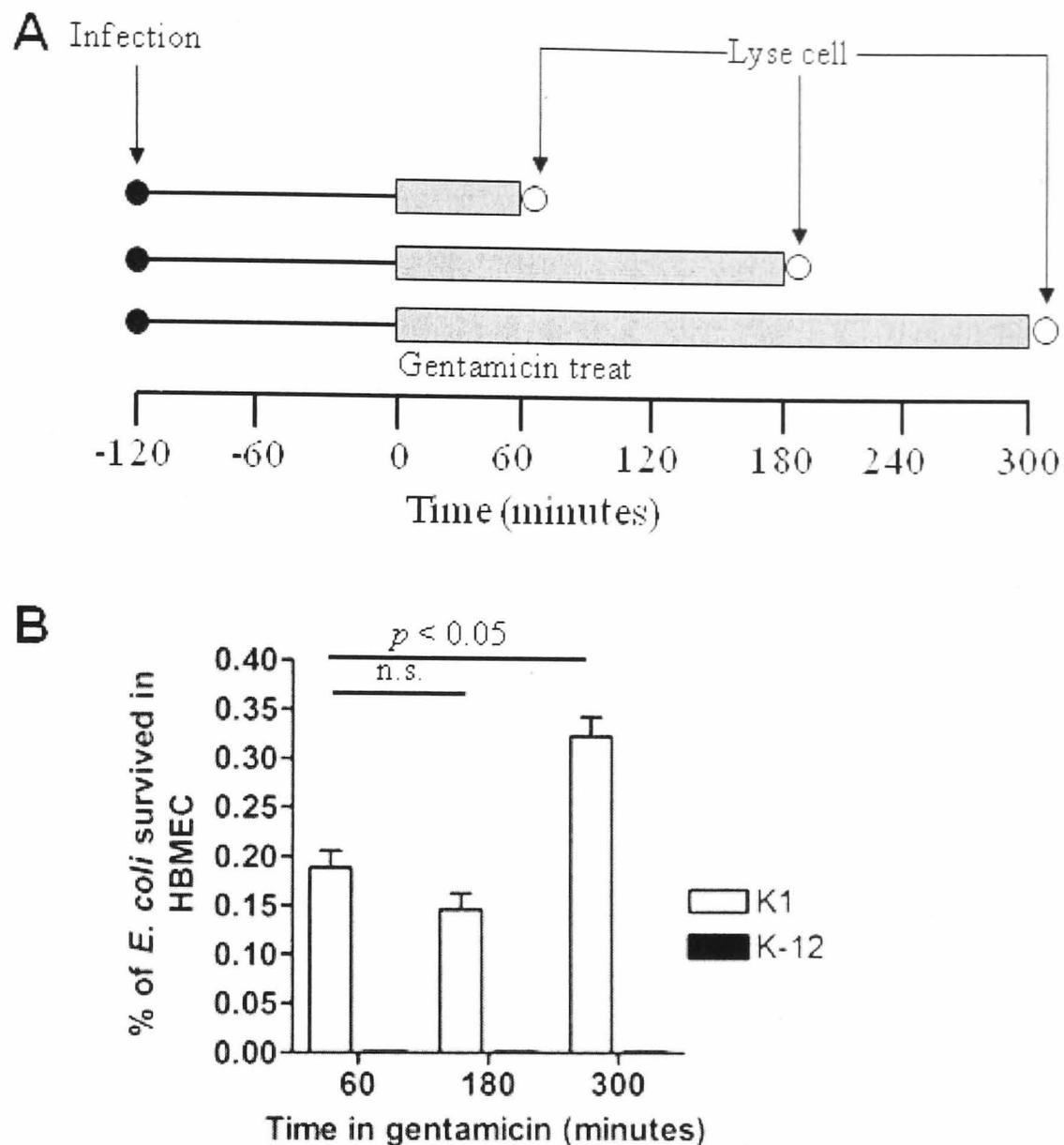
Figure 3.2. Intracellular survival of *E. coli* K1 in HBMEC. (A) Schematic of experimental design. To determine the intracellular survival of the bacteria, HBMEC were infected with *E. coli* K1 or K-12 at MOI of 100 for different time intervals. The infected cells were washed and incubated in medium containing 100 µg/ml gentamicin for the time periods indicated. Cells were washed and lysed. The cell lysates were plated on LB agar to enumerate the number of bacteria. (B) Quantitation of the intracellular survival. The result represents the percentage of recovered intracellular bacteria. Results are from one representative experiment of three independent repeats performed in triplicate and presented as mean of triplicates ± SD.

3.3.1.1 *E. coli* K1 bearing *M. tuberculosis* codon optimized fluorescent reporter vectors invasion of HBMEC

E. coli K1 transformed with *M. tuberculosis* codon optimized fluorescent reporter vectors were initially screened with a cheap *Acanthamoeba* phagocytosis assay and were found to retain virulence when compared to untransformed *E. coli* K1 (data not shown). The final application of the virulent fluorescent *E. coli* K1 strain is for studying the

interactions of the fluorescent bacterial strain with HBMEC, which is a non-phagocytic cell type used as a blood-brain barrier model *in vitro*. Therefore, the fluorescent *E. coli* K1 strains, which had demonstrated to be virulent in *Acanthamoeba*, had to demonstrate similar virulence trait in HBMEC.

K1pmCherry3 and K1pEnvy1 were selected for further screening with HBMEC. Invasion assays were performed at MOI of 100 for 60 minutes (Figure 3.3). The percentages of recovered intracellular bacteria for K1pmCherry3, and K1pEnvy1 were significantly lower than untransformed K1 ($p < 0.01$, using *t*-test, one-tailed distribution). It was also observed that the doubling time for all K1 and K-12 transformed with the *Mycobacterium* sp. codon-optimised fluorescent reporter constructs were longer than the untransformed K1 and K-12, respectively (data not shown). It appears that although the bacterial strains were equally able to infect *Acanthamoeba*, the virulence of the bacteria transformed with *M. tuberculosis* codon optimized fluorescent reporter constructs was impaired in their ability to invade HBMEC. These transformed bacteria were therefore not suitable for use in future experiments.
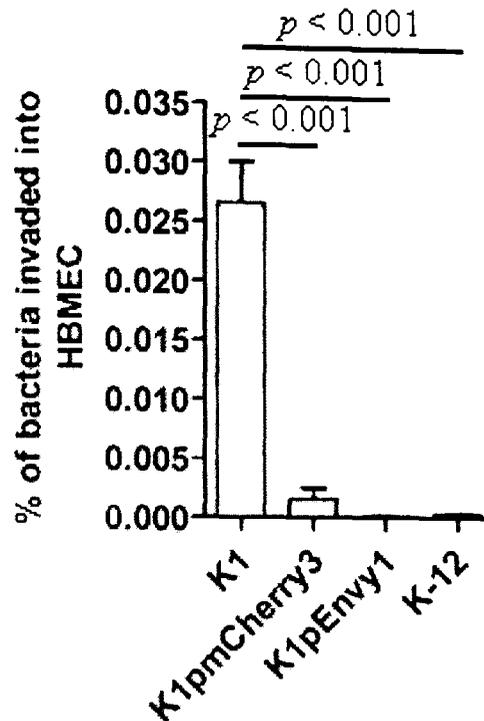
Figure 3.3. Screening of virulence of *E. coli* K1 expressing fluorescent protein in HBMEC. To determine the virulence of the K1 expressing fluorescent protein, invasion assays were performed by infecting HBMEC with either native *E. coli* K1, K-12 or fluorescent protein expressing *E. coli* K1 strains at MOI of 100 for 60 minutes, followed by incubation in media containing gentamicin for 1 hour. The result represents the percentage of bacteria invaded into HBMEC. Results are from one representative experiment of two independent repeats performed in triplicate and presented as mean of triplicates ± SD.

3.3.1.2 pFPV25.1-transformed *E. coli* K1 invasion of HBMEC

pFPV25.1 plasmid contains *E. coli* codon optimised GFP reporter gene, *gfpmut3a*, fused downstream of a *Salmonella typhimurium* (*S. typhimurium*) promoter, *rpsM* (Figure 3.4A) (Valdivia and Falkow, 1996). This construct had been extensively used in studies involved *S. typhimurium* (Cheminay *et al.*, 2005; Radtke *et al.*, 2007; Gerlach *et al.*, 2008), and enteropathogenic *E. coli* (EPEC) (Unsworth *et al.*, 2007; Marchès *et al.*, 2008); therefore, this plasmid was tested for use in *E. coli* K1.

As with other constructs, pFPV25.1 was transformed into K1 and K-12 as previously described, and the fluorescence stability was confirmed using a confocal microscope (Figure 3.4B). All pFPV25.1-transformed K1 (K1-GFP) fluoresced when observed with a confocal microscope. The growth profile of the K1-GFP was slightly lower when compared to native K1 (Figure 3.4C), with the doubling time of K1-GFP was

approximately 36.3 minutes, and the K1 doubling time was 35 minutes in this specific experiment.

To determine whether the virulence of K1-GFP is retained, HBMEC invasion assays were performed (Figure 3.4D). The percentage of recovered intracellular K1-GFP was roughly 40% lower than that of native K1, however this was shown to be not significant ($p > 0.05$, using t-test, one-tailed distribution). The reduction in the K1-GFP invasion efficiency was deemed to be acceptable for further experiments, as the transformant bacteria were still invasive when compared to the non-pathogenic *E. coli* K-12 (Figure 3.4D) and the previous transformed strains (Figure 3.3).
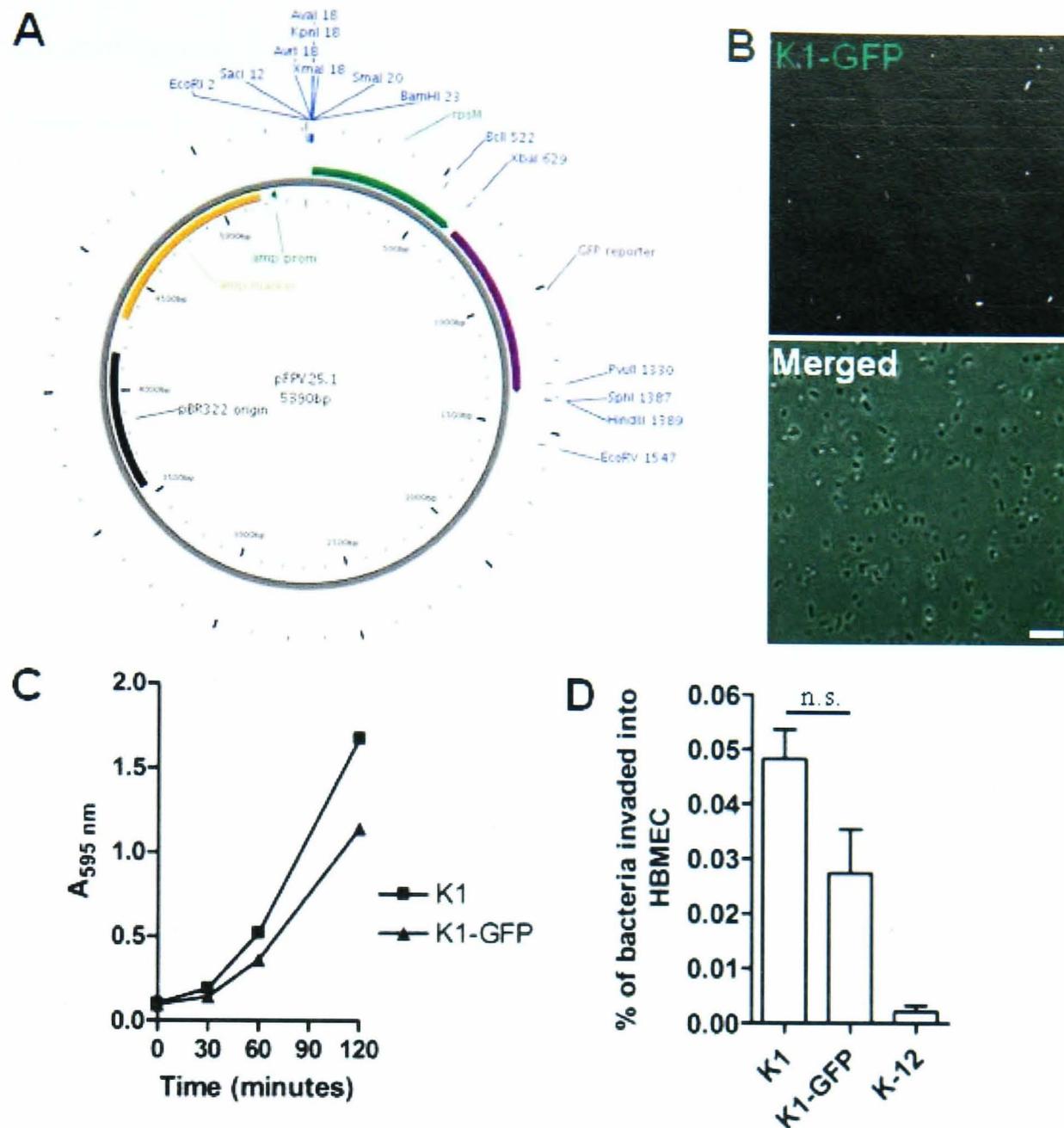
Figure 3.4. Screening of virulence *E. coli* K1 transformed with pFPV25.1 construct in HBMEC. (A) The illustration shows the pFPV25.1 plasmid map. Unique restriction enzyme cutting sites are indicated in blue. (B) The confocal micrograph shows fluorescent *E. coli* K1 transformed with pFPV25.1 (K1-GFP). Scale bar: 10 μm. (C) The growth kinetics of K1-GFP and untransformed *E. coli* K1 in LB broth. The results show the absorbance at 595 nm of the bacterial cultures at the time intervals indicated. (D) To determine the virulence of the transformed K1, invasion assays were performed by incubating HBMEC with either *E. coli* K1, K-12 or K1-GFP at MOI of 100 for 120 minutes, followed by incubation in media containing gentamicin. The result represents the percentage of bacteria invaded into HBMEC. Results are from one representative experiment of two independent repeats performed in triplicate and presented as mean of triplicates ± SD.

It has been shown previously that the bacterial K1 polysialic acid capsule is crucial for bacterial intracellular survival in HBMEC, no defect was observed in the HBMEC invasion by K1 capsule deletion mutant (Kim *et al.*, 2003). Thus, the apparent lower invasion efficiency of K1-GFP seen in Figure 3.4D may be due to impairment in K1

101

polysialic acid capsule expression, leading to the killing of the intracellular bacteria rather than a reduction in bacterial invasion. To examine the presence of K1 polysialic acid capsule on K1-GFP, the transformed bacteria were smeared onto a cover slip, fixed with formaldehyde, and stained with PK1A-GFP probe, which binds K1 polysialic acid capsule specifically (Jokilammi et al., 2004; Zelmer et al., 2008), in the absent of detergent. As the transformed bacteria already expressed GFP, visualization of the bound PK1A probe was facilitated by counter-staining with a mouse anti-GFP antibody, followed by Fluoprobes 642-conjugated anti-mouse antibody. An experimental control which K1-GFP smear was not stained with the PK1A-GFP probe, but was stained with the anti-GFP antibody, followed by Fluoprobes 642-conjugated anti-mouse antibody, did not detect any signal in the far red channel (Figure 3.5B). This result showed that the intracellular GFP of K1-GFP was not detected by the anti-GFP antibody when staining was performed without permeabilization with detergent. Hence, the staining showed the presence of K1 polysialic acid capsule on the untransformed K1 and K1-GFP (Figure 3.5A and C respectively). Therefore, the reduction in the K1-GFP invasion efficiency was not caused by intracellular bacterial killing as the result of the absence of K1 polysialic acid capsule expression on the transformant, but was probably due to a defect in other bacterial determinants that are essential for HBMEC invasion.
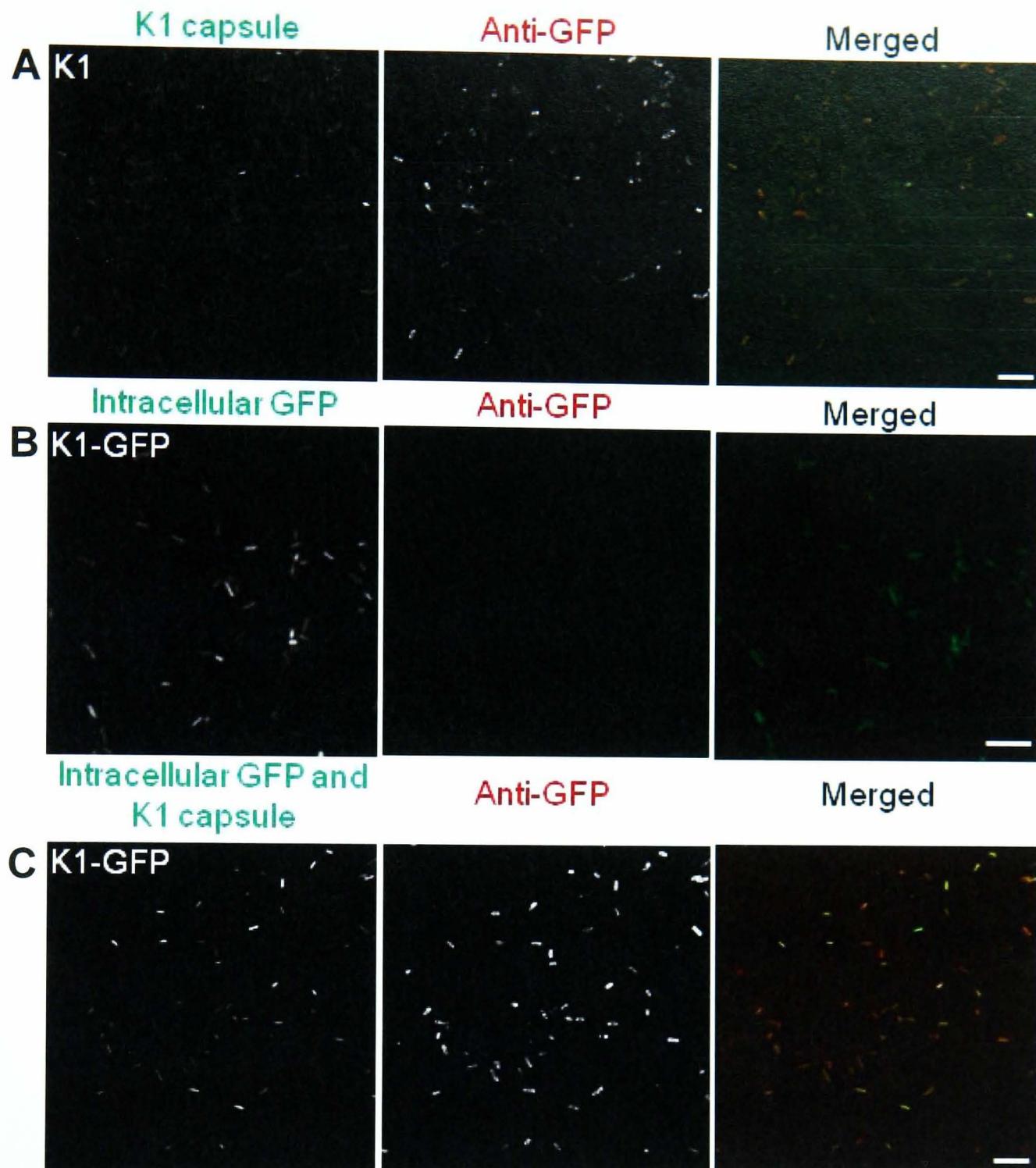
Figure 3.5. The presence of K1 polysialic acid capsule on K1-GFP. To examine the presence of K1 polysialic acid capsule on K1 and K1-GFP, the bacterial culture was smeared on a glass cover slip, air-dried, and fixed with 2% (v/v) formaldehyde. The bacterial smear was stained with 10 µg/ml of PK1A-GFP probe in PBS, then by mouse anti-GFP clone 3E6, and followed by Fluoprobes 642 conjugated donkey anti-mouse antibody without permeabilizing by detergent. As an experimental control (B), K1-GFP was stained with mouse anti-GFP antibody, followed by Fluoprobes 642 conjugated donkey anti-mouse antibody only. (A and C) The images show the presence of the bacterial K1 capsule on K1 and K1-GFP respectively. Contrast of all images was enhanced. GFP signal from intracellular GFP of K1-GFP and from PK1A-GFP probe (green); signal resulted from anti-GFP staining (red). Scale bar: 10 µm (A and C); 5 µm (B).

3.3.1.3 Deletion of *rpsM* promoter from pFPV25.1 and the transformed bacterial invasion of HBMEC

It was previously shown that cytoplasmic fluorescent protein expression affects *Salmonella* virulence (Knodler *et al.*, 2005; Clark *et al.*, 2009). To investigate if GFP expression was the major factor that affects the transformed bacterial invasion and survival in HBMEC, the *rpsM* gene was deleted from pFPV25.1, to construct a promoterless construct that does not expression GFP, as illustrated in Figure 3.6.
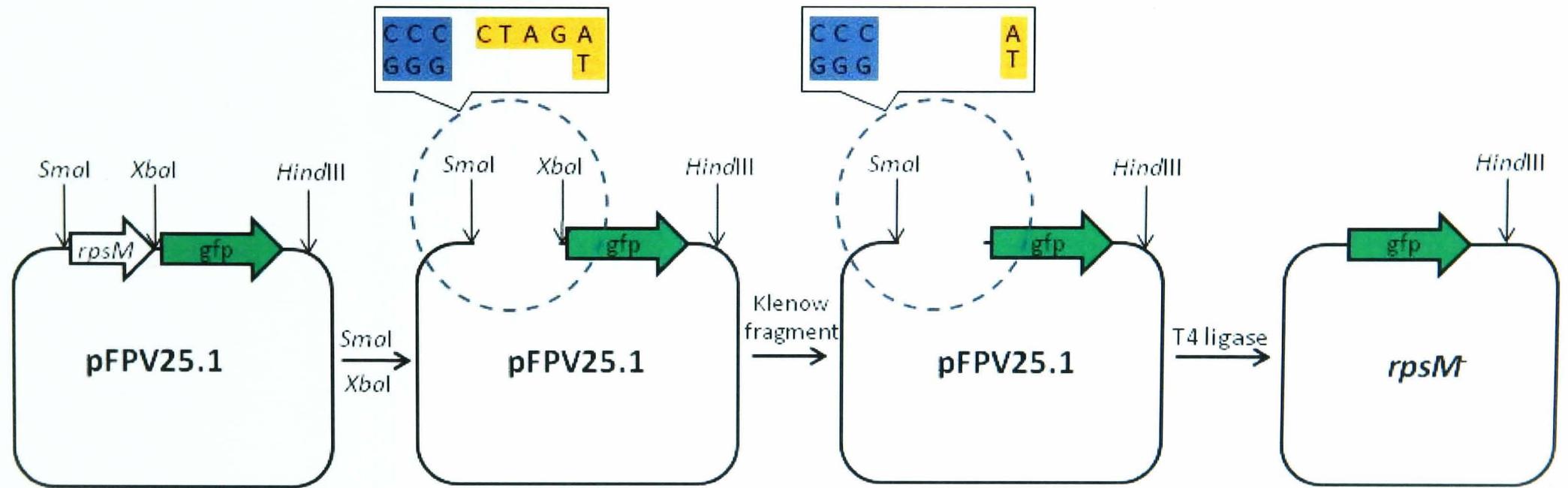
Figure 3.6. Deletion of *rpsM* from pFPV25.1. The illustration summarizes steps involved in deleting *rpsM* gene in pFPV25.1 using standard cloning techniques. pFPV25.1 was digested with *Sma*I and *Xba*I, blunted with Klenow fragment, and re-ligated. The resulting construct was a promoterless bacterial expression vector, *rpsM*.

The construct was transformed into *E. coli* K1 by electroporation. As the promoter had been deleted, there was no GFP expression in the transformed bacteria, therefore, to additionally confirm the transformed *E. coli* K1 that grew on a ampicillin selection LB agar plate, the plasmid DNA was extracted and linearised by *Hind*III digestion for the expected 4786 bp band compared to the plasmid with intact promoter of 5390 bp (Figure 3.7A). The quality of the plasmid DNA extracted from *E. coli* K1 was poor compared to *E. coli* DH5α strain, a standard *E. coli* cloning strain, possibly due to the presence of nucleases in the pathogenic strain. The growth kinetics of the transformed bacteria, K1rpsM⁻, was slightly lower than K1, with the doubling time of 32.43 minutes (Figure 3.7B), which is similarly observed in other fluorescent protein-expressing K1.

In order to demonstrate the invasion efficiency of the K1rpsM⁻, HBMEC invasion assays were performed (Figure 3.9C). Interestingly, the percentage of recovered intracellular K1rpsM⁻ was nearly 2-fold and slightly lower than that of K1 and K1-GFP. The observation might suggest that the reduction in the invasion efficiency of fluorescent protein-expressing K1 is not caused by the expression of fluorescent protein, but the presence of the plasmid DNA alone might be a metabolic burden to the bacteria, hence, the bacterial virulence is affected. Alternatively, the presence of certain genetic components on the expression vector, such as antibiotic resistance gene, contribute to the loss of the bacterial virulence trait (Abromaitis *et al.*, 2005).
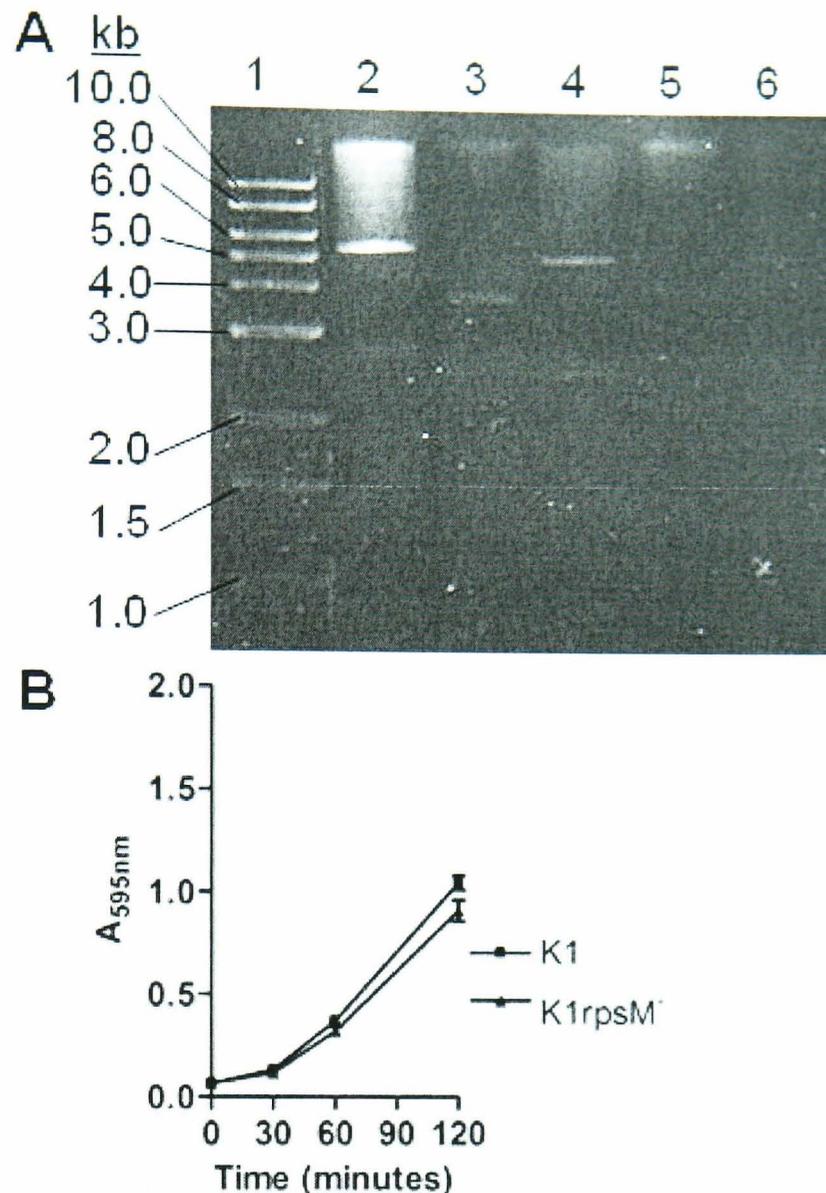
Figure 3.7. Screening of *E. coli* K1 transformed with rpsM⁻ plasmid DNA and the growth kinetics of the transformed *E. coli* K1. (A) *Sma*I and *Xba*I digestion resulted in the deletion of *rpsM,* the promoter for *gfp* in pFPV25.1. Therefore, *E. coli* K1 transformed with rpsM⁻ (K1rpsM⁻) does not express GFP. To screen for K1rpsM⁻, plasmid DNA was extracted from the bacteria, and digested with *Hind*III. The gel photograph shows the products generated from *Hind*III digestion of the extracted rpsM⁻ plasmid DNA. Lanes: 1, 1 kb DNA ladder; 2, pFPV25.1 digested with *Hind*III (5390 bp); 3, undigested *rpsM* extracted from transformed *E. coli* DH5α (cloning strain); 4, *rpsM* extracted from *E. coli* DH5α digested with *Hind*III (4786 bp); 5, undigested *rpsM* extracted from transformed *E. coli* K1; 6, *rpsM* extracted from *E. coli* K1 digested with *Hind*III (4786 bp). (B) The growth kinetics of the transformant in LB broth were compared to the untransformed *E. coli* K1. The results show the absorbance at 595 nm of the bacterial cultures at the time intervals indicated.

3.3.1.4 Construction of pFPV-mCherry and the mCherry-expressing *E. coli* K1 invasion of HBMEC

Whilst K1-GFP was shown to fluoresce and to retain the bacterial virulence trait in HBMEC infection, the major aim of this study was to apply the fluorescent bacterial strain for studying the interaction of the bacteria with cellular markers, which the majority of the

available cellular markers containing mammalian expression vectors are also GFP-tagged. Therefore, it was of crucial importance to have an *E. coli* K1 strain expressing other fluorescent proteins, with excitation and emission spectra that did not overlap with GFP, but that still retained virulence.

We chose mCherry as a candidate to test for its known brightness, photostability, and distinct excitation and emission spectra from GFP. The cloning strategy was performed as illustrated in Figure 3.8. All the transformed *E. coli* K1 were found to be fluorescent when they were screened with a confocal microscope (Figure 3.9A). The variability in the fluorescent intensity of the bacteria in Figure 3.9A was due to different focal plane of the bacteria when the image was acquired from live bacteria. The growth kinetics of the transformed bacteria, K1-Cherry, was slightly lower than K1 (Figure 3.9B), the doubling time of K1-Cherry was approximately 36.47 minutes compared to the doubling time of K1, which was 35 minutes in this experiment.

As with other constructs, to determine the virulence of K1-Cherry, HBMEC invasion assays were performed by infecting HBMEC with either *E. coli* K1, K-12, K1-GFP, K1-Cherry or K1rpsM⁻ (Figure 3.9C). The results indicate that K1rpsM⁻, and K1-GFP exhibit a decrease in HBMEC invasion efficiency, however, the decrease was not statistical significant, and they remain significantly more invasive than the non-pathogenic *E. coli* K-12 laboratory strain. In contrast, the invasion efficiency of K1-Cherry was very similar to the native K1 (Figure 3.9C). Therefore, mCherry expression seems to have no adverse effect on *E. coli* K1 virulence.
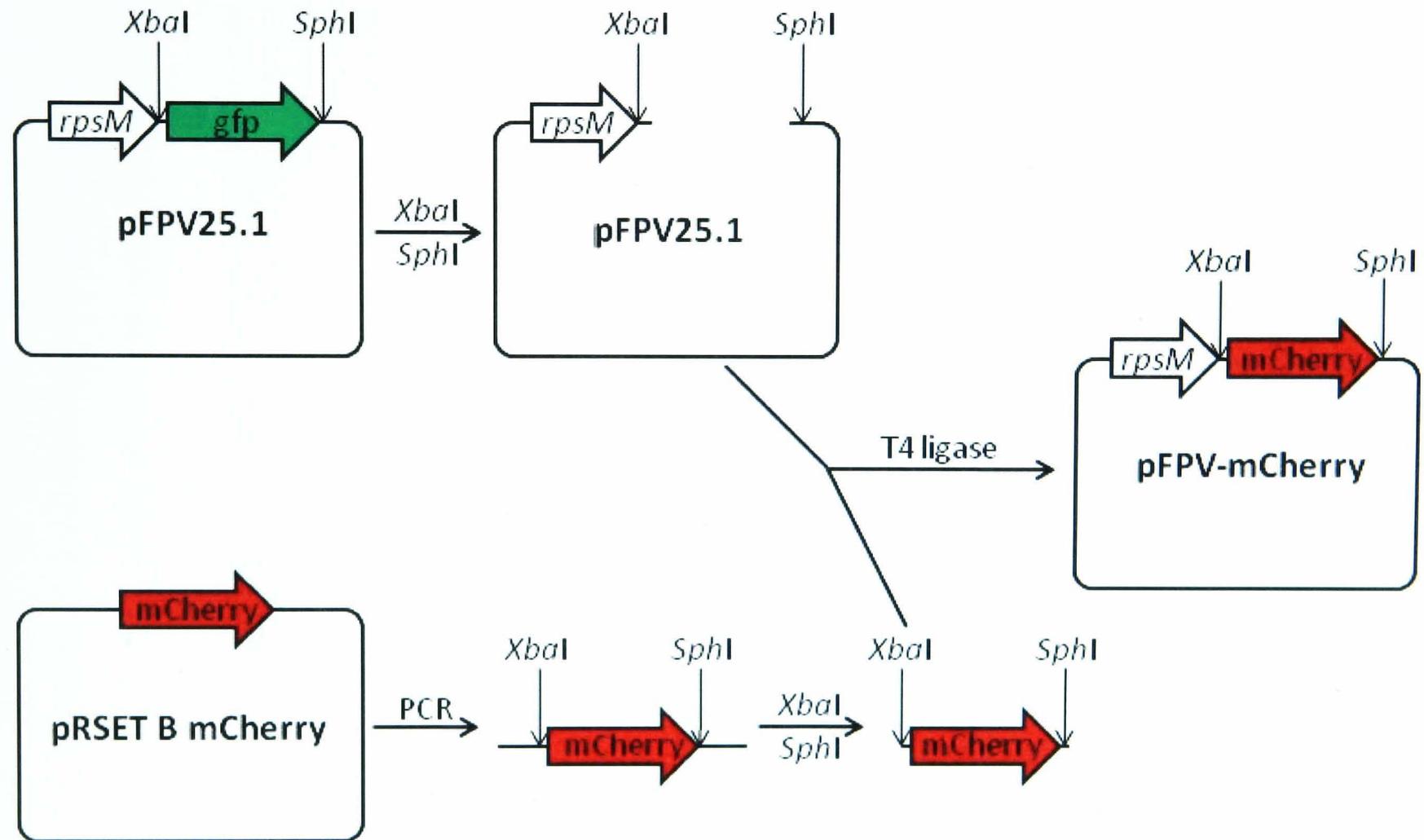
Figure 3.8. Cloning strategy for constructing a bacterial expression vector carrying mCherry fluorescent protein cDNA. The illustration summarizes steps involved in replacing *gfp* gene in pFPV25.1. Briefly, mCherry gene was PCR amplified from pRSET-mCherry with forward primer flanked with *Xba*I restriction site and reverse primer flanked with *Sph*I restriction site. The resulting amplicons were digested with *Xba*I and *Sph*I and ligated into the corresponding sites of pFPV25.1, thereby replacing the *gfp* gene.
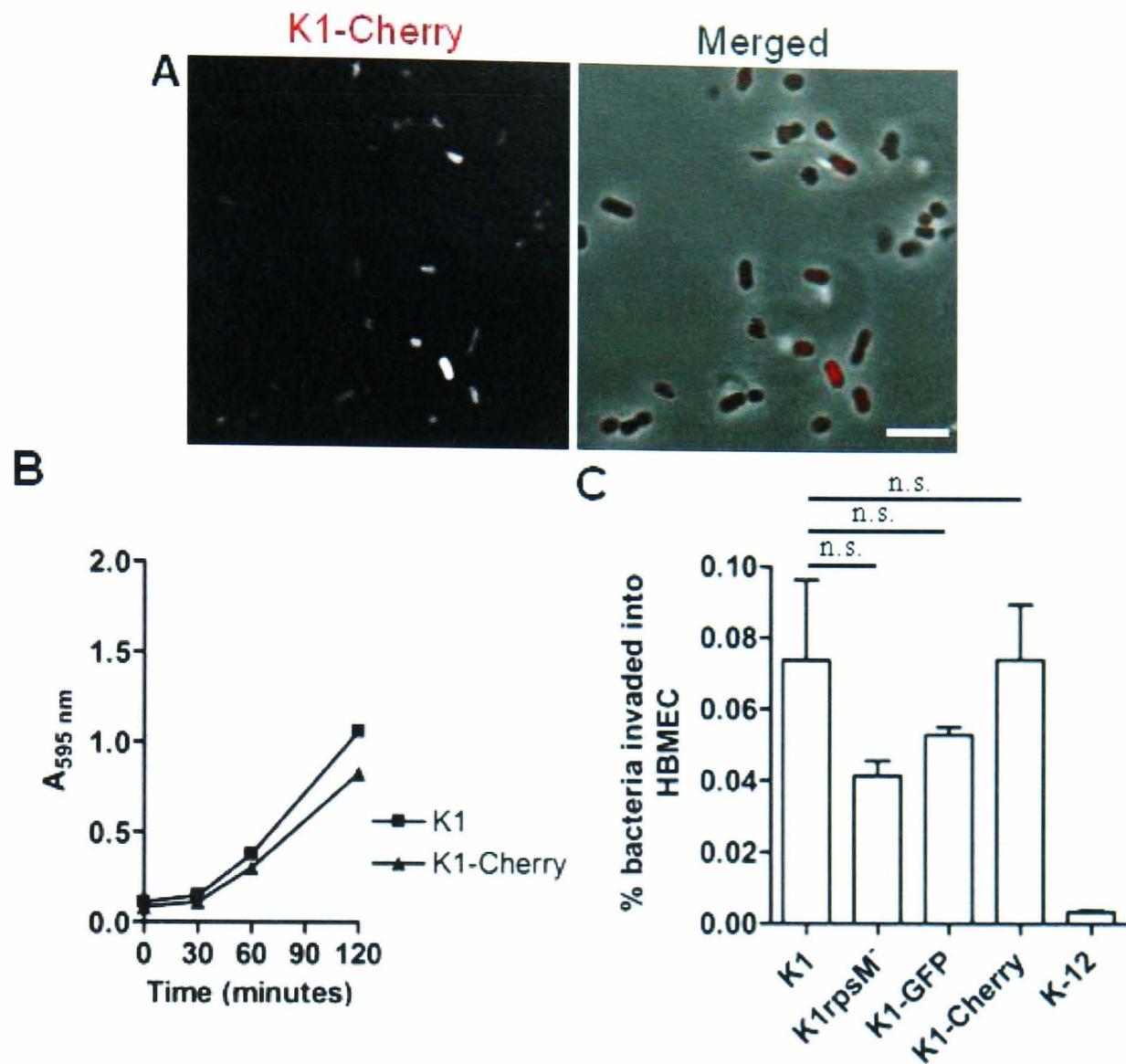
Figure 3.9. Screening of virulence _E. coli_ K1 expressing fluorescent protein in HBMEC. (A) A confocal micrograph to show fluorescent K1-Cherry. Scale bar: 5 μm. (B) The growth kinetics of the transformant in LB broth were compared to the untransformed _E. coli_ K1. The results show the absorbance at 595 nm of the bacterial cultures at the time intervals indicated. (C) To determine the virulence of the transformed K1, invasion assays were performed by infecting HBMEC with either _E. coli_ K1 or K-12 or K1-GFP or K1-Cherry or K1rpsM⁻ at MOI of 100 for 2 hours, followed by incubation in media containing gentamicin for 1 hour. The result represents the percentage of bacteria invaded into HBMEC. Results are from one representative experiment of two independent repeats performed in triplicate and presented as mean of triplicates ± SD.

3.3.2 Transcytosis of _E. coli_ K1 across HBMEC

During an infection, it is thought that _E. coli_ K1 invade and transcytose from the endothelial cells of BBB to the CNS and subsequently trigger the infiltration of immune cells, which results in inflammation of the meninges (Siegel and McCracken, 1981; Kim _et al._, 1992; Zelmer _et al._, 2008). To model the BBB _in vitro_, HBMEC, which are polarized

endothelial cells, were grown on collagen-coated Transwell inserts as illustrated in Figure 3.10A. Upon complete confluency, tight junction formation was induced by culturing the cells in the presence of hydrocortisone (Franke *et al.*, 2000).The formation of tight junctions and the integrity of the HBMEC monolayer were evidenced by an increase in transendothelial electrical resistance (TEER) (Figure 3.10B). When the TEER reading reached approximately 20 Ωcm^2, the monolayer's permeability to 4 kDa FITC-conjugated dextran was assessed (Figure 3.10C). A small amount of fluorescent signal could be detected in the media collected from the basolateral compartment 90 minutes after the introduction of the FITC-conjugated dextran to the apical compartment. However, when the HBMEC containing insert was compared with a cell-free insert (empty insert), the amount of fluorescent signal detected in media collected from basolateral compartment of empty insert was approximately 10-fold higher than that collected from the HBMEC containing insert after 90 minutes of incubation (Figure 3.10C).
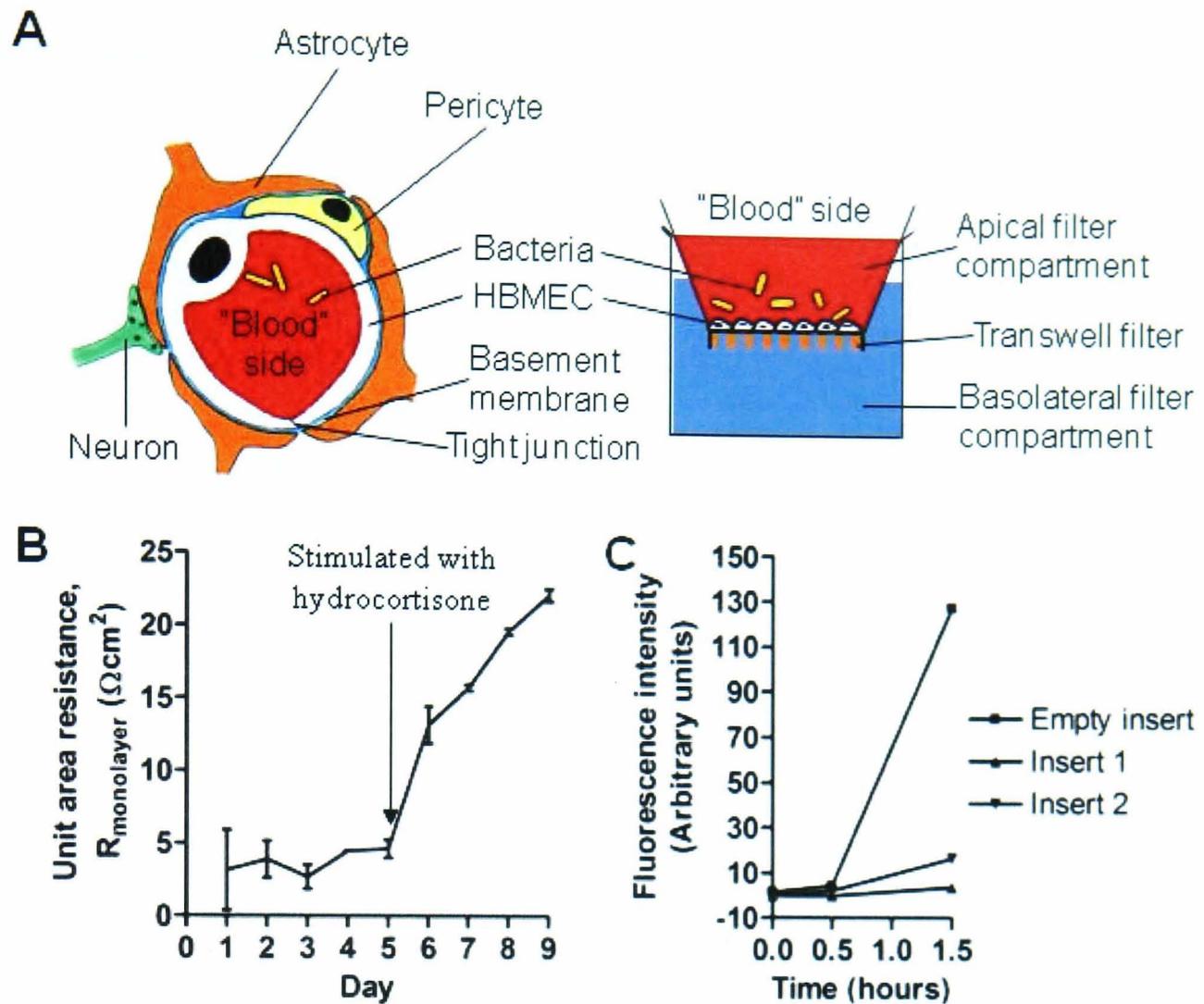
Figure 3.10. *in vitro* blood-brain barrier (BBB) model. (A) An illustration of how the BBB *in vitro* relates to the Transwell insert model. (B) To determine the permeability of HBMEC, cells were seeded onto a collagen-coated Transwell insert. When the cells on the Transwell membrane reached complete confluency, the medium was replaced with HBMEC growth media containing 1.0 µg/ml hydrocortisone for stimulating the formation of barrier properties. The transendothelial electrical resistance (TEER) measurements were monitored. The graph shows the TEER measurements (Ωcm^2) throughout the culture duration. Results are one representative experiment of 4 independent repeats performed in triplicate and presented as mean of triplicates ± SD. (C) To demonstrate the barrier properties of HBMEC cultured on Transwell insert on day 9, 4 kDa FITC-conjugated dextran (0.1 mg/ml) (Sigma-Aldrich) was added to the apical chamber of cells. After addition of the reagent, medium was sampled at the indicated time intervals. The permeability was quantified as fluorescence intensity of the FITC that passed from the apical chamber to the basolateral chamber.

Although FITC-conjugated dextran transportation through HBMEC monolayer was reduced, the TEER of the HBMEC line used in this study was lower than the reported TEER for other immortalized HBMEC, HCMEC/D3, which ranged from 60 to 80 Ωcm^2 (Weksler *et al.*, 2005; Cucullo *et al.*, 2008). To confirm that the HBMEC used in this study were able to form intercellular junctions, confluent HBMEC were stained for cadherin, a

transmembrane protein associated with intercellular junctions. The distribution of the staining suggests that the cells are able to form intercellular junctions (Figure 3.11). In addition, F-actin staining also revealed cell periphery localization indicative of intercellular junction formation (Figure 3.11).
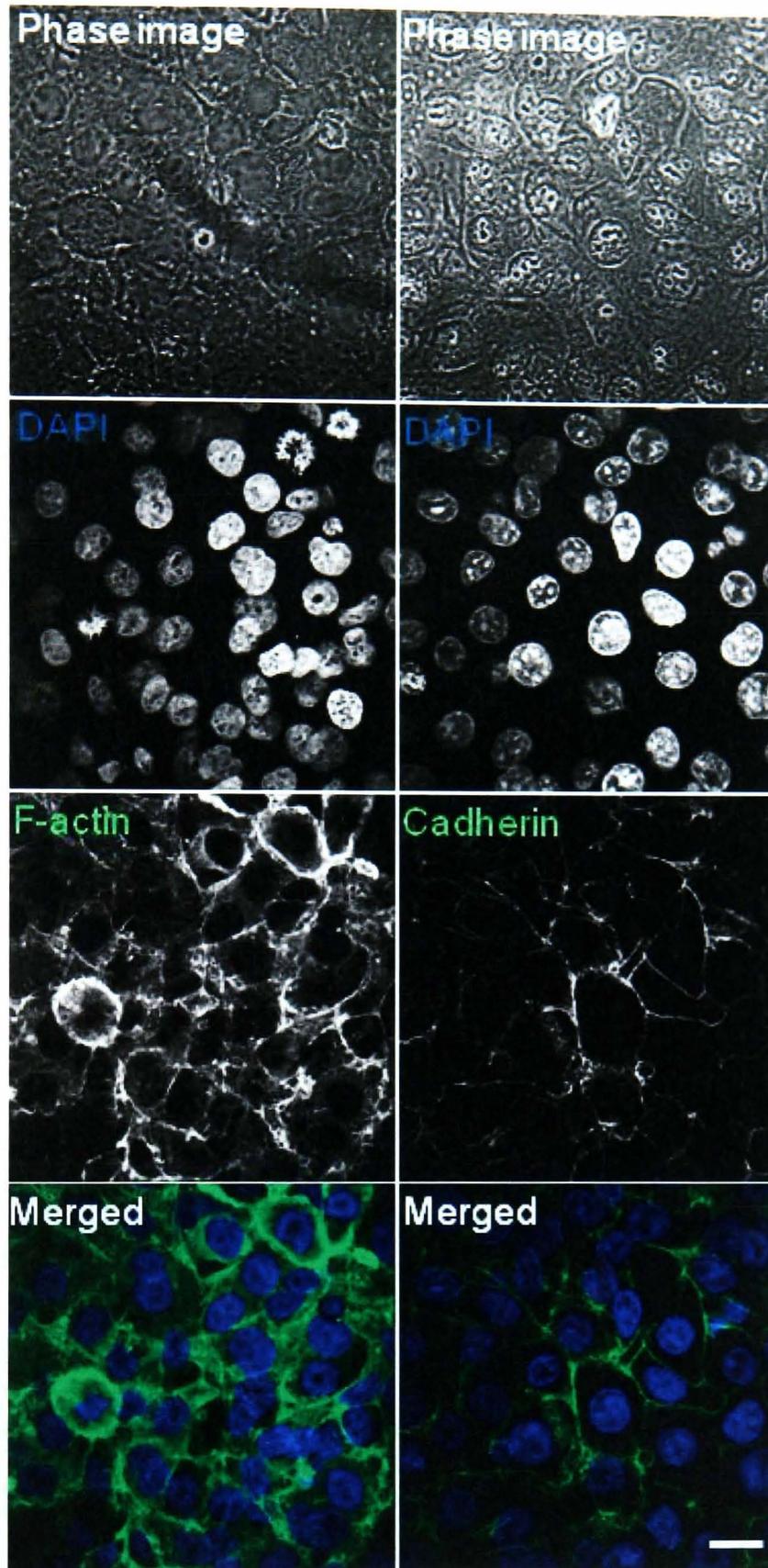
Figure 3.11 Immunostaining of cadherin and F-actin of HBMEC. Confluent monolayers of HBMEC cells (passage 15) were fixed with either 2% (v/v) formaldehyde (F-actin) or methanol (cadherin), immunostained for cadherin with mouse anti-pan cadherin, and followed by Fluoprobes 488 conjugated donkey anti-mouse antibody, or stained with 30 μg/ml phalloidin-TRITC. F-actin and cadherin (green), nuclei (blue). Scale bar: 20 μm.

After confirming the successful production of an integral monolayer of HBMEC on

the Transwell inserts, a transcytosis assay was performed to study the kinetics of the

114

bacterial traversal of HBMEC. After the TEER reading of HBMEC on Transwell insert reached at least 20 Ωcm^2, cells were infected with approximately 1 x 10^8 cfu/ml of either K1 or K-12. Samples of media were taken from the basolateral compartment at the indicated times, and these were serially diluted before being plated on LB agar plates to enable bacterial growth and quantification. K1 were detected in the basolateral compartment at 8 hours post-infection (Figure 3.12), while K-12 were absent at all the time intervals studied. These results clearly demonstrate that the non-pathogenic *E. coli* K-12 are unable to traverse HBMEC, while *E. coli* K1 are able to invade and subsequently traverse HBMEC.
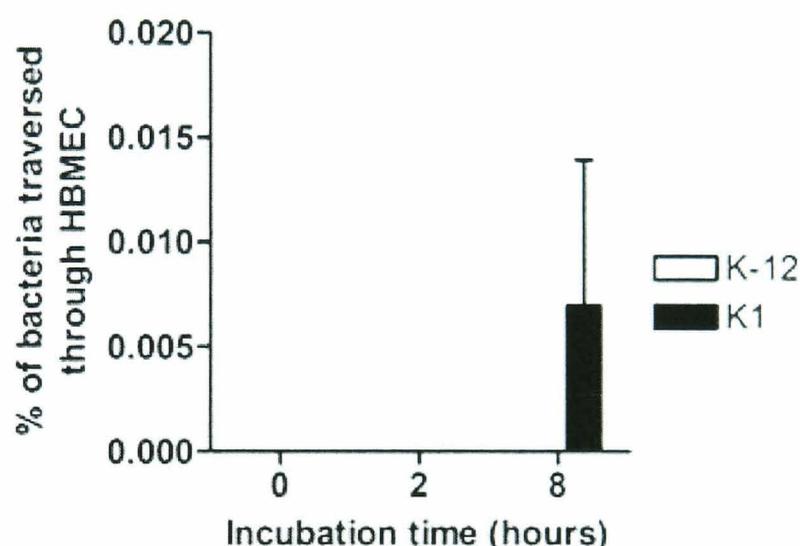
Figure 3.12. Transcytosis of *E. coli* K1 and K-12 through HBMEC. To study the bacterial transcytosis kinetics, HBMEC on Transwell membranes were incubated with approximately 1 x 10^8 cfu/ml of either *E. coli* K1 or K-12. Media were sampled from the basolateral chamber at the indicated time intervals. The result represents the percentages of bacteria traversed through HBMEC. Results are from one representative experiment of three independent repeats performed in triplicate and presented as mean of triplicates ± SD.

3.3.2.1 K1-Cherry transcytosis of HBMEC

Although K1-Cherry had been shown to retain the ability to invade HBMEC at the similar efficiency as the native K1 (Figure 3.9), the transformed bacteria further had to retain the ability to traverse an HBMEC monolayer grown on Transwell filter inserts. To determine whether the mCherry expression affected the ability of K1 to traverse HBMEC, a transcytosis assay was performed by co-infecting HBMEC cultured on Transwell filter

inserts with either *E. coli* K1 and K-12, or K1-Cherry and K-12 (Figure 3.13). As shown in Figure 3.12, K-12 did not traverse HBMEC monolayer on Transwell insert, therefore, K-12 were used as an indicator of the monolayer's integrity, and K-12 could be differentiated from K1 or K1-Cherry by the distinct small dark pink colony on MacConkey agar, while K1 and K1-Cherry appear as big white or light pink colony on MacConkey agar.

HBMEC monolayers on Transwell filter inserts were incubated with approximately 1×10^8 cfu/ml of each bacterial strain. Media from the basolateral compartment was collected at various time intervals, and the serially diluted specimens were plated on MacConkey agar. At 8 hours, *E. coli* K1 was detected in the basolateral compartment, and the percentages of the bacteria that traversed the HBMEC monolayer increased significantly from 0.25% at 8 hours to 77.42% at 12 hours post-infection (Figure 3.13A). The absence of *E. coli* K-12 at both intervals indicated that the HBMEC monolayer remained intact during the infection. In contrast, during K1-Cherry co-infection with K-12, K-12 were detected in the basolateral compartment after 12 hours (Figure 3.13B). The percentages of K1-Cherry traversed HBMEC were 0.54% at 8 hours and increased to 40% after 12 hours infection.

In conclusion, although K1-Cherry was able to invade HBMEC as efficiently as native K1, K1-Cherry affects HBMEC monolayer integrity, possibly by deforming the intercellular tight junctions. Therefore, K1-Cherry was suitable for further imaging experiments but not as appropriate for bacterial transcytosis studies.
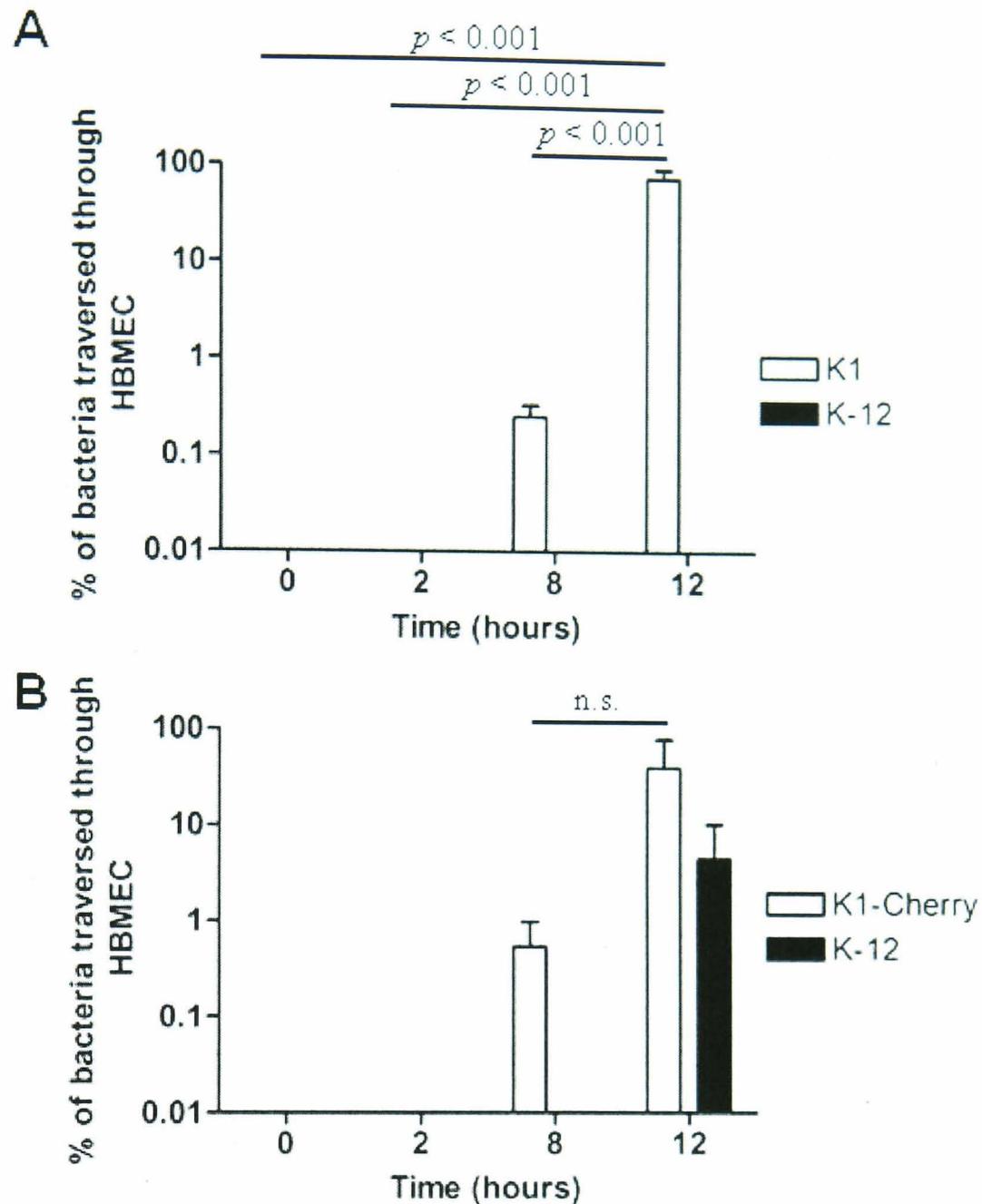
Figure 3.13. Transcytosis of *E. coli* K1 expressing mCherry through HBMEC. To determine the virulence of the K1-Cherry, transcytosis assays were performed by incubating HBMEC with either K1 and K-12 (A) or K1-Cherry and K-12 (B) with approximately 1×10^8 cfu/ml of each bacterial strain. At the time intervals indicated, media were sampled, and plated on MacConkey agar. The results represent the percentages of bacteria traversed through HBMEC. Results are from one representative experiment of two independent repeats performed in triplicate and presented as mean of triplicates ± SD.

3.4 Discussion

The major objective of this study was to construct a fluorescent *E. coli* K1 strain that retains the bacterial virulence trait. To assess the virulence of the fluorescent bacterial strains, an *Acanthamoeba* phagocytosis assay and HBMEC invasion assay were initially employed (data not shown). After various attempts, one of the constructs, pFPV25.1, which contains *E. coli* codon-optimised *gfp* gene fused downstream of a *S. Typhimurium* promoter, *rpsM*, retained bacterial invasiveness. Interestingly, the replacement of *gfp* gene

117

with a mammalian codon optimised *mCherry* gene in pFPV25.1 seemed to have no detrimental effect on the bacterial invasiveness, although the intracellular growth of K1-Cherry in comparison to untransformed K1 is not known.

To enable the application of confocal microscopy imaging for studying *E. coli* K1 interactions with various cellular markers, particularly as the majority of the available mammalian expression constructs encode GFP chimaeric proteins, an *E. coli* K1 strain expressing mCherry was constructed. mCherry was chosen for the fluorescent protein's photostability and brightness (Shaner *et al.*, 2005). Further, mCherry is expressed as a monomer, which avoids the potential formation of toxic aggregates in the bacteria as observed in some dimeric or tetrameric fluorescent proteins, such as DsRed, and tdTomato (Shaner *et al.*, 2004; Shaner *et al.*, 2005). mCherry also offers a potential advantage over other fluorescent proteins, as mCherry expression and fluorescence in *M. tuberculosis* was not affected by hypoxic conditions (Carroll *et al.*, 2010). The long excitation wavelength of mCherry also reduces the phototoxicity effect on live cells, and allows live-cell imaging of the infection (Tsien, 1998). Furthermore, mCherry-expressing *E. coli* K1 also provide a tool for future deep tissue *in vivo* imaging experiments, as the long excitation wavelength is able to penetrate tissue efficiently (Carroll *et al.*, 2010).

Previously, an *E. coli* K1 strain expressing GFP was used to study bacterial interaction with vimentin in HBMEC, but the authors did not demonstrate the virulence of the transformed strain (Chi *et al.*, 2010). Several studies have shown that the production of fluorescent protein and/or the presence of plasmid DNA in *Salmonella enterica* abrogates bacterial virulence in both epithelial and macrophage cell lines as well as *in vivo* (Knodler *et al.*, 2005; Clark *et al.*, 2009). In this study, although the growth kinetics of the fluorescent protein-expressing bacteria are slightly lower than the growth kinetics of the native *E. coli* K1, we found no evidence of correlation in the abrogation of the bacterial virulence and fluorescent protein expression, as bacteria harbouring a promoterless

plasmid DNA, which did not express fluorescent protein, also demonstrated a marginally decreased efficiency in HBMEC invasion. The reduction in the bacterial HBMEC invasion efficiency could be due to the metabolic burden caused by harbouring extra copies of plasmid in the bacteria. Interestingly, we found that expression of a mammalian codon optimised mCherry under the control of a *Salmonella* promoter, *rpsM*, did not affect the bacterial invasiveness. In fact, the bacteria invaded HBMEC as efficiently as the native bacteria; whereas a decrease in invasion efficiency was observed for *E. coli* K1 expressing an *E. coli*-codon optimised GFP under the control of *rpsM* (pFPV25.1).

Although we showed that mammalian codon-optimised mCherry did not affect the reporter's expression as well as virulence trait in *E. coli* K1, one of our preliminary data additionally observed that expression of *Mycobacterium* sp. (GC-rich organism) codon-optimised fluorescent proteins in both *E. coli* K1 and non-pathogenic *E. coli* K-12 affected the bacterial growth kinetics (data not shown). These fluorescent *E. coli* K1 strains further demonstrated distinct levels of virulence in two different cell types, in which the bacteria were able to infect and to survive in *Acanthamoeba*, which is an active phagocytic cell (data not shown); while they failed to invade non-phagocytic HBMEC. This observation suggests that expression of the *Mycobacterium* sp. codon-optimised fluorescent proteins in *E. coli* K1 might have affected the expression of a set of bacterial virulence factors, main factors essential for HBMEC invasion, but probably not the factors that are required for the bacterial intracellular survival. In order to further understand the effects of the expression of *Mycobacterium* sp. codon-optimised fluorescent proteins on the bacterial virulence factors expression, it would be important to study the expression and the form variations of the bacterial polysialic K1 capsule in both native and transformed bacterial strains, as well as the expression of some of the known bacterial virulence factors that are required for the bacteria adhesion and invasion of HBMEC, such as Type 1 fimbriae, OmpA, and Cnf1.

Additionally, several lines of evidence have demonstrated that the presence of a tetracycline resistance gene (tet^R), or chloramphenicol resistance gene (Cm^R), on a cloning vector might have an adverse effect on *Salmonella* survival in macrophages, and could impair the bacterial invasiveness of epithelial cells (Abromaitis *et al.*, 2005; Clark *et al.*, 2009). However, Clark *et al.* (2009) further demonstrated that the DNA copy number determined the outcome of fluorescent reporter expression in *Salmonella* virulence by showing that chromosomally-encoded GFP, also carrying a Cm^R gene, did not affect *Salmonella* invasion. In this study, there was no direct evidence on the correlation of gene copy number and the transformed bacterial virulence, but plasmid copy number might contribute to the loss of virulent traits in transformed *E. coli* K1 which would need to be tested against chromosomal integration. However, the major hindrance for stably integrating fluorescent protein gene into the *E. coli* K1 genome is the lack of access to the bacterial genome data in public databases, although the findings from the sequencing projects have been published (Xie *et al.*, 2006).

Another risk of having a bacterial strain harbouring a fluorescent reporter construct is the stability of the construct in the bacteria. It was shown that plasmids expressing fluorescent proteins from the *Mycobacterium bovis hsp60* promoter were unstable in *Mycobacterium smegmatis* (Carroll *et al.*, 2010). In this study, it was observed that all K1-Cherry expressed mCherry when the bacteria were cultured for 2 hours without antibiotic selection (data not shown) and upon cell infection (see Chapter 6), bacteria maintained fluorescence for 20 hours or more without antibiotic selection, which suggested that the pFPV-mCherry construct was stably maintained in K1-Cherry.

In this study, the HBMEC demonstrated lower TEER than the TEER reported by Stins *et al.* (2001), as well as the TEER measurement for other immortalized HBMEC, HCMEC/D3, which ranged from 60 to 80 Ωcm^2 (Weksler *et al.*, 2005; Cucullo *et al.*, 2008). The low TEER detected in our system might indicate an inability of these cells to

form a tight monolayer on the Transwell® membrane. Alternatively, the low TEER might be caused by the presence of FBS in the medium during TEER measurement. It has been previously reported that primary brain endothelial cells (PBEC) were less permeable to sucrose under FBS-free condition, and it was also evidenced by an increase in the TEER reading in that experimental condition (Franke et al., 2000). It was also speculated that the content of growth factors in the growth medium used for cell maintainence might also affect the tight junctional proteins expression of these cells, hence, different TEER was observed from Stins et al. (2001). The reduction in FITC-dextran and the non-invasive E. coli K-12 translocation in transwells with hydrocortisone-stimulated HBMEC, in combination with the distribution of cadherin and actin suggest that the cells are capable of forming intercellular interactions. However, the expression of several other major tight junctional proteins, such as claudin-5, occludin, ZO-1, and JAM-A, need to be studied, to further characterize the tight junction phenotype of the HBMEC.

Despite the low TEER of the HBMEC on Transwell, it was demonstrated that E. coli K1, but not non-pathogenic E. coli K-12, could traverse HBMEC monolayer cultured on Transwell insert (Figure 3.12). The result from this study also confirmed the published result by Stins et al. 2001, whereby we demonstrated that the HBMEC monolayer on Transwell insert remained intact during the bacterial infection, as E. coli K-12 was absent in the basolateral compartment of the Transwell filter insert when co-infection of both E. coli K1 and K-12 was performed. Although E. coli K1 expressing mCherry (K1-Cherry) were shown to retain the ability to invade HBMEC, the presence of non-pathogenic E. coli K-12 in the basolateral compartment at late time point of K1-Cherry and K-12 co-infection of the HBMEC monolayer on Transwell filter insert might suggest the leakage of the monolayer. Immunofluorescent staining of the K1-Cherry infected HBMEC on Transwell membrane with either fluorophore conjugated-phalloidin (for F-actin) or specific tight junction antibodies, such as occludin, and claudin 5, might be able to confirm the observed

results. F-actin co-localizes with tight junction proteins in intact polarized epithelium and endothelium, and the staining also allows detection of the presence of an intercellular gap, which is an indicator of permeable tissue monolayer (Martins-Green et al., 2008). It might also be interesting to study the bacterial factors that are affected by the fluorescent protein expression, which led to the change in bacterial virulence and disruption of HBMEC monolayer integrity during infection.

The negative effect of the K1-Cherry on the HBMEC monolayer in the Transwell insert was a disappointing discovery. Despite this effect, the fluorescent bacteria were still considered to be a useful tool for studying HBMEC invasion in this study. Alternative approaches include the application of PK1A-GFP and E. coli K1 specific antibody to label the bacteria along with antibodies to cellular markers; however, these methods come with their own caveats. Essentially, access to E. coli K1-specific and certain cell marker antibodies was limited; as such GFP-tagged cellular markers were the primary tool for studying intracellular markers that E. coli K1 may interact with. Although an alternative non-antibody E. coli K1 probe, the endosialidase-GFP probe (PK1A-GFP), was available, the application of this probe in studying the bacteria interaction with various GFP-tagged cellular markers would require changing the GFP tag of the cellular proteins to red fluorescent protein (RFP), which frequently changes the conformation of cytosolic protein (Ward, T., personal communication), and the functionality of each construct would thus need to be validated before use. Also, the application of PK1A-GFP and E. coli K1-specific antibody for the bacterial staining only works in fixed tissue, but fixation (as well as the application of detergent for cell permeabilization) of GFP-tagged cytosolic and membrane proteins often results with redistribution of the proteins (Tanaka et al., 2010; Schnell et al., 2012). On the other hand, labelling of the bacteria with fluorescent dye was not considered, as one of the preliminary data showed that FITC-labelled, and the labelling buffer-exposed E. coli K1 demonstrated lower invasion of HBMEC than that of untreated

E. coli K1 (data not shown). Similar observation was made in *Mycobacterium tuberculosis* study (Schaible, U., personal communication). Therefore, the availability of K1-Cherry allows live-cell imaging of infected HBMEC overexpressing GFP-tagged cellular markers. Although some caution is needed with the results obtained from this system, important results could be further verified with the use of untransformed bacteria in a fixed tissue system if time and antibody availability allowed.

In conclusion, the level of bacterial virulence can be affected by the presence of plasmids, and cytoplasmic production of fluorescent proteins. An mCherry-expressing *E. coli* K1 strain that retains bacterial invasiveness was successfully constructed in this study and this can therefore be used in future live-cell imaging experiments for studying the bacterial invasion of HBMEC.

4. Optimization of HBMEC transfection efficiency

4.1 Introduction

Genetic materials (such as DNA, RNA, and siRNA) can be delivered into eukaryotic cell via chemical, lipid, physical, or viral vector-mediated methods (Kingston, 2001). The availability of these gene delivery technologies allows the study of a gene function and expression in a cell (Hawley-Nelson *et al.*, 2008). The technology also allows production of correctly folded protein, especially for proteins that require special post-translational modification, such as glycoprotein, for structural studies or as a therapeutic or diagnostic agent (Chan *et al.*, 2002; Bowden *et al.*, 2008).

Viral vectors, such as retroviral, adenoviral, and baculoviral systems, usually give promising cell transduction efficiency (Kingston, 2001). However, for infection study, the major concern with this transfection approach is the potential cellular changes resulting from viral vector-uptake on bacterial infection of the transduced cells.

Several common non-viral vector transfection approaches, such as calcium phosphate transfection, liposome-mediated transfection, and electroporation, offer alternative approaches for introducing genetic material into mammalian cells. For calcium phosphate-, and liposome-mediated transfection, negatively charged DNA is bound to the positively charged surface of calcium, or cationic lipid. Following the attachment of calcium-DNA or lipid-DNA complexes on the cell surface, uptake of the complex is triggered via uncharacterized pathways (Kingston, 2001; Kingston *et al.*, 2003; Hawley-Nelson *et al.*, 2008).

Electroporation uses an electric field to open up micro-sized pores transiently in the plasma membrane to allow diffusion of macromolecules, such as DNA, into the cells. This approach is applicable to all cell types under optimized experimental settings (Potter, 2003). In the past decade, eukaryotic cell electroporation (particularly specific 'difficult' or

primary cell types) has been further improved by the introduction of Nucleofection technology (Lonza, Germany), which involves electroporating cells under optimized electroporation conditions in special proprietary buffers. The technology offers greatly improved transfection efficiency and cell viability to various generic cell lines and primary cells. Endothelial cells, which are notoriously difficult to transfect, have also benefited from this technology (Doulet *et al.*, 2006; Lui-Roberts *et al.*, 2008; Kang *et al.*, 2009).

In previous studies, Lipofectamine™ 2000 was used for transfecting plasmid DNA into HBMEC, and transfected cells were treated with antibiotic for stable clone selection (Khan *et al.*, 2002; Sukumaran and Prasadarao, 2002; Sukumaran *et al.*, 2002; Rudrabhatla *et al.*, 2006). Although stable transfection offers 100% of the selected cells expressing the exogenous protein of interest, the efficiency of the gene incorporation into the genome is low, and typically require 2 – 3 months to generate a stable cell line. One part of this study involved the application of a collection of GFP tagged cellular markers and their mutant forms to screen for their effects on *E. coli* K1 invasion and intracellular survival in HBMEC. Hence, it is practically unfeasible to generate stable cell lines for all constructs used within the limited time of this study. Further, the majority of constructs used code for peripheral membrane proteins (for example Rab GTPases), which are poorly expressed in stable cells (Ward, personal communication). Therefore, a transient transfection protocol that provides high transfection efficiency is required for this study.

4.2 Objectives and aims

The aim of this chapter was to optimise HBMEC transfection efficiency, with the specific objectives being:

- To optimise nucleofection parameters with Amaxa® Nucleofector® Kit.
- To optimise HBMEC transfection efficiency with different liposomal and non-liposomal based transfection reagents.

4.3 Results

4.3.1 Plasmid DNA transfection with Amaxa Nucleofection kit

Using human umbilical vein endothelial cells (HUVEC) specific Amaxa Nucleofection kit, plasmid DNA transfection rate up to 70% and siRNA transfection rate of 90% have been achieved for HUVEC (Cutler, personal communication; Lui-Roberts *et al.*, 2008). As recommended by the Cutler lab (MRC Laboratory for Molecular Cell Biology, UCL, London), two Amaxa Nucleofection kits, namely HUVEC Nucleofector® Kit-OLD (Old) and Amaxa® HUVEC Nucleofector® Kit (New), were tested for plasmid DNA nucleofection into HBMEC. For pmaxGFP nucleofection performed with New, two alternative nucleofection programs, U-001 and A-034, were applied as suggested by the manufacturer. GFP expression was screened with a confocal microscope at 24 and 48 hours post-nucleofection. The number of GFP-expressing cells and total number of cells in phase images were counted manually, and transfection efficiency was expressed as the percentage of GFP-expressing cells (Figure 4.1). At 24 and 48 hours post-nucleofection, the transfection efficiency was less than 20% for nucleofection performed with both kits (Figure 4.1A). Although nucleofection performed with New by applying program A-034 (New/A-034) gave lower transfection efficiency than the transfection efficiency for nucleofection performed with either Old, or with New by applying program U-001 (New/U-001), more cells were attached to coverslips, and fewer rounded cells were observed (data not shown). Therefore, nucleofection with New/A-034 was chosen for further optimizing nucleofection conditions by altering concentration of pmaxGFP (Figure 4.1B). HBMEC nucleofection with 5µg plasmid DNA successfully brought up the transfection efficiency to approximately a fold higher than the transfection efficiency for nucleofection with 2µg of plasmid DNA, although no difference was observed in the transfection efficiency at both time points.

126
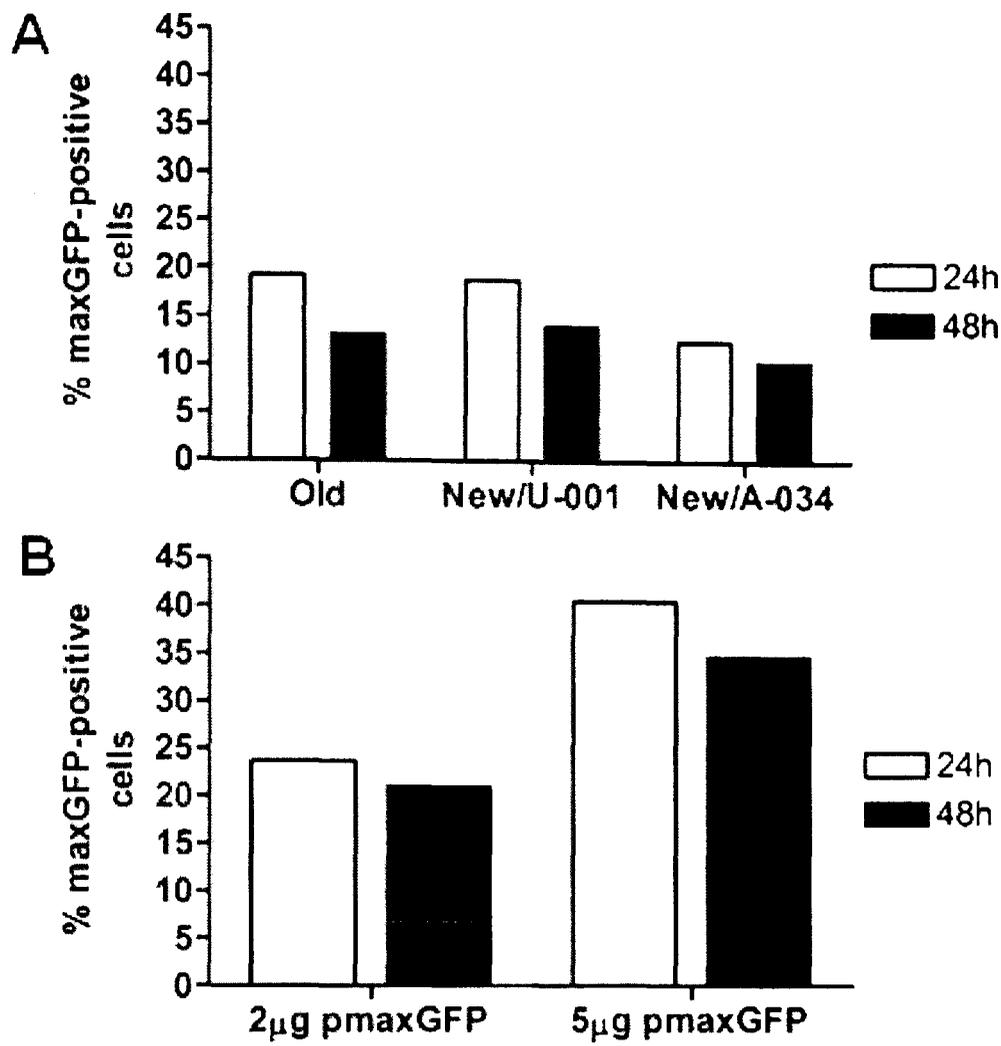
Figure 4.1. Optimization of HBMEC transfection with Amaxa Nucleofector kit. (A) To optimize plasmid DNA nucleofection of HBMEC, HBMEC were nucleofected with 2 μg pmaxGFP by either HUVEC Nucleofector® Kit-OLD (program U-001) (Old) or Amaxa® HUVEC Nucleofector® Kit [program U-001 (New/U-001) or A-034 (New/A-034)]. pmaxGFP expression was assessed and imaged with a confocal microscope 24 and 48 hours after nucleofection. Transfection efficiency is expressed as a percentage of maxGFP-expressing cells over total number of cells. Results are from one experiment. (B) Optimization of New/A-034 was performed by nucleofecting HBMEC with either 2 μg or 5 μg pmaxGFP, and transfection efficiency was assessed after 24 and 48 hours. Transfection efficiency is expressed as a percentage of maxGFP-expressing cells over total number of cells. Results are from one experiment.

Nucleofection with PBS was tried as described by Kang *et al.* (2009), which claimed high transfection efficiency in arterial and venous endothelial cells, but resulted with no transfected cells. The cost of a nucleofection kit is high, but the transfection efficiency of HBMEC was generally unsatisfactory with no more than 80% efficiency which would be very difficult for screening purposes, hence alternative transfection reagents were tried.

4.3.2 Plasmid DNA transfection with liposomal- and non-liposomal-based transfection reagents

In the majority of previous studies, Lipofectamine™ has been widely used for transfecting plasmid DNA into HBMEC (Reddy *et al.*, 2000a; Sukumaran *et al.*, 2002; Prasadarao *et al.*, 2003; Sissons *et al.*, 2005). Therefore, different transfection conditions with Lipofectamine™ LTX was applied to HBMEC with different concentrations of pN1-EGFP with or without PLUS reagent in Opti-MEM® reduced serum medium. To avoid experimental bias, tiled images were acquired with a confocal microscope 24 and 48 hours post-transfection. The number of GFP-expressing cells and total number of cells in phase images were counted manually, and transfection efficiency was expressed as the percentage of GFP-expressing cells (Figure 4.2). There was no difference observed in the transfection efficiency between 500 ng and 1000 ng of plasmid DNA used at both time points. However, the application of PLUS reagent in transfection reactions improved the transfection efficiency by at least a fold for both plasmid DNA concentration at both time points. The results show that plasmid DNA can be transfected into HBMEC by Lipofectamine™ LTX, and the transfection efficiency is improved by PLUS reagent to approximately 30%, although this level of transfection efficiency was still unsatisfactory for screening purposes.
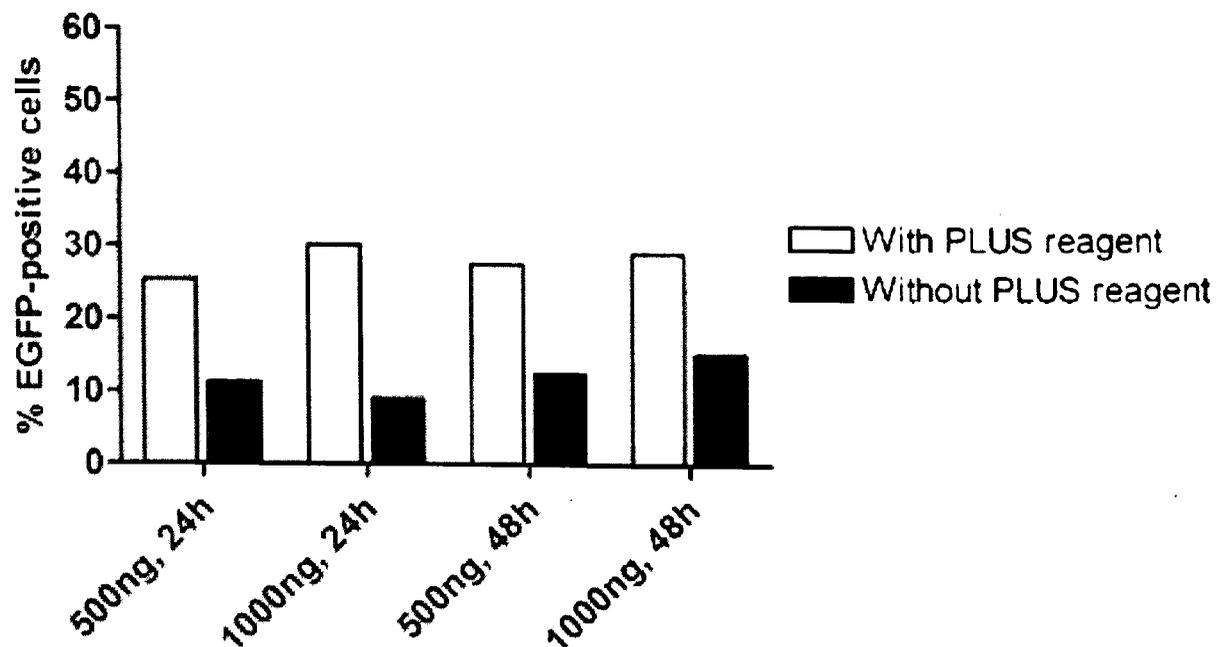
Figure 4.2. The effect of PLUS reagent on HBMEC transfection efficiency. To optimize plasmid DNA transfection of HBMEC with Lipofectamine™ LTX, HBMEC were incubated with either 500 ng or 1000 ng of pN1-EGFP-lipid complex in the presence or absence of PLUS reagent. EGFP expression was assessed and tile images were taken with a confocal microscope 24 and 48 hours after transfection. Transfection efficiency is expressed as a percentage of EGFP-expressing cells over total number of cells. The results represent the percentage of EGFP-positive HBMEC. Results are from one experiment.

In the attempt to optimize HBMEC transfection efficiency, various lipid-based and cationic polymers proprietary transfection reagents were applied for transfecting pN1-EGFP into HBMEC (Figure 4.3A). 24 hours post-transfection, the general transfection efficiency for all transfection reagents was below 30%, and the lowest transfection efficiency, below 10%, was obtained for transfection performed with FuGENE® HD. However, for transfection performed with jetPRIME™, HBMEC transfection efficiency was increased significantly to approximately 50% when 1 µg of plasmid DNA and 2 µl of jetPRIME™ were employed (Figure 4.3A). Western blotting confirmed an increase in the GFP protein levels for transfection performed with 1 µg of plasmid DNA and 2 µl of jetPRIME™ compared to the other transfection methods (Figure 4.3B). Some rounded cells, presumably dead cells, were frequently observed (data not shown). In conclusion, HBMEC transient transfection efficiency was significantly improved by increasing plasmid DNA concentration and volume of jetPRIME™ in the transfection mixture.
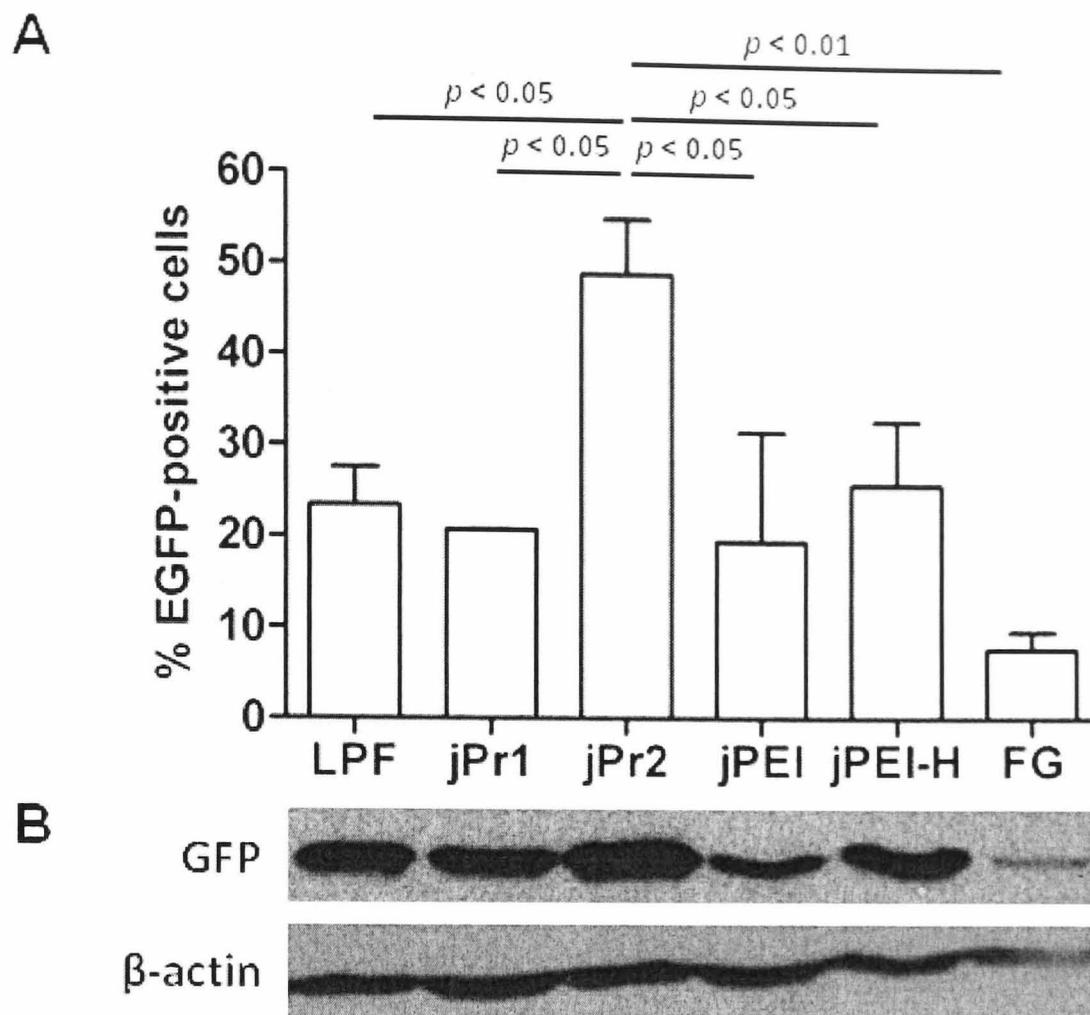
Figure 4.3. Optimization of HBMEC transfection using different transfection reagents. (A) HBMEC cells were transfected with pN1-EGFP using different transfectants. LPF, Lipofectamine™ LTX and PLUS™ reagent with 0.5 μg plasmid DNA; jPr1, 1 μl jetPRIME™ with 0.5 μg plasmid DNA; jPr2, 2 μl jetPRIME™ with 1 μg plasmid DNA; jPEI, jetPEI™ with 1 μg plasmid DNA; jPEI-H, jetPEI™-HUVEC with 2 μg plasmid DNA; FG, FuGENE® HD with 0.5 μg plasmid DNA. 24 hours post-transfection, GFP expression was assessed by acquiring tiled images with a confocal microscope. Transfection efficiency is expressed as a percentage of EGFP-expressing cells over total number of cells. Results are representative of two independent experiments performed in duplicate and presented as mean ± standard deviation. Statistical significance was evaluated with analysis of variance and Newman-Keuls post hoc analysis. (B) Total GFP protein in the transfected cell lysate was determined by Westen blotting analysis, lanes equivalent to chart above.

4.4 Discussion

This study showed that HBMEC can be transfected with plasmid DNA using a Nucleofection kit, although the transfection efficiency was unsatisfactory for screening purposes. It was possibly due to the differences between HUVEC and HBMEC, as studies have reported the heterogeneity of different endothelial cells (Swerlick *et al.*, 1992; Salcedo *et al.*, 2000; Man *et al.*, 2008), and the heterogeneity of microvascular endothelial cells isolated from different anatomical sites (Invernici *et al.*, 2005; Lu *et al.*, 2007).

Hence, the optimized HUVEC nucleofection condition might not be suitable for HBMEC nucleofection, and the HBMEC nucleofection conditions would need extensive optimization.

As the cost for a nucleofection kit is high, but with low efficiency, alternative transfection reagents were explored. Plasmid DNA could be transfected into HBMEC by Lipofectamine™ LTX, and the transfection efficiency was improved by pre-complexing plasmid DNA with PLUS reagent before the addition of Lipofectamine™ reagent. The best transfection efficiency obtained from transfection performed with liposomal-based transfection reagents (Lipofectamine™ LTX, and FuGENE® HD) was approximately 30%. In addition to liposomal-based transfection reagents, cationic polymer (non-liposomal) transfection reagents, including jetPRIME™, jetPEI™, and jetPEI™-HUVEC, were applied. Among these transfection reagents, HBMEC transfection efficiency was significantly increased to approximately 50% by altering plasmid DNA : jetPRIME™ ratios. As observed with HUVEC specific Amaxa Nucleofection kits, the HBMEC transfection efficiency achieved with HUVEC specific jetPEI, jetPEI™-HUVEC, was less satisfactory, probably due to the differences between HUVEC and HBMEC, as discussed above. Despite the significant improvement in the HBMEC transfection efficiency as observed from EGFP expression in pN1-EGFP transfection with jetPRIME™, the transfection efficiency was found to vary for different recombinant constructs used later in the study, presumably due to effects of exogenous protein expression in cells.

Viral vectors offer another approach for introducing genetic materials into cells with generally high transduction efficiency. Most of these viral vectors enter into cells via a receptor-specific endocytic pathway, and some of these vectors, especially those originated from retroviruses, stably integrate the transferred gene into the genome of the transduced cells (Ramezani and Hawley, 2002; Lindemann and Schnittler, 2009). In general, viral vector transduction yields high transduction efficiency in most cell lines:

however, the transduction efficiency for endothelial cells varies from 40 – 90% (Shichinohe *et al.*, 2001; Cefai *et al.*, 2005; Anliker *et al.*, 2010). Interestingly, Anliker *et al.* (2010) constructed measles viral haemagglutinin-pseudotyped lentiviral vectors based on single-chain antibodies recognizing cell-surface antigens, which specifically targeted endothelial cells via CD105, a transmembrane glycoprotein predominantly expressed on endothelial cells (Fonsatti and Maio, 2004). The CD105-targeted viral vector resulted in transduction efficiency of HUVEC of approximately 80%, while the transduction efficiency of human dermal microvascular endothelial cells (HDMEC) was 60.5% (Anliker *et al.*, 2010). This finding further demonstrated the differences of HUVEC from other sources of endothelial cells. Despite the endothelial cells variations, pseudotyped lentiviral vectors might be useful in improving HBMEC transfection efficiency. The major concern for this approach is the triggering of inflammatory responses after exposing the cells with viral vectors, which might affect the transduced cells responses to *E. coli* K1 infection.

Although common routine transfection methods are used for *in vitro* studies, researchers in the field of drug or gene delivery have strong interests in developing non-viral-based nano-sized delivery vehicles for efficient delivery into vessels and blood-brain barrier endothelial cells (Dufes *et al.*, 2004; Zhang *et al.*, 2009; Georgieva *et al.*, 2011; Liu *et al.*, 2011). In the efforts of developing delivery vehicles, various transfection methods have been developed, such as a peptide based delivery system targeting caveolae-mediated endocytosis (Liu *et al.*, 2011), glucose-bearing delivery vesicle (Dufes *et al.*, 2004), and DNA intercalating conjugates with a short nuclear localization signal (NLS) peptide (Zhang *et al.*, 2009). However, the transfection efficiency of these alternative vectors remains unsatisfactory for clinical treatment.

5. *E. coli* K1 invasion of human brain microvascular endothelial cells via a caveolae-, flotillin 1-, and dynamin-independent pathway

5.1 Introduction

Phagocytosis is a process that involves internalization of large particles into specialized cells such as phagocytic protozoa, and phagocytic leukocytes of the immune system. It functions to clear pathogens, such as bacteria or yeast, apoptotic cells, and cell debris (Conner and Schmid, 2003), although some pathogens can piggyback on the phagocytic process and then create a propagatory intracellular niche. The process is an active and regulated process involving specific cell surface receptors and signalling cascades that regulate actin cytoskeleton rearrangement (Conner and Schmid, 2003; Kumari *et al.*, 2010).

As with phagocytic cells, non-phagocytic cells are able to take up fluid and small molecules via pinocytosis, such as clathrin-mediated endocytosis, caveolae-mediated endocytosis, and flotillin-mediated endocytosis, which are classified by the requirement of dynamin during vesicle scission at the plasma membrane (Conner and Schmid, 2003; Doherty and McMahon, 2009). Pathogenic bacteria have also been demonstrated to gain entry into non-phagocytic cells via these endocytic pathways, in addition to the classical classification of bacterial entry based on trigger and zipper mechanisms (Finlay and Cossart, 1997; Cossart and Sansonetti, 2004). It was found that endocytic coats and accessory proteins are recruited during bacterial invasion of non-phagocytic cells via zipper mechanism, but are not recruited to those bacteria, such as *Salmonella enterica* Typhimurium, and *Shigella*, which trigger host entry by injecting bacterial effectors and lead to actin cytoskeleton rearrangement (Veiga *et al.*, 2007). The requirement of dynamin and examples of pathogens that utilise specific endocytic pathways for cell entry are summarized in Table 1.1.

Dynamin is a 100 kDa GTPase, which is able to form helical tubes on lipid nanotubes *in vitro* (Sweitzer and Hinshaw, 1998: Stowell *et al.*, 1999). and assemble at the neck of an endocytic vesicle for vesicle scission (Iversen *et al.*, 2003). In mammalian cells, there are three closely related dynamin isoforms identified. Dynamin 1 (Dyn1) is found specifically in neuronal tissue (Scaife and Margolis, 1990; Sontag *et al.*, 1994), and there are eight splice variants identified (Cao *et al.*, 1998); whereas dynamin 2 (Dyn2), which has four splice variants, is ubiquitously expressed (Nakata *et al.*, 1993; Cook *et al.*, 1994: Sontag *et al.*, 1994; Cao *et al.*, 1998). Dynamin 3 (Dyn3) is expressed predominantly in testes, brain, lung and heart, and has 13 splice variants (Nakata *et al.*, 1993; Cao *et al.*, 1998). It was shown that each splice variant of dynamin isoforms is targeted to distinct cellular locations in Clone 9 cells, a normal rat hepatocyte cell line (Cao *et al.*, 1998), and has different endocytic functions (Cao *et al.*, 2007). Interestingly, the functions of Dyn1 and Dyn2 are indistinguishable in non-polarized epitheloid cell line, HeLa; however, in polarized epithelial cell lines, such as MDCK, both dynamins have distinct endocytic functions at the different membrane surfaces (Altschuler *et al.*, 1998). The role of dynamin in endocytosis is often studied using either the chemical inhibitor Dynasore or overexpressing a mutant form of the dynamin protein. Overexpression of the K44A or S45N mutant, which demonstrates weak guanosine triphosphate (GTP) affinity *in vitro* and thus unable to release the endocytic vesicle from the plasma membrane, is sufficient to inhibit transferrin uptake via clathrin-mediated endocytosis as well as SV40 uptake via caveolae-mediated endocytosis (Marks *et al.*, 2001; Pelkmans *et al.*, 2002; Ferguson and De Camilli, 2012).

Caveolin-1 is a major protein in caveolae, and it has two isoforms, namely caveolin-1α (full length caveolin-1) and caveolin-1β (Parton and Simons, 2007: Parat, 2009). Caveolin-1β is a product of alternate translation, and it lacks 31 amino acids found at the N-terminal of caveolin-1α (Parat, 2009). It has also been proposed that caveolin-1β

is unable to form caveolae in the absence of caveolin-1α (Fujimoto *et al.*, 2000). Caveolin-1 is inserted into plasma membrane lipid bilayers in a wedge-like manner, with its N- and C-termini in the cytoplasm (Figure 1.6) (Parton, 2003). The protein is palmitoylated at the cysteine residue 133, 143, and 156 at the C termini (Dietzen *et al.*, 1995), which has been shown to be essential for cholesterol binding and chaperone complex formation for cholesterol transportation to caveolae, but it is not required for caveolin-1 localization to caveolae (Dietzen *et al.*, 1995; Uittenbogaard and Smart, 2000). The tyrosine residue 14 of caveolin-1 is phosphorylated by cellular Src tyrosine kinase (Li *et al.*, 1996). Abrogation of caveolin-1 phosphorylation by mutating this tyrosine residue to phenylalanine (Cav1 Y14F) might block the downstream effectors, and thus inhibits albumin uptake in rat lung microvascular endothelial cells (RLMEC) via caveolae-mediated endocytosis (Hu *et al.*, 2006). Expression of Cav1 Y14F mutant in caveolin-1 knockout cells also inhibited raft internalization although caveolae was formed on the plasma membrane, suggesting that the non-phosphorylatable caveolin-1 mutant is still recruited to the plasma membrane, but defective in internalisation (del Pozo *et al.*, 2005). As such, Cav Y14F mutant provides a useful tool in studying caveolin-mediated endocytosis.

In addition to clathrin-mediated endocytosis, which requires dynamin for vesicle scission from the plasma membrane, dynamin has also been implicated in caveolae-mediated endocytosis, whereby overexpression of GDP-locked dynamin K44A mutant inhibits caveolar budding and cholera toxin B (a ligand used for studying caveolae-mediated endocytosis) uptake in fibroblasts and endothelial cells (Oh *et al.*, 1998; Shajahan *et al.*, 2004; Yao *et al.*, 2005). The tyrosine residue 231 and 596 of Dyn2 are required for caveolin-1 binding; however, only overexpression of non-phosphorylatable Dyn2 Y597F mutant in rat lung microvascular endothelial cells successfully inhibit albumin and cholera toxin B uptake to the level observed in cells overexpressing the Dyn2 K44A mutant (Shajahan *et al.*, 2004).

There are a number of endocytic pathways that are independent of dynamin, including flotillin-mediated endocytosis (Glebov *et al.*, 2006), Arf6-mediated endocytosis (Donaldson *et al.*, 2009), and the CLIC/GEEC endocytosis pathway (Kumari *et al.*, 2008). These endocytic pathways are still not very well-studied and it is unclear how membrane scission on the plasma membrane occurs in these pathways in the absence of dynamin.

E. coli K1 invasion of HBMEC has been proposed to be receptor-dependent, via the zipper mechanism, where actin cytoskeleton rearrangement is induced upon bacterial surface antigen attachment to a specific receptor on the host cell surface (Prasadarao *et al.*, 1999). Numerous host cell receptors have been identified in parallel with the identification of bacterial virulence determinants required for host cell binding and invasion (Prasadarao, 2002; Chung *et al.*, 2003; Khan *et al.*, 2007). Upon *E. coli* K1 binding to a cell receptor on HBMEC surface, a cascade of signalling molecules as detailed in 1.6.1, such as the signal transducer and activator of transcription 3 (stat3), focal adhesion kinase (FAK), phosphatidylinositol-3-kinase (PI3K), and protein kinase Cα (PKCα), RhoA, are activated and results in actin polymerization, which leads to bacterial invasion into HBMEC (Prasadarao *et al.*, 1999; Reddy *et al.*, 2000a; Reddy *et al.*, 2000b; Prasadarao, 2002; Khan *et al.*, 2003; Maruvada *et al.*, 2008). It has been shown that the bacterial invasion of HBMEC is clathrin-independent (Prasadarao *et al.*, 1999), but may be caveolae-mediated (Sukumaran *et al.*, 2002). These authors also showed association of intracellular *E. coli* K1 with caveolin-1, and proposed that the caveolin-1 pathway was involved in bacterial transcytosis (Sukumaran *et al.*, 2002). The caveolae-mediated endocytosis pathway is thought to be dynamin-dependent *in vitro* and *in vivo* (Oh *et al.*, 1998; Pelkmans *et al.*, 2002; Yao *et al.*, 2005); however, the role of dynamin and the functional role of endocytic pathway during *E. coli* K1 invasion of HBMEC is not clear.

5.2 Objectives and aims

The aim of this chapter was to investigate the endocytic pathway used by *E. coli* K1 to invade HBMEC. The specific objectives are:

- To study the role of dynamin for *E. coli* K1 invasion of HBMEC.

- To study the requirement of caveolin-1 for *E. coli* K1 invasion of HBMEC.

- To study the requirement and the role of flotillin 1 for *E. coli* K1 invasion of HBMEC.

5.3 Results

5.3.1 *E. coli* K1 invasion of HBMEC is dynamin-independent

The caveolae-mediated endocytic pathway has previously been implicated in *E. coli* K1 invasion of HBMEC (Sukumaran *et al.*, 2002). The authors also reported association of intracellular *E. coli* K1 with caveolin-1, hence, they proposed that caveolin-1 was involved in the bacterial transcytosis. However, the authors did not investigate the involvement of dynamin, which has been found to be required in vesicle membrane fission in caveolae-mediated endocytosis both *in vitro* and *in vivo* (Oh *et al.*, 1998; Pelkmans *et al.*, 2002; Shajahan *et al.*, 2004; Yao *et al.*, 2005), during *E. coli* K1 invasion HBMEC.

Both Dyn1 and Dyn2 have been implicated in caveolae-mediated endocytosis (Oh *et al.*, 1998; Pelkmans *et al.*, 2002; Shajahan *et al.*, 2004; Yao *et al.*, 2005), but the majority of previous endothelial studies have focussed on Dyn2-dependent endocytic mechanisms as this isoform is ubiquitously expressed in mammalian tissues (Cook *et al.*, 1994), whereas Dyn1 is more usually associated with neuronal tissue. Therefore, Dyn2 was initially selected to study its role during *E. coli* K1 invasion of HBMEC. Among the four Dyn2 splice variants (Cao *et al.*, 1998), Dyn2(aa) and Dyn2(ab) have been shown to interact directly with caveolin-1 *in vitro* (Yao *et al.*, 2005), and overexpression of GDP-locked Dyn2(aa)K44A (also termed dominant negative) mutant has been shown to inhibit

cholera toxin B internalization into rat fibroblasts and endothelium (Shajahan *et al.*, 2004; Yao *et al.*, 2005). We hypothesized that overexpression of Dyn2(aa)K44A mutant would inhibit *E. coli* K1 invasion of HBMEC if the bacteria invaded HBMEC via a caveolae-mediated endocytic pathway. Dynasore, a cell-permeable inhibitor of Dyn1, Dyn2, and dynamin-related protein 1 (Drp1) (Macia *et al.*, 2006), was not applied as HBMEC used in this study are sensitive to a lot of chemical inhibitors (Kim, K.S., personal communication).

To study the role of dynamin during the bacterial invasion quantitatively, HBMEC were transiently transfected with GFP-tagged Dyn2 chimaera, either wild type or dominant negative [Dyn2(aa)K44A GFP]. LDLR A18 GFP, which expressed GFP-tagged recycling-deficient mutant of the low-density-lipoprotein receptor (LDLR) on the plasma membrane, was transfected into HBMEC as a transfection control. After 5 hours incubation of plasmid DNA-jetPRIME™ complex with HBMEC, media was removed and replenished with fresh media, and further incubated for approximately 16 hours. Cells were infected with K1-Cherry for 2 hours, incubated for 1 hour in media containing gentamicin to kill off extracellular bacteria and then imaged on the confocal microscope. Tiled z-stack confocal imaging was performed to acquire a large field and to minimise experimental bias, and GFP-expressing cells were manually scored for the presence of intracellular K1-Cherry (Figure 5.1A). The transfection efficiency of Dyn2(aa)WT, Dyn2(aa)K44A, and LDLR A18 GFP, was $19.5 \pm 1.6\%$, $19.1 \pm 2.8\%$, and $11.7 \pm 3.8\%$, respectively. Quantification of the infected GFP-expressing cells showed no inhibition in bacterial invasion in cells overexpressing Dyn2(aa)K44A GFP. In fact, there was a modest enhancement in *E. coli* K1 internalization into these cells compared to cells expressing wild type Dyn2, though it was not statistically significant.

As the endothelium specific dynamin isoform is unknown, the role of the neuronal specific Dyn1 on *E. coli* K1 invasion was studied in similar manner (Figure 5.1B). The

transfection efficiency of Dyn1WT, Dyn1K44A, and LDLR A18 GFP, was 41.4 ± 7.0%, 20.9 ± 6.0%, and 38.3 ± 3.9%, respectively. As with Dyn2, the bacterial entry was not inhibited in cells that overexpressed dominant negative Dyn1 (Dyn1K44A-GFP) and again there was a trend to a slight increase in bacterial uptake in mutant over wild type Dyn1 expression.
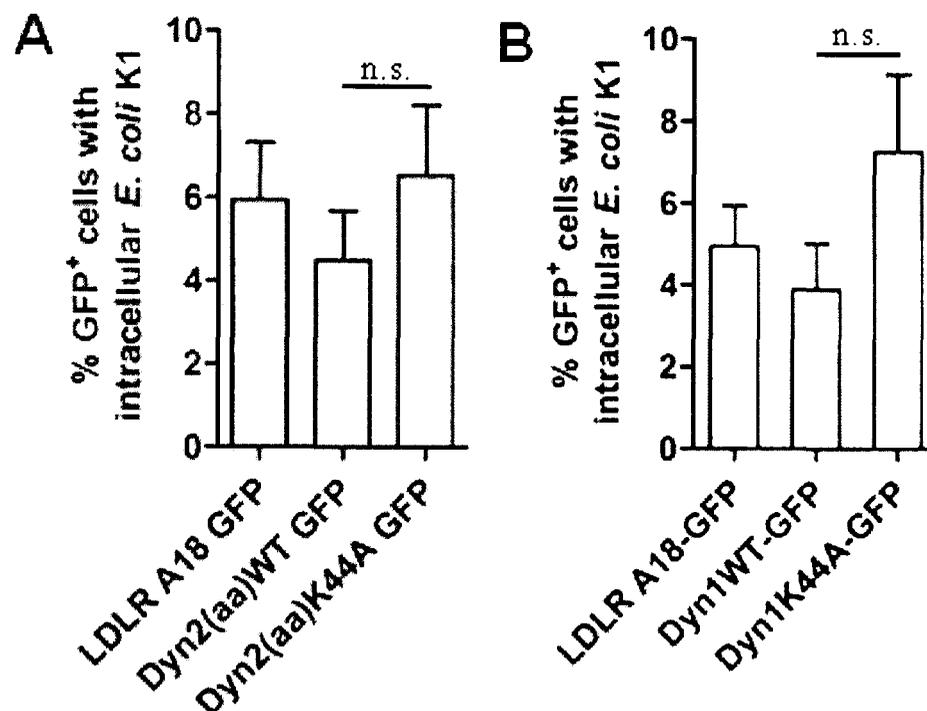
Figure 5.1. Overexpression of dominant negative dynamin 1 and 2 do not inhibit *E. coli* K1 invasion of HBMEC. (A) and (B) To study the requirement of dynamin during *E. coli* K1 invasion, HBMEC cells were transiently transfected with GFP tagged Dyn2 or Dyn1 chimaera: either wild type (WT), or dominant negative mutant (K44A). LDLR A18 GFP was transfection control. Cells were infected with K1-Cherry at MOI of 100 for 2 hours, followed by 1 hours incubation in gentamicin containing media, and processed for microscopy. GFP chimaera-expressing cells were scored for the presence of intracellular K1-Cherry. Data shown are the mean ± SEM from three independent experiments; at least 50 GFP-expressing cells were counted per sample.

5.3.2 *E. coli* K1 invasion of HBMEC is caveolin-1-independent

Caveolae-mediated endocytosis has been implicated to be dynamin-dependent (Oh *et al.*, 1998; Pelkmans *et al.*, 2002), however, the data above suggested that overexpression of dominant negative forms of both dynamin 1 and 2 did not inhibit *E. coli* K1 invasion of HBMEC. Hence, the requirement of caveolin-1 during *E. coli* K1 invasion of HBMEC was reassessed. To address the requirement of caveolin-1 during *E. coli* K1 invasion, HBMEC were infected with *E. coli* K1, fixed at various time points post infection, and

immunostained for caveolin-1. Caveolin-1 staining revealed bright punctate structures at the cell periphery and at the juxtanuclear position as well as in the cytoplasm (Figure 5.2A). After 30 minutes of infection, invading *E. coli* were found localized in compartments weakly stained for caveolin-1 (Figure 5.2A).
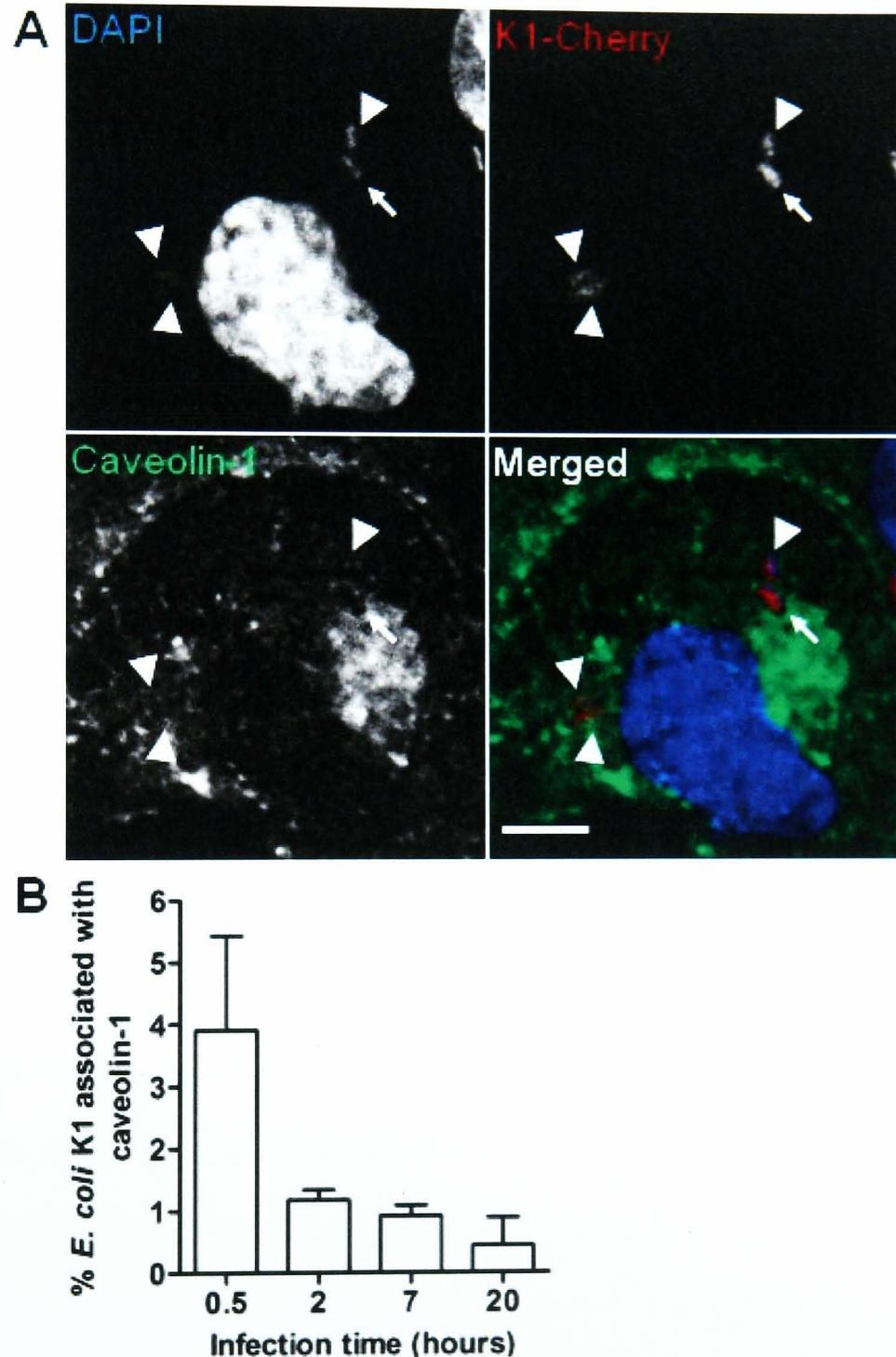
Figure 5.2. Association of *E. coli* K1 with caveolin-1 decreases over time of infection. (A) HBMEC were infected with K1-Cherry at MOI of 100 for 30 minutes, and fixed with 2% formaldehyde, and immunostained for caveolin-1. Caveolin-1 is shown in green, bacteria in red, nuclei in blue. The white arrow indicates bacterium localising with caveolin-1; white arrow heads indicate bacteria that do not localise with caveolin-1. A single confocal slice is shown. Scale bar: 5 μm. (B) Quantification of the observed phenotype in (A) at various times p.i. Data shown are the mean ± SEM from two independent experiments; ≥100 bacteria were counted per sample.

Quantification of the observed phenotype in Figure 5.2A showed that only about 4% of the bacteria were closely associated with caveolin-1 after 30 minutes infection, and the percentages reduced to about 1% and 0.5% at 2 and 20 hours post infection (p.i.). Therefore, association of *E. coli* K1 with caveolin-1 seemed to be a rare event which occurred at the early time point when the bacteria were invading the cell. This would therefore suggest that caveolae-mediated uptake is not a major route of invasion for *E. coli* K1 into HBMEC.

To further address the role of caveolin-1 during *E. coli* K1 uptake, various GFP-tagged caveolin-1 mutant constructs were applied. Caveolin-1 phosphorylation has been demonstrated to be required for albumin uptake via caveolae (Hu *et al.*, 2006), and overexpression of caveolin-1 Y14F phosphorylation mutant, which is unable to be phosphorylated by Src family protein kinases (Labrecque *et al.*, 2004), in COS-1 cells partially inhibits *Campylobacter jejuni* invasion (Watson and Galán, 2008). To study the effect of caveolin-1 tyrosine phosphorylation on *E. coli* K1 invasion, GFP-tagged caveolin-1 Y14A mutant (Caveolin-1 Tyr14. N.B. this mutant is also non-phosphorylatable) was transiently overexpressed in HBMEC, and the cells were then infected with K1-Cherry. Quantification of the infected GFP-expressing cells showed no inhibition in the bacterial internalization as compared to cells overexpressing wild type caveolin-1 (Caveolin-1 WT-GFP) (Figure 5.3). Similar results were seen by overexpressing the non-phosphorylatable isoform, caveolin-1β (Caveolin-1β-GFP), which lacks the 31 amino acids of the N-terminal of full length caveolin-1 (caveolin-1α) as a result of alternate initiation during translation.

Caveolin-1 is also post-translationally modified by palmitoylation at the three cysteine residues at the hydrophobic region at the C-terminal. Whilst this is not required for the plasma membrane localization of caveolin-1, it is required for transport of newly synthesized cholesterol to the plasma membrane (Dietzen *et al.*, 1995; Uittenbogaard and

Smart, 2000; Parat and Fox, 2001). Previous studies showed that depletion of cholesterol from HBMEC leads to reduction of *E. coli* K1 invasion (Sukumaran *et al.*, 2002; Chi *et al.*, 2010). We hypothesized that the lack of cholesterol on the plasma membrane that results from overexpression of a caveolin-1 mutant that cannot be palmitoylated is able to block *E. coli* K1 invasion of HBMEC if the bacterial entry is cholesterol dependent. To test this hypothesis, HBMEC were transfected with a GFP-tagged caveolin-1 palmitoylation mutant construct, in which the 133, 143, and 156 cysteine residues were mutated to serine (Caveolin-1 palm⁻) (Parat *et al.*, 2003), infected with K1-Cherry, and imaged 3 hours p.i. (Figure 5.3). Quantification of the number of infected GFP-expressing cells revealed no inhibitory effect of the mutant on *E. coli* K1 internalization. These cumulative results strongly indicated that in our infection model, caveolae are not used as a route of invasion for *E. coli* K1 into HBMEC.
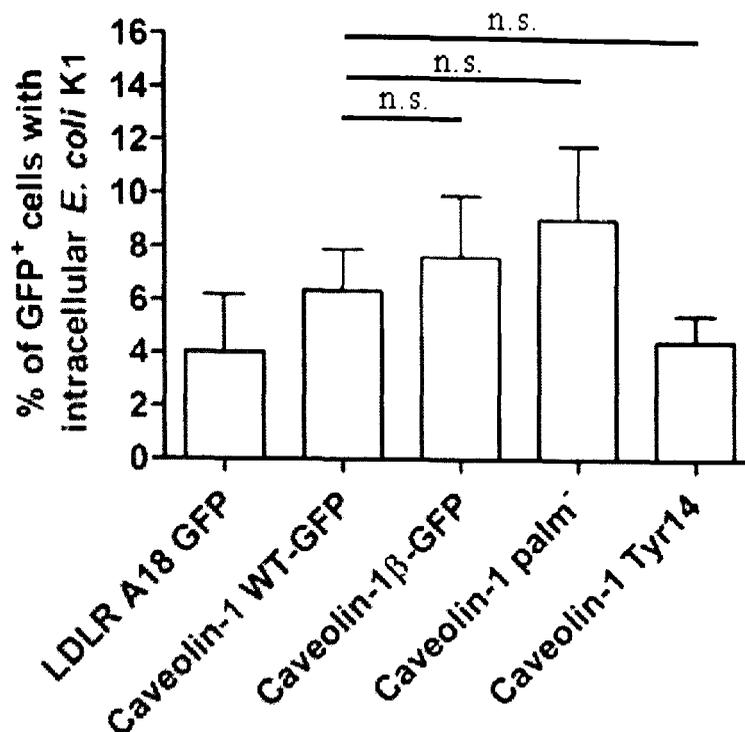
Figure 5.3. Overexpression of caveolin-1β isoform and caveolin-1 mutants do not affect *E. coli* K1 invasion of HBMEC. To study the effect of different caveolin-1 mutants and caveolin-1β isoform on *E. coli* K1 invasion of HBMEC, HBMEC were transiently transfected with GFP-tagged caveolin-1 chimaerae: either wild type (WT), caveolin-1β, palmitoylation mutant (palm⁻), or phosphorylation mutant (Tyr14) as indicated. Cells were infected with K1-Cherry at MOI of 100 and were imaged 3 hours p.i. Data shown are the mean ± SEM from two independent experiments; ≥100 GFP cells were counted per sample and experiment. LDLR A18 was used as transfection control. The transfection efficiency of each construct was: LDLR A18 GFP = 34.24 ± 8.8%; Caveolin-1 WT-GFP = 41.8 ± 13.9%; Caveolin-1β-GFP = 29.8 ± 10.3%; Caveolin-1 palm⁻ = 32.3 ± 12.1%; Caveolin-1 Tyr14 = 43.2 ± 5.8%.

To investigate this further, an invasion assay was performed with mouse lung endothelial cells (MLEC) isolated from wild type (WT) and caveolin-1 knockout (Cav1 K/O) mice and cultured as described. MLEC were used instead of brain microvascular endothelial cells (BMEC) due to the technical difficulty to isolate a sufficient quantity of BMEC from mice, and the difficulty in culturing them beyond a single passage (Liebner, S., personal communication). The results from the invasion assay performed in RPMI-1640 media showed that the number of recovered intracellular *E. coli* K1 per cell was approximately 40-fold higher than the number of recovered intracellular non-pathogenic *E. coli* K-12 per cell (Figure 5.4). This data indicated that MLEC could be used as an alternative *in vitro* model for studying *E. coli* K1 pathogenesis. When the invasion assay was performed with MLEC Cav1 K/O, *E. coli* K1 invasion of MLEC was not inhibited as

would be expected if caveolin were required for bacterial entry. However, the number of recovered intracellular *E. coli* K1 per cell was approximately 2-fold higher than the number of bacteria recovered from MLEC WT, although this observed increase in intracellular bacteria was not statistically significant, while there was no comparable increase in K12 uptake into MLEC Cav1 K/O cells. Overall, our data indicates that in our system *E. coli* K1 invasion of HBMEC is not dependent on caveolae-mediated endocytosis.
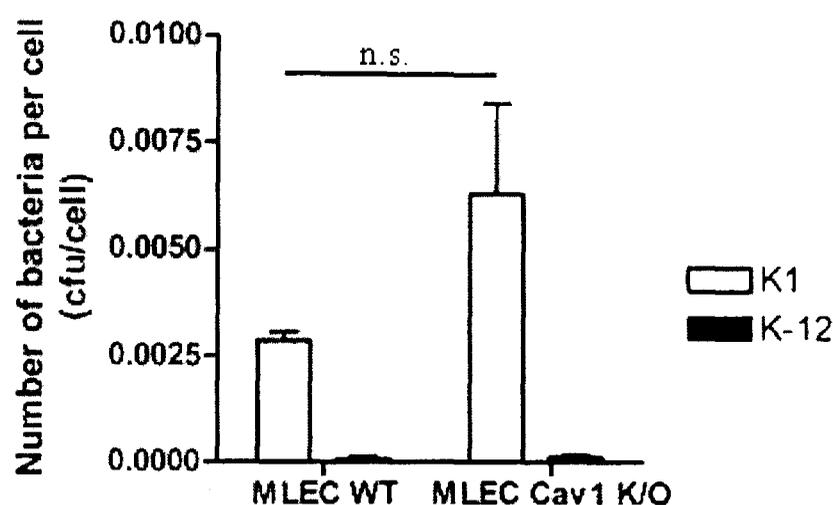
Figure 5.4. Caveolin-1 knockout does not inhibit *E. coli* K1 invasion of MLEC. To confirm the requirement of caveolin-1 during *E. coli* K1 invasion of endothelial cells, MLEC purified from wild type and caveolin-1 knockout mice were infected with either *E. coli* K1 or K-12 at MOI of 100 for 2 hours, followed by 30 minutes incubation in gentamicin containing media. The results represent the mean number of bacteria per cell. Results are from one representative experiment of three independent repeats performed in triplicate and presented as mean of triplicates ± SEM.

5.3.3 Flotillin 1 is recruited to invading and intracellular *E. coli* K1

All the evidence from this study suggested that *E. coli* K1 invasion of HBMEC is dynamin- and caveolae-independent. Therefore, other dynamin-independent endocytic pathways were explored. Cholesterol has been shown to be required for *E. coli* K1 invasion of HBMEC by treating the cells with chemical inhibitors, such as filipin, methyl-β-cyclodextrin, and nystatin (Sukumaran *et al.*, 2002; Chi *et al.*, 2010). We therefore investigated the potential role of flotillin 1, which is associated with cholesterol and lipid raft microdomains, and independent of dynamin, during *E. coli* K1 invasion. To address the involvement of flotillin 1 during *E. coli* K1 uptake, HBMEC were infected with *E. coli*

K1. Cells were fixed over a time course from 0.5 hours p.i. to overnight and differential bacterial staining was performed to discriminate between extra- and intracellular bacteria. Flotillin 1 staining revealed bright punctate structures at the cell periphery and in the cytoplasm (Figure 5.5A). After 30 minutes infection, flotillin 1 could be found concentrated at bacterial attachment sites; 2 hours post-infection, strong co-localization of flotillin 1 with intracellular bacteria were observed (Figure 5.5A). In Figure 5.5B, quantification of *E. coli* K1 association with flotillin 1 over time showed that the association of flotillin 1 with extracellular bacteria was approximately 5%, and the percentage decreased to about 1% by 2 hours. For the intracellular bacteria, the percentages of bacteria co-localized with flotillin 1 increased sharply from about 5% at 30 minutes after infection to approximately 30% after 2 hours infection, and this association remained fairly constant at later time points. In comparison, caveolin-1 associated *E. coli* K1 was 4% and 1% at 30 minutes and 2 hours p.i., respectively (Figure 5.2B). These results suggest that flotillin 1 might have a role during *E. coli* K1 invasion of HBMEC.
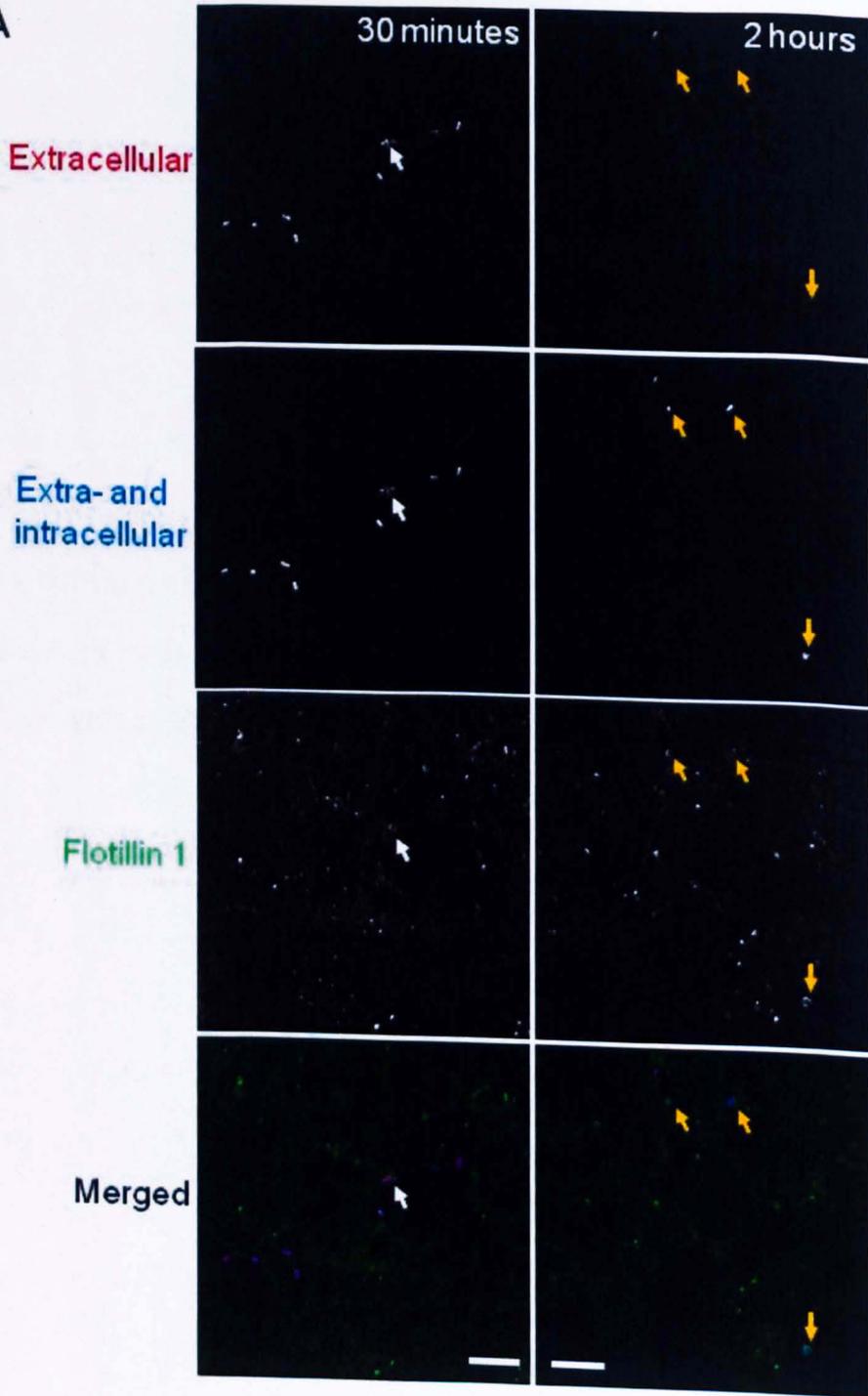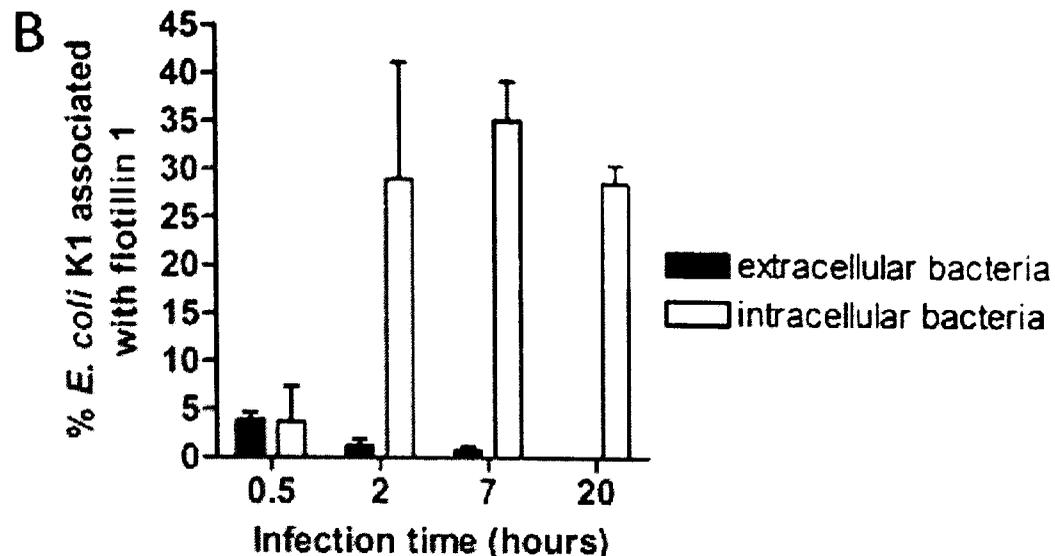
Figure 5.5. Association of flotillin 1 with extra- and intracellular _E. coli_ K1 over time of infection. (A) HBMEC were infected with _E. coli_ K1 for the times indicated, fixed, and differential bacterial and flotillin 1 staining was performed as described in Chapter 2. Flotillin 1 is shown in green, extracellular bacteria in purple, intracellular bacteria in blue. A single confocal slice is shown. Flotillin 1 is associated with extracellular bacteria on the cell surface (white arrows), and concentrated around intracellular bacteria at the later time point (yellow arrows). Scale bars: 10 μm. (B) Quantification of bacteria-flotillin 1 association as in (A) at various time of infection. Data shown are the mean ± SEM from two independent experiments; ≥100 bacteria were counted per sample.

5.3.4 _E. coli_ K1 invasion of flotillin 1 knockout MLEC is enhanced

To elucidate the role of flotillin 1 during _E. coli_ K1 infection, an invasion assay was performed with flotillin 1 knockout MLEC (MLEC Flot1 K/O) (Figure 5.6A). At 150 minutes p.i., in the absence of flotillin 1, the intracellular bacterial density per cell for both _E. coli_ K1 and non-pathogenic _E. coli_ K-12 was significantly higher than the recovered bacteria from MLEC WT. The mean number of intracellular _E. coli_ K1 per cell recovered from MLEC Flot1 K/O was approximately 25-fold higher than the mean number of the intracellular bacteria per cell recovered from MLEC WT ($p < 0.01$). In MLEC WT, there was almost no _E. coli_ K-12 recovered; however, in MLEC Flot1 K/O, the mean number of intracellular _E. coli_ K-12 was about 0.02, which was about 60% increased compared to the mean number of _E. coli_ K-12 recovered from MLEC WT ($p < 0.0001$).

Despite being a plasma membrane protein, flotillin 1 has also been implicated as a late endosomal marker (Dermine _et al._, 2001; Glebov _et al._, 2006; Riento _et al._, 2009). Therefore, the increase in recovered intracellular bacteria from MLEC Flot1 K/O cells

could result either from enhanced bacterial entry into the cells, or from a defective late endosomal/lysosomal pathway due to flotillin 1 knockout, potentially preventing targeting of bacteria to lysosomal destruction. To address this question, both MLEC WT and MLEC Flot1 K/O cells were infected with *E. coli* K1 for 30 minutes, fixed, and differential bacterial staining was performed (Figure 5.6B). There were no intracellular bacteria found in MLEC WT after 30 minutes of infection. In contrast, approximately 8% of Flot1 K/O cells were found to contain intracellular bacteria. This result suggested that the increased number of recovered intracellular bacteria from MLEC Flot1 K/O lysates was due to enhanced bacterial entry.
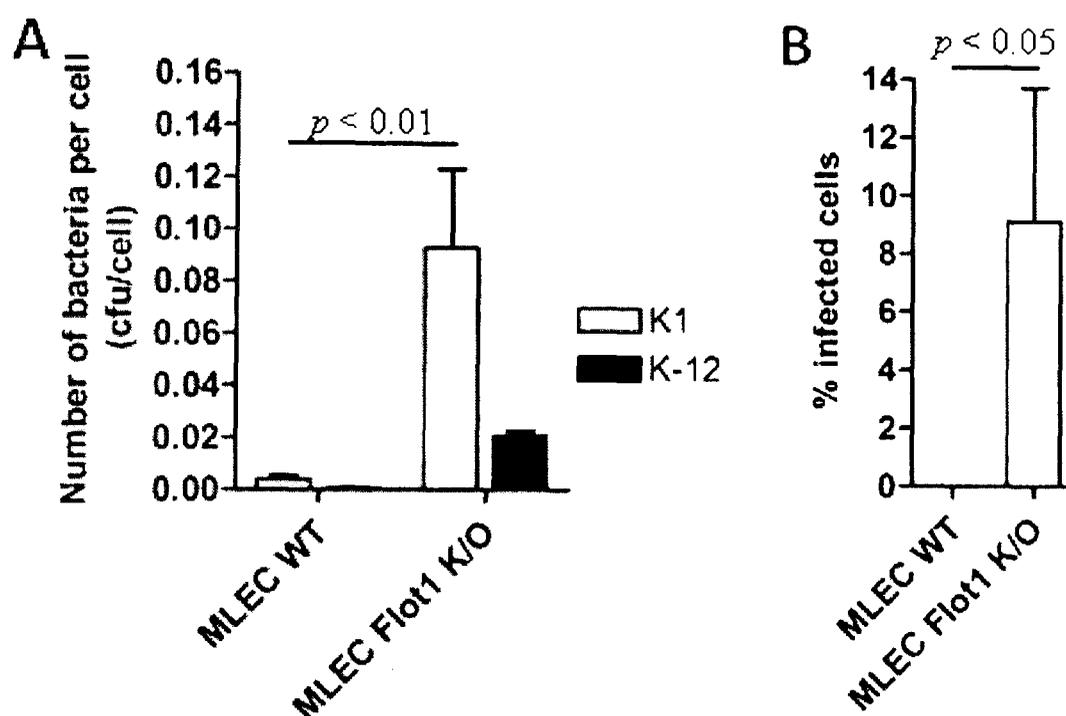
Figure 5.6. Flotillin 1 knockout enhances *E. coli* K1 uptake into MLEC. (A) To study the role of flotillin 1 during *E. coli* K1 invasion of endothelial cells, MLEC purified from wild type and flotillin 1 knockout mice were infected with either *E. coli* K1 or K-12 at MOI of 100 for 2 hours, followed by 30 minutes incubation in gentamicin containing media. The results represent the mean number of bacteria per cell. Results are from one representative experiment of three independent repeats performed in triplicate and presented as mean of triplicates ± SEM. (B) To confirm the enhanced recovered intracellular bacteria was due to increased bacterial invasion, wild type and flotillin 1 knockout MLEC were infected with *E. coli* K1 for 30 minutes, fixed with formaldehyde, and differential bacterial staining was performed. Cells containing intracellular bacteria were counted. Data shown are the mean ± SEM from two independent experiments; ≥40 cells were counted per sample.

5.3.5 Flotillin as cellular regulatory barrier model

Caveolin-1, flotillin 1, and flotillin 2 are lipid raft associated membrane proteins in mammalian cells. Previous studies have shown that knockdown or knockout of either protein leads to the alteration of expression levels of the other proteins in the target cells (Chintagari *et al.*, 2008; Vassilieva *et al.*, 2009; Ludwig *et al.*, 2010). To characterize the knockout MLEC used in this study, cells were stained for caveolin-1, flotillin 1, and flotillin 2 (Figure 5.7). The immunofluorescence micrographs showed that caveolin-1 distribution in both MLEC Flot1 K/O and MLEC WT was similar, where bright punctate structures were observed in the cytoplasm and cell periphery, although the protein expression might be lower in the flotillin 1 knockout cells than the wild type cells (Figure 5.7A. N.B. Contrast has been enhanced in these micrographs.). However, in MLEC Cav1 K/O cells, for cells immunostained for flotillin 1, there was no punctate structure found in the cells (Figure 5.7B). Contrastingly, comparison of the flotillin 2 phenotype in the different MLEC cell lines revealed that in WT cells bright punctate structures were observed (Figure 5.7C). These were also present in MLEC Cav1 K/O, but loss of the phenotype was observed in MLEC Flot1 K/O. These observed phenotypes might suggest that the loss of flotillin 1 and 2 caused the plasma membrane of MLEC Flot1 K/O to become more penetrable to bacteria.

A

DAPI	Caveolin-1	Merged
MLEC WT		
MLEC Flot1 K/O		

B

DAPI	Flotillin 1	Merged
MLEC WT		
MLEC Cav1 K/O		
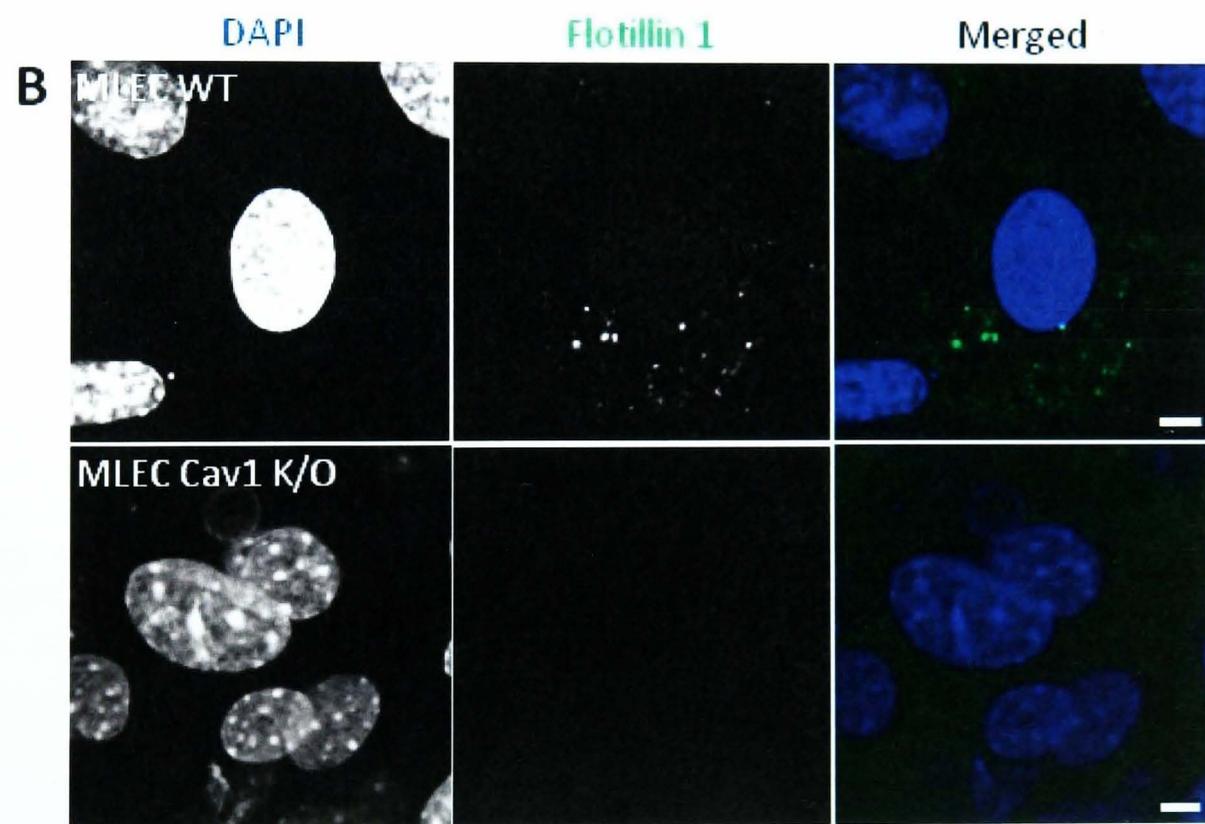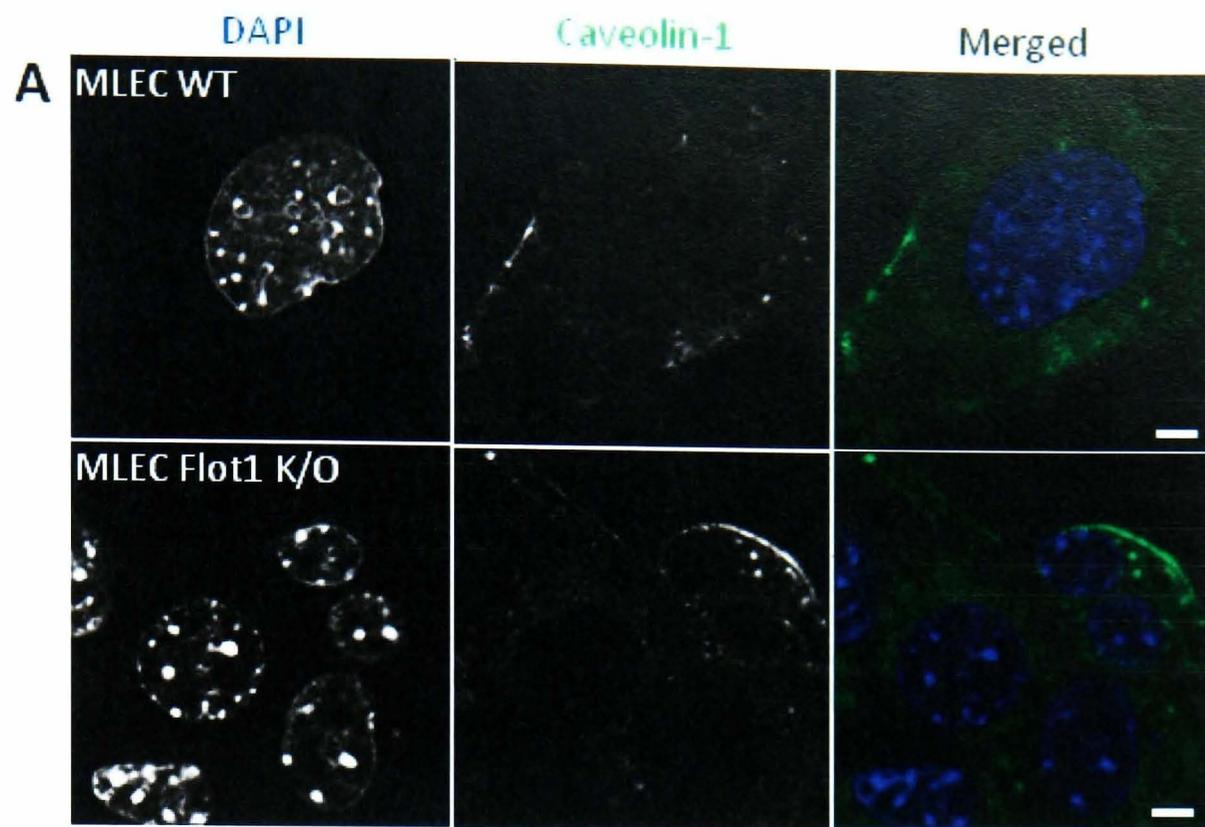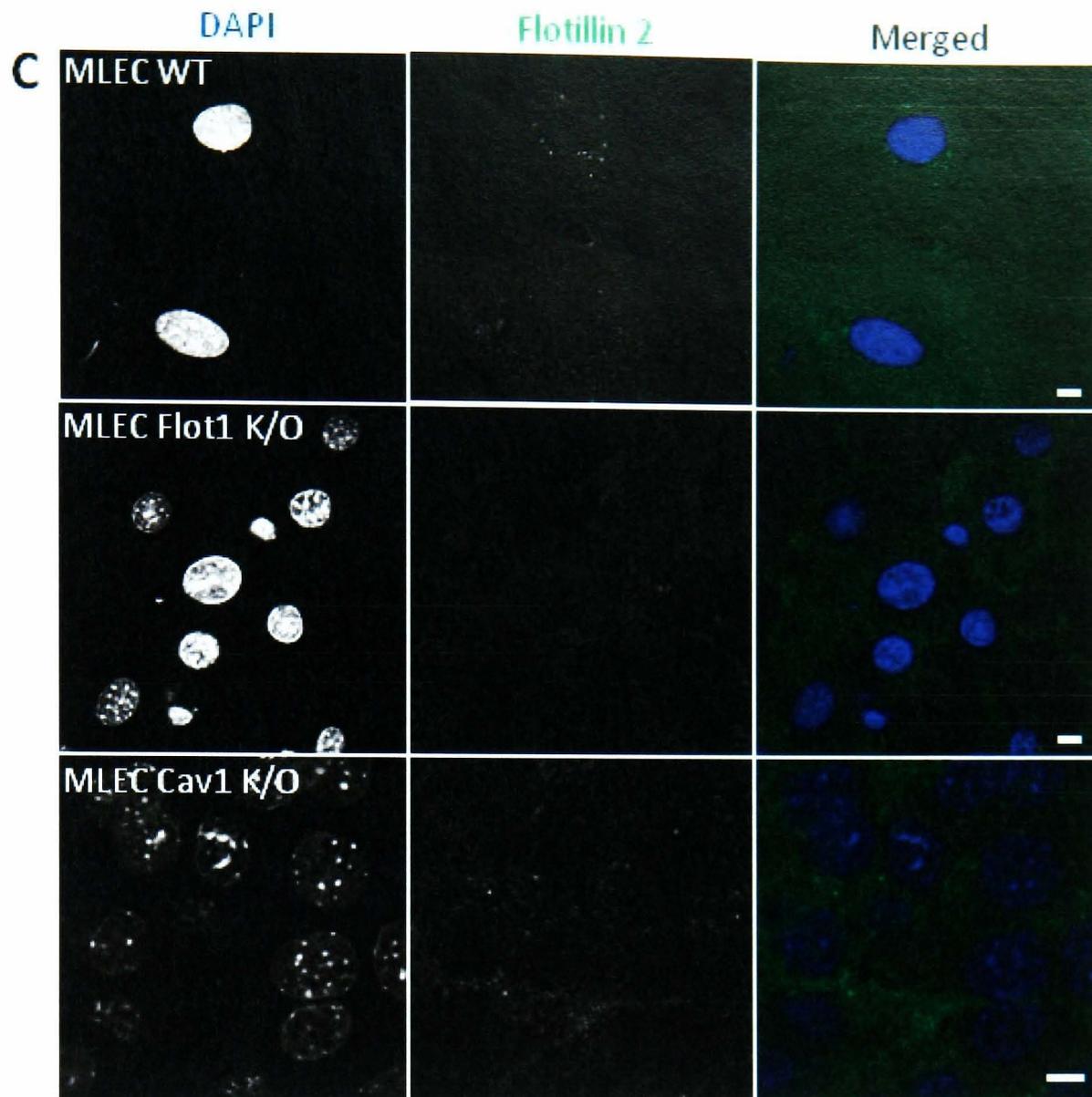
Figure 5.7. Flotillin 1 and flotillin 2 distributions are altered in caveolin-1 and flotillin 1 knockout MLEC. (A) MLEC WT and MLEC Flot1 K/O were stained with anti-caveolin-1 (green). Bright punctate structures were observed in the cytoplasm and cell periphery of both cells. (B) MLEC WT and MLEC Cav1 K/O were stained with anti-flotillin 1 (green). Bright punctate structures were observed in MLEC WT, but absent in MLEC Cav1 K/O. (C) MLEC WT, MLEC Flot1 K/O, and MLEC Cav1 K/O were stained with anti-flotillin 2 (green). Bright punctate structures were observed in MLEC WT and MLEC Cav1 K/O, but absent in MLEC Flot1 K/O. Scale bars: 5 µm.

To test the hypothesis that flotillin may have a barrier function in preventing bacterial invasion, GFP-tagged flotillin 1, flotillin 2, caveolin-1, and LDLR A18 were transfected into HBMEC, infected with K1-Cherry at MOI of 100 for 2 hours, followed by 1 hour incubation in media containing gentamicin, and imaged with a confocal microscope. The number of GFP-expressing HBMEC with intracellular K1-Cherry was scored manually. As an experimental control, infection of untransfected HBMEC was included (Figure 5.8). The percentage of infected HBMEC overexpressing GFP-tagged flotillin 1

after 3 hours infection was about 3-fold lower than the percentage of infected HBMEC overexpressing GFP-tagged caveolin-1 and LDLR A18 at the similar infection time point. In HBMEC overexpressing GFP-tagged flotillin 2, no infected cells were found after 3 hours infection. This preliminary observation suggests that overexpression of flotillin 1 or flotillin 2 has inhibitory effect on *E. coli* K1 invasion of HBMEC.
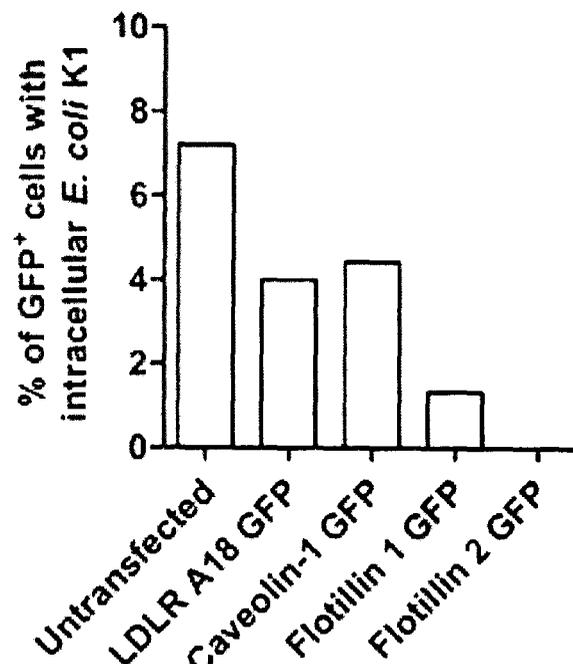
Figure 5.8. Overexpression of GFP tagged flotillin 1 and flotillin 2 affect *E. coli* K1 entry of HBMEC. To study the effect of flotillin 1 and flotillin 2 overexpression in HBMEC on *E. coli* K1 invasion, HBMEC were transiently transfected with a GFP-tagged constructs as indicated. Untransfected HBMEC was included as experimental control. Cells were infected with K1-Cherry at MOI of 100 for 2 hours, incubated in media containing 100 µg/ml gentamicin for 1 hour, and imaged. Data shown are from one experiment.

5.4 Discussion

E. coli K1 invasion of HBMEC is dynamin- and caveolin-1 independent

Some bacteria, such as *Salmonella* Typhimurium, invade non-phagocytic cells by injecting bacterial effectors via T3SS, which leads to membrane ruffle formation and results in bacterial uptake (Gerlach *et al.*, 2008). Some *E. coli* K1 clinical isolates were found to possess T3SS, and this T3SS was shown to be required for bacterial invasion of HBMEC and intracellular survival (Yao *et al.*, 2006; Yao *et al.*, 2009). The *E. coli* K1 strain used in this study, E44 strain, does not have T3SS, however, it harbours genes for

general secretory pathway (GSP), which are also present in uropathogenic *E. coli* strain CFT073 and other Gram negative bacteria (Welch *et al.*, 2002; Yao *et al.*, 2006). Studies performed with E44 proposed that the K1 bacterial invasion of HBMEC was via receptor-mediated, clathrin-independent "zippering" mechanism (Prasadarao *et al.*, 1999). Later, Sukumaran *et al.* (2002) reported that *E. coli* K1 hijacked the caveolae-mediated pathway for entry into HBMEC, and the authors also proposed that caveolin-1 was involved in bacterial transcytosis.

Caveolae-mediated endocytosis has been implicated to be dynamin-dependent via a GTP-dependent fission process (Oh *et al.*, 1998; Yao *et al.*, 2005). Further evidence to support the requirement for dynamin in caveolae-mediated endocytosis has been demonstrated by the recruitment of Dyn2 during SV40 internalization into a fibroblast cell line (Pelkmans *et al.*, 2001; Pelkmans *et al.*, 2002), and that phosphorylation of tyrosine 231 and 597 of dynamin 2 is required for caveolin-1 binding, as shown by expression of non-Src-phosphorylatable Dyn2 Y597F mutant in microvessel endothelial cells, which abolished albumin and cholera toxin subunit B uptake (Shajahan *et al.*, 2004). Therefore, we hypothesized that overexpression of GDP-bound Dyn2 K44A mutant, which has also been shown to abolish caveolae-mediated endocytosis in endothelium (Shajahan *et al.*, 2004), might block *E. coli* K1 invasion of HBMEC, if the bacteria utilized the caveolae-mediated pathway for HBMEC entry. However, we did not find any inhibitory effect on the bacterial internalization in cells overexpressing GDP-bound Dyn2 (Figure 5.1A). Different isoforms and splice variants of dynamin exist in mammalian cells (Cao *et al.*, 1998; Hinshaw, 2000), and furthermore different dynamin isoforms regulate receptor-mediated endocytosis at the different membrane surfaces in polarized MDCK cells (Altschuler *et al.*, 1998). Since HBMEC are polarized cells, we repeated the experiments with GDP-bound Dyn1 (Figure 5.1B), but again *E. coli* K1 invasion was not inhibited. As observed by Watson and Galan (2008) in their study of *Campylobacter jejuni* invasion of

COS-1 cells, minor enhancement in *E. coli* K1 uptake in cells overexpressing GDP-bound dynamin was also observed in this study. These data suggest that dynamin is not required for *E. coli* K1 internalization into HBMEC. However, it should be noted that the functionality of the dominant negative mutants in our system has not been validated. Whilst the phenotype of the cells overexpressing the K44A mutants is similar to that previously published, it is possible that HBMEC dynamin-dependant endocytosis is still functioning. To ensure the observation with *E. coli* K1 was not due to non-functioning GDP-bound dynamin mutants in HBMEC, the inhibitive effect of the mutants on endocytosis should be confirmed by studying the uptake of transferrin, a ligand for clathrin-mediated endocytosis. A functional GDP-bound dynamin mutant is anticipated to inhibit transferrin uptake into HBMEC overexpressed the mutant. Furthermore, since dynamin isoforms seem to have redundant functions (Altschuler *et al.*, 1998), there is a possibility that the other endogenous dynamin isoforms and splice variants might take over the role in cells overexpressing a specific GDP-locked dynamin isoform or splice variant.

Although it appears that dynamin is not required for *E. coli* K1 uptake in our system, the observation does not completely eliminate the involvement of caveolae-mediated endocytosis. Recently, it was reported that the uptake of cholera toxin B (CTB), which is a ligand commonly used for studying caveolae-mediated endocytosis, was not inhibited in Dyn2 knockout fibroblasts (Liu *et al.*, 2008). Therefore, the absolute requirement for dynamin in caveolae-mediated endocytosis seems to be unclear and a role for caveolin that might be dynamin-independent was investigated further. Immunofluorescence staining of *E. coli* K1-infected HBMEC showed weak staining of the bacteria with caveolin-1 (Figure 5.2A), as compared to Sukumaran *et al.* (2002) who showed strong staining of the bacteria with caveolin-1. The observed discrepancy could be due to channel cross-talk in their results, because very high intensity of nonspecific background signals was shown in their micrographs, which they indicated as specific

bacterial staining (using anti-K1 or anti-S-fimbriae antibody). Further, our findings showed that the association of the bacteria with caveolin-1 was a rare event, with only approximately 4% of the bacterial population associated with caveolin-1 after 30 minutes infection (Figure 5.2B), and the percentage of association further decreased to about 1% at the end of 2 hours infection.

Overexpression of tyrosine 14 mutant, caveolin-1 Y14F, in COS-1 cells has been shown previously to partially inhibit *Campylobacter jejuni* invasion (Watson and Galán, 2008), however, in this study overexpression of caveolin-1 Y14A in HBMEC had no inhibitory effect on *E. coli* K1 invasion. This result was further backed up by expressing the GFP-tagged caveolin-1β isoform, which is not phosphorylatable, in HBMEC. Instead of inhibiting *E. coli* K1 internalization into HBMEC, which might be expected if caveolin-1 is required for uptake, a mild increase in the number of cells with intracellular bacteria was observed when overexpressing caveolin-1β. The functionality of caveolin-1 Y14A and caveolin-1β in HBMEC need to be validated by studying the uptake of lactosylceramide (LacCer), which was a specific ligand for caveolae-mediated endocytosis (Singh *et al.*, 2003) to substantiate these observations.

To further support our data that caveolin-1 is not required for *E. coli* K1 infection, an invasion assay was performed with MLEC isolated from either wild type or caveolin-1 knockout mice. The main reason for using lung endothelia was due to the technical difficulty to isolate of brain microvascular endothelium in sufficient quantity from mice and the difficulty to then culture the cells *in vitro* (Liebner, S., personal communication). Although bacterial invasion efficiency of MLEC is low, MLEC are still a valid *in vitro* model for studying *E. coli* K1 pathogenesis, as parallel infection with the non-pathogenic *E. coli* K-12 showed that these bacteria did not invade MLEC. Further, it was also shown previously that *E. coli* K1 was able to invade other endothelial cells with lower invasion efficiency (Prasadarao *et al.*, 1996a). Importantly, an invasion assay performed with

caveolin-1 knockout in MLEC did not inhibit *E. coli* K1 invasion (Figure 5.4). Although this evidence, in combination with our data using non-phosphorylatable caveolin-1 mutant expression in HBMECs, suggests that *E. coli* K1 invasion is independent of caveolin-1, the possible effects of alterations in other signalling pathways or receptor expression on the plasma membrane caused by the removal of caveolin-1 in the knockout cells cannot be disregarded (Barth *et al.*, 2007; Matthews *et al.*, 2008). Recently, Siddiqui *et al.* (2011) demonstrated the absence of caveolin-1 led to destabilization of adherens junctions and activation of endothelial nitric oxide synthase (eNOS) in endothelial cells. The eNOS nitrated GTPase activating protein (GAP) p190RhoGAP-A, resulting in impaired GAP and RhoA activation (Siddiqui *et al.*, 2011). Since RhoA was required for *E. coli* K1 invasion of HBMEC (Khan *et al.*, 2002), the upregulation of RhoA in caveolin-1 knockout cells could facilitate the bacteria invasion of caveolin-1 knockout MLEC.

In addition to studying the role of caveolin-1 during *E. coli* K1 invasion of HBMEC, we were also interested in studying the requirement of cholesterol for bacterial invasion of HBMEC. It was previously shown that *E. coli* K1 invasion of HBMEC was blocked by a number of cholesterol inhibitors (Sukumaran *et al.*, 2002; Chi *et al.*, 2010). Caveolin-1 is irreversibly palmitoylated at the three cysteine residues in the hydrophobic region at the C-terminal (Figure 1.6) (Dietzen *et al.*, 1995; Parat and Fox, 2001). Mutation of these cysteine residues affects caveolin-chaperone complex formation and abolishes transport of newly synthesized cholesterol to plasma membrane caveolae (Dietzen *et al.*, 1995; Smart *et al.*, 1996; Uittenbogaard and Smart, 2000; Fu *et al.*, 2004). We found no inhibitory effect of the caveolin-1 palmitoylation mutant on *E. coli* K1 internalization of HBMEC. However, this observation is insufficient to rule out the role of cholesterol during *E. coli* K1 invasion of HBMEC, as caveolin-1 knockout mice displayed normal mRNA and protein levels of cholesterol transport protein Niemann-Pick C1-like 1 (NPC1L1) in intestinal mucosa, and did not show any defect in cholesterol transportation (Valasek *et al.*,

2005). Therefore, overexpression of the caveolin-1 palmitoylation mutant might not have completely abolished the cellular cholesterol trafficking pathway, and cholesterol could be transported or acquired via alternative pathways. This could be more directly tested by depleting cholesterol with β-trimethyl cyclodextrin, which is less toxic than filipin (Schneider, B., personal communication), or by cholesterol inhibiting agents, such as simvastatin, and lovastatin, if the cells can withstand these treatments.

Loss of flotillin 1 enhanced *E. coli* K1 internalization

Since cholesterol had been previously implicated in *E. coli* K1 invasion of HBMEC (Sukumaran *et al.*, 2002; Chi *et al.*, 2010), we therefore looked at the requirement of flotillin, which is associated with lipid rafts (Glebov *et al.*, 2006), during the bacterial invasion of HBMEC. Although flotillin endocytosis is relatively rare (Doherty and McMahon, 2009; Riento *et al.*, 2009), it has been shown to endocytose a proportion of cholera toxin B, and this uptake is dynamin-independent (Glebov *et al.*, 2006). Other than the uptake of cholera toxin B, flotillin is required for uptake of plasma membrane components such as glycosyl-phosphatidylinositol (GPI)-linked proteins and glycosphingolipids (Glebov *et al.*, 2006; Frick *et al.*, 2007). Flotillin 1 has been shown to co-localize with lysosomal transmembrane glycoprotein, LAMP1 (Dermine *et al.*, 2001), in addition to its localization on plasma membrane. It was suggested that the presence of flotillin 1 on the phagolysosomal membrane might be involved in actin accumulation and polymerization (Dermine *et al.*, 2001). No known pathogen is documented to invade eukaryotic cells via a flotillin-dependent pathway, although some bacteria have been found to associate with flotillin intracellularly (Li *et al.*, 2008a). For example, *Campylobacter jejuni* and *Brucella abortus* associate with flotillin 1 transiently (Arellano-Reynoso *et al.*, 2005; Watson and Galán, 2008), while in *Mycobacterium marinum* infection of monocytes,

flotillin 1 was found on the bacterial replication phagosomes which lack LAMP1 (Hagedorn and Soldati, 2007).

Quantification of the population of *E. coli* K1 associated with flotillin 1 revealed that a small population of *E. coli* K1 (5%) associated with flotillin 1 after 30 minutes infection, but the bacterial population which associated with flotillin 1 increased to about 30% after 2 hours infection (Figure 5.5A and B). The role of flotillin 1 on intracellular bacteria-containing vacuoles is unknown. In this study, the population of *E. coli* K1 associated with flotillin 1 remained stable at later time points. The low initial colocalisation with flotillin might suggest that *E. coli* K1 do not require flotillin for uptake, but that *E. coli* K1 might hijack a flotillin 1 pathway once inside the cell, and utilize the cytoskeletal machinery for intracellular transportation to the other membrane surface.

To elucidate the role of flotillin 1 during *E. coli* K1 infection, the invasion assay was performed with MLEC isolated from flotillin 1 knockout mice. Instead of an inhibitory effect on the bacterial entry, we observed a 25-fold increase in *E. coli* K1 density recovered from the cell lysate of flotillin 1 knockout MLEC in comparison to wild type MLEC. This trend was also observed for infection performed with non-pathogenic *E. coli* K-12. The observed increase in intracellular bacteria could be due to either increased bacterial uptake, or a non-functioning lysosomal degradation pathway, due to the fact that flotillin 1 has been found on late endosomes (Dermine *et al.*, 2001). However, after 30 minutes infection with *E. coli* K1, which should be insufficient for the bacteria-containing vacuoles to mature to late endosomal stage and to fuse with lysosomes, there was no infected wild type MLEC, while 8% of the flotillin 1 knockout MLEC were infected. This observation strongly supported the hypothesis that the enhanced number of intracellular bacteria recovered from flotillin 1 knockout MLEC was due to increased bacterial uptake rather than an inhibition in lysosomally targeted bacterial lysis. There is a possibility that in these flotillin 1 knockout MLEC, the equilibrium of membrane protein populations are

disrupted following the total absence of flotillin 1 in these cells, hence the bacterial internalization might be shunted to another endocytic pathway. Therefore, this result might need to be confirmed with flotillin 1 knockdown by flotillin 1 specific siRNA in HBMEC, where a small amount of flotillin 1 remains in the knockdown cells, and might maintain the equilibrium of the membrane protein populations. On the other hand, the functionality of the lysosomal degradation pathway in MLEC Flot1K/O can be studied by comparing the number of recovered intracellular *E. coli* K-12, which have been shown to be unable to survive intracellularly (Figure 3.5), in Flot1K/O MLEC at early and extended time points of infection. A significant reduction in the number of recovered intracellular *E. coli* K-12 from Flot1K/O MLEC at the extended time point of infection would be expected if the lysosomal pathway remains functional in the knockout cells. Alternatively, the functionality of the lysosomal degradation pathway can be studied by assessing the long-lived protein degradation as described in (Razi *et al.*, 2009).

Flotillin as a regulatory cell barrier

Although caveolae and flotillin form distinct microdomains, their cellular expressions and protein stability are interdependent (Solis *et al.*, 2007; Chintagari *et al.*, 2008; Vassilieva *et al.*, 2009; Ludwig *et al.*, 2010). In conjunction with previous published data on caveolin-1, flotillin 1, and flotillin 2 expression levels in protein knockdown or knockout cells, as well as our immunofluorescence observations on the protein distributions, we propose that both flotillin 1 and flotillin 2 distributions on the plasma membrane might have a role as a regulatory cellular barrier. This is evidenced by the loss of flotillin 2 punctate structures in flotillin 1 knockout MLEC, which showed enhanced bacterial internalization for both *E. coli* strains; whereas in caveolin-1 knockout MLEC, only flotillin 1 distribution was affected, and a mild increase which was not statistically significant in *E. coli* K1 uptake into the knockout MLEC was observed. It is also possible

that the inhibitory effect on *E. coli* K1 uptake into caveolin-1 knockout MLEC is cancelled by the loss of flotillin 1, but some flotillin 2 is still expressed on the surface of these cells. Hence, the increase in bacterial internalization was not as great as in flotillin 1 knockout MLEC.

Previously, Hoffmann *et al.* (2010) observed increased membrane fluidity in caveolin-1 knockout fibroblasts, which was corroborated by strong increased mobility of GFP-GPI in these knockout cells based on FRAP experiment. The increased GFP-GPI mobility correlated with enhanced *Staphylococcus aureus* uptake in caveolin-1 knockout fibroblasts (Hoffmann *et al.*, 2010). Since membrane fluidity is known to be influenced by cholesterol (Spector and Yorek, 1985), the absence of both flotillin isoforms on the plasma membrane might affect the cholesterol content of the plasma membrane, which made the membrane more easily penetrable by the bacteria.

It is known that some plasma membrane rafts interact with cytoskeletal structures (Maxfield, 2002; Meiri, 2005; Langhorst *et al.*, 2007; Sverdlov *et al.*, 2009; Ludwig *et al.*, 2010), and this interaction has been hijacked by certain pathogens, such as SV40, for invading non-phagocytic mammalian cells (Pelkmans *et al.*, 2001; Pelkmans *et al.*, 2002). Rather than facilitating pathogen entry by raft-cytoskeleton interactions, it was found that tyrosine-phosphorylated caveolin-1 induced cytoskeleton rearrangements at *Neisseria gonorrhoeae* attachment sites and blocked the bacterial internalization into a human cervix carcinoma cell line, ME-180 (Boettcher *et al.*, 2010). We speculate that the enhanced *E. coli* K1 into flotillin 1 knockout MLEC could also link to an impact on cytoskeletal structures, as flotillin 2 has been shown to interact with F-actin via its stomatin, prohibitin, flotillin, and HflK/C (SPFH) domain, and the protein lateral mobility is modulated by the actin cytoskeleton (Langhorst *et al.*, 2007; Langhorst *et al.*, 2008a). This model is also supported by our data where bacterial internalization was inhibited in HBMEC overexpressing-GFP-tagged flotillin 1 and flotillin 2 (Figure 5.8). Therefore, we propose

that flotillin might act as cellular regulatory barrier either by regulating plasma membrane cholesterol or by modulating plasma membrane-cytoskeleton interactions and, hence, protect eukaryotic cells from pathogen invasion.

6. Intracellular *E. coli* K1 interacts with various organellar markers, revealing the potential bacterial transcytosis pathway in HBMEC

6.1 Introduction

After entry into host cells, bacteria successfully escape the direct attack from the host immunity, but the intracellular environment is also unfriendly to the bacteria. Indeed, intracellular bacteria face "intracellular immunity" from the host cell degradation mechanism, and the bacteria have to obtain nutrients and biosynthetic precursors, as well as evade detection by the host's immune system (Bhavsar *et al.*, 2007; Ham *et al.*, 2011).

In order to survive intracellularly, pathogenic bacteria have evolved diverse strategies to modulate host cellular machinery to make a cosy and protected intracellular niche for survival and replication (Brumell and Scidmore, 2007; Ham *et al.*, 2011). To escape from lysosomal degradation, some bacteria, such as *Listeria monocytogenes* (Tweten, 2005; Henry *et al.*, 2006), *Mycobacterium marinum* (Stamm *et al.*, 2003; Hagedorn and Soldati, 2007), *Burkholderia pseudomallei* (Sitthidet et al., 2011), and *Shigella flexneri* (Sansonetti et al., 1986), trigger rupture of the phagosome and escape into the cytosol. *Listeria* is the best-studied pathogen to employ this strategy, whereby the bacterium secretes listeriolysin O for delaying endosomal maturation and for the formation of transmembrane pores on the vacuolar membrane (Tweten, 2005), thereby escaping from the late endosome-like compartment into the cytosol (Henry *et al.*, 2006). The expression of GTP-locked Rab5 (Rab5Q79L) mutant showed co-localization of the bacteria with Rab5Q79L, but did not block the bacterial escape into the cytosol (Henry *et al.*, 2006). In the cytosol, these bacteria replicate and acquire host actin for cell-cell spreading *in vitro* (Hagedorn and Soldati, 2007).

On the other hand, those invasive bacteria that reside and replicate in membrane-bound vesicles must delay or block endosomal maturation to avoid fusion with lysosomes

by modifying the endosomal membrane (Gruenberg and van der Goot, 2006). To prevent lysosomal fusion, pathogenic *Brucella* secretes cyclic β-1.2-glucan (CβG) that is structurally similar to cyclodextrins and disrupts lipid rafts (Arellano-Reynoso *et al.*, 2005). *Brucella*-containing vacuoles eventually fuse with the endoplasmic reticulum (ER) after transient acquisition of late endocytic markers (Celli *et al.*, 2003; Starr *et al.*, 2008).

For *Salmonella enterica* serovar Typhimurium, once inside the cells, the bacterium secretes bacterial virulence effectors into the cytosol via T3SS, and the *Salmonella*-containing vacuoles (SCV) undergo standard endosomal maturation to late endosomes, without interacting with mannose-6-phosphate-containing late endosomes or lysosomes (Méresse *et al.*, 1999; Steele-Mortimer *et al.*, 1999). In macrophage cell line, SpiC, one of the bacterial effectors encodes within SPI-2 pathogenicity island, is thought to prevent fusion of SCV with lysosomes (Uchiya *et al.*, 1999). In fact, it was shown that before SCV mature to late endosomal stage, various regulators of endocytic recycling, including Arf6, Rab4, syntaxin 13, and Rab11, are transiently associated with SCV. These recycling regulators are not only required for recycling cell surface protein from SCV, but they are also essential for acquisition of lysosomal glycoproteins to SCV (Smith *et al.*, 2005). SCV also recruit Rab7-interacting lysosomal protein (RILP) to allow migration to the perinuclear region, where the bacterial vacuoles are associated with Golgi (Salcedo and Holden, 2003; Guignot *et al.*, 2004).

The obligate intracellular bacteria *Chlamydia* species have evolved an unique strategy for the bacterial intracellular survival and replication. *Chlamydiae* replicate in a specialized compartment that is not acidified and does not fuse with lysosomes (Heinzen *et al.*, 1996), but the bacterium-containing compartment is enriched with host lipids, such as sphingomyelin and cholesterol, which are acquired via golgi-dependent transportation, and the acquisition is a bacterially driven process (Carabeo *et al.*, 2003). Additionally, screening with a panel of GFP-tagged Rab GTPases constructs revealved that the

chlamydial compartment is also decorated with various Rab GTPases, such as Rab11, Rab4, Rab1, Rab6, and Rab14 (Rzomp *et al.*, 2003). The functional roles of most of these GTPases on the chlamydial compartment are not clear, but the association of Rab11a with the compartment has been shown to regulate the development of the bacterial elementary bodies (an infectious form of the bacteria) by affecting Golgi fragmentation via the golgin-84 dependent pathway (Lipinski *et al.*, 2009). Recently, it was demonstrated that the bacterium secretes a serine protease, chlamydial protease-like activity factor (CPAF), which regulates the membrane integrity of the bacterial compartment, prevents superinfection by degrading early *Chlamydia* effectors, Tarp, during infection of a pre-infected cell, as well as interfering with the caspase-1 apoptotic pathway of infected cells (Jorgensen *et al.*, 2011).

Although the majority of invasive bacteria survive intracellularly by avoiding fusion with lysosomes, *Coxiella burnetii*, the etiologic agent that causes Q fever, evolved a radically opposite strategy. *Coxiella*-containing vacuole (CCV) fuses with the autophagosome before the vacuole fuses with lysosome and its vacuole is decorated with lysosomal glycoproteins, vacuolar H^+-ATPase, Rab7, cathepsin D, and other lysosomal hydrolytic enzymes (Beron *et al.*, 2002; Brumell and Scidmore, 2007; Romano *et al.*, 2007; Voth and Heinzen, 2007). The acidic environment is required for stimulating the intracellular bacteria to become metabolically active, and also to activate the bacterial type 4 secretion system in order to evade the host innate immune signalling pathways (Newton and Roy, 2011).

In order to establish a successful infection, pathogenic bacteria not only survive intracellularly, but they need to disseminate systemically. However, the host's body is structured with various barriers of sheets of epithelial and endothelial cells. Therefore, to disseminate to other anatomical sites, the bacteria need to traverse through these polarized barrier cells.

To date, most knowledge on transcytosis pathways in polarized epithelial cells has been contributed by studies of immunoglobulins, and macromolecules. such as albumin, and insulin (Ghitescu and Bendayan, 1992; Predescu and Palade, 1993; Apodaca, 2001: Minshall *et al.*, 2003; Ducharme *et al.*, 2007; Tzaban *et al.*, 2009). However. it is unknown if similar membrane trafficking pathways exist in flat endothelial cells. Several pathogens are known to traverse polarized epithelial or endothelial cells, but bacterial transcytotic pathways are poorly understood (Nikitas *et al.*, 2011), and the majority of previous studies mainly focused on the requirement for microfilaments, motor proteins, and microtubules (Bomsel, 1997; Bras and Ketley, 1999; Eyngor *et al.*, 2007; Hu *et al.*. 2008; Wang *et al.*. 2008). Recently, uropathogenic *E. coli* (UPEC) traslocation across renal medullary collecting duct (MCD) was demonstrated to depend on lipid rafts via a Toll-like receptor 4 (TLR4)-dependent process. The authors correlated the decrease in bacterial translocation across cholesterol-depleted MCD with the downregulation of proinflammatory mediator expression (Chassin *et al.*, 2008).

A previous study has shown that the majority of *E. coli* K1 acquire the early endosomal marker, transferrin receptor (TfR), after 30 minutes of infection (Kim *et al.*, 2003). The association with TfR gradually decreased at later time points of infection, while the population of bacteria associated with late endosomal marker, LAMP1, increased over time of infection (Kim *et al.*, 2003). *E. coli* K1 has been shown to survive intracellularly in a late endosomal-like compartment devoid of lysosomal enzymes (Kim *et al.*, 2003). The bacterium is able to traverse an HBMEC monolayer *in vitro* without affecting the monolayer's integrity (Stins *et al.*, 2001), but to date the transcytosis pathway has not been identified.

6.2 Objectives and aims

The aim of this chapter was to identify the intracellular fate of *E. coli* K1 and a potential transcytosis pathway in HBMEC. The specific objectives are as below:

- To screen the interactions of *E. coli* K1 with various cellular compartments by transfecting HBMEC with various GFP-tagged chimaerae.

- To study the identified pathway(s) for *E. coli* K1 traversal of HBMEC cells.

6.3 Results

6.3.1 *E. coli* K1 containing compartment is not arrested at early endosomal stage

A pervious study showed that *E. coli* K1 did not replicate intracellularly in HBMEC (Prasadarao *et al.*, 1999), but data from our intracellular survival assay showed that *E. coli* K1 could survive and replicate in HBMEC up to 7 hours p.i. (Figure 3.2). Therefore, we were interested to study the host proteins that were present on the bacterial containing compartments. We first analyzed the *E. coli* K1 compartmentation in HBMEC by infecting HBMEC transiently overexpressing GFP-tagged Rab5 chimaerae with K1-Cherry for 2 hours, followed by 1 hour incubation in media containing gentamicin, and processed for live-cell imaging. Wild type Rab5 (Rab5WT) was found diffuse in the cytoplasm with vesicular structures observed at the perinuclear region and some at the cytoplasm (Figure 6.1A). K1-Cherry were found in areas that exclude cytosolic Rab5WT expression and had no membrane accumulation of Rab5 around them. This observation demonstrated that *E. coli* K1 did not arrest endosomal maturation at early endosomal stage, evidenced by the absence of Rab5 accumulation on the *E. coli* K1 containing vacuoles (ECV) 3 hours p.i. in HBMEC transiently overexpressing GFP-tagged Rab5WT. We also looked for co-localization of GFP-Rab5 with K1-Cherry at an early time point (30 minutes p.i.) in fixed cells; however, no co-localization of Rab5 with K1-Cherry observed (data not shown). One possibility is that the interaction of Rab5 and ECV is rapid and transient, or

Rab5 is not involved in the ECV development. We further investigated the interaction of K1-Cherry with early endosome by infecting HBMEC with *E. coli* K1 for 30 minutes, fixed, and stained for early endosomal antigen 1 (EEA1) (Figure 6.1D), which is an effector of Rab5 (Galperin and Sorkin, 2003). EEA1 staining showed bright punctate structures in the cell cytoplasm and some weak signal of EEA1 around the bacteria was observed, which might suggest that ECV did fuse with early endosomes during its maturation, but once again this interaction might be too rapid and transient to be detectable in our assay.

To overcome the possibility that any interactions of *E. coli* K1 were too short to be detected, we investigated if Rab5 mutant chimaerae might have an effect on the protein localization with ECV. Rab5Q79L and Rab5S34N are GTP- and GDP-locked Rab5 mutants, respectively, which the GTPase activity of these mutants has been well-characterized (Stenmark *et al.*, 1994). The defects in these mutants prevent normal vesicle fusion and maturation, as such if *E. coli* K1 did interact with Rab5-associated vesicles, normal vesicle progress would be stalled, and an accumulation of Rab5 and *E. coli* K1 expected. In HBMEC overexpressed Rab5Q79L, large vesicular structures were observed in the cytoplasm, and K1-Cherry was located in an enlarged vacuole (Figure 6.1B). Whereas in HBMEC overexpressed Rab5S34N, diffuse punctate signal was observed (Figure 6.1C), and K1-Cherry was localized in the cytoplasm without any protein accumulation around them.

As overexpression of GDP-locked Rab5 (Rab5S34N) was shown to inhibit *Coxiella burnetii* entry of CHO cells (Romano *et al.*, 2007), to ensure that *E. coli* K1 internalization into HBMEC overexpressing GFP-tagged Rab5S34N was not affected, HBMEC overexpressing GFP-Rab5 chimaerae were infected with K1-Cherry at MOI of 100 for 2 hours, followed by incubation in media containing gentamicin for 1 or 5 hours, and processed for live-cell imaging. The number of GFP-expressing cells with intracellular

K1-Cherry was quantified. We did not find any evidence of the inhibition of *E. coli* K1 invasion in HBMEC overexpressing GDP-locked Rab5 (Rab5S34N) 3 and 7 hours p.i. (Figure 6.1E) as would be expected if Rab5-associated vesicles were involved in the intracellular survival of *E. coli* K1. Therefore, our results suggested that ECV interact transiently with early endosomal markers, and the interaction was only observed in cells overexpressing Rab5Q79L mutant. On the other hand, *E. coli* K1 invasion of HBMEC was not affected in HBMEC overexpressing Rab5 chimaera.

A
K1-Cherry | GFP-Rab5WT | Merged

B
K1-Cherry | GFP-Rab5Q79L | Merged

C
K1-Cherry | GFP-Rab5S34N | Merged

D
E. coli K1 | EEA1 | Merged

E
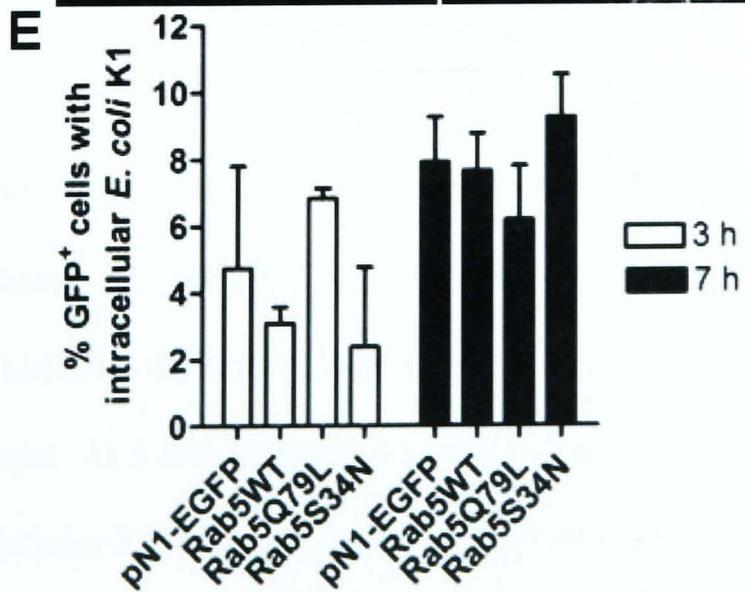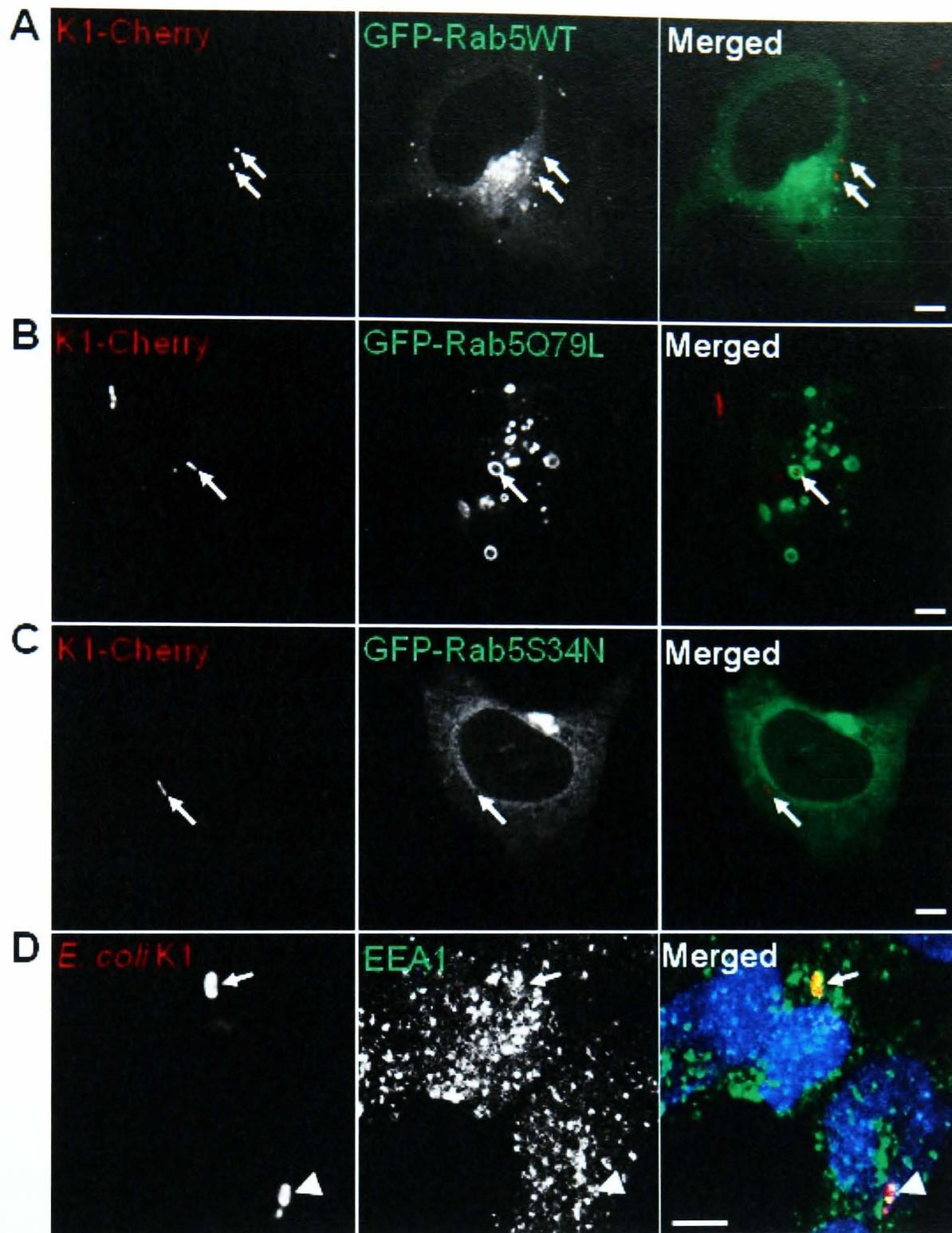
Figure 6.1. The *E. coli* K1-containing vacuole is not arrested at an early endosomal stage. (A) - (C) Representative confocal micrographs of HBMEC cells transiently expressing GFP-Rab5WT (A), GFP-Rab5Q79L (B), and GFP-Rab5S34N (C) that were infected with mCherry-expressing *E. coli* K1 (K1-Cherry) (red) at MOI of 100 for 2 hours, followed by 1 hour incubation in media containing gentamicin, and were imaged with a confocal microscope as described in Chapter 2. The white arrows indicate intracellular K1-Cherry. (D) Representative confocal micrograph of HBMEC infected with *E. coli* K1 (red) at 30 minutes p.i., fixed and immunostained for EEA1 and visualized by FluoProbes®-488-conjugated secondary antibodies (green). Nuclei were stained with DAPI (blue). A single confocal slice is shown. The white arrows indicate bacterium localising with EEA1, and the white arrow heads indicate bacterium that does not localise with EEA1. Scale bars: 5 μm. (E) To investigate overexpression of GFP-tagged Rab5 on K1-Cherry invasion, HBMEC were transfected with GFP-tagged Rab5 chimaerae, infected with K1-Cherry as above, followed by 1 or 5 hours incubation in media containing gentamicin, and imaged as in (A) – (C). pN1-EGFP was included as the experimental control. GFP-expressing HBMEC with intracellular *E. coli* K1 were scored by confocal microscopy at 3 and 7 hours p.i. Data are mean ± SEM from two independent experiments.

6.3.2 *E. coli* K1 does not utilize endosomal recycling pathway

Rab11 is one of the Rab GTPases that regulates endosomal recycling at the juxtanuclear recycling endosome. To determine whether *E. coli* K1 utilizes the Rab11a recycling pathway, HBMEC were transiently transfected with GFP-tagged Rab11 chimaera, either Rab11a wild type (Rab11aWT) (Figure 6.2A), or GTP-locked Rab11a (Rab11aQ70L) (Figure 6.2B), or GDP-locked Rab11a (Rab11aS25N) (Figure 6.2C), infected with K1-Cherry as described above, followed by incubation in media containing gentamicin for 1 or 18 hours, and imaged. Both GDP- and GTP-locked Rab11a mutants were applied in case ECV association with Rab11a was transient. Bright punctate structures were observed in the cytoplasm and juxtanuclear position of HBMEC overexpressing Rab11aWT; while only bright punctate structures were observed in the cytoplasm of HBMEC overexpressing Rab11aQ70L. In HBMEC overexpressing Rab11aS25N, the GFP signal was dispersed in the cytoplasm, no punctate structure was observed. At 3 and 20 hours p.i., none of the Rab11a chimaera localized specifically with intracellular K1-Cherry. No localization of intracellular K1-Cherry with GFP-Rab11aWT, and GFP-Rab11aQ70L suggests that Rab11a is not involved in regulation of the pathway hijacked by intracellular *E. coli* K1 during the bacterial infection of HBMEC.

A
K1-Cherry | GFP-Rab11aWT | Merged
3 h p.i.
20 h p.i.

B
K1-Cherry | GFP-Rab11aQ70L | Merged
3 h p.i.
20 h p.i.

171
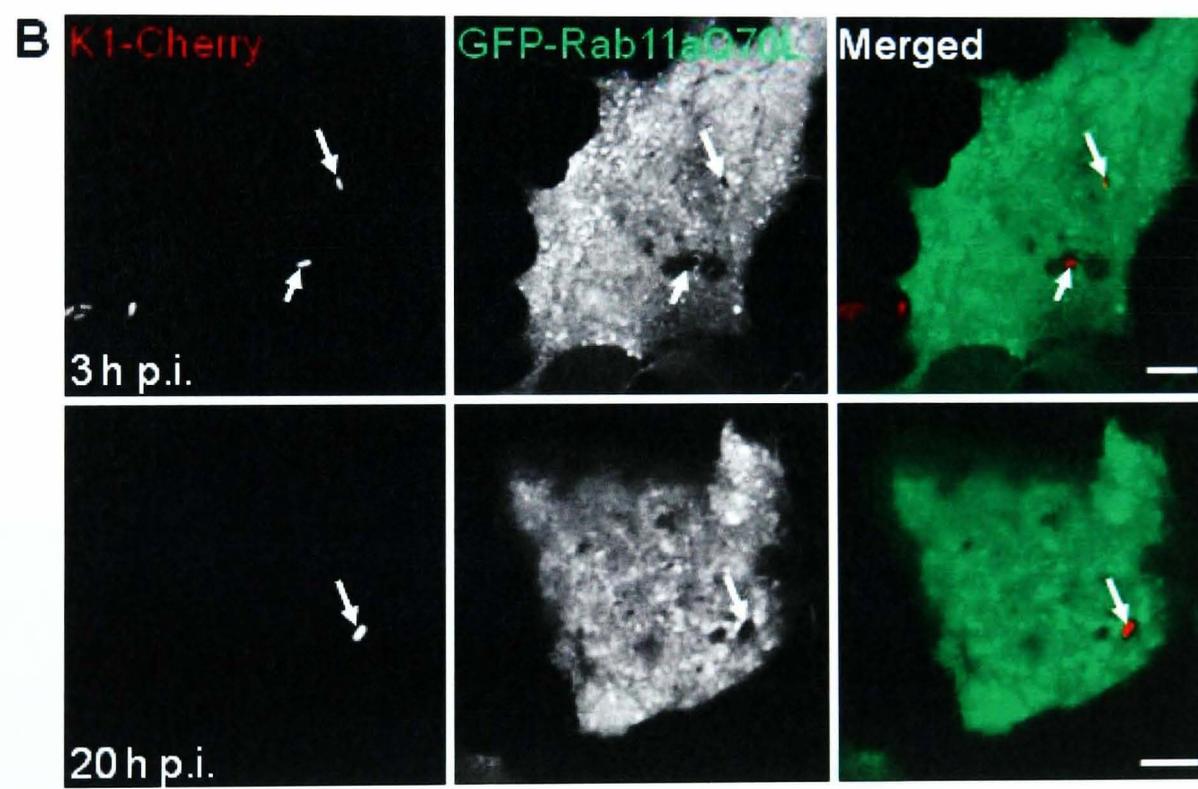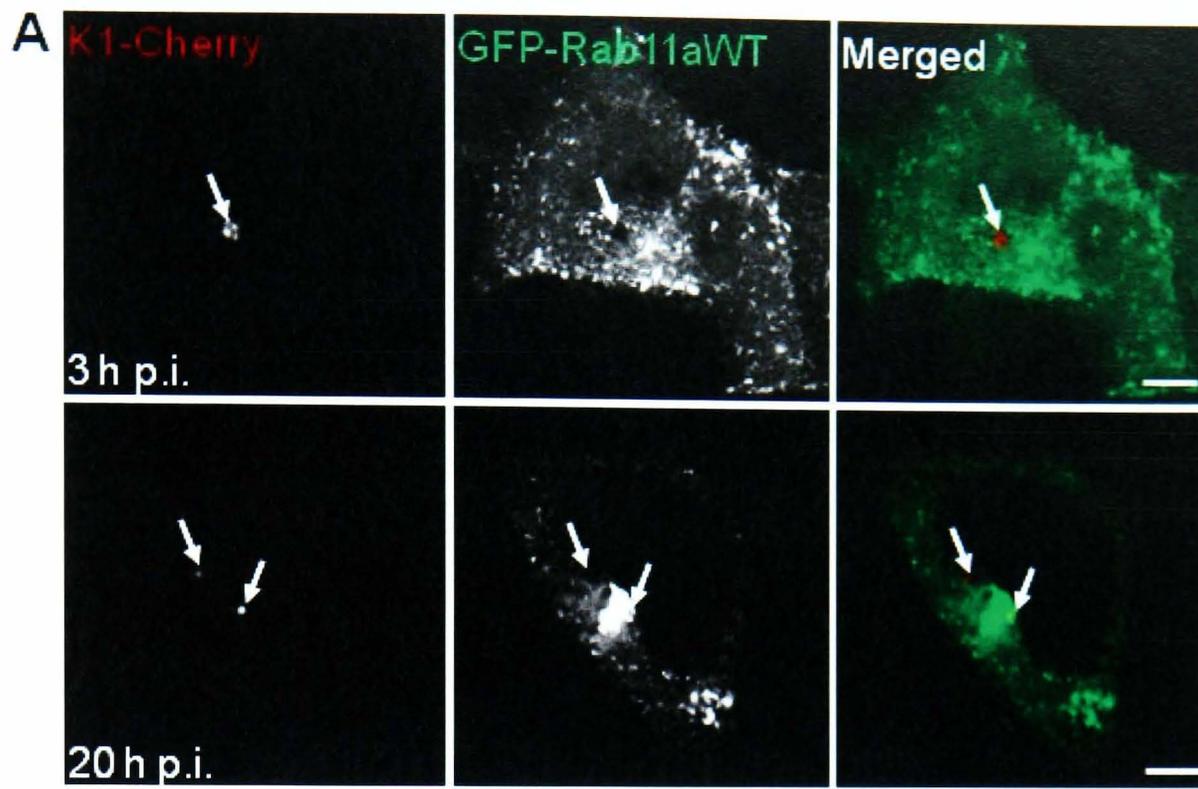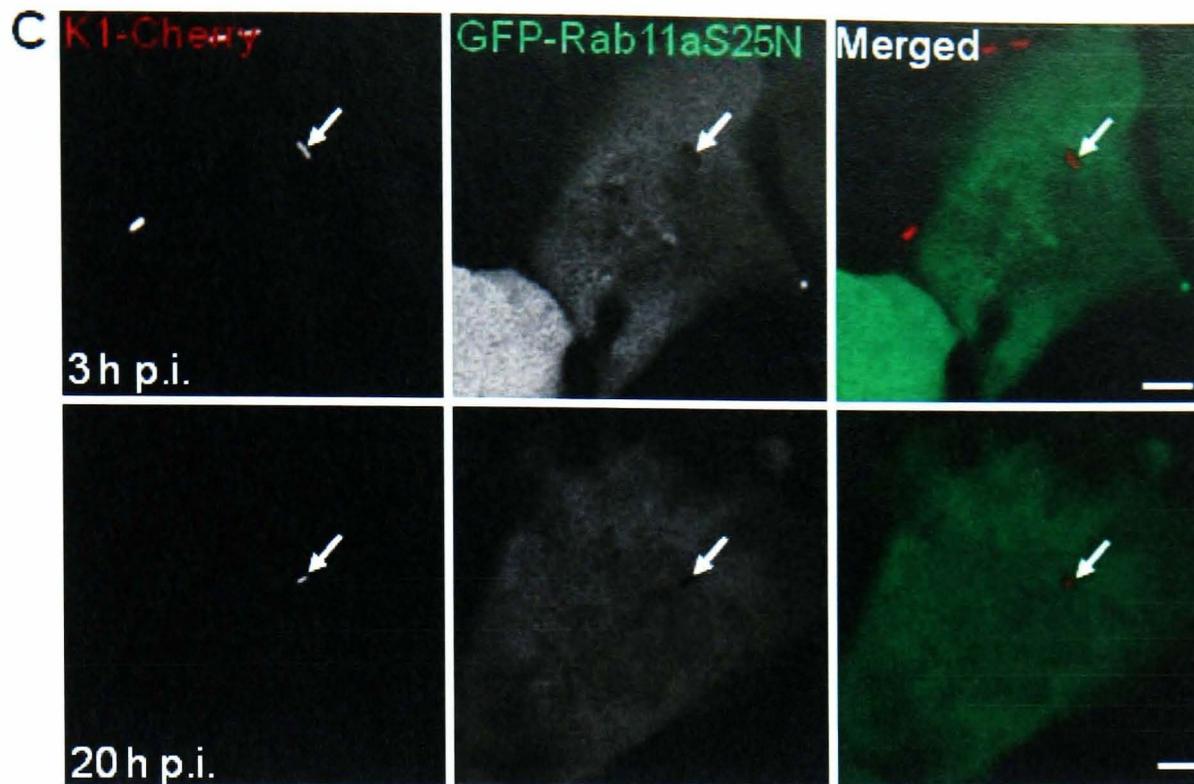
Figure 6.2. *E. coli* K1-containing vacuoles do not acquire Rab11a during endosomal maturation. (A) - (C) Representative confocal micrographs of HBMEC cells transiently expressing GFP-Rab11aWT (A), GFP-Rab11aQ79L (B), and GFP-Rab11aS25N (C) that were infected with K1-Cherry (red) at MOI of 100 for 2 hours, followed by incubation in media containing gentamicin for 1 or 18 hours, and imaged with a confocal microscope as described in Chapter 2. The white arrows indicate intracellular K1-Cherry. Scale bars: 5 μm.

6.3.3 *E. coli* K1 localizes in a late endosomal/lysosomal compartment

Kim *et al.* (2003) also showed that the K1 capsule prevented the ECV that acquired characteristics of late endosome (positive for Rab7 and LAMP1) from fusion with lysosomes 2 hours p.i., evidenced by the absence of cathepsin D co-localization with ECV. We further investigated the role of Rab7 on ECV development by infecting HBMEC transiently overexpressing wild type Rab7 (Rab7WT) with K1-Cherry as described for 2 hours, and imaged live with a confocal microscope. Two mutant forms of Rab7 GTP-locked Rab7 (Rab7Q67L), or GDP-locked Rab7 (Rab7T22N), were also used in case any association with Rab7 was transient. Vesicular and punctate structures were observed in the cytoplasm and juxtanuclear position of HBMEC expressing Rab7WT (Figure 6.3A), and K1-Cherry was localized in a membrane bound compartment decorated with Rab7 in the cell cytoplasm. It was observed that all the intracellular K1-Cherry were localized in

Rab7WT compartments (data not shown). In HBMEC overexpressing Rab7Q67L (Figure 6.3B), large vesicular structures were observed and K1-Cherry were localized in the mutant protein decorated compartments. In contrast to HBMEC overexpressing Rab7WT and Rab7Q67L, diffuse punctate signals were seen in the cytoplasm of HBMEC overexpressing Rab7T22N (Figure 6.3C). In these Rab7T22N-expressing HBMEC, clumps of K1-Cherry were found localised in areas devoid of cytoplasmic Rab7T22N.

To ensure that the bacterial invasion was not affected by the overexpression of these Rab7 chimaerae in HBMEC, HBMEC expressing GFP-Rab7 chimaerae were infected with K1-Cherry as described in section 6.3.1 and processed for imaging (Figure 6.3D). The number of K1-Cherry infected GFP-Rab7 chimaerae expressing HBMEC were counted. The preliminary data showed that the number of infected Rab7Q67L-expressing HBMEC was lower than the number of infected HBMEC overexpressing either Rab7WT or Rab7T22N; however, the number of infected Rab7Q67L-expressing HBMEC increased sharply to about 10%, which was higher than that of other infected Rab7 chimaerae-expressing HBMEC. This data is inconclusive and the experiment needs to be repeated.

We further asked if ECV-Rab7 association is transient or stable. To address this question, time-lapse imaging of HBMEC transiently overexpressing GFP-tagged wild type Rab7 with K1-Cherry was performed 2 hours p.i. (Figure 6.3E). K1-Cherry was found to remain in Rab7-enriched compartments for prolonged periods of time (here shown approximately 6 hours). Intriguingly, cross-sectional view of the last time point revealed that the bacteria in the Rab7 compartments were localized at the basolateral membrane surface; while at 2 hours p.i., cross-sectional view revealed that the bacteria were very close to the apical surface of the cell (Figure 6.3F).

A K1-Cherry   GFP-Rab7WT   Merged

B K1-Cherry   GFP-Rab7Q67L   Merged

C K1-Cherry   GFP-Rab7T22N   Merged

D
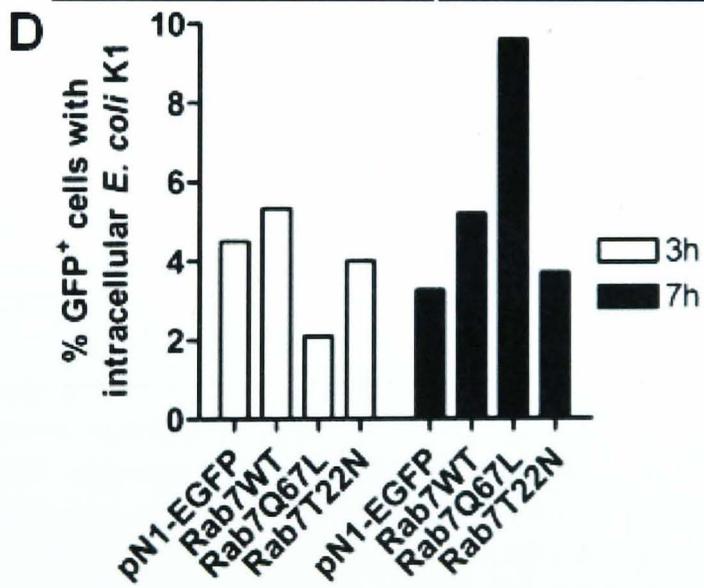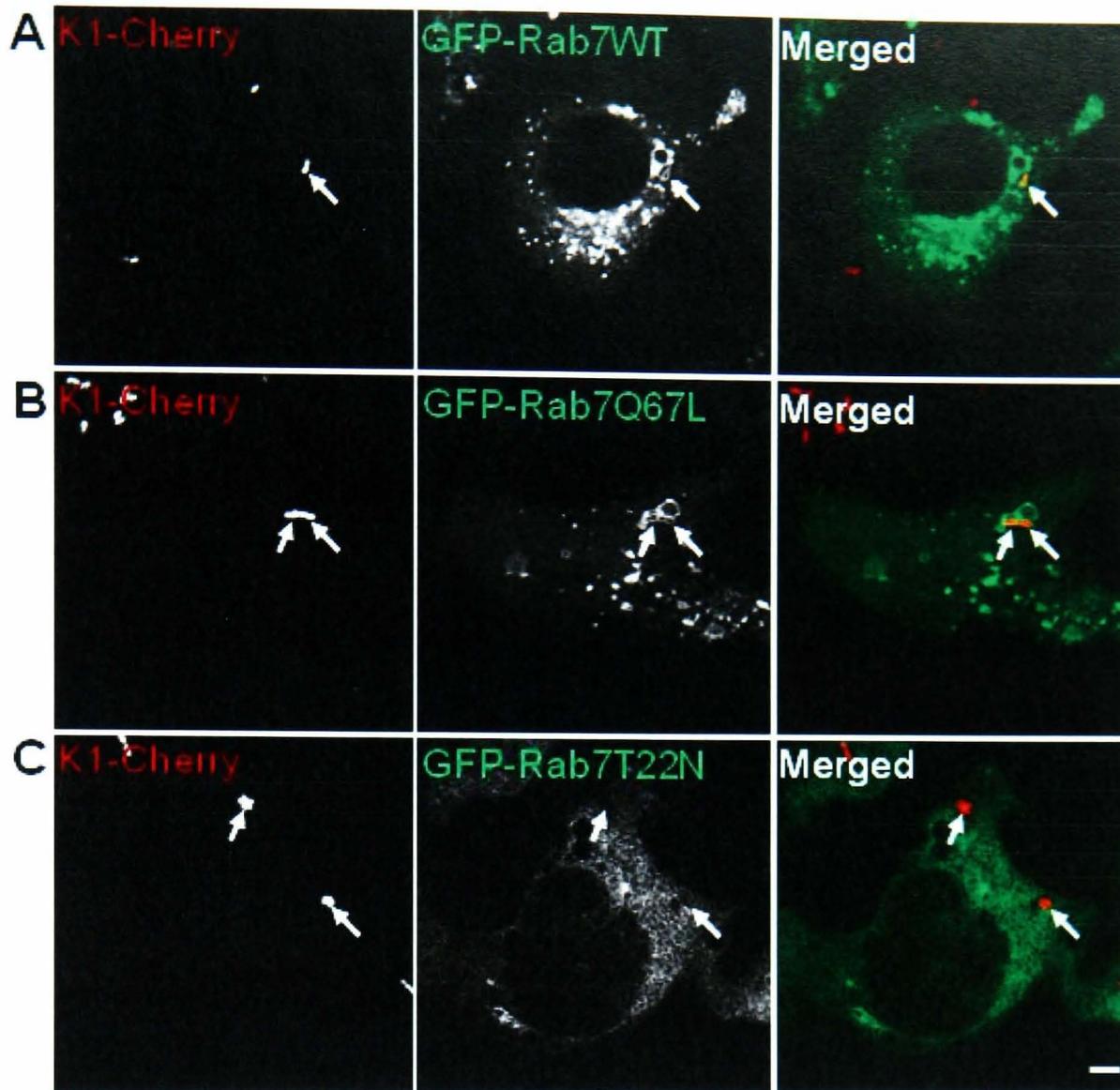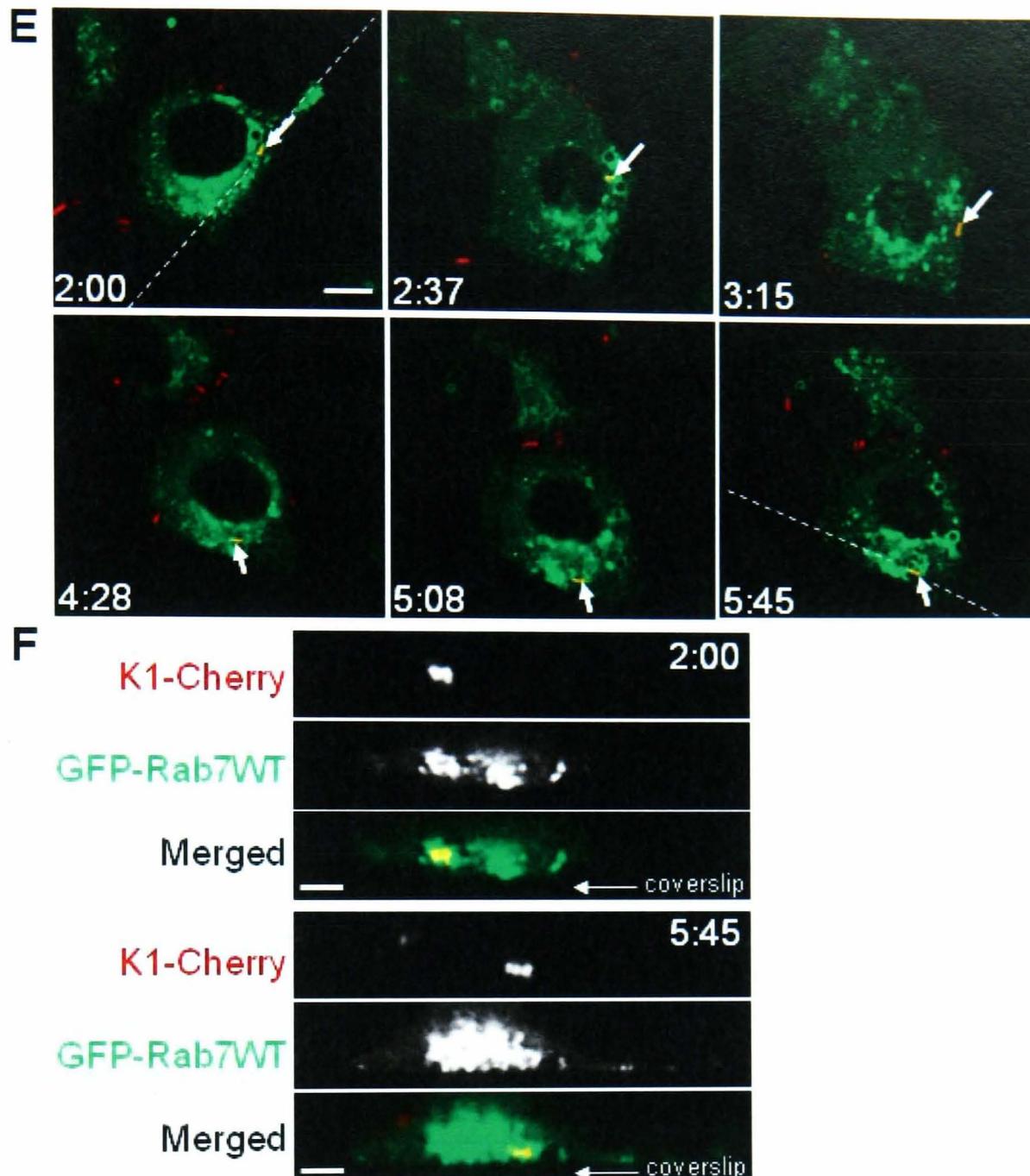
Figure 6.3. Localization of intracellular *E. coli* K1 in Rab7 compartments. (A) - (C) Representative confocal micrographs of HBMEC cells transiently expressing GFP-Rab7WT (A), GFP-Rab7Q67L (B), and GFP-Rab7T22N (C) that were then infected with K1-Cherry (red) at MOI of 100 for 2 hours. Transfected, infected HBMEC cells were imaged at 2 hours p.i. with a confocal microscope as described in Chapter 2. The white arrows indicate intracellular K1-Cherry. (D) To investigate overexpression of GFP-tagged Rab7 chimaerae on K1-Cherry invasion, HBMEC overexpressing GFP-tagged Rab7 chimaerae were infected with K1-Cherry at MOI of 100 for 2 hours, followed by incubation in media containing gentamicin for 1 or 5 hours, and imaged as in (A) – (C). pN1-EGFP was included as the experimental control. GFP-expressing HBMEC with intracellular *E. coli* K1 were scored by confocal microscopy at 3 and 7 hours p.i. Data are from one experiment. (E) Representative frames of time-lapse imaging of K1-Cherry infected GFP-Rab7WT-expressing HBMEC 2 hours p.i. The elapsed time (hours: minutes) is indicated at the lower left hand corner of each panel. The white arrows indicate intracellular K1-Cherry co-localized with Rab7. Scale bars: 5 μm. The white dotted lines indicate the position of cross-sectional view in (F). (F) The micrographs show the cross-sectional view of infected cells at 2:00 and 5:45 timepoints. Scale bar: 5 μm.

175

In agreement with Kim *et al.* (2003), our live-cell imaging results also revealed localization of the bacteria in LAMP1-positive compartments at 3 and 20 hours p.i. (Figure 6.4A and B). We also observed that the intracellular K1-Cherry in LAMP1 compartments appeared intact and brightly fluorescent 20 hours p.i. (Figure 6.4B). Intriguingly, several the bacteria were located in these LAMP1 compartments 20 hours p.i., while individual bacillus was observed in LAMP1 compartments 3 hours p.i. This observation might suggest intracellular bacterial replication in LAMP1 compartment at later time point, which was supported by increased number of recovered intracellular *E. coli* K1 7 hours p.i. (Figure 3.5)
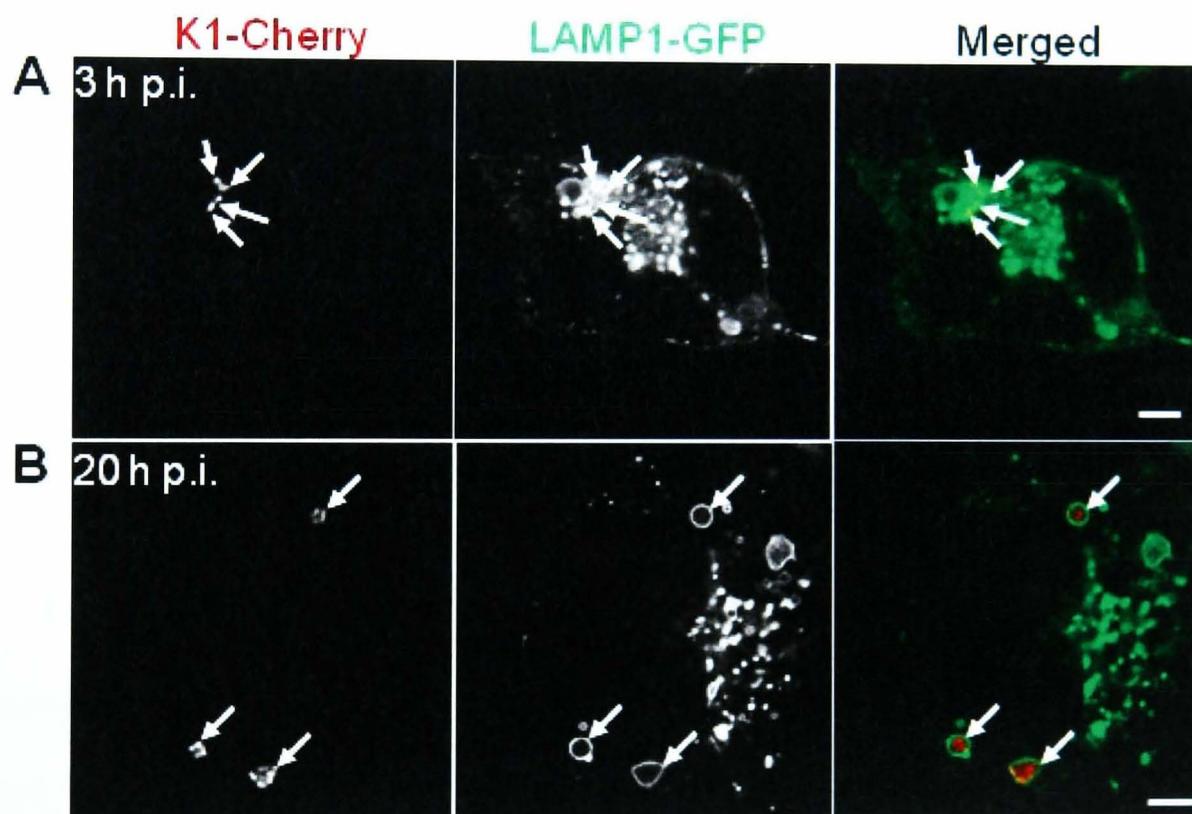
Figure 6.4. *E. coli* **K1-containing vacuoles acquire the lysosomal membrane glycoprotein, LAMP1.** (A) and (B) Representative confocal micrographs of HBMEC cells transiently expressing LAMP1-GFP that were infected with K1-Cherry (red) at MOI of 100, followed by 1 or 18 hours incubation in media containing gentamicin, imaged at 3 (A), and 20 hours p.i. (B) with a confocal microscope. The white arrows indicate intracellular K1-Cherry. Scale bars: 5 μm.

We further investigated the interaction of Rab9 chimaerae with *E. coli* K1. GFP-Rab9 chimaera, either wild type Rab9 (Rab9WT), or GTP-locked Rab9 (Rab9Q66L), or

GDP-locked Rab9 (Rab9S21N), was transfected into HBMEC, and the transfected cells were infected with K1-Cherry as described (Figure 6.5). The cells were imaged with a confocal microscope 3 and 20 hours p.i. Both GDP- and GTP-locked mutants were also used in case any association with Rab9 was transient. In HBMEC overexpressing Rab9WT, vesicular structures were concentrated at the juxtanuclear position as well as in the cytoplasm (Figure 6.5A), whereas in HBMEC overexpressing Rab9Q66L, fluorescent signal was diffuse in the cytoplasm with some large vacuolar structures observed (Figure 6.5B). In HBMEC overexpressing Rab9S21N, fluorescent signal was diffuse in cytoplasm, but some enlarged vacuolar structures were observed, with some of these structures appeared at juxtanuclear position (Figure 6.5C). We found that intracellular K1-Cherry were localized in Rab9WT and Rab9Q66L-enriched compartments at 3 and 20 hours p.i. in HBMEC transiently overexpressing respective GFP-tagged Rab9 chimaerae (Figure 6.5A and B respectively), but not with Rab9S21N (Figure 6.5C). Interestingly, similar with the observation with bacteria localized in LAMP1 compartment, several K1-Cherry was found in an individual Rab9WT compartment at 20 hours p.i., which might suggest bacterial replication.

From these results we conclude that ECV development might involve early endosomal markers, in which the interaction might be rapid and transient. ECV was not directed to recycling endosomes which involved Rab11, but the vacuole matured to late endosome-like compartment with Rab7, Rab9, and LAMP1 detected on the vacuole.

A

K1-Cherry	GFP-Rab9WT	Merged
3 h p.i.		
20 h p.i.		

B

K1-Cherry	GFP-Rab9Q66L	Merged
3 h p.i.		
20 h p.i.		
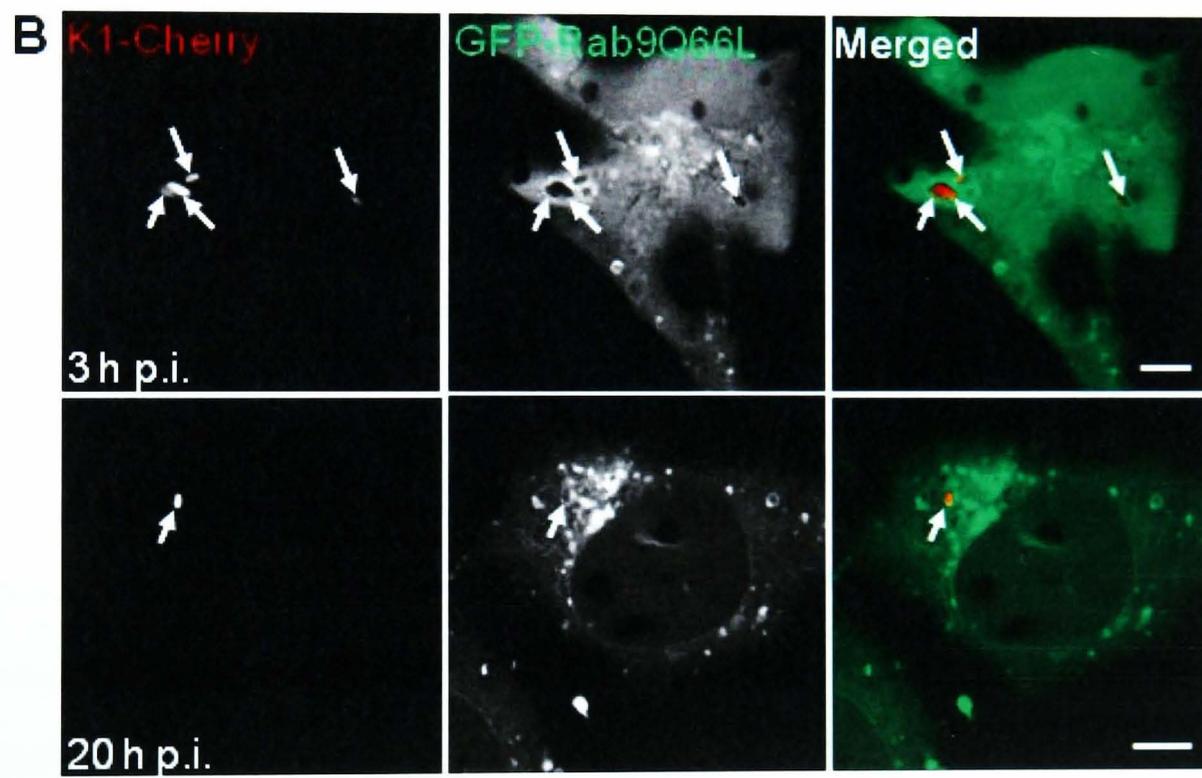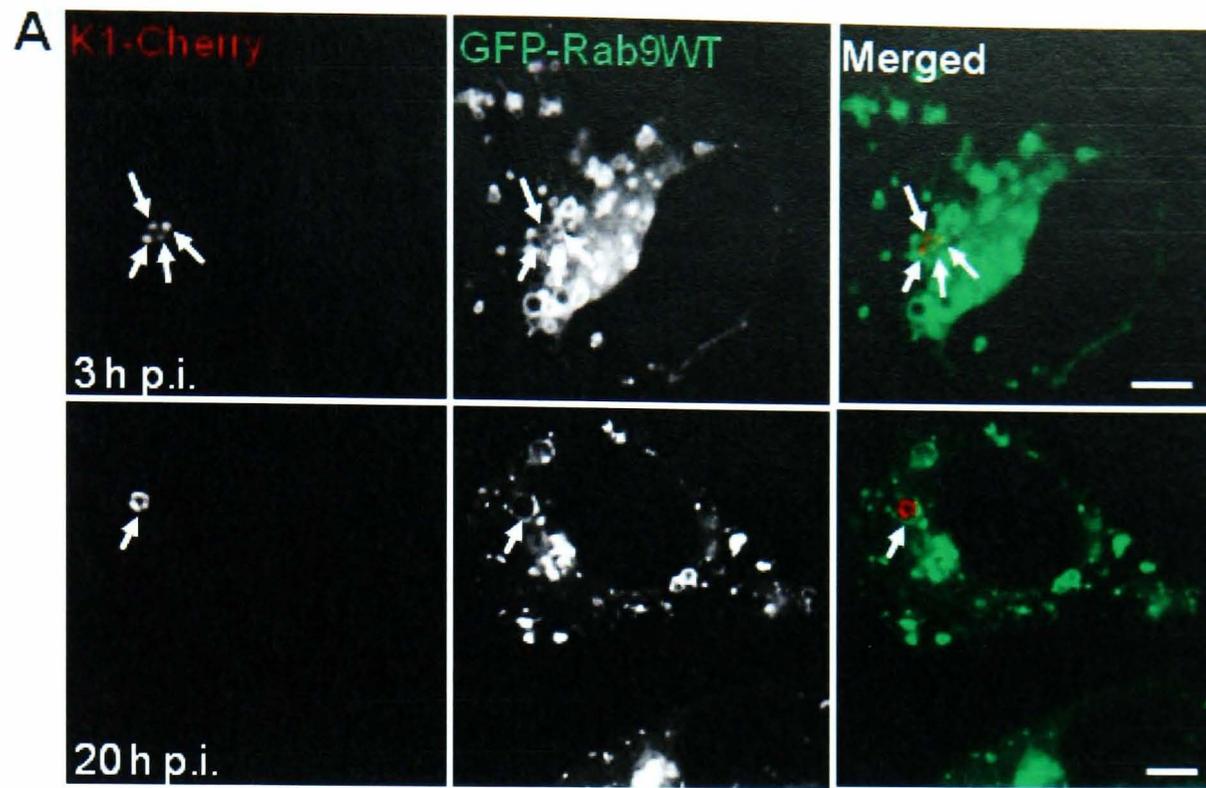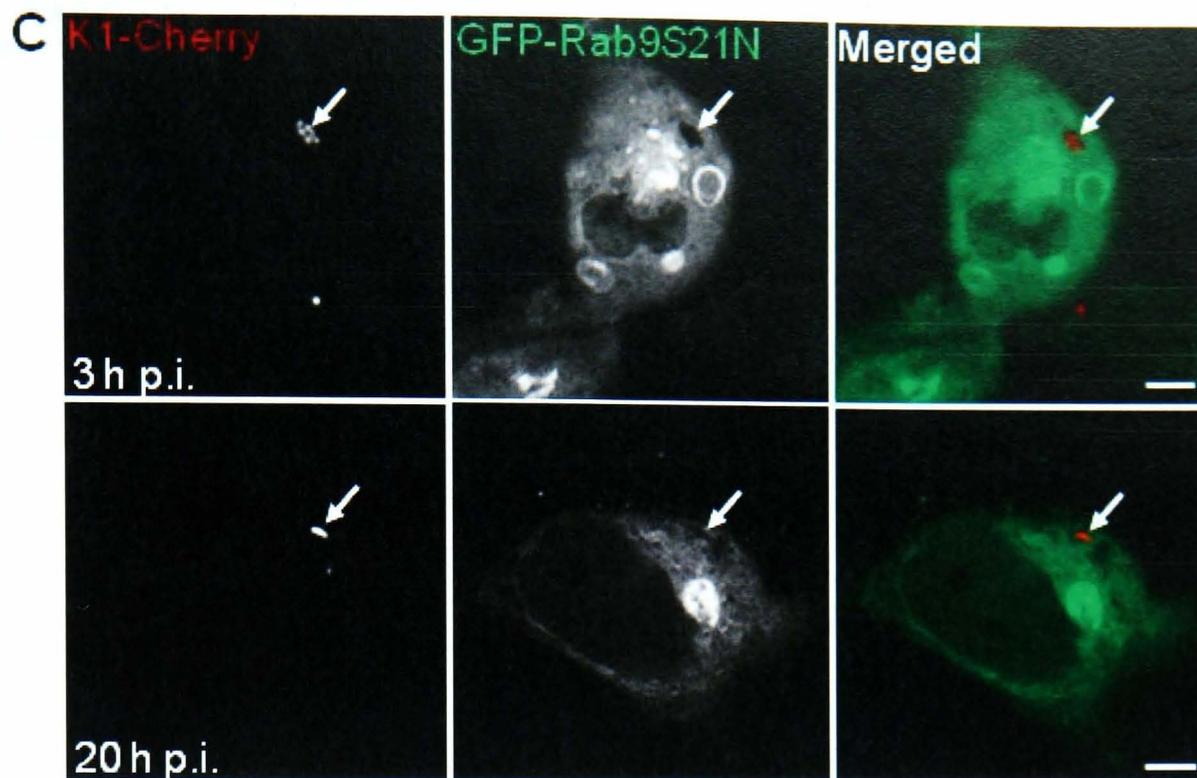
Figure 6.5. ***E. coli*** **K1-containing vacuoles acquire Rab9 during endosomal maturation.** (A) - (C) Representative confocal micrographs of HBMEC cells transiently expressing GFP-Rab9WT (A), GFP-Rab9Q66L (B), and GFP-Rab9S21N (C) that were infected with K1-Cherry (red) at MOI of 100 for 2 hours, followed by incubation in media containing gentamicin for 1 or 18 hours, and imaged at 3, and 20 hours p.i. with a confocal microscope as described in Chapter 2. The white arrows indicate intracellular K1-Cherry. Scale bars: 5 μm.

6.4 Discussion

The *E. coli* K1 invasion pathway of HBMEC has been studied extensively for the past two decades (Prasadarao *et al.*, 1993; Huang *et al.*, 1995; Prasadarao *et al.*, 1996a; Prasadarao *et al.*, 1996b; Reddy *et al.*, 2000a; Reddy *et al.*, 2000b; Khan *et al.*, 2003; Prasadarao *et al.*, 2003; Maruvada *et al.*, 2008; Liu *et al.*, 2010); however, the trafficking pathways involved in bacterial intracellular survival are poorly understood. The classical degradative endocytic pathway to the lysosome is prevented by the presence of the K1 capsule, which is essential for the bacterial intracellular survival by preventing lysosomal fusion with the ECV (Hoffman *et al.*, 1999; Kim *et al.*, 2003).

In this study, we showed that *E. coli* K1 does not arrest endosomal maturation at early endosomal stage and that overexpression of various GFP-tagged Rab5 chimaerae does not affect the bacterial invasion of HBMEC. Intracellular *E. coli* K1 does not localize to the Rab11a recycling compartment, but the bacteria were found to localize in late

179

endosomal compartments, which are positive for Rab7, Rab9, and LAMP1. Time-lapse imaging revealed that the intracellular bacteria were associated with Rab7 2 hours p.i. and remain associated throughout the imaging time point.

Numerous pathogenic bacteria, such as *Campylobacter jejuni*, *Coxiella burnetii*, and *Salmonella enterica* serovar Typhimurium, localize in late endosomal-like compartments, but the bacteria-containing vacuoles do not fuse with lysosomes (Méresse *et al.*, 1999; Beron *et al.*, 2002; Watson and Galán, 2008). Although cathepsin D has previously been shown to be absent from ECV (Kim *et al.*, 2003), we were unable to repeat this finding and to demonstrate the absence of cathepsin D from the Rab7/LAMP1/Rab9-associated ECV at later time points of infection, due to reagent compatibility (data not shown). However, intracellular mCherry-expressing *E. coli* K1 remained intact and brightly fluorescent 20 hours p.i. (Figure 6.4B, 6.5A – C), which might indicate the bacteria were viable (Hagedorn and Soldati, 2007). *in vitro* study has also demonstrated that fluorescent protein fails to retain in bactericidal compound-killed *Mycobacterium tuberculosis*, while the protein is stably maintained in bacteriostatic compound-treated bacteria (Carroll *et al.*, 2010). Recently, the application of a fluorescence dilution bacterial reporter system found that a large population of *Salmonella* Typhimurium does not replicate upon entry into macrophages, but enters a dormant stage, in which the bacteria are unculturable on laboratory medium, but some are able to respond to an extracellular chemical inducer, and equally there is no evidence of their being killed intracellularly (Helaine *et al.*, 2010). The *Salmonella* findings open up a critical question of the viability and dormancy of intracellular *E. coli* K1 in various identified cellular compartments in this study, especially at late time points of infection. One of the results from this study showed that *E. coli* K1 could survive intracellularly 7 hours p.i. (Figure 3.2), but a very low number of viable bacteria were recovered 20 hours p.i. (data not shown), which was possibly due to bacterial dormancy, or bacterial killing, or the majority

of the bacteria having egressed from the infected cells at late time point and by gentamicin in the media.

In the previous chapter, ≥30% intracellular bacteria were found to be associated with flotillin 1, while comparison to more traditional endocytic markers in this chapter additionally found that the intracellular bacteria were localized in late endosomal compartments that are positive for Rab7 (Figure 6.3A and E), Rab9 (Figure 6.5A), and LAMP1 (Figure 6.4A and B). With these observations, we questioned the correlation between flotillin 1 and these late endosomal markers on ECV. Flotillin 1 is considered as a late endosomal marker and co-localizes with LAMP1 (Dermine *et al.*, 2001), but live intracellular *Mycobacterium marinum* (*M. marinum*) are found to replicate in flotillin 1 compartments that are devoid of LAMP1 in human peripheral monocytes (Hagedorn and Soldati, 2007). Therefore, it is important to characterize if those flotillin 1-associated ECV exist as an independent compartment or associate with LAMP1, and which of these compartments provides a safe niche for the bacteria. These experiments are ongoing. Furthermore, to elucidate the specific endosomal stage at which flotillin 1 is recruited to ECV, the presence of flotillin 1 on ECV in cells overexpressing the dominant negative Rab proteins should be studied.

During this study, it was also hoped to identify a potential transcytosis pathway that *E. coli* K1 hijack for crossing HBMEC, however, our data is so far insufficient to address this question. HBMEC are rich with caveolae, which is rationale to speculate the caveolae as the major endocytic and also transcytotic pathway for the cells (Minshall *et al.*, 2003). However, this study showed that only approximately 4% of *E. coli* K1 was associated with caveolin-1 at the early infection time point, and this further reduced to less than 1% at later time points of infection. Therefore, it is very unlikely that *E. coli* K1 traverses to the basolateral surface via a caveolae-mediated pathway. Based on the current data, we speculated that *E. coli* K1 could potentially harness late/lysosomal, flotillin 1-dependent

pathway for traversing HBMEC (Figure 6.6, model 2), which has been proposed for exosome egress (Lakkaraju and Rodriguez-Boulan, 2008; Thery *et al.*, 2009). Further, the cellular markers present on ECV are typically identified on exosomes (Chertova *et al.*, 2006; Simons and Raposo, 2009; Chen *et al.*, 2011). Alternatively, ECV associated with flotillin 1 (independent of LE markers) might be the route by which the bacterial population traverses and exocytoses from HBMEC (model 1) (Figure 6.6). The presence of flotillin 1 on ECV could have a role in the recruitment of actin and other motor proteins onto the endosome (Dermine *et al.*, 2001), as flotillin binds F-actin via its stomatin, prohibitin, flotillin, and HflK/C (SPFH) domain (Langhorst *et al.*, 2007). In addition to actin and motor proteins recruitment to ECV, the actin binding ability of flotillin could be required for vesicles docking onto the target membrane, and for exocytosis (Nightingale *et al.*, 2011). Overall, other potential transcytotic markers, such as Rab25 and Rab1a, will be investigated in future experiments. Once a potential transcytotic marker is identified on ECV, the endosomal stage which the marker is recruited can be identified with the application of the available Rab dominant negative mutant constructs.
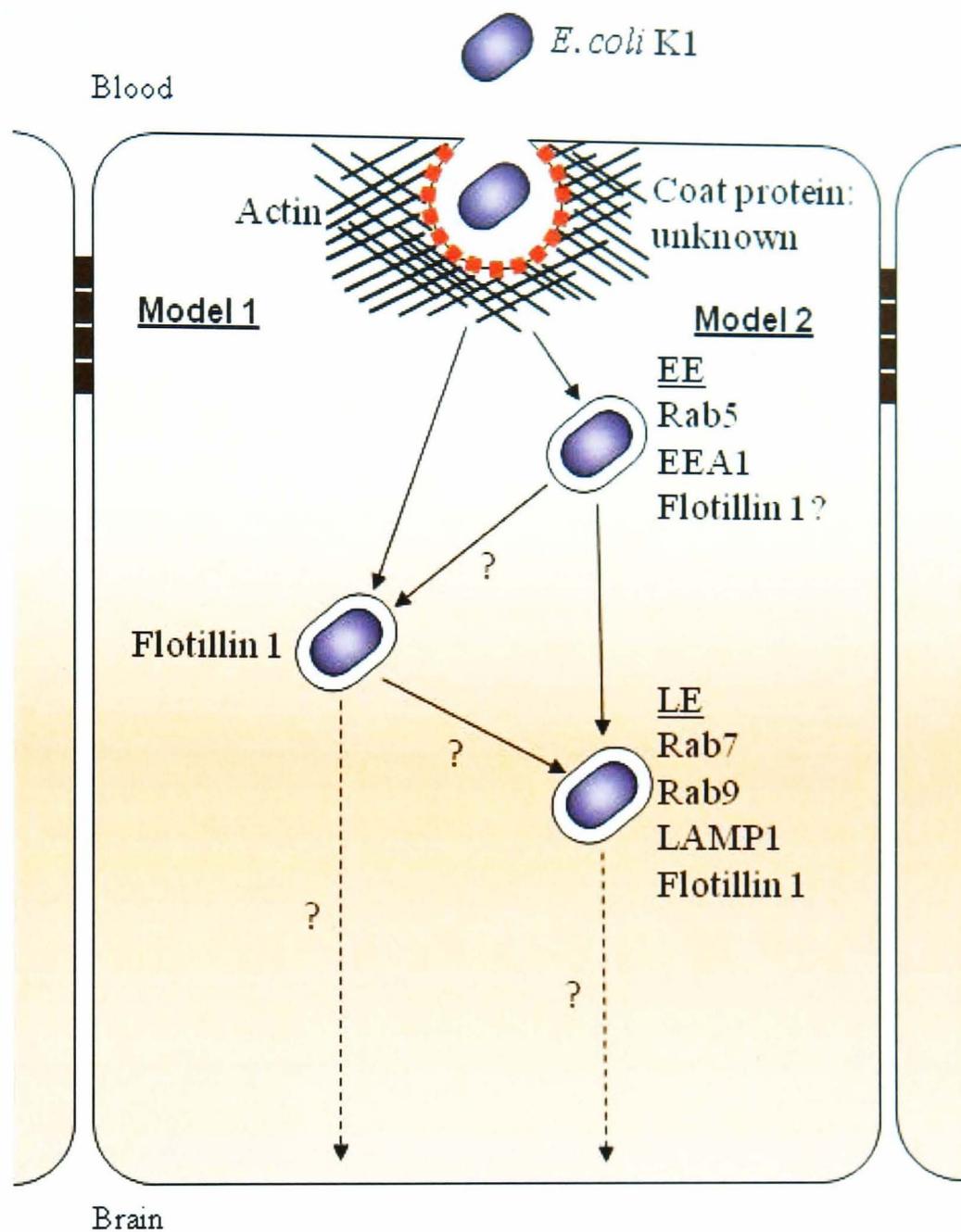
Figure 6.6. Potential *E. coli* K1 transcytotic pathway in HBMEC. *E. coli* K1 enters HBMEC via an actin-dependent process with unknown endocytic pathway. After internalization, the ECV transiently acquires different markers of the classical endocytic pathway. We speculated that *E. coli* K1 might traverse HBMEC via either flotillin 1 (model 1) or late endosomes (LE) with flotillin 1 (model 2) pathway. EE, early endosome; LE, late endosome.

7. General discussion and conclusion

E. coli is one of the bacteria predominantly isolated from neonatal bacterial meningitis cases (Osrin *et al.*, 2004; May *et al.*, 2005; Wu *et al.*, 2009; Talbert *et al.*, 2010; Gaschignard *et al.*, 2011), with high mortality rate observed in some countries (May *et al.*, 2005; Wu *et al.*, 2009). The majority of the *E. coli* strains isolated from neonatal meningitis cases possess K1 capsule (Robbins *et al.*, 1974; Sarff *et al.*, 1975), which is structurally homologous to, and immuno-cross-reactive with, the α-2,8-linked polysialic acid (polySia) glycan highly expressed on the developing brain and kidney of newborn mammals (Finne *et al.*, 1983a; Roth *et al.*, 1987; Harvey *et al.*, 2001).

For this study, an immortalized HBMEC line, which was generated by transfecting primary HBMEC isolated from patients aged 4 – 7-year-old with SV40 large T antigen (Stins *et al.*, 2001), representing the BBB, was applied to study *E. coli* K1 pathogenesis *in vitro*. Early in the study, we tried *E. coli* K1 infection on mouse brain endothelioma cell lines (bEnd5), an *in vitro* BBB model commonly applied for T cell migration studies (Steiner *et al.*, 2011), but this resulted in no intracellular bacteria recovered from infected bEnd5 lysates (data not shown). With the HBMEC model, *E. coli* K1 invasion efficiency was approximately 0.1% of the initial bacterial inoculums (Figure 3.2), which agreed with the published *E. coli* K1 invasion efficiency by Prasadarao *et al.* (1996). In fact, this level of bacterial invasion efficiency is low, and the bacterial invasion is FCS-dependent, which is a major experimental hindrance for studies that involve cholesterol depletion. The low bacterial invasion efficiency leads to some degree of experimental difficulty, especially in the studies of the bacterial entry pathways. Despite various optimization steps that were performed, such as determination of the optimum MOI, bacteria-HBMEC incubation time, total volume of experimental media used during infection, and centrifugation of the bacteria to the cell surface for synchronizing the infection, only minor improvements were

184

achieved. The observed low bacterial invasion could be an outcome of age-related differences in the HBMEC used, as indirectly evidenced by an earlier study that demonstrated the age-related susceptibility of an infant rat model in developing *Haemophilus influenza* type b-associated meningitis (Moxon *et al.*, 1977), and a similar observation was made with *E. coli* K1 infection *in vivo* (Zelmer, A., personal communication)(Mushtaq *et al.*, 2005). The difference in neonate- and adult-derived mouse brain microvascular endothelial cells (BMEC) was also demonstrated by different level of protease secretion following glutamate induction, though both endothelial cells exhibited similar phenotypes (Legros *et al.*, 2009). Therefore, we hypothesize that *E. coli* K1 would invade neonate-derived HBMEC more efficiently than HBMEC derived from patients aged 4 – 7 years of age such as the HBMEC used in this study. Owing to the involvement of complicated ethical issues in obtaining and utilizing human tissues either from live or dead patients lately (Carmichael, 2011; Marchant, 2011), neonate BMEC could be obtained from other species such as bovine and porcine, as no difference was reported in *E. coli* K1 invasion efficiency of BMEC derived from other species (Prasadarao *et al.*, 1996a).

An additional difficulty in this invasion model is that HBMEC, like other endothelial cells, are also resistance to plasmid DNA transfection, either by lipid- or polymer-based transfectants, or by electroporation (Kovala *et al.*, 2000; Segura *et al.*, 2001; Kang *et al.*, 2009; Anliker *et al.*, 2010). In this study, various transfection reagents were tried, but the transfection efficiency usually ranged between 10 - 30% (Figure 4.2). Transfection efficiency of about 50% was achieved by altering the amount of pN1-EGFP plasmid DNA and jetPRIME™ used per transfection reaction (Figure 4.3), however, with other recombinant constructs this ranged between 20 – 45%. The current transfection efficiency could probably be further improved with gene-specific lentiviral vectors, which were psudotyped with mutated truncated measles viral haemagglutinin, and displayed a

single-chain variable fragment (scFv) specific to CD105, an endothelial cell specific marker (Anliker *et al.*, 2010). However, it has been documented that the application of lentiviral vector for transducing monocyte-derived dendritic cells resulted with decrease CD1d presentation (Garg *et al.*, 2011). Therefore, there is a possibility that transduced cells might respond differently to infection.

Confocal microscopy imaging was one of the experimental techniques heavily applied in this study. To enable visualization of the bacteria under a confocal microscope, fluorescent *E. coli* K1 were required, either by surface-labelling with fluorescent dye, or by immunostaining with specific antibody, or by cytoplasmic expression of fluorescent protein. There is a limited choice of *E. coli* K1-specific antibodies, and bacterial surface-labelling with FITC dye led to unexpected imaging channel cross-talk, as well as a decrease in bacterial invasion of HBMEC. Therefore, in Chapter 3, we described the making of fluorescent bacteria that retain bacterial virulence by transforming the bacteria with various bacterial expression vectors expressing fluorescent protein. All the transformed bacteria fluoresced under a confocal microscope, but the majority of them demonstrated impairment in bacterial invasion of HBMEC, except *E. coli* K1 transformed with pFPV25.1, which has been widely applied in *Salmonella* (Cheminay *et al.*, 2005; Radtke *et al.*, 2007; Gerlach *et al.*, 2008), and pathogenic *E. coli* studies (Radtke *et al.*, 2007; Marchès *et al.*, 2008). Surprisingly, the invasiveness of transformed *E. coli* K1 bearing pFPV-mCherry construct, in which the *gfpmut3a* gene of pFPV25.1 was replaced with mammalian codon-optimised mCherry cDNA, was closely similar to the untransformed bacteria (Figure 3.19). Even so, our results show that the presence of plasmid DNA and expression of fluorescent proteins could affect bacterial virulence, and the possibility that the fluorescent protein gene or the plasmid DNA copy number might also affect bacterial virulence gene expression must be kept in consideration when interpreting results (Clark *et al.*, 2009; Valdivia, R., personal communication). The

mCherry-expressing *E. coli* K1 not only served as a useful tool for this study, retaining virulence in the assays here, but also might be a valuable tool for future preliminary *in vivo* live animal imaging, in which the application of the longer excitation wavelength needed for mCherry also enables better deep tissue penetration and is less prone to tissue autofluorescence.

E. coli K1 entry has been proposed to be receptor-dependent and via zipper mechanism (Prasadarao *et al.*, 1999), which was further supported by the absence of T3SS in the RS218 clinical strain or the E44 strain used in all studies by Kim's group for the past two decades (Yao *et al.*, 2006). The molecular events that lead to actin polymerization at the bacterial adhesion site have been very well-studied (Prasadarao *et al.*, 1999; Reddy *et al.*, 2000a; Reddy *et al.*, 2000b; Prasadarao, 2002; Khan *et al.*, 2003; Maruvada *et al.*, 2008). The endocytic pathway manipulated by the bacteria for HBMEC entry was reported to be clathrin-independent (Prasadarao *et al.*, 1999), and caveolae-dependent (Sukumaran *et al.*, 2002). Based on the current knowledge of caveolae-mediated entry, dynamin is required for caveolar fission *in vitro* and *in vivo* (Oh *et al.*, 1998; Pelkmans *et al.*, 2002; Yao *et al.*, 2005), and dynamin might also have a role in actin cytoskeleton recruitment (Lee and De Camilli, 2002). However, previous studies have not investigated the role of dynamin during *E. coli* K1 internalization. Given the proposed entry site of caveolae, we hypothesized that overexpression of GDP-locked dynamin would inhibit the bacterial uptake into HBMEC. To our surprise, we found no inhibitory effect on the *E. coli* K1 entry in HBMEC overexpressing GDP-locked dynamin 1 or 2 (Figure 5.1A and B). Although these constructs have been widely used in previous studies (Cao *et al.*, 1998; Watson and Galán, 2008; Rahn *et al.*, 2011) the uptake of a known specific ligand, such as transferrin (clathrin-mediated endocytosis), into HBMEC overexpressing GDP-locked dynamin need to be assessed to ensure this observation was not due to non-functioning GDP-locked dynamin mutants. Dynamin inhibitors, such as dynasore (Macia *et al.*, 2006), could be

applied for blocking dynamin isoforms in cells and studied their effects on *E. coli* K1 invasion of HBMEC. Since dynasore is a broad spectrum inhibitor, the application of this inhibitor for studying *E. coli* K1 invasion of HBMEC would rule out the possibility that other endogenous dynamin isoforms and splice variants take over roles in cells overexpressing a GDP-locked dynamin isoform.

To confirm the findings by Sukumaran *et al.* (2002), we revisited the role of caveolin-1 during *E. coli* K1 infection of HBMEC, and found that only about 4% of the bacteria were localized in compartments weakly stained for caveolin-1 at 30 minutes p.i., i.e., at a timepoint where we would expect to see bacteria undergoing invasion, and that population of bacteria further reduced to approximately 1% at later timepoints indicating no obvious association with caveolin-1 during uptake or with the intracellular ECV (Figure 5.2A and B). Furthermore, the application of caveolin-1 mutants had no effect on *E. coli* K1 internalization. Importantly, *E. coli* K1 invasion of caveolin-1 knockout MLEC was not inhibited. However, this observation is insufficient to completely rule out the bacterial invasion via non-caveolae-mediated endocytic pathway, as Siddiqui *et al.* (2011) demonstrated the absence of caveolin-1 led to destabilization of adherens junctions, activation of endothelial nitric oxide synthase (eNOS) in endothelial cells, which impaired GTPase activating protein (GAP) p190RhoGAP-A by nitrating tyrosine residue 1105, and led to RhoA activation (Siddiqui *et al.*, 2011). RhoA was shown to be required for *E. coli* K1 invasion of HBMEC (Khan *et al.*, 2002), therefore, the inhibitory effect of bacterial invasion in caveolin-1 knockout MLEC might be cancelled by RhoA. To further elucidate the role of caveolin-1 during *E. coli* K1 invasion, caveolin-1 Y14A mutant, which is non-phosphorylatable and its expression in cells inhibited caveolae-mediated endocytosis (del Pozo *et al.*, 2005; Hu *et al.*, 2006), could be transfected into caveolin-1 knockout MLEC, and infect with the bacteria. It is hypothesized that the bacterial invasion of caveolin-1

Y14A expressing caveolin-1 knockout MLEC would be inhibited if caveolae-mediated endocytosis is exploited by *E. coli* K1 for cell invasion.

At this stage of the study, our findings are contradictory to the Sukumaran *et al.* (2002) findings, where they reported inhibition in *E. coli* K1 invasion in HBMEC overexpressing dominant negative caveolin-1 (caveolin-1 with two amino acids mutation at the scaffolding domain for phosphor-PKCα interaction), and strong staining of the invading and intracellular bacteria with caveolin-1. As discussed above, further experiments are needed to further substantiate our findings; however, there are also several ambiguities in their findings. First, in the panel of micrographs that was indicated as bacteria-specific staining, very strong non-specific background was observed, and appears to show staining of the entire cell periphery. This strongly suggests that the caveolin-1 signal on the bacteria that they observed could be signal resulting from channel crosstalk with bacterial staining. Secondly, the authors stated that the presented micrographs were from 30 minutes p.i. (MOI unknown, but it was stated that 1×10^7 *E. coli* K1 were used for infection), and a high number of bacteria was observed in the panels that they claimed to be intracellular. We have never seen such a high number of intracellular bacteria at 30 minutes p.i., a maximum single bacterium per cell is more frequently observed in our hands at the similar time point. We only see clumps of intracellular bacteria at much later timepoints (see below). Thirdly, filipin was applied to deplete cholesterol from HBMEC plasma membrane in their study, and a dose-dependent reduction in recovered intracellular *E. coli* K1 was reported. We tried to repeat this experiment, but 30 minutes incubation with 1 or 4 μg/ml of filipin in FCS-free media resulted in massive cell detachment from the well, probably due to the sensitivity of HBMEC to some chemical inhibitors (Kim, K.S., personal communication).

Since no link was found between *E. coli* K1 invasion and dynamin- and caveolin-1-mediated endocytic uptake, which endocytic pathway that the bacteria manipulated for

invading HBMEC was explored. We chose to focus on the flotillin-mediated pathway, which forms distinct lipid raft microdomains on the plasma membrane and the pathway is dynamin-independent. Both flotillin 1 and flotillin 2 co-localize and co-assemble into microdomains distinct from caveolae microdomains (Frick et al., 2007). It has been shown that knockout of flotillin 1 causes concomitant reduction in flotillin 2 expression (Ludwig et al., 2010), and this study showed that in flotillin 1 knockout MLEC, flotillin 2 distribution was disrupted as evidenced by the absence of flotillin 2 punctate staining. We observed weak flotillin 1 signal accumulated beneath approximately 5% of extracellular bacterial population and 5% of the intracellular bacterial population were associated with flotillin 1 at 30 minutes p.i. (Figure 5.5A and B). The intracellular bacteria that associated with flotillin 1 increased to about 30% at 2 hour p.i. However, in flotillin 1 knockout MLEC, instead of blocking the bacterial internalization as would be expected if flotillin 1 were required for uptake, both E. coli K1 and non-pathogenic E. coli K-12 intracellular density was significantly enhanced at 150 minutes p.i. (Figure 5.6A). The enhanced bacterial density was caused by enhanced bacterial invasion into flotillin 1 knockout MLEC, and not because of non-functioning lysosomal pathway (Figure 5.6B). These results show that E. coli K1 does not require the flotillin 1-mediated pathway for invading HBMEC, and the bacterial invasion should also be flotillin 2 independent since both flotillin 1 and flotillin 2 co-assemble to form microdomains and their expression are interdependent.

The data in this study suggest that E. coli K1 endocytosis is dynamin-independant, and the precise endocytic pathway utilized is still unclear. There are three major dynamin-independent endocytic pathways, namely the Arf-6-regulated pathway, the Cdc42-regulated pathway, and macropinocytosis (Mayor and Pagano, 2007; Kumari and Mayor, 2008; Mercer and Helenius, 2009; Howes et al., 2010; Kumari et al., 2010). Arf6 and Cdc42 dominant active and dominant negative constructs have been sourced and will be

tested in HBMEC to study their effects on *E. coli* K1 invasion. To date, there is no singular cellular target to study macropinocytosis, a number of different cellular markers together are needed to imply the activity of the macropinocytic pathway. It is interesting to note that current experimental criteria to implicate macropinocytosis specifically exclude a dependency on the Rho GTPase RhoA (Mercer and Helenius, 2009). Activation of RhoA during *E. coli* K1 invasion of HBMEC has been published previously (Khan *et al.*, 2002; Khan *et al.*, 2003). Furthermore, overexpression of dominant negative RhoA T19N mutant reduces *E. coli* invasion; while overexpression of the dominant positive form (RhoA G14V) increased invasion (Khan *et al.*, 2002). Rho A has also been proposed as a clathrin-independant but dynamin-dependent endocytic pathway for interleukin 2 (IL2) receptor (Lamaze *et al.*, 2001), which is contradictory with the dynamin-independent findings in this study. Since RhoA is one of the key signalling molecules involved in the regulation and dynamics of the actin cytoskeleton, the activation of RhoA seen in *E. coli* K1 infection of HBMEC may be a bystander effect due to the actin rearrangement triggered during infection. Indeed, a dependency of *E. coli* K1 invasion on RhoA has not been shown.

Enhanced intracellular bacterial density was observed in flotillin 1 knockout MLEC, which we believed was a result of enhanced bacterial uptake, evidenced by higher number of infected flotillin 1 knockout cells than the number of infected wild type cells after 30 minutes infection (Figure 5.6B). We hypothesize that the cholesterol content of the plasma membrane might have been depleted in the flotillin 1 knockout cells; hence, the membrane fluidity might be enhanced, and could lead to facilitated penetration by the bacteria. Alternatively, flotillin 1 might have a role in regulating cellular cytoskeletal structures (Langhorst *et al.*, 2008a), that might form a cellular barrier at the bacterial attachment sites, or the absent of flotillin 1 disrupt the cytoskeletal signalling pathway as observed in caveolin-1 knockout endothelial cells (Siddiqui *et al.*, 2011). This cellular barrier hypothesis might explain one of our preliminary data, wherein HBMEC

overexpressing either GFP-tagged flotillin 1 or flotillin 2 showed a lower rate of infection than HBMEC overexpressing other GFP-tagged recombinant constructs at 3 hours p.i. (Figure 5.8).

The general role of flotillin 1 *in vivo* is not known. Flotillin 1 knockout mice do survive, although a defect in neutrophil and monocyte recruitment in response to chemoattractant has been observed (Ludwig *et al.*, 2010). In addition to have a key role in host defense system, the data from this study as well as the results from others suggest that flotillin 1 might actively maintain integral barrier against external environment at the cellular and systemic level (Li *et al.*, 2008b). Therefore, future study should look into the susceptibility of flotillin 1 knockout animals to infections (particularly enteric and neurotropic pathogens), as well as autoimmune and allergy diseases, such as Crohn's disease and Asthma.

Another part of this project was to study the *E. coli* K1 intracellular survival by screening the organellar markers on the bacterial compartments. We found that the post invasion ECV had the characteristics of late endosomes. Intriguingly, at 20 hours p.i., we observed clumps of intact and fluorescent intracellular bacteria localized in these late endosomal compartments, which we believe to result from intracellular bacterial replication, also evidenced from our survival assay data (Figure 3.2). There was no evidence of *E. coli* K1 clumping in culture based on live microscopy examination (data not shown). Again, this finding is contradictory with previous publication which claimed that *E. coli* K1 did not replicate intracellularly based on transmission electron micrographs, as TEM micrograph only shows small regions of interest, there is potential bias in figure selection (Prasadarao *et al.*, 1999; Sukumaran and Prasadarao, 2002). This study also found 35% of intracellular bacteria were localized in flotillin 1 compartments at late time points of infection, to understand the distribution of flotillin 1 and late endosomal markers (Rab7 and LAMP1) on the ECV is a high priority. More detailed analysis of the host cell

factors present on the ECV could be achieved by performing a proteome analysis with mass spectrometry of purified ECV as described in (Urwyler *et al.*, 2009).

A previous study showed that the inhibition of lysosomal fusion is achieved by the presence of the K1 capsule on the bacteria (Kim *et al.*, 2003), but the lysosomal inhibition strategy that involves the K1 capsule is unknown. Therefore, other bacterial factors may involve in inhibiting ECV fusion with lysosomes. The bacteria might secrete bacterial virulence factors into the cytosol of infected HBMEC via the bacterial GSP system, which might be the alternative secretion system in the absence of T3SS (Yao *et al.*, 2006), and interfere with host factors (such as GTPases, vATPases, components of homotypic fusion and vacuole protein sorting (HOPS) complex, N-ethylmaleimide sensitive factor (NSF), etc.) required for late endosome-lysosome fusion. Further, the bacteria were shown to contain *icmF* and *icmH* in one of the bacterial pathogenicity islands (Xie *et al.*, 2006). The *Legionella* homologues of these proteins encode a type IV secretion system required for *Legionella* species' intracellular survival by avoiding trafficking to lysosomes in human macrophages (VanRheenen *et al.*, 2004). To study if the *icmF*, *icmH*, and other potential bacterial secretory proteins are translocated into the cytosol of infected HBMEC, split-GFP teachnology could be applied, whereby the bacterial proteins are tagged with the 13-amino-acid 11th strand of the GFP β-barrel (GFP11), and the non-fluorescent complementary fragment of the first ten strands of GFP (GFP1-10) is expressed in HBMEC (Van Engelenburg and Palmer, 2010). Fluorescent signal is resulted if the GFP11-tagged bacterial protein is translocated into the cytosol and complemented with GFP1-10 in HBMEC. After the identification of secreted bacterial proteins, gene specific knockout bacterial mutants could be constructed for screening of bacterial factors that are required for inhibiting lysosomal fusion to ECV.

The ability of *E. coli* K1 to traverse HBMEC cultured on a Transwell® insert without disrupting the monolayer's integrity was described a decade ago (Stins *et al.*,

2001), but the cellular pathway has never been studied. Sukumaran *et al.* (2002) proposed the bacteria utilized caveolin-1 for HBMEC traversal based on their observation of co-localization between the intracellular bacteria and caveolin-1. However, there are some ambiguities with their findings as discussed previously, and we only found about 1% of bacteria weakly associated with caveolin-1 at later time points of infection. Therefore, we believe that caveolin-1 is unlikely to form the basis of the bacterial transcytosis pathway, unless the 1% population of *E. coli* K1 weakly associated with caveolin-1 is sufficient for the bacteria to egress from HBMEC at the basolateral membrane. Based on our findings in Chapter 6, we speculated that *E. coli* K1 might egress from HBMEC via late/lysosomal [N.B. Lysosomal membrane proteins, such as LAMP1, are actively interacting with plasma membrane, and are involved in membrane repairing (Divangahi *et al.*, 2009).], or a flotillin 1-dependent pathway. The role of flotillin 1 on the intracellular vacuoles might have a role in recruiting motor proteins for intracellular transportation, for docking of the vacuoles to the target membrane surface, or for releasing the cargo. The low transfection efficiency of HBMEC is the major experimental obstacle for studying bacterial transcytosis pathway. An alternative experimental approach would be the application of tannic acid, which only fixes the membrane surface in contact, at the basolateral compartment of Transwell® filter insert to arrest the bacteria at the basolateral membrane surface (Polishchuk *et al.*, 2004), and the infected HBMEC on the Transwell® filter insert is fixed and immunostained for organellar markers.

Although HBMEC has been widely applied for studying the *E. coli* K1 pathogenesis (Huang *et al.*, 1995; Reddy *et al.*, 2000a; Stins *et al.*, 2001; Kim *et al.*, 2003; Khan *et al.*, 2007), the precise bacterial entry site *in vivo* remains controversial. The current model is based on findings by Kim *et al.* (1992), where, in a newborn (5-day-old) rat model, the authors found the bacteria present in the perivascular area of the subarachnoid space, but not in the choroid plexus, where the BCSFB is found (see section

1.4). The group further showed that the bacteria invaded isolated brain microvascular endothelium more efficiently than endothelial cells isolated from other anatomical sites *in vitro* (Prasadarao *et al.*, 1996a). More than a decade later, Zelmer *et al.* (2008) found evidence to support the alternative BCSFB entry site in their newborn (2-day-old) rat model. The observed discrepancy by both groups is complex and multifactorial, where one of the factors could be the age of the animals used, or the different route of bacterial administration in these studies. The precise bacterial entry site in the animal could be elucidated by the application of multiphoton microscopy for deep tissue live animal imaging (Melican and Richter-Dahlfors, 2009; Melican *et al.*, 2011), in conjunction with innovative thin-skull microsurgery procedure (Marker *et al.*, 2010). The main challenge for this experimental approach is to keep the fragile, hypothermia-prone newborn animal alive and physiologically stable during the surgery procedure as well as during imaging. Live animal deep tissue imaging is also important to confirm previous *in vitro* findings that have arisen from the HBMEC model, as differences in *Listeria monocytogenes* infection cycle both *in vitro* and *in vivo* has been demonstrated recently (Nikitas *et al.*, 2011). Further, an infection is more heterogeneous than merely *E. coli* K1-HBMEC interactions in culture medium, and would also depend upon a complex interaction between the pathogen and capillary endothelium as well as various tissues, including microglial cells, astrocytes, immune cells, inflammatory factors, etc. It has also been shown that approximately 40% of plasma membrane proteins failed to express on the plasma membrane of purified endothelial cells maintained *in vitro* (Durr *et al.*, 2004), which might affect the results obtained *in vitro* and *in vivo*. All the future *in vivo* imaging works can be achieved by the mCherry-expressing *E. coli* K1 constructed in this study.

Conclusion

The purpose of this study was to investigate the interactions of *E. coli* K1 with HBMEC in order to elucidate the pathway by which the bacteria cross the BBB into the CNS. To this end, an mCherry-expressing *E. coli* K1 that retains the bacterial invasiveness of HBMEC was constructed. Our data suggest *E. coli* K1 invade HBMEC via a caveolae-, dynamin-, and flotillin-independent pathway. Once inside the cells, *E. coli* K1 were found to localize in late endosome-like compartment. We speculate that the bacteria may cross BBB via late/lysosomal pathway. Interestingly, when MLEC knockout cells were used to model bacterial infection, the absence of flotillin 1 was found to enhance bacterial invasion compared to wild type. We further suggest flotillin has an essential role in maintaining the cell wall as a barrier to the external environment. In addition, flotillin appears to be an important component in maintaining mucosal membrane integrity, having significant impacts in diseases such as Crohn's disease and asthma (Li *et al.*, 2008b). Thus, the results in this study not only have an impact in the understanding of how *E. coli* K1 traverse the BBB, but are also of interest in relation to the role of flotillin in maintaining cellular barrier integrity.

8. References

Abbott, N.J., Chugani, D.C., Zaharchuk, G., Rosen, B.R. and Lo, E.H. (1999). Delivery of imaging agents into brain. *Adv Drug Deliv Rev* **37**, 253-277.

Abbott, N.J., Ronnback, L. and Hansson, E. (2006). Astrocyte-endothelial interactions at the blood-brain barrier. *Nat Rev Neurosci* **7**, 41-53.

Abromaitis, S., Faucher, S., Béland, M., Curtiss III, R. and Daigle, F. (2005). The presence of the *tet* gene from cloning vectors impairs *Salmonella* survival in macrophages. *FEMS Microbiol Lett* **242**, 305-312.

Achtman, M., Mercer, A., Kusecek, B., Pohl, A., Heuzenroeder, M., Aaronson, W., Sutton, A. and Silver, R.P. (1983). Six widespread bacterial clones among *Escherichia coli* K1 isolates. *Infect Immun* **39**, 315-335.

Aghamohammadzadeh, S. and Ayscough, K.R. (2009). Differential requirements for actin during yeast and mammalian endocytosis. *Nat Cell Biol* **11**, 1039-1042.

Alarcon, A., Pena, P., Salas, S., Sancha, M. and Omenaca, F. (2004). Neonatal early onset *Escherichia coli* sepsis: trends in incidence and antimicrobial resistance in the era of intrapartum antimicrobial prophylaxis. *Pediatr Infect Dis J* **23**, 295-299.

Allt, G. and Lawrenson, J.G. (1997). Is the pial microvessel a good model for blood-brain barrier studies? *Brain Res Brain Res Rev* **24**, 67-76.

Alsam, S., Sissons, J., Dudley, R. and Khan, N.A. (2005). Mechanisms associated with *Acanthamoeba castellanii* (T4) phagocytosis. *Parasitol Res* **96**, 402-409.

Altschuler, Y., Barbas, S.M., Terlecky, L.J., Tang, K., Hardy, S., Mostov, K.E. and Schmid, S.L. (1998). Redundant and distinct functions for dynamin-1 and dynamin-2 isoforms. *J Cell Biol* **143**, 1871-1881.

Anderson, R.G., Brown, M.S. and Goldstein, J.L. (1977). Role of the coated endocytic vesicle in the uptake of receptor-bound low density lipoprotein in human fibroblasts. *Cell* **10**, 351-364.

Anliker, B., Abel, T., Kneissl, S., Hlavaty, J., Caputi, A., Brynza, J., Schneider, I.C., Munch, R.C., Petznek, H., Kontermann, R.E., Koehl, U., Johnston, I.C., Keinanen, K., Muller, U.C., Hohenadl, C., Monyer, H., Cichutek, K. and Buchholz, C.J. (2010). Specific gene transfer to neurons, endothelial cells and hematopoietic progenitors with lentiviral vectors. *Nat Methods* **7**, 929-935.

Apodaca, G. (2001). Endocytic traffic in polarized epithelial cells: role of the actin and microtubule cytoskeleton. *Traffic* **2**, 149-159.

Arellano-Reynoso, B., Lapaque, N., Salcedo, S., Briones, G., Ciocchini, A.E., Ugalde, R., Moreno, E., Moriyon, I. and Gorvel, J.P. (2005). Cyclic β-1,2-glucan is a brucella virulence factor required for intracellular survival. *Nat Immunol* **6**, 618-625.

Arthur, F.E., Shivers, R.R. and Bowman, P.D. (1987). Astrocyte-mediated induction of tight junctions in brain capillary endothelium: an efficient *in vitro* model. *Brain Res* **433**, 155-159.

Babuke, T. and Tikkanen, R. (2007). Dissecting the molecular function of reggie/flotillin proteins. *Eur J Cell Biol* **86**, 525-532.

Baltimore, R.S., Huie, S.M., Meek, J.I., Schuchat, A. and O'Brien, K.L. (2001). Early-onset neonatal sepsis in the era of group B streptococcal prevention. *Pediatrics* **108**, 1094-1098.

Barbero, P., Bittova, L. and Pfeffer, S.R. (2002). Visualization of Rab9-mediated vesicle transport from endosomes to the trans-Golgi in living cells. *J Cell Biol* **156**, 511-518.

Barnhart, M.M., Schilling, J.D., Bäckhed, F., Dahlfors, A.R., Normark, S. and Hultgren, S.J. (2002) Host-pathogen interactions: structure and function of pili. In *Methods in Microbiology*, Sansonetti, P. and Zychlinsky, A. (eds.). Academic Press, pp. 133-159.

Barth, K., Weinhold, K., Guenther, A., Young, M.T., Schnittler, H. and Kasper, M. (2007). Caveolin-1 influences P2X7 receptor expression and localization in mouse lung alveolar epithelial cells. *FEBS J* **274**, 3021-3033.

Benmerah, A. and Lamaze, C. (2007). Clathrin-coated pits: vive la difference? *Traffic* **8**, 970-982.

Beron, W., Gutierrez, M.G., Rabinovitch, M. and Colombo, M.I. (2002). *Coxiella burnetii* localizes in a Rab7-labeled compartment with autophagic characteristics. *Infect. Immun.* **70**, 5816-5821.

Bhattacharyya, S., Warfield, K.L., Ruthel, G., Bavari, S., Aman, M.J. and Hope, T.J. (2010). Ebola virus uses clathrin-mediated endocytosis as an entry pathway. *Virology* **401**, 18-28.

Bhavsar, A.P., Guttman, J.A. and Finlay, B.B. (2007). Manipulation of host-cell pathways by bacterial pathogens. *Nature* **449**, 827-834.

Bizzarro, M.J., Dembry, L.M., Baltimore, R.S. and Gallagher, P.G. (2008). Changing patterns in neonatal *Escherichia coli* sepsis and ampicillin resistance in the era of intrapartum antibiotic prophylaxis. *Pediatrics* **121**, 689-696.

Blasig, I.E., Giese, H., Schroeter, M.L., Sporbert, A., Utepbergenov, D.I., Buchwalow, I.B., Neubert, K., Schonfelder, G., Freyer, D., Schimke, I., Siems, W.E., Paul, M., Haseloff, R.F. and Blasig, R. (2001). *NO and oxyradical metabolism in new cell lines of rat brain capillary endothelial cells forming the blood-brain barrier. *Microvasc Res* **62,** 114-127.

Bloch, C.A. and Orndorff, P.E. (1990). Impaired colonization by and full invasiveness of *Escherichia coli* K1 bearing a site-directed mutation in the type 1 pilin gene. *Infect Immun* **58,** 275-278.

Boettcher, J.P., Kirchner, M., Churin, Y., Kaushansky, A., Pompaiah, M., Thorn, H., Brinkmann, V., Macbeath, G. and Meyer, T.F. (2010). Tyrosine-phosphorylated caveolin-1 blocks bacterial uptake by inducing Vav2-RhoA-mediated cytoskeletal rearrangements. *PLoS Biol* **8.**

Bomsel, M. (1997). Transcytosis of infectious human immunodeficiency virus across a tight human epithelial cell line barrier. *Nat Med* **3,** 42-47.

Bonacorsi, S. and Bingen, E. (2005). Molecular epidemiology of *Escherichia coli* causing neonatal meningitis. *Int J Med Microbiol* **295,** 373-381.

Bortolussi, R., Ferrieri, P., Bjorksten, B. and Quie, P.G. (1979). Capsular K1 polysaccharide of *Escherichia coli*: relationship to virulence in newborn rats and resistance to phagocytosis. *Infect Immun* **25,** 293-298.

Bourdoulous, S., Olivier, P.C. and Nassif, X. (2002) Methods for studying the mechanisms of microbial entry into the central nervous system. In *Method Microbiol*, Sansonetti, P. and Zychlinsky, A. (eds.). Academic Press, pp. 419-437.

Bowden, T.A., Crispin, M., Harvey, D.J., Aricescu, A.R., Grimes, J.M., Jones, E.Y. and Stuart, D.I. (2008). Crystal structure and carbohydrate analysis of Nipah virus attachment glycoprotein: a template for antiviral and vaccine design. *J Virol* **82,** 11628-11636.

Bras, A.M. and Ketley, J.M. (1999). Transcellular translocation of *Campylobacter jejuni* across human polarised epithelial monolayers. *FEMS Microbiol Lett* **179,** 209-215.

Braun, J.S., Novak, R., Herzog, K.H., Bodner, S.M., Cleveland, J.L. and Tuomanen, E.I. (1999). Neuroprotection by a caspase inhibitor in acute bacterial meningitis. *Nat Med* **5,** 298-302.

Brown, F.D., Rozelle, A.L., Yin, H.L., Balla, T. and Donaldson, J.G. (2001). Phosphatidylinositol 4,5-bisphosphate and Arf6-regulated membrane traffic. *J Cell Biol* **154,** 1007-1017.

Brumell, J.H. and Scidmore, M.A. (2007). Manipulation of Rab GTPase function by intracellular bacterial pathogens. *Microbiol. Mol. Biol. Rev.* **71,** 636-652.

Bucci, C., Thomsen, P., Nicoziani, P., McCarthy, J. and van Deurs, B. (2000). Rab7: a key to lysosome biogenesis. *Mol. Biol. Cell* **11,** 467-480.

Burns, J.L., Griffith, A., Barry, J.J., Jonas, M. and Chi, E.Y. (2001). Transcytosis of gastrointestinal epithelial cells by *Escherichia coli* K1. *Pediatr Res* **49,** 30-37.

Butt, A.M. and Jones, H.C. (1992). Effect of histamine and antagonists on electrical resistance across the blood-brain barrier in rat brain-surface microvessels. *Brain Res* **569,** 100-105.

Cabanes, D., Sousa, S., Cebria, A., Lecuit, M., Garcia-del Portillo, F. and Cossart, P. (2005). Gp96 is a receptor for a novel *Listeria monocytogenes* virulence factor, Vip, a surface protein. *EMBO J* **24,** 2827-2838.

Cao, H., Chen, J., Awoniyi, M., Henley, J.R. and McNiven, M.A. (2007). Dynamin 2 mediates fluid-phase micropinocytosis in epithelial cells. *J Cell Sci* **120,** 4167-4177.

Cao, H., Garcia, F. and McNiven, M.A. (1998). Differential distribution of dynamin isoforms in mammalian cells. *Mol. Biol. Cell* **9,** 2595-2609.

Capitani, G., Eidam, O., Glockshuber, R. and Grutter, M.G. (2006). Structural and functional insights into the assembly of type 1 pili from *Escherichia coli*. *Microbes Infect* **8,** 2284-2290.

Carabeo, R.A., Mead, D.J. and Hackstadt, T. (2003). Golgi-dependent transport of cholesterol to the *Chlamydia trachomatis* inclusion. *Proc Natl Acad Sci U S A* **100,** 6771-6776.

Carmichael, M. (2011). Newborn screening: a spot of trouble. *Nature* **475,** 156-158.

Carroll, P., Schreuder, L.J., Muwanguzi-Karugaba, J., Wiles, S., Robertson, B.D., Ripoll, J., Ward, T.H., Bancroft, G.J., Schaible, U.E. and Parish, T. (2010). Sensitive detection of gene expression in mycobacteria under replicating and non-replicating conditions using optimized far-red reporters. *PLoS One* **5,** e9823.

Cefai, D., Simeoni, E., Ludunge, K.M., Driscoll, R., von Segesser, L.K., Kappenberger, L. and Vassalli, G. (2005). Multiply attenuated, self-inactivating lentiviral vectors efficiently transduce human coronary artery cells *in vitro* and rat arteries *in vivo*. *J Mol Cell Cardiol* **38,** 333-344.

Celli, J., de Chastellier, C., Franchini, D.M., Pizarro-Cerda, J., Moreno, E. and Gorvel, J.P. (2003). *Brucella* evades macrophage killing via VirB-dependent sustained interactions with the endoplasmic reticulum. *J. Exp. Med.* **198,** 545-556.

Chan, L.C., Young, P.R., Bletchly, C. and Reid, S. (2002). Production of the baculovirus-expressed dengue virus glycoprotein NS1 can be improved dramatically with optimised regimes for fed-batch cultures and the addition of the insect moulting hormone, 20-Hydroxyecdysone. *J Virol Methods* **105**, 87-98.

Chassin, C., Vimont, S., Cluzeaud, F., Bens, M., Goujon, J.M., Fernandez, B., Hertig, A., Rondeau, E., Arlet, G., Hornef, M.W. and Vandewalle, A. (2008). TLR4 facilitates translocation of bacteria across renal collecting duct cells. *J Am Soc Nephrol* **19**, 2364-2374.

Cheminay, C., Mohlenbrink, A. and Hensel, M. (2005). Intracellular *Salmonella* inhibit antigen presentation by dendritic cells. *J Immunol* **174**, 2892-2899.

Chen, T., Guo, J., Yang, M., Zhu, X. and Cao, X. (2011). Chemokine-containing exosomes are released from heat-stressed tumor cells via lipid raft-dependent pathway and act as efficient tumor vaccine. *J Immunol* **186**, 2219-2228.

Chertova, E., Chertov, O., Coren, L.V., Roser, J.D., Trubey, C.M., Bess, J.W., Jr., Sowder, R.C., 2nd, Barsov, E., Hood, B.L., Fisher, R.J., Nagashima, K., Conrads, T.P., Veenstra, T.D., Lifson, J.D. and Ott, D.E. (2006). Proteomic and biochemical analysis of purified human immunodeficiency virus type 1 produced from infected monocyte-derived macrophages. *J Virol* **80**, 9039-9052.

Chi, F., Jong, T.D., Wang, L., Ouyang, Y., Wu, C., Li, W. and Huang, S.H. (2010). Vimentin-mediated signalling is required for IbeA+ *E. coli* K1 invasion of human brain microvascular endothelial cells. *Biochem J* **427**, 79-90.

Chintagari, N.R., Gou, D. and Liu, L. (2008). Knockdown of flotillin-2 inhibits lung surfactant secretion by alveolar type II cells. *Cell Res* **18**, 701-703.

Chung, J.W., Hong, S.J., Kim, K.J., Goti, D., Stins, M.F., Shin, S., Dawson, V.L., Dawson, T.M. and Kim, K.S. (2003). 37-kDa laminin receptor precursor modulates cytotoxic necrotizing factor 1-mediated RhoA activation and bacterial uptake. *J Biol Chem* **278**, 16857-16862.

Clague, M.J. (1998). Molecular aspects of the endocytic pathway. *Biochem J* **336 (Pt 2)**, 271-282.

Clark, L., Martinez-Argudo, I., Humphrey, T.J. and Jepson, M.A. (2009). GFP plasmid-induced defects in *Salmonella* invasion depend on plasmid architecture, not protein expression. *Microbiology* **155**, 461-467.

Colino, J. and Outschoorn, I. (1999). The form variation of the capsular polysaccharide K1 is not a critical virulence factor of *Escherichia coli* in a neonatal mouse model of infection. *Microb Pathog* **27**, 187-196.

Conner, S.D. and Schmid, S.L. (2003). Regulated portals of entry into the cell. *Nature* 422. 37-44.

Cook, T.A., Urrutia, R. and McNiven, M.A. (1994). Identification of dynamin 2. an isoform ubiquitously expressed in rat tissues. *Proc Natl Acad Sci U S A* 91, 644-648.

Cordero, L., Rau, R., Taylor, D. and Ayers, L.W. (2004). Enteric gram-negative bacilli bloodstream infections: 17 years' experience in a neonatal intensive care unit. *Am J Infect Control* 32, 189-195.

Cossart, P. and Sansonetti, P.J. (2004). Bacterial Invasion: the paradigms of enteroinvasive pathogens. *Science* 304, 242-248.

Coureuil, M., Lecuyer, H., Scott, M.G., Boularan, C., Enslen, H., Soyer, M., Mikaty, G., Bourdoulous, S., Nassif, X. and Marullo, S. (2010). Meningococcus hijacks a β2-adrenoceptor/β-arrestin pathway to cross brain microvasculature endothelium. *Cell* 143, 1149-1160.

Coureuil, M., Mikaty, G., Miller, F., Lecuyer, H., Bernard, C., Bourdoulous, S., Dumenil, G., Mege, R.M., Weksler, B.B., Romero, I.A., Couraud, P.O. and Nassif, X. (2009). Meningococcal type IV pili recruit the polarity complex to cross the brain endothelium. *Science* 325, 83-87.

Cross, A.S., Kim, K.S., Wright, D.C., Sadoff, J.C. and Gemski, P. (1986). Role of lipopolysaccharide and capsule in the serum resistance of bacteremic strains of *Escherichia coli. J Infect Dis* 154, 497-503.

Croxen, M.A. and Finlay, B.B. (2010). Molecular mechanisms of Escherichia coli pathogenicity. *Nat Rev Microbiol* 8, 26-38.

Cucullo, L., Couraud, P.O., Weksler, B., Romero, I.A., Hossain, M., Rapp, E. and Janigro, D. (2008). Immortalized human brain endothelial cells and flow-based vascular modeling: a marriage of convenience for rational neurovascular studies. *J Cereb Blood Flow Metab* 28, 312-328.

Cureton, D.K., Massol, R.H., Saffarian, S., Kirchhausen, T.L. and Whelan, S.P. (2009). Vesicular stomatitis virus enters cells through vesicles incompletely coated with clathrin that depend upon actin for internalization. *PLoS Pathog* 5, e1000394.

Damke, H., Baba, T., Warnock, D.E. and Schmid, S.L. (1994). Induction of mutant dynamin specifically blocks endocytic coated vesicle formation. *J Cell Biol* 127, 915-934.

Damke, H., Binns, D.D., Ueda, H., Schmid, S.L. and Baba, T. (2001). Dynamin GTPase domain mutants block endocytic vesicle formation at morphologically distinct stages. *Mol Biol Cell* **12,** 2578-2589.

Damm, E.M., Pelkmans, L., Kartenbeck, J., Mezzacasa, A., Kurzchalia, T. and Helenius, A. (2005). Clathrin- and caveolin-1-independent endocytosis: entry of simian virus 40 into cells devoid of caveolae. *J Cell Biol* **168,** 477-488.

Daneman, R. and Rescigno, M. (2009). The gut immune barrier and the blood-brain barrier: are they so different? *Immunity* **31,** 722-735.

de Louvois, J. (1994). Acute bacterial meningitis in the newborn. *J Antimicrob Chemother* **34 Suppl A,** 61-73.

del Pozo, M.A., Balasubramanian, N., Alderson, N.B., Kiosses, W.B., Grande-Garcia, A., Anderson, R.G. and Schwartz, M.A. (2005). Phospho-caveolin-1 mediates integrin-regulated membrane domain internalization. *Nat Cell Biol* **7,** 901-908.

Dellagrammaticas, H.D., Christodoulou, C., Megaloyanni, E., Papadimitriou, M., Kapetanakis, J. and Kourakis, G. (2000). Treatment of gram-negative bacterial meningitis in term neonates with third generation cephalosporins plus amikacin. *Biol Neonate* **77,** 139-146.

Dermine, J.F., Duclos, S., Garin, J., St-Louis, F., Rea, S., Parton, R.G. and Desjardins, M. (2001). Flotillin-1-enriched lipid raft domains accumulate on maturing phagosomes. *J Biol Chem* **276,** 18507-18512.

Deszo, E.L., Steenbergen, S.M., Freedberg, D.I. and Vimr, E.R. (2005). *Escherichia coli* K1 polysialic acid O-acetyltransferase gene, neuO, and the mechanism of capsule form variation involving a mobile contingency locus. *Proc Natl Acad Sci U S A* **102,** 5564-5569.

Dharmawardhane, S., Schurmann, A., Sells, M.A., Chernoff, J., Schmid, S.L. and Bokoch, G.M. (2000). Regulation of macropinocytosis by p21-activated kinase-1. *Mol Biol Cell* **11,** 3341-3352.

Dietzen, D.J., Hastings, W.R. and Lublin, D.M. (1995). Caveolin is palmitoylated on multiple cysteine residues. Palmitoylation is not necessary for localization of caveolin to caveolae. *J Biol Chem* **270,** 6838-6842.

Dietzman, D.E., Fischer, G.W. and Schoenknecht, F.D. (1974). Neonatal *Escherichia coli* septicemia--bacterial counts in blood. *J Pediatr* **85,** 128-130.

Dinarello, C.A. (1989). Interleukin-1 and its biologically related cytokines. *Adv Immunol* **44,** 153-205.

Divangahi, M., Chen, M., Gan, H., Desjardins, D., Hickman, T.T., Lee, D.M., Fortune, S., Behar, S.M. and Remold, H.G. (2009). *Mycobacterium tuberculosis* evades macrophage defenses by inhibiting plasma membrane repair. *Nat Immunol* **10**, 899-906.

Doherty, G.J. and McMahon, H.T. (2009). Mechanisms of Endocytosis. *Annu Rev Biochem* **78**, 857-902.

Donaldson, J.G., Porat-Shliom, N. and Cohen, L.A. (2009). Clathrin-independent endocytosis: a unique platform for cell signaling and PM remodeling. *Cell Signal* **21**, 1-6.

Doran, K.S., Engelson, E.J., Khosravi, A., Maisey, H.C., Fedtke, I., Equils, O., Michelsen, K.S., Arditi, M., Peschel, A. and Nizet, V. (2005). Blood-brain barrier invasion by group B *Streptococcus* depends upon proper cell-surface anchoring of lipoteichoic acid. *J Clin Invest* **115**, 2499-2507.

Doulet, N., Donnadieu, E., Laran-Chich, M.P., Niedergang, F., Nassif, X., Couraud, P.O. and Bourdoulous, S. (2006). *Neisseria meningitidis* infection of human endothelial cells interferes with leukocyte transmigration by preventing the formation of endothelial docking structures. *J. Cell Biol.* **173**, 627-637.

Drecktrah, D., Knodler, L.A., Howe, D. and Steele-Mortimer, O. (2007). *Salmonella* trafficking is defined by continuous dynamic interactions with the endolysosomal system. *Traffic* **8**, 212-225.

Drecktrah, D., Levine-Wilkinson, S., Dam, T., Winfree, S., Knodler, L.A., Schroer, T.A. and Steele-Mortimer, O. (2008). Dynamic behavior of *Salmonella*-induced membrane tubules in epithelial cells. *Traffic* **9**, 2117-2129.

Ducharme, N.A., Williams, J.A., Oztan, A., Apodaca, G., Lapierre, L.A. and Goldenring, J.R. (2007). Rab11-FIP2 regulates differentiable steps in transcytosis. *Am J Physiol Cell Physiol* **293**, C1059-1072.

Dufes, C., Gaillard, F., Uchegbu, I.F., Schatzlein, A.G., Olivier, J.C. and Muller, J.M. (2004). Glucose-targeted niosomes deliver vasoactive intestinal peptide (VIP) to the brain. *Int J Pharm* **285**, 77-85.

Durr, E., Yu, J., Krasinska, K.M., Carver, L.A., Yates, J.R., Testa, J.E., Oh, P. and Schnitzer, J.E. (2004). Direct proteomic mapping of the lung microvascular endothelial cell surface *in vivo* and in cell culture. *Nat Biotech* **22**, 985-992.

Efe, J.A., Botelho, R.J. and Emr, S.D. (2005). The Fab1 phosphatidylinositol kinase pathway in the regulation of vacuole morphology. *Curr Opin Cell Biol* **17**, 402-408.

Engqvist-Goldstein, A.E. and Drubin, D.G. (2003). Actin assembly and endocytosis: from yeast to mammals. *Annu Rev Cell Dev Biol* **19**, 287-332.

Ernst, J.D., Decazes, J.M. and Sande, M.A. (1983). Experimental pneumococcal meningitis: role of leukocytes in pathogenesis. *Infect Immun* **41**, 275-279.

Eyngor, M., Chilmonczyk, S., Zlotkin, A., Manuali, E., Lahav. D., Ghittino, C.. Shapira. R., Hurvitz, A. and Eldar, A. (2007). Transcytosis of *Streptococcus iniae* through skin epithelial barriers: an in vitro study. *FEMS Microbiol Lett* **277**, 238-248.

Feig, L.A. (1999). Tools of the trade: use of dominant-inhibitory mutants of Ras-family GTPases. *Nat Cell Biol* **1**, E25-27.

Feig, L.A. and Cooper, G.M. (1988). Inhibition of NIH 3T3 cell proliferation by a mutant ras protein with preferential affinity for GDP. *Mol Cell Biol* **8**, 3235-3243.

Ferguson, S.M. and De Camilli, P. (2012). Dynamin, a membrane-remodelling GTPase. *Nat Rev Mol Cell Biol* **13**, 75-88.

Ferguson, S.M., Raimondi, A., Paradise, S., Shen, H., Mesaki, K., Ferguson, A., Destaing, O., Ko, G., Takasaki, J., Cremona, O., E, O.T. and De Camilli, P. (2009). Coordinated actions of actin and BAR proteins upstream of dynamin at endocytic clathrin-coated pits. *Dev Cell* **17**, 811-822.

Filias, A., Theodorou, G.L., Mouzopoulou, S., Varvarigou, A.A., Mantagos, S. and Karakantza, M. (2011). Phagocytic ability of neutrophils and monocytes in neonates. *BMC Pediatr* **11**, 29.

Finlay, B.B. and Cossart, P. (1997). Exploitation of mammalian host cell functions by bacterial pathogens. *Science* **276**, 718-725.

Finne, J. (1982). Occurrence of unique polysialosyl carbohydrate units in glycoproteins of developing brain. *J Biol Chem* **257**, 11966-11970.

Finne, J., Finne, U., Deagostini-Bazin, H. and Goridis, C. (1983a). Occurrence of alpha 2-8 linked polysialosyl units in a neural cell adhesion molecule. *Biochem Biophys Res Commun* **112**, 482-487.

Finne, J., Leinonen, M. and Makela, P.H. (1983b). Antigenic similarities between brain components and bacteria causing meningitis. Implications for vaccine development and pathogenesis. *Lancet* **2**, 355-357.

Fonsatti, E. and Maio, M. (2004). Highlights on endoglin (CD105): from basic findings towards clinical applications in human cancer. *J Transl Med* **2**, 18.

Frank, P.G., Woodman, S.E., Park, D.S. and Lisanti, M.P. (2003). Caveolin, caveolae, and endothelial cell function. *Arterioscler Thromb Vasc Biol* **23**, 1161-1168.

Franke, H., Galla, H. and Beuckmann, C.T. (2000). Primary cultures of brain microvessel endothelial cells: a valid and flexible model to study drug transport through the blood-brain barrier *in vitro*. *Brain Res Brain Res Protoc* **5,** 248-256.

Frasa, H., Procee, J., Torensma, R., Verbruggen, A., Algra, A., Rozenberg-Arska, M., Kraaijeveld, K. and Verhoef, J. (1993). *Escherichia coli* in bacteremia: O-acetylated K1 strains appear to be more virulent than non-O-acetylated K1 strains. *J Clin Microbiol* **31,** 3174-3178.

Frick, M., Bright, N.A., Riento, K., Bray, A., Merrified, C. and Nichols, B.J. (2007). Coassembly of flotillins induces formation of membrane microdomains, membrane curvature, and vesicle budding. *Curr Biol* **17,** 1151-1156.

Fu, Y., Hoang, A., Escher, G., Parton, R.G., Krozowski, Z. and Sviridov, D. (2004). Expression of caveolin-1 enhances cholesterol efflux in hepatic cells. *J Biol Chem* **279,** 14140-14146.

Fujimoto, T., Kogo, H., Nomura, R. and Une, T. (2000). Isoforms of caveolin-1 and caveolar structure. *J Cell Sci* **113,** 3509-3517.

Gaidarov, I., Chen, Q., Falck, J.R., Reddy, K.K. and Keen, J.H. (1996). A functional phosphatidylinositol 3,4,5-trisphosphate/phosphoinositide binding domain in the clathrin adaptor AP-2 α subunit. Implications for the endocytic pathway. *J Biol Chem* **271,** 20922-20929.

Gaidarov, I. and Keen, J.H. (1999). Phosphoinositide-AP-2 interactions required for targeting to plasma membrane clathrin-coated pits. *J Cell Biol* **146,** 755-764.

Galperin, E. and Sorkin, A. (2003). Visualization of Rab5 activity in living cells by FRET microscopy and influence of plasma-membrane-targeted Rab5 on clathrin-dependent endocytosis. *J Cell Sci* **116,** 4799-4810.

Garg, S., Sharma, M., Ung, C., Tuli, A., Barral, D.C., Hava, D.L., Veerapen, N., Besra, G.S., Hacohen, N. and Brenner, M.B. (2011). Lysosomal trafficking, antigen presentation, and microbial killing are controlled by the Arf-like GTPase Arl8b. *Immunity* **35,** 182-193.

Garrett, W.S., Chen, L.M., Kroschewski, R., Ebersold, M., Turley, S., Trombetta, S., Galan, J.E. and Mellman, I. (2000). Developmental control of endocytosis in dendritic cells by Cdc42. *Cell* **102,** 325-334.

Gaschignard, J., Levy, C., Romain, O., Cohen, R., Bingen, E., Aujard, Y. and Boileau, P. (2011). Neonatal Bacterial Meningitis: 444 Cases in 7 Years. *Pediatr Infect Dis J* **30,** 212-217.

Gauthier, N.C., Monzo, P., Gonzalez, T., Doye, A., Oldani, A., Gounon, P., Ricci, V., Cormont, M. and Boquet, P. (2007). Early endosomes associated with dynamic F-actin structures are required for late trafficking of *H. pylori* VacA toxin. *J Cell Biol* **177**, 343-354.

Gauthier, N.C., Monzo, P., Kaddai, V., Doye, A., Ricci, V. and Boquet, P. (2005). *Helicobacter pylori* VacA cytotoxin: a probe for a clathrin-independent and Cdc42-dependent pinocytic pathway routed to late endosomes. *Mol Biol Cell* **16**, 4852-4866.

Georgieva, J.V., Kalicharan, D., Couraud, P.O., Romero, I.A., Weksler, B., Hoekstra, D. and Zuhorn, I.S. (2011). Surface characteristics of nanoparticles determine their intracellular fate in and processing by human blood-brain barrier endothelial cells in vitro. *Mol Ther* **19**, 318-325.

Gerlach, R.G., Cláudio, N., Rohde, M., Jäckel, D., Wagner, C. and Hensel, M. (2008). Cooperation of *Salmonella* pathogenicity islands 1 and 4 is required to breach epithelial barriers. *Cell Microbiol* **10**, 2364-2376.

Ghitescu, L. and Bendayan, M. (1992). Transendothelial transport of serum albumin: a quantitative immunocytochemical study. *J Cell Biol* **117**, 745-755.

Glebov, O.O., Bright, N.A. and Nichols, B.J. (2006). Flotillin-1 defines a clathrin-independent endocytic pathway in mammalian cells. *Nat Cell Biol* **8**, 46-54.

Glode, M.P., Sutton, A., Moxon, E.R. and Robbins, J.B. (1977). Pathogenesis of neonatal *Escherichia coli* meningitis: induction of bacteremia and meningitis in infant rats fed *E. coli* K1. *Infect. Immun.* **16**, 75-80.

Golachowska, M.R., Hoekstra, D. and van, I.S.C. (2010). Recycling endosomes in apical plasma membrane domain formation and epithelial cell polarity. *Trends Cell Biol* **20**, 618-626.

Goldenberg, N.M., Grinstein, S. and Silverman, M. (2007). Golgi-bound Rab34 is a novel member of the secretory pathway. *Mol Biol Cell* **18**, 4762-4771.

Grab, D.J., Nikolskaia, O., Kim, Y.V., Lonsdale-Eccles, J.D., Ito, S., Hara, T., Fukuma, T., Nyarko, E., Kim, K.J., Stins, M.F., Delannoy, M.J., Rodgers, J. and Kim, K.S. (2004). African trypanosome interactions with an *in vitro* model of the human blood-brain barrier. *J Parasitol* **90**, 970-979.

Greiffenberg, L., Goebel, W., Kim, K.S., Weiglein, I., Bubert, A., Engelbrecht, F., Stins, M. and Kuhn, M. (1998). Interaction of *Listeria monocytogenes* with human brain microvascular endothelial cells: InlB-dependent invasion, long-term intracellular

growth, and spread from macrophages to endothelial cells. *Infect Immun* **66**, 5260-5267.

Gruenberg, J. and van der Goot, F.G. (2006). Mechanisms of pathogen entry through the endosomal compartments. *Nat Rev Mol Cell Biol* **7**, 495-504.

Guignot, J., Caron, E., Beuzon, C., Bucci, C., Kagan, J., Roy, C. and Holden, D.W. (2004). Microtubule motors control membrane dynamics of Salmonella-containing vacuoles. *J Cell Sci* **117**, 1033-1045.

Hagedorn, M. and Soldati, T. (2007). Flotillin and RacH modulate the intracellular immunity of *Dictyostelium* to *Mycobacterium marinum* infection. *Cell Microbiol* **9**, 2716-2733.

Haglund, C.M. and Welch, M.D. (2011). Host-pathogen interactions: Pathogens and polymers: Microbe-host interactions illuminate the cytoskeleton. *J Cell Biol* **195**, 7-17.

Ham, H., Sreelatha, A. and Orth, K. (2011). Manipulation of host membranes by bacterial effectors. *Nat Rev Microbiol* **9**, 635-646.

Harvey, D., Holt, D.E. and Bedford, H. (1999). Bacterial meningitis in the newborn: a prospective study of mortality and morbidity. *Semin Perinatol* **23**, 218-225.

Harvey, H.A., Swords, W.E. and Apicella, M.A. (2001). The mimicry of human glycolipids and glycosphingolipids by the lipooligosaccharides of pathogenic neisseria and haemophilus. *J Autoimmun* **16**, 257-262.

Hawley-Nelson, P., Ciccarone, V. and Moore, M.L. (2008). Transfection of cultured eukaryotic cells using cationic lipid reagents. *Curr Protoc Mol Biol* **Chapter 9**, Unit 9 4.

Hazenbos, W.L., van den Berg, B.M., van't Wout, J.W., Mooi, F.R. and van Furth, R. (1994). Virulence factors determine attachment and ingestion of nonopsonized and opsonized *Bordetella pertussis* by human monocytes. *Infect. Immun.* **62**, 4818-4824.

Headings, D.L. and Overall, J.C., Jr. (1977). Outbreak of meningitis in a newborn intensive care unit caused by a single *Escherichia coli* K1 serotype. *J Pediatr* **90**, 99-102.

Heinzen, R.A., Scidmore, M.A., Rockey, D.D. and Hackstadt, T. (1996). Differential interaction with endocytic and exocytic pathways distinguish parasitophorous vacuoles of *Coxiella burnetii* and *Chlamydia trachomatis*. *Infect Immun* **64**, 796-809.

Helaine, S., Thompson, J.A., Watson, K.G., Liu, M., Boyle, C. and Holden, D.W. (2010). Dynamics of intracellular bacterial replication at the single cell level. *Proc Natl Acad Sci U S A* **107,** 3746-3751.

Henley, J.R., Krueger, E.W., Oswald, B.J. and McNiven, M.A. (1998). Dynamin-mediated internalization of caveolae. *J Cell Biol* **141,** 85-99.

Henne, W.M., Boucrot, E., Meinecke, M., Evergren, E., Vallis, Y., Mittal, R. and McMahon, H.T. (2010). FCHo proteins are nucleators of clathrin-mediated endocytosis. *Science* **328,** 1281-1284.

Henry, R., Shaughnessy, L., Loessner, M.J., Alberti-Segui, C., Higgins, D.E. and Swanson, J.A. (2006). Cytolysin-dependent delay of vacuole maturation in macrophages infected with *Listeria monocytogenes*. *Cell Microbiol* **8,** 107-119.

Herskovits, J.S., Burgess, C.C., Obar, R.A. and Vallee, R.B. (1993). Effects of mutant rat dynamin on endocytosis. *J Cell Biol* **122,** 565-578.

Hinshaw, J.E. (2000). Dynamin and its role in membrane fission. *Annu Rev Cell Dev Biol* **16,** 483-519.

Hoehne, M., de Couet, H.G., Stuermer, C.A. and Fischbach, K.F. (2005). Loss- and gain-of-function analysis of the lipid raft proteins Reggie/Flotillin in Drosophila: they are posttranslationally regulated, and misexpression interferes with wing and eye development. *Mol Cell Neurosci* **30,** 326-338.

Hoffman, J.A., Wass, C., Stins, M.F. and Kim, K.S. (1999). The capsule supports survival but not traversal of *Escherichia coli* K1 across the blood-brain barrier. *Infect Immun* **67,** 3566-3570.

Hoffmann, C., Berking, A., Agerer, F., Buntru, A., Neske, F., Chhatwal, G.S., Ohlsen, K. and Hauck, C.R. (2010). Caveolin limits membrane microdomain mobility and integrin-mediated uptake of fibronectin-binding pathogens. *J Cell Sci* **123,** 4280-4291.

Holt, D.E., Halket, S., de Louvois, J. and Harvey, D. (2001). Neonatal meningitis in England and Wales: 10 years on. *Arch. Dis. Child. Fetal Neonatal Ed.* **84,** F85-89.

Howes, M.T., Kirkham, M., Riches, J., Cortese, K., Walser, P.J., Simpson, F., Hill, M.M., Jones, A., Lundmark, R., Lindsay, M.R., Hernandez-Deviez, D.J., Hadzic, G., McCluskey, A., Bashir, R., Liu, L., Pilch, P., McMahon, H., Robinson, P.J., Hancock, J.F., Mayor, S. and Parton, R.G. (2010). Clathrin-independent carriers form a high capacity endocytic sorting system at the leading edge of migrating cells. *J Cell Biol* **190,** 675-691.

Hu, G., Schwartz, D.E., Shajahan, A.N., Visintine, D.J., Salem, M.R., Crystal, G.J., Albrecht, R.F., Vogel, S.M. and Minshall, R.D. (2006). Isoflurane, but not sevoflurane, increases transendothelial albumin permeability in the isolated rat lung: role for enhanced phosphorylation of caveolin-1. *Anesthesiology* **104**, 777-785.

Hu, L., Tall, B.D., Curtis, S.K. and Kopecko, D.J. (2008). Enhanced microscopic definition of *Campylobacter jejuni* 81-176 adherence to, invasion of, translocation across, and exocytosis from polarized human intestinal Caco-2 cells. *Infect. Immun.* **76**, 5294-5304.

Huang, S.H., Chen, Y.H., Fu, Q., Stins, M., Wang, Y., Wass, C. and Kim, K.S. (1999). Identification and characterization of an *Escherichia coli* invasion gene locus, *ibeB*, required for penetration of brain microvascular endothelial cells. *Infect Immun* **67**, 2103-2109.

Huang, S.H., Wass, C., Fu, Q., Prasadarao, N.V., Stins, M. and Kim, K.S. (1995). *Escherichia coli* invasion of brain microvascular endothelial cells *in vitro* and *in vivo*: molecular cloning and characterization of invasion gene *ibe10*. *Infect Immun* **63**, 4470-4475.

Hundorfean, G., Zimmer, K.P., Strobel, S., Gebert, A., Ludwig, D. and Buning, J. (2007). Luminal antigens access late endosomes of intestinal epithelial cells enriched in MHC I and MHC II molecules: in vivo study in Crohn's ileitis. *Am J Physiol Gastrointest Liver Physiol* **293**, G798-808.

Hybiske, K. and Stephens, R.S. (2007). Mechanisms of *Chlamydia trachomatis* entry into nonphagocytic cells. *Infect Immun* **75**, 3925-3934.

Idrissi, F.Z., Grotsch, H., Fernandez-Golbano, I.M., Presciatto-Baschong, C., Riezman, H. and Geli, M.I. (2008). Distinct acto/myosin-I structures associate with endocytic profiles at the plasma membrane. *J. Cell Biol.* **180**, 1219-1232.

Inoue, Y., Tanaka, N., Tanaka, Y., Inoue, S., Morita, K., Zhuang, M., Hattori, T. and Sugamura, K. (2007). Clathrin-dependent entry of severe acute respiratory syndrome coronavirus into target cells expressing ACE2 with the cytoplasmic tail deleted. *J Virol* **81**, 8722-8729.

Invernici, G., Ponti, D., Corsini, E., Cristini, S., Frigerio, S., Colombo, A., Parati, E. and Alessandri, G. (2005). Human microvascular endothelial cells from different fetal organs demonstrate organ-specific CAM expression. *Exp Cell Res* **308**, 273-282.

Iversen, T.G., Skretting, G., van Deurs, B. and Sandvig, K. (2003). Clathrin-coated pits with long, dynamin-wrapped necks upon expression of a clathrin antisense RNA. *Proc Natl Acad Sci U S A* **100,** 5175-5180.

Jain, S.K., Paul-Satyaseela, M., Lamichhane, G., Kim, K.S. and Bishai. W.R. (2006). *Mycobacterium tuberculosis* invasion and traversal across an in vitro human blood-brain barrier as a pathogenic mechanism for central nervous system tuberculosis. *J Infect Dis* **193,** 1287-1295.

Join-Lambert, O., Morand, P.C., Carbonnelle, E., Coureuil, M., Bille, E., Bourdoulous, S. and Nassif, X. (2010). Mechanisms of meningeal invasion by a bacterial extracellular pathogen, the example of *Neisseria meningitidis*. *Prog Neurobiol* **91,** 130-139.

Jokilammi, A., Ollikka, P., Korja, M., Jakobsson, E., Loimaranta, V., Haataja. S., Hirvonen, H. and Finne, J. (2004). Construction of antibody mimics from a noncatalytic enzyme-detection of polysialic acid. *J Immunol Methods* **295,** 149-160.

Jorgensen, I., Bednar, M.M., Amin, V., Davis, B.K., Ting, J.P., McCafferty, D.G. and Valdivia, R.H. (2011). The *Chlamydia* protease CPAF regulates host and bacterial proteins to maintain pathogen vacuole integrity and promote virulence. *Cell Host Microbe* **10,** 21-32.

Kaksonen, M., Toret, C.P. and Drubin, D.G. (2005). A modular design for the clathrin- and actin-mediated endocytosis machinery. *Cell* **123,** 305-320.

Kang, J., Ramu, S., Lee, S., Aguilar, B., Ganesan, S.K., Yoo, J., Kalra, V.K., Koh, C.J. and Hong, Y.-K. (2009). Phosphate-buffered saline-based nucleofection of primary endothelial cells. *Anal Biochem* **386,** 251-255.

Kaper, J.B., Nataro, J.P. and Mobley, H.L. (2004). Pathogenic *Escherichia coli*. *Nat Rev Microbiol* **2,** 123-140.

Khan, A.G., Pickl-Herk, A., Gajdzik, L., Marlovits, T.C., Fuchs, R. and Blaas, D. (2011). Entry of a heparan sulphate-binding HRV8 variant strictly depends on dynamin but not on clathrin, caveolin, and flotillin. *Virology* **412,** 55-67.

Khan, N.A., Kim, Y., Shin, S. and Kim, K.S. (2007). FimH-mediated *Escherichia coli* K1 invasion of human brain microvascular endothelial cells. *Cell Microbiol* **9,** 169-178.

Khan, N.A., Shin, S., Chung, J.W., Kim, K.J., Elliott, S., Wang, Y. and Kim. K.S. (2003). Outer membrane protein A and cytotoxic necrotizing factor-1 use diverse signaling

mechanisms for *Escherichia coli* K1 invasion of human brain microvascular endothelial cells. *Microb Pathog* **35**, 35-42.

Khan, N.A., Wang, Y., Kim, K.J., Chung, J.W., Wass, C.A. and Kim, K.S. (2002). Cytotoxic necrotizing factor-1 contributes to *Escherichia coli* K1 invasion of the central nervous system. *J. Biol. Chem.* **277**, 15607-15612.

Kim, K.J., Elliott, S.J., Di Cello, F., Stins, M.F. and Kim, K.S. (2003). The K1 capsule modulates trafficking of *E. coli*-containing vacuoles and enhances intracellular bacterial survival in human brain microvascular endothelial cells. *Cell Microbiol* **5**, 245-252.

Kim, K.S. (2008). Mechanisms of microbial traversal of the blood-brain barrier. *Nat Rev Micro* **6**, 625-634.

Kim, K.S., Itabashi, H., Gemski, P., Sadoff, J., Warren, R.L. and Cross, A.S. (1992). The K1 capsule is the critical determinant in the development of *Escherichia coli* meningitis in the rat. *J Clin Invest* **90**, 897-905.

Kinchen, J.M. and Ravichandran, K.S. (2008). Phagosome maturation: going through the acid test. *Nat Rev Mol Cell Biol* **9**, 781-795.

Kingston, R.E. (2001) Introduction of DNA into Mammalian Cells. In *Curr Protoc Mol Biol*. John Wiley & Sons, Inc.

Kingston, R.E., Chen, C.A. and Rose, J.K. (2003). Calcium phosphate transfection. *Curr Protoc Mol Biol* **Chapter 9,** Unit 9 1.

Kirkham, M., Fujita, A., Chadda, R., Nixon, S.J., Kurzchalia, T.V., Sharma, D.K., Pagano, R.E., Hancock, J.F., Mayor, S. and Parton, R.G. (2005). Ultrastructural identification of uncoated caveolin-independent early endocytic vehicles. *J Cell Biol* **168,** 465-476.

Kitazawa, T., Hosoya, K., Watanabe, M., Takashima, T., Ohtsuki, S., Takanaga, H., Ueda, M., Yanai, N., Obinata, M. and Terasaki, T. (2001). Characterization of the amino acid transport of new immortalized choroid plexus epithelial cell lines: a novel *in vitro* system for investigating transport functions at the blood-cerebrospinal fluid barrier. *Pharm Res* **18,** 16-22.

Knodler, A., Feng, S., Zhang, J., Zhang, X., Das, A., Peranen, J. and Guo, W. (2010). Coordination of Rab8 and Rab11 in primary ciliogenesis. *Proc Natl Acad Sci U S A* **107,** 6346-6351.

Knodler, L.A., Bestor, A., Ma, C., Hansen-Wester, I., Hensel, M., Vallance, B.A. and Steele-Mortimer, O. (2005). Cloning vectors and fluorescent proteins can significantly inhibit *Salmonella enterica* virulence in both epithelial cells and

macrophages: implications for bacterial pathogenesis studies. *Infect. Immun.* **73**, 7027-7031.

Kovala, A.T., Harvey, K.A., McGlynn, P., Boguslawski, G., Garcia, J.G.N. and English. D. (2000). High-efficiency transient transfection of endothelial cells for functional analysis. *FASEB J* **14**, 2486-2494.

Kreitzer, G., Schmoranzer, J., Low, S.H., Li, X., Gan, Y., Weimbs, T., Simon. S.M. and Rodriguez-Boulan, E. (2003). Three-dimensional analysis of post-golgi carrier exocytosis in epithelial cells. *Nat Cell Biol* **5**, 126-136.

Kumabe, T., Tominaga, T., Kondo, T., Yoshimoto, T. and Kayama, T. (1996). Intraoperative radiation therapy and chemotherapy for huge choroid plexus carcinoma in an infant--case report. *Neurol Med Chir (Tokyo)* **36**, 179-184.

Kumari, S., Borroni, V., Chaudhry, A., Chanda, B., Massol. R., Mayor, S. and Barrantes, F.J. (2008). Nicotinic acetylcholine receptor is internalized via a Rac-dependent. dynamin-independent endocytic pathway. *J Cell Biol* **181**, 1179-1193.

Kumari, S. and Mayor, S. (2008). ARF1 is directly involved in dynamin-independent endocytosis. *Nat Cell Biol* **10**, 30-41.

Kumari, S., Mg, S. and Mayor, S. (2010). Endocytosis unplugged: multiple ways to enter the cell. *Cell Res* **20**, 256-275.

Labrecque, L., Nyalendo, C., Langlois, S., Durocher, Y., Roghi, C., Murphy, G., Gingras, D. and Beliveau, R. (2004). Src-mediated tyrosine phosphorylation of caveolin-1 induces its association with membrane type 1 matrix metalloproteinase. *J Biol Chem* **279**, 52132-52140.

Lakkaraju, A. and Rodriguez-Boulan, E. (2008). Itinerant exosomes: emerging roles in cell and tissue polarity. *Trends Cell Biol* **18**, 199-209.

Lamaze, C., Dujeancourt, A., Baba, T., Lo, C.G., Benmerah, A. and Dautry-Varsat, A. (2001). Interleukin 2 receptors and detergent-resistant membrane domains define a clathrin-independent endocytic pathway. *Mol Cell* **7**, 661-671.

Lamberti, Y.A., Hayes, J.A., Perez Vidakovics, M.L., Harvill, E.T. and Rodriguez, M.E. (2010). Intracellular trafficking of *Bordetella pertussis* in human macrophages. *Infect. Immun.* **78**, 907-913.

Langhorst, M.F., Jaeger, F.A., Mueller, S., Sven Hartmann, L., Luxenhofer. G. and Stuermer, C.A. (2008a). Reggies/flotillins regulate cytoskeletal remodeling during neuronal differentiation via CAP/ponsin and Rho GTPases. *Eur J Cell Biol* **87**, 921-931.

Langhorst, M.F., Reuter, A., Jaeger, F.A., Wippich, F.M., Luxenhofer, G., Plattner, H. and Stuermer, C.A. (2008b). Trafficking of the microdomain scaffolding protein reggie-1/flotillin-2. *Eur J Cell Biol* **87**, 211-226.

Langhorst, M.F., Solis, G.P., Hannbeck, S., Plattner, H. and Stuermer, C.A. (2007). Linking membrane microdomains to the cytoskeleton: regulation of the lateral mobility of reggie-1/flotillin-2 by interaction with actin. *FEBS Lett* **581**, 4697-4703.

Lassiter, H.A., Watson, S.W., Seifring, M.L. and Tanner, J.E. (1992). Complement factor 9 deficiency in serum of human neonates. *J Infect Dis* **166**, 53-57.

Lee, E. and De Camilli, P. (2002). Dynamin at actin tails. *Proc Natl Acad Sci U S A* **99**, 161-166.

Lee, J., Shin, S., Teng, C.H., Hong, S.J. and Kim, K.S. (2005). FimH adhesin of *Escherichia coli* K1 type 1 fimbriae activates BV-2 microglia. *Biochem Biophys Res Commun* **334**, 917-923.

Legros, H., Launay, S., Roussel, B.D., Marcou-Labarre, A., Calbo, S., Catteau, J., Leroux, P., Boyer, O., Ali, C., Marret, S., Vivien, D. and Laudenbach, V. (2009). Newborn- and adult-derived brain microvascular endothelial cells show age-related differences in phenotype and glutamate-evoked protease release. *J Cereb Blood Flow Metab* **29**, 1146-1158.

Leung, S.M., Ruiz, W.G. and Apodaca, G. (2000). Sorting of membrane and fluid at the apical pole of polarized Madin-Darby canine kidney cells. *Mol Biol Cell* **11**, 2131-2150.

Levine, E.M., Ghai, V., Barton, J.J. and Strom, C.M. (1999). Intrapartum antibiotic prophylaxis increases the incidence of gram-negative neonatal sepsis. *Infect Dis Obstet Gynecol* **7**, 210-213.

Levy, O. (2007). Innate immunity of the newborn: basic mechanisms and clinical correlates. *Nat Rev Immunol* **7**, 379-390.

Li, Q., Zhang, Q., Wang, C., Li, N. and Li, J. (2008a). Invasion of enteropathogenic *Escherichia coli* into host cells through epithelial tight junctions. *FEBS J* **275**, 6022-6032.

Li, Q., Zhang, Q., Wang, M., Zhao, S., Ma, J., Luo, N., Li, N., Li, Y., Xu, G. and Li, J. (2008b). Interferon-γ and tumor necrosis factor-α disrupt epithelial barrier function by altering lipid composition in membrane microdomains of tight junction. *Clin Immunol* **126**, 67-80.

Li, S., Seitz, R. and Lisanti, M.P. (1996). Phosphorylation of caveolin by src tyrosine kinases. The alpha-isoform of caveolin is selectively phosphorylated by v-Src in vivo. *J Biol Chem* **271,** 3863-3868.

Li, Z., Dai, J., Zheng, H., Liu, B. and Caudill, M. (2002). An integrated view of the roles and mechanisms of heat shock protein gp96-peptide complex in eliciting immune response. *Front Biosci* **7,** d731-751.

Liberali, P., Kakkonen, E., Turacchio, G., Valente, C., Spaar, A., Perinetti, G., Bockmann, R.A., Corda, D., Colanzi, A., Marjomaki, V. and Luini, A. (2008). The closure of Pak1-dependent macropinosomes requires the phosphorylation of CtBP1/BARS. *EMBO J* **27,** 970-981.

Lindemann, D. and Schnittler, H. (2009). Genetic manipulation of endothelial cells by viral vectors. *Thromb Haemost* **102,** 1135-1143.

Lingwood, D. and Simons, K. (2010). Lipid rafts as a membrane-organizing principle. *Science* **327,** 46-50.

Lipinski, A.R., Heymann, J., Meissner, C., Karlas, A., Brinkmann, V., Meyer, T.F. and Heuer, D. (2009). Rab6 and Rab11 regulate *Chlamydia trachomatis* development and golgin-84-dependent Golgi fragmentation. *PLoS Pathog* **5,** e1000615.

Liu, C., Yu, W., Chen, Z., Zhang, J. and Zhang, N. (2011). Enhanced gene transfection efficiency in CD13-positive vascular endothelial cells with targeted poly(lactic acid)-poly(ethylene glycol) nanoparticles through caveolae-mediated endocytosis. *J Control Release* **151,** 162-175.

Liu, J., Deyoung, S.M., Zhang, M., Dold, L.H. and Saltiel, A.R. (2005). The stomatin/prohibitin/flotillin/HflK/C domain of flotillin-1 contains distinct sequences that direct plasma membrane localization and protein interactions in 3T3-L1 adipocytes. *J Biol Chem* **280,** 16125-16134.

Liu, N.Q., Lossinsky, A.S., Popik, W., Li, X., Gujuluva, C., Kriederman, B., Roberts, J., Pushkarsky, T., Bukrinsky, M., Witte, M., Weinand, M. and Fiala, M. (2002). Human immunodeficiency virus type 1 enters brain microvascular endothelia by macropinocytosis dependent on lipid rafts and the mitogen-activated protein kinase signaling pathway. *J Virol* **76,** 6689-6700.

Liu, W., Zhao, W.D., Yan, J.C., Ren, Z.Y., Fang, W.G., Zhu, L., Shang, D.S. and Chen, Y.H. (2010). Involvement of Src tyrosine kinase in *Escherichia coli* invasion of human brain microvascular endothelial cells. *FEBS Lett* **584,** 27-32.

Liu, Y.W., Surka, M.C., Schroeter, T., Lukiyanchuk, V. and Schmid, S.L. (2008). Isoform and splice-variant specific functions of dynamin-2 revealed by analysis of conditional knock-out cells. *Mol. Biol. Cell* **19**, 5347-5359.

Lu, L., Yang, P.Y., Rui, Y., Kang, H., Zhang, J., Zhang, J.P. and Feng, W.H. (2007). Comparative proteome analysis of rat brain and coronary microvascular endothelial cells. *Physiol Res* **56**, 159-168.

Ludwig, A., Otto, G.P., Riento, K., Hams, E., Fallon, P.G. and Nichols, B.J. (2010). Flotillin microdomains interact with the cortical cytoskeleton to control uropod formation and neutrophil recruitment. *J Cell Biol* **191**, 771-781.

Lui-Roberts, W.W., Ferraro, F., Nightingale, T.D. and Cutler. D.F. (2008). Aftiphilin and gamma-synergin are required for secretagogue sensitivity of Weibel-Palade bodies in endothelial cells. *Mol Biol Cell* **19**, 5072-5081.

Lundmark, R., Doherty, G.J., Vallis, Y., Peter, B.J. and McMahon, H.T. (2008). Arf family GTP loading is activated by, and generates, positive membrane curvature. *Biochem J* **414**, 189-194.

Macia, E., Ehrlich, M., Massol, R., Boucrot, E., Brunner, C. and Kirchhausen, T. (2006). Dynasore, a cell-permeable inhibitor of dynamin. *Dev Cell* **10**, 839-850.

Mairey, E., Genovesio, A., Donnadieu, E., Bernard, C., Jaubert, F., Pinard, E., Seylaz, J., Olivo-Marin, J.C., Nassif, X. and Dumenil, G. (2006). Cerebral microcirculation shear stress levels determine *Neisseria meningitidis* attachment sites along the blood-brain barrier. *J Exp Med* **203**, 1939-1950.

Mallegol, J., Van Niel, G., Lebreton, C., Lepelletier, Y., Candalh, C., Dugave, C., Heath, J.K., Raposo, G., Cerf-Bensussan, N. and Heyman, M. (2007). T84-intestinal epithelial exosomes bear MHC class II/peptide complexes potentiating antigen presentation by dendritic cells. *Gastroenterology* **132**, 1866-1876.

Man, S., Ubogu, E.E., Williams, K.A., Tucky, B., Callahan, M.K. and Ransohoff, R.M. (2008). Human brain microvascular endothelial cells and umbilical vein endothelial cells differentially facilitate leukocyte recruitment and utilize chemokines for T cell migration. *Clin Dev Immunol* **2008**, 384982.

Marchant, J. (2011). 'Flawed' infant death papers not retracted. *Nature* **476**, 263-264.

Marchès, O., Covarelli, V., Dahan, S., Cougoule, C., Bhatta, P., Frankel, G. and Caron, E. (2008). EspJ of enteropathogenic and enterohaemorrhagic *Escherichia coli* inhibits opsono-phagocytosis. *Cell Microbiol* **10**, 1104-1115.

Marker, D.F., Tremblay, M.E., Lu, S.M., Majewska, A.K. and Gelbard, H.A. (2010). A thin-skull window technique for chronic two-photon *in vivo* imaging of murine microglia in models of neuroinflammation. *J Vis Exp.*

Marks, B., Stowell, M.H., Vallis, Y., Mills, I.G., Gibson. A., Hopkins. C.R. and McMahon, H.T. (2001). GTPase activity of dynamin and resulting conformation change are essential for endocytosis. *Nature* **410,** 231-235.

Martins-Green, M., Petreaca, M. and Yao, M. (2008). An assay system for *in vitro* detection of permeability in human "endothelium". *Methods Enzymol* **443,** 137-153.

Maruvada, R., Argon, Y. and Prasadarao, N.V. (2008). *Escherichia coli* interaction with human brain microvascular endothelial cells induces signal transducer and activator of transcription 3 association with the C-terminal domain of Ec-gp96, the outer membrane protein A receptor for invasion. *Cell Microbiol* **10,** 2326-2338.

Matthews, L.C., Taggart, M.J. and Westwood, M. (2008). Modulation of caveolin-1 expression can affect signalling through the phosphatidylinositol 3-kinase/Akt pathway and cellular proliferation in response to insulin-like growth factor I. *Endocrinology* **149,** 5199-5208.

Maxfield, F.R. (2002). Plasma membrane microdomains. *Curr Opin Cell Biol* **14,** 483-487.

May, M., Daley, A.J., Donath, S. and Isaacs, D. (2005). Early onset neonatal meningitis in Australia and New Zealand, 1992-2002. *Arch. Dis. Child. Fetal Neonatal Ed.* **90,** F324-327.

Mayor, S. and Pagano, R.E. (2007). Pathways of clathrin-independent endocytosis. *Nat Rev Mol Cell Biol* **8,** 603-612.

McMahon, H.T. and Boucrot, E. (2011). Molecular mechanism and physiological functions of clathrin-mediated endocytosis. *Nat Rev Mol Cell Biol* **12,** 517-533.

Meiri, K.F. (2005). Lipid rafts and regulation of the cytoskeleton during T cell activation. *Philos Trans R Soc Lond B Biol Sci* **360,** 1663-1672.

Melican, K. and Richter-Dahlfors, A. (2009). Multiphoton imaging of host-pathogen interactions. *Biotechnol J* **4,** 804-811.

Melican, K., Sandoval, R.M., Kader, A., Josefsson, L., Tanner, G.A., Molitoris, B.A. and Richter-Dahlfors, A. (2011). Uropathogenic *Escherichia coli* P and Type 1 fimbriae act in synergy in a living host to facilitate renal colonization leading to nephron obstruction. *PLoS Pathog* **7,** e1001298.

Mercer, J. and Helenius, A. (2008). Vaccinia virus uses macropinocytosis and apoptotic mimicry to enter host cells. *Science* **320,** 531-535.

Mercer, J. and Helenius, A. (2009). Virus entry by macropinocytosis. *Nat Cell Biol* **11**, 510-520.

Méresse, S., Steele-Mortimer, O., Finlay, B.B. and Gorvel, J.P. (1999). The rab7 GTPase controls the maturation of *Salmonella typhimurium*-containing vacuoles in HeLa cells. *EMBO J* **18**, 4394-4403.

Messick, J.B. and Rikihisa, Y. (1993). Characterization of *Ehrlichia risticii* binding, internalization, and proliferation in host cells by flow cytometry. *Infect Immun* **61**, 3803-3810.

Metkar, S., Awasthi, S., Denamur, E., Kim, K.S., Gangloff, S.C., Teichberg, S., Haziot, A., Silver, J. and Goyert, S.M. (2007). Role of CD14 in responses to clinical isolates of *Escherichia coli*: effects of K1 capsule expression. *Infect Immun* **75**, 5415-5424.

Michell, R.H., Heath, V.L., Lemmon, M.A. and Dove, S.K. (2006). Phosphatidylinositol 3,5-bisphosphate: metabolism and cellular functions. *Trends Biochem Sci* **31**, 52-63.

Minshall, R.D., Sessa, W.C., Stan, R.V., Anderson, R.G.W. and Malik, A.B. (2003). Caveolin regulation of endothelial function. *Am J Physiol Lung Cell Mol Physiol* **285**, L1179-1183.

Mosso, C., Galvan-Mendoza, I.J., Ludert, J.E. and del Angel, R.M. (2008). Endocytic pathway followed by dengue virus to infect the mosquito cell line C6/36 HT. *Virology* **378**, 193-199.

Moxon, E.R., Glode, M.P., Sutton, A. and Robbins, J.B. (1977). The infant rat as a model of bacterial meningitis. *J Infect Dis* **136 Suppl**, S186-190.

Mulholland, K. (1998). Serious infections in young infants in developing countries. *Vaccine* **16**, 1360-1362.

Mushtaq, N., Redpath, M.B., Luzio, J.P. and Taylor, P.W. (2004). Prevention and cure of systemic *Escherichia coli* K1 infection by modification of the bacterial phenotype. *Antimicrob. Agents Chemother.* **48**, 1503-1508.

Mushtaq, N., Redpath, M.B., Luzio, J.P. and Taylor, P.W. (2005). Treatment of experimental *Escherichia coli* infection with recombinant bacteriophage-derived capsule depolymerase. *J Antimicrob Chemother* **56**, 160-165.

Nachman, R.L. and Rafii, S. (2008). Platelets, petechiae, and preservation of the vascular wall. *N Engl J Med* **359**, 1261-1270.

Nagy, Z., Peters, H. and Huttner, I. (1984). Fracture faces of cell junctions in cerebral endothelium during normal and hyperosmotic conditions. *Lab Invest* **50**, 313-322.

Nakata, T., Takemura, R. and Hirokawa, N. (1993). A novel member of the dynamin family of GTP-binding proteins is expressed specifically in the testis. *J Cell Sci* **105** (Pt 1), 1-5.

Nassif, X., Bourdoulous, S., Eugene, E. and Couraud, P.O. (2002). How do extracellular pathogens cross the blood-brain barrier? *Trends Microbiol* **10**, 227-232.

Neumann-Giesen, C., Falkenbach, B., Beicht, P., Claasen, S., Luers, G., Stuermer, C.A., Herzog, V. and Tikkanen, R. (2004). Membrane and raft association of reggie-1/flotillin-2: role of myristoylation, palmitoylation and oligomerization and induction of filopodia by overexpression. *Biochem J* **378**, 509-518.

Newton, H.J. and Roy, C.R. (2011). The *Coxiella burnetii* Dot/Icm System Creates a Comfortable Home through Lysosomal Renovation. *MBio* **2**.

Nightingale, T.D., White, I.J., Doyle, E.L., Turmaine, M., Harrison-Lavoie, K.J., Webb, K.F., Cramer, L.P. and Cutler, D.F. (2011). Actomyosin II contractility expels von Willebrand factor from Weibel-Palade bodies during exocytosis. *J Cell Biol* **194**, 613-629.

Nikitas, G., Deschamps, C., Disson, O., Niault, T., Cossart, P. and Lecuit, M. (2011). Transcytosis of *Listeria monocytogenes* across the intestinal barrier upon specific targeting of goblet cell accessible E-cadherin. *J Exp Med* **208**, 2263-2277.

Nowicki, B., Rhen, M., Väisänen-Rhen, V., Pere, A. and Korhonen, T.K. (1985). Kinetics of phase variation between S and type-1 fimbriae of *Escherichia coli*. *FEMS Microbiol Lett* **28**, 237-242.

Oh, P., McIntosh, D.P. and Schnitzer, J.E. (1998). Dynamin at the neck of caveolae mediates their budding to form transport vesicles by GTP-driven fission from the plasma membrane of endothelium. *J Cell Biol* **141**, 101-114.

Orihuela, C.J., Mahdavi, J., Thornton, J., Mann, B., Wooldridge, K.G., Abouseada, N., Oldfield, N.J., Self, T., Ala'Aldeen, D.A. and Tuomanen, E.I. (2009). Laminin receptor initiates bacterial contact with the blood brain barrier in experimental meningitis models. *J Clin Invest* **119**, 1638-1646.

Osrin, D., Vergnano, S. and Costello, A. (2004). Serious bacterial infections in newborn infants in developing countries. *Curr Opin Infect Dis* **17**, 217-224.

Parat, M.O. (2009). The biology of caveolae: achievements and perspectives. *Int Rev Cell Mol Biol* **273**, 117-162.

Parat, M.O., Anand-Apte, B. and Fox, P.L. (2003). Differential caveolin-1 polarization in endothelial cells during migration in two and three dimensions. *Mol. Biol. Cell* **14**, 3156-3168.

Parat, M.O. and Fox, P.L. (2001). Palmitoylation of caveolin-1 in endothelial cells is post-translational but irreversible. *J Biol Chem* **276**, 15776-15782.

Parkkinen, J., Korhonen, T.K., Pere, A., Hacker, J. and Soinila, S. (1988). Binding sites in the rat brain for *Escherichia coli* S fimbriae associated with neonatal meningitis. *J Clin Invest* **81**, 860-865.

Parolini, I., Sargiacomo, M., Galbiati, F., Rizzo, G., Grignani, F., Engelman, J.A., Okamoto, T., Ikezu, T., Scherer, P.E., Mora, R., Rodriguez-Boulan. E., Peschle, C. and Lisanti, M.P. (1999). Expression of caveolin-1 is required for the transport of caveolin-2 to the plasma membrane. Retention of caveolin-2 at the level of the golgi complex. *J Biol Chem* **274**, 25718-25725.

Parton, R.G. (2003). Caveolae--from ultrastructure to molecular mechanisms. *Nat Rev Mol Cell Biol* **4**, 162-167.

Parton, R.G. and Simons, K. (2007). The multiple faces of caveolae. *Nat Rev Mol Cell Biol* **8**, 185-194.

Patterson, G.H. and Lippincott-Schwartz, J. (2002). A Photoactivatable GFP for Selective Photolabeling of Proteins and Cells. *Science* **297**, 1873-1877.

Pearse, B.M. (1976). Clathrin: a unique protein associated with intracellular transfer of membrane by coated vesicles. *Proc Natl Acad Sci U S A* **73**, 1255-1259.

Pearse, B.M. (1982). Coated vesicles from human placenta carry ferritin, transferrin, and immunoglobulin G. *Proc Natl Acad Sci U S A* **79**, 451-455.

Pelkmans, L. and Helenius, A. (2002). Endocytosis via caveolae. *Traffic* **3**, 311-320.

Pelkmans, L., Kartenbeck, J. and Helenius, A. (2001). Caveolar endocytosis of simian virus 40 reveals a new two-step vesicular-transport pathway to the ER. *Nat Cell Biol* **3**, 473-483.

Pelkmans, L., Puntener, D. and Helenius, A. (2002). Local actin polymerization and dynamin recruitment in SV40-induced internalization of caveolae. *Science* **296**, 535-539.

Pluschke, G., Mercer, A., Kusecek, B., Pohl, A. and Achtman, M. (1983). Induction of bacteremia in newborn rats by *Escherichia coli* K1 is correlated with only certain O (lipopolysaccharide) antigen types. *Infect. Immun.* **39**, 599-608.

Polin, R.A. and Harris, M.C. (2001). Neonatal bacterial meningitis. *Semin Neonatol* **6**, 157-172.

Polishchuk, R., Pentima, A.D. and Lippincott-Schwartz, J. (2004). Delivery of raft-associated. GPI-anchored proteins to the apical surface of polarized MDCK cells by a transcytotic pathway. *Nat Cell Biol* **6**, 297-307.

Potter, H. (2003). Transfection by electroporation. *Curr Protoc Mol Biol* **Chapter 9,** Unit 9 3.

Praefcke, G.J.K. and McMahon, H.T. (2004). The dynamin superfamily: universal membrane tubulation and fission molecules? *Nat Rev Mol Cell Biol* **5,** 133-147.

Prasadarao, N.V. (2002). Identification of *Escherichia coli* outer membrane protein A receptor on human brain microvascular endothelial cells. *Infect. Immun.* **70,** 4556-4563.

Prasadarao, N.V., Srivastava, P.K., Rudrabhatla, R.S., Kim, K.S., Huang, S.H. and Sukumaran, S.K. (2003). Cloning and expression of the *Escherichia coli* K1 outer membrane protein A receptor, a gp96 homologue. *Infect Immun* **71,** 1680-1688.

Prasadarao, N.V., Wass, C.A., Hacker, J., Jann, K. and Kim, K.S. (1993). Adhesion of S-fimbriated *Escherichia coli* to brain glycolipids mediated by *sfaA* gene-encoded protein of S-fimbriae. *J Biol Chem* **268,** 10356-10363.

Prasadarao, N.V., Wass, C.A. and Kim, K.S. (1996a). Endothelial cell GlcNAcβ1-4GlcNAc epitopes for outer membrane protein A enhance traversal of *Escherichia coli* across the blood-brain barrier. *Infect Immun* **64,** 154-160.

Prasadarao, N.V., Wass, C.A., Stins, M.F., Shimada, H. and Kim, K.S. (1999). Outer membrane protein A-promoted actin condensation of brain microvascular endothelial cells is required for *Escherichia coli* invasion. *Infect. Immun.* **67,** 5775-5783.

Prasadarao, N.V., Wass, C.A., Weiser, J.N., Stins, M.F., Huang, S.H. and Kim, K.S. (1996b). Outer membrane protein A of *Escherichia coli* contributes to invasion of brain microvascular endothelial cells. *Infect Immun* **64,** 146-153.

Predescu, D. and Palade, G.E. (1993). Plasmalemmal vesicles represent the large pore system of continuous microvascular endothelium. *Am J Physiol* **265,** H725-733.

Predescu, S.A., Predescu, D.N. and Malik, A.B. (2007). Molecular determinants of endothelial transcytosis and their role in endothelial permeability. *Am J Physiol Lung Cell Mol Physiol* **293,** L823-842.

Pron, B., Taha, M.K., Rambaud, C., Fournet, J.C., Pattey, N., Monnet, J.P., Musilek, M., Beretti, J.L. and Nassif, X. (1997). Interaction of *Neisseria meningitidis* with the components of the blood-brain barrier correlates with an increased expression of PilC. *J Infect Dis* **176,** 1285-1292.

Qazi, S.N., Rees, C.E., Mellits, K.H. and Hill, P.J. (2001). Development of gfp vectors for expression in *Listeria monocytogenes* and other low G+C Gram positive bacteria. *Microb Ecol* **41,** 301-309.

Quagliarello, V.J., Long, W.J. and Scheld, W.M. (1986). Morphologic alterations of the blood-brain barrier with experimental meningitis in the rat. Temporal sequence and role of encapsulation. *J Clin Invest* **77**, 1084-1095.

Quagliarello, V.J., Wispelwey, B., Long, W.J., Jr. and Scheld, W.M. (1991). Recombinant human interleukin-1 induces meningitis and blood-brain barrier injury in the rat. Characterization and comparison with tumor necrosis factor. *J Clin Invest* **87**, 1360-1366.

Radtke, A.L., Delbridge, L.M., Balachandran, S., Barber, G.N. and O'Riordan, M.X.D. (2007). TBK1 protects vacuolar integrity during intracellular bacterial infection. *PLoS Pathog* **3**, e29.

Raghu, H., Sharma-Walia, N., Veettil, M.V., Sadagopan, S. and Chandran, B. (2009). Kaposi's sarcoma-associated herpesvirus utilizes an actin polymerization-dependent macropinocytic pathway to enter human dermal microvascular endothelial and human umbilical vein endothelial cells. *J Virol* **83**, 4895-4911.

Rahn, E., Petermann, P., Hsu, M.J., Rixon, F.J. and Knebel-Morsdorf, D. (2011). Entry pathways of herpes simplex virus type 1 into human keratinocytes are dynamin- and cholesterol-dependent. *PLoS One* **6**, e25464.

Ramezani, A. and Hawley, R.G. (2002). Overview of the HIV-1 lentiviral vector system. *Curr Protoc Mol Biol* **Chapter 16**, Unit 16 21.

Ramilo, O., Saez-Llorens, X., Mertsola, J., Jafari, H., Olsen, K.D., Hansen, E.J., Yoshinaga, M., Ohkawara, S., Nariuchi, H. and McCracken, G.H., Jr. (1990). Tumor necrosis factor alpha/cachectin and interleukin 1 beta initiate meningeal inflammation. *J Exp Med* **172**, 497-507.

Raymond, J., Lopez, E., Bonacorsi, S., Poyart, C., Moriette, G., Jarreau, P.H. and Bingen, E. (2008). Evidence for transmission of *Escherichia coli* from mother to child in late-onset neonatal infection. *Pediatr Infect Dis J* **27**, 186-188.

Razani, B., Engelman, J.A., Wang, X.B., Schubert, W., Zhang, X.L., Marks, C.B., Macaluso, F., Russell, R.G., Li, M., Pestell, R.G., Di Vizio, D., Hou, H., Jr., Kneitz, B., Lagaud, G., Christ, G.J., Edelmann, W. and Lisanti, M.P. (2001). Caveolin-1 null mice are viable but show evidence of hyperproliferative and vascular abnormalities. *J Biol Chem* **276**, 38121-38138.

Razi, M., Chan, E.Y. and Tooze, S.A. (2009). Early endosomes and endosomal coatomer are required for autophagy. *J Cell Biol* **185**, 305-321.

Reddy, M.A., Prasadarao, N.V., Wass, C.A. and Kim, K.S. (2000a). Phosphatidylinositol 3-kinase activation and interaction with focal adhesion kinase in *Escherichia coli*

K1 invasion of human brain microvascular endothelial cells. *J. Biol. Chem.* **275**, 36769-36774.

Reddy, M.A., Wass, C.A., Kim, K.S., Schlaepfer, D.D. and Prasadarao, N.V. (2000b). Involvement of focal adhesion kinase in *Escherichia coli* invasion of human brain microvascular endothelial cells. *Infect. Immun.* **68**, 6423-6430.

Richterova, Z., Liebl, D., Horak, M., Palkova, Z., Stokrova, J., Hozak, P., Korb, J. and Forstova, J. (2001). Caveolae are involved in the trafficking of mouse polyomavirus virions and artificial VP1 pseudocapsids toward cell nuclei. *J Virol* **75**, 10880-10891.

Ridley, A.J., Paterson, H.F., Johnston, C.L., Diekmann, D. and Hall, A. (1992). The small GTP-binding protein rac regulates growth factor-induced membrane ruffling. *Cell* **70**, 401-410.

Riederer, M.A., Soldati, T., Shapiro, A.D., Lin, J. and Pfeffer, S.R. (1994). Lysosome biogenesis requires Rab9 function and receptor recycling from endosomes to the trans-Golgi network. *J. Cell Biol.* **125**, 573-582.

Riento, K., Frick, M., Schafer, I. and Nichols, B.J. (2009). Endocytosis of flotillin-1 and flotillin-2 is regulated by Fyn kinase. *J Cell Sci* **122**, 912-918.

Ring, A., Weiser, J.N. and Tuomanen, E.I. (1998). *Pneumococcal* trafficking across the blood-brain barrier. Molecular analysis of a novel bidirectional pathway. *J Clin Invest* **102**, 347-360.

Robbins, J.B., McCracken, G.H., Jr., Gotschlich, E.C., Orskov, F., Orskov, I. and Hanson, L.A. (1974). *Escherichia coli* K1 capsular polysaccharide associated with neonatal meningitis. *N Engl J Med* **290**, 1216-1220.

Romano, P.S., Gutierrez, M.G., Beron, W., Rabinovitch, M. and Colombo, M.I. (2007). The autophagic pathway is actively modulated by phase II *Coxiella burnetii* to efficiently replicate in the host cell. *Cell Microbiol* **9**, 891-909.

Roth, J., Taatjes, D.J., Bitter-Suermann, D. and Finne, J. (1987). Polysialic acid units are spatially and temporally expressed in developing postnatal rat kidney. *Proc Natl Acad Sci U S A* **84**, 1969-1973.

Rubin, L.L. and Staddon, J.M. (1999). The cell biology of the blood-brain barrier. *Annual Review of Neuroscience* **22**, 11-28.

Rudrabhatla, R.S., Selvaraj, S.K. and Prasadarao, N.V. (2006). Role of Rac1 in *Escherichia coli* K1 invasion of human brain microvascular endothelial cells. *Microbes Infect* **8**, 460-469.

Ruthel, G., Ribot, W.J., Bavari, S. and Hoover, T.A. (2004). Time-lapse confocal imaging of development of *Bacillus anthracis* in macrophages. *J Infect Dis* **189**, 1313-1316.

Rutishauser, U. (2008). Polysialic acid in the plasticity of the developing and adult vertebrate nervous system. *Nat Rev Neurosci* **9**, 26-35.

Rzomp, K.A., Scholtes, L.D., Briggs, B.J., Whittaker, G.R. and Scidmore, M.A. (2003). Rab GTPases are recruited to chlamydial inclusions in both a species-dependent and species-independent manner. *Infect. Immun.* **71**, 5855-5870.

Sabharanjak, S., Sharma, P., Parton, R.G. and Mayor, S. (2002). GPI-anchored proteins are delivered to recycling endosomes via a distinct cdc42-regulated, clathrin-independent pinocytic pathway. *Dev Cell* **2**, 411-423.

Salcedo, R., Resau, J.H., Halverson, D., Hudson, E.A., Dambach, M., Powell, D., Wasserman, K. and Oppenheim, J.J. (2000). Differential expression and responsiveness of chemokine receptors (CXCR1-3) by human microvascular endothelial cells and umbilical vein endothelial cells. *FASEB J* **14**, 2055-2064.

Salcedo, S.P. and Holden, D.W. (2003). SseG, a virulence protein that targets *Salmonella* to the Golgi network. *EMBO J* **22**, 5003-5014.

Sansonetti, P.J., Ryter, A., Clerc, P., Maurelli, A.T. and Mounier, J. (1986). Multiplication of *Shigella flexneri* within HeLa cells: lysis of the phagocytic vacuole and plasmid-mediated contact hemolysis. *Infect Immun* **51**, 461-469.

Sarff, L.D., McCracken, G.H., Schiffer, M.S., Glode, M.P., Robbins, J.B., Orskov, I. and Orskov, F. (1975). Epidemiology of *Escherichia coli* K1 in healthy and diseased newborns. *Lancet* **1**, 1099-1104.

Sato, K., Ernstrom, G.G., Watanabe, S., Weimer, R.M., Chen, C.H., Sato, M., Siddiqui, A., Jorgensen, E.M. and Grant, B.D. (2009). Differential requirements for clathrin in receptor-mediated endocytosis and maintenance of synaptic vesicle pools. *Proc Natl Acad Sci U S A* **106**, 1139-1144.

Saukkonen, K.M., Nowicki, B. and Leinonen, M. (1988). Role of type 1 and S fimbriae in the pathogenesis of *Escherichia coli* O18:K1 bacteremia and meningitis in the infant rat. *Infect Immun* **56**, 892-897.

Scaife, R. and Margolis, R.L. (1990). Biochemical and immunochemical analysis of rat brain dynamin interaction with microtubules and organelles *in vivo* and *in vitro*. *J Cell Biol* **111**, 3023-3033.

Schlossman, D.M., Schmid, S.L., Braell, W.A. and Rothman, J.E. (1984). An enzyme that removes clathrin coats: purification of an uncoating ATPase. *J Cell Biol* **99**, 723-733.

Schneider, A., Rajendran, L., Honsho, M., Gralle, M., Donnert, G., Wouters, F., Hell, S.W. and Simons, M. (2008). Flotillin-dependent clustering of the amyloid precursor protein regulates its endocytosis and amyloidogenic processing in neurons. *J Neurosci* **28**, 2874-2882.

Schneider, B., Gross, R. and Haas, A. (2000). Phagosome acidification has opposite effects on intracellular survival of *Bordetella pertussis* and *B. bronchiseptica*. *Infect. Immun.* **68**, 7039-7048.

Schneider, B., Schueller, C., Utermoehlen, O. and Haas, A. (2007). Lipid microdomain-dependent macropinocytosis determines compartmentation of *Afipia felis*. *Traffic* **8**, 226-240.

Schnell, U., Dijk, F., Sjollema, K.A. and Giepmans, B.N. (2012). Immunolabeling artifacts and the need for live-cell imaging. *Nat Methods* **9**, 152-158.

Schnitzer, J.E., Oh, P., Pinney, E. and Allard, J. (1994). Filipin-sensitive caveolae-mediated transport in endothelium: reduced transcytosis, scavenger endocytosis, and capillary permeability of select macromolecules. *J. Cell Biol.* **127**, 1217-1232.

Schroder, A., Kland, R., Peschel, A., von Eiff, C. and Aepfelbacher, M. (2006). Live cell imaging of phagosome maturation in *Staphylococcus aureus* infected human endothelial cells: small colony variants are able to survive in lysosomes. *Med Microbiol Immunol* **195**, 185-194.

Schubert, W., Frank, P.G., Razani, B., Park, D.S., Chow, C.W. and Lisanti, M.P. (2001). Caveolae-deficient endothelial cells show defects in the uptake and transport of albumin in vivo. *J Biol Chem* **276**, 48619-48622.

Seaman, M.N.J. (2004). Cargo-selective endosomal sorting for retrieval to the Golgi requires retromer. *J Cell Biol* **165**, 111-122.

Segura, I., Gonzalez, M.A., Serrano, A., Abad, J.L., Bernad, A. and Riese, H.H. (2001). High transfection efficiency of human umbilical vein endothelial cells using an optimized calcium phosphate method. *Anal Biochem* **296**, 143-147.

Seidman, C.E., Struhl, K., Sheen, J. and Jessen, T. (2001). Introduction of plasmid DNA into cells. *Curr Protoc Mol Biol* **Chapter 1,** Unit1 8.

Shajahan, A.N., Timblin, B.K., Sandoval, R., Tiruppathi, C., Malik, A.B. and Minshall, R.D. (2004). Role of Src-induced dynamin-2 phosphorylation in caveolae-mediated endocytosis in endothelial cells. *J Biol Chem* **279**, 20392-20400.

Shaner, N.C., Campbell, R.E., Steinbach, P.A., Giepmans, B.N., Palmer, A.E. and Tsien, R.Y. (2004). Improved monomeric red, orange and yellow fluorescent proteins derived from *Discosoma* sp. red fluorescent protein. *Nat Biotechnol* **22**, 1567-1572.

Shaner, N.C., Steinbach, P.A. and Tsien, R.Y. (2005). A guide to choosing fluorescent proteins. *Nat Meth* **2**, 905-909.

Sheff, D.R., Daro, E.A., Hull, M. and Mellman, I. (1999). The receptor recycling pathway contains two distinct populations of early endosomes with different sorting functions. *J Cell Biol* **145**, 123-139.

Shichinohe, T., Bochner, B.H., Mizutani, K., Nishida, M., Hegerich-Gilliam, S., Naldini, L. and Kasahara, N. (2001). Development of lentiviral vectors for antiangiogenic gene delivery. *Cancer Gene Ther* **8**, 879-889.

Shin, J.S., Gao, Z. and Abraham, S.N. (2000). Involvement of cellular caveolae in bacterial entry into mast cells. *Science* **289**, 785-788.

Shogomori, H. and Futerman, A.H. (2001). Cholera toxin is found in detergent-insoluble rafts/domains at the cell surface of hippocampal neurons but is internalized via a raft-independent mechanism. *J Biol Chem* **276**, 9182-9188.

Siddiqui, M.R., Komarova, Y.A., Vogel, S.M., Gao, X., Bonini, M.G., Rajasingh, J., Zhao, Y.Y., Brovkovych, V. and Malik, A.B. (2011). Caveolin-1-eNOS signaling promotes p190RhoGAP-A nitration and endothelial permeability. *J Cell Biol* **193**, 841-850.

Siegel, J.D. and McCracken, G.H., Jr. (1981). Sepsis neonatorum. *N Engl J Med* **304**, 642-647.

Silver, R.P., Aaronson, W., Sutton, A. and Schneerson, R. (1980). Comparative analysis of plasmids and some metabolic characteristics of *Escherichia coli* K1 from diseased and healthy individuals. *Infect Immun* **29**, 200-206.

Simberkoff, M.S., Moldover, N.H. and Rahal, J., Jr. (1980). Absence of detectable bactericidal and opsonic activities in normal and infected human cerebrospinal fluids. A regional host defense deficiency. *J Lab Clin Med* **95**, 362-372.

Simons, K. and Gerl, M.J. (2010). Revitalizing membrane rafts: new tools and insights. *Nat Rev Mol Cell Biol* **11**, 688-699.

Simons, K. and Sampaio, J.L. (2011). Membrane organization and lipid rafts. *Cold Spring Harb Perspect Biol* **3**, a004697.

Simons, M. and Raposo, G. (2009). Exosomes-vesicular carriers for intercellular communication. *Curr Opin Cell Biol* **21**, 575-581.

Singh, R.D., Puri, V., Valiyaveettil, J.T., Marks, D.L., Bittman, R. and Pagano, R.E. (2003). Selective caveolin-1-dependent endocytosis of glycosphingolipids. *Mol Biol Cell* **14**, 3254-3265.

Sissons, J., Kim, K.S., Stins, M., Jayasekera, S., Alsam, S. and Khan, N.A. (2005). *Acanthamoeba castellanii* induces host cell death via a phosphatidylinositol 3-kinase-dependent mechanism. *Infect Immun* **73**, 2704-2708.

Sitthidet, C., Korbsrisate, S., Layton, A.N., Field, T.R., Stevens, M.P. and Stevens, J.M. (2011). Identification of motifs of *Burkholderia pseudomallei* BimA required for intracellular motility, actin binding, and actin polymerization. *J Bacteriol* **193**, 1901-1910.

Smart, E.J., Ying, Y., Donzell, W.C. and Anderson, R.G. (1996). A role for caveolin in transport of cholesterol from endoplasmic reticulum to plasma membrane. *J Biol Chem* **271**, 29427-29435.

Smith, A.C., Cirulis, J.T., Casanova, J.E., Scidmore, M.A. and Brumell, J.H. (2005). Interaction of the *Salmonella*-containing vacuole with the endocytic recycling system. *J. Biol. Chem.* **280**, 24634-24641.

Smith, A.L. (1987). Pathogenesis of *Haemophilus influenzae* meningitis. *Pediatr Infect Dis J* **6**, 783-786.

Solis, G.P., Hoegg, M., Munderloh, C., Schrock, Y., Malaga-Trillo, E., Rivera-Milla, E. and Stuermer, C.A. (2007). Reggie/flotillin proteins are organized into stable tetramers in membrane microdomains. *Biochem J* **403**, 313-322.

Sontag, J.M., Fykse, E.M., Ushkaryov, Y., Liu, J.P., Robinson, P.J. and Sudhof, T.C. (1994). Differential expression and regulation of multiple dynamins. *J Biol Chem* **269**, 4547-4554.

Spector, A.A. and Yorek, M.A. (1985). Membrane lipid composition and cellular function. *J Lipid Res* **26**, 1015-1035.

Stamm, L.M., Morisaki, J.H., Gao, L.-Y., Jeng, R.L., McDonald, K.L., Roth, R., Takeshita, S., Heuser, J., Welch, M.D. and Brown, E.J. (2003). *Mycobacterium marinum* escapes from phagosomes and is propelled by actin-based motility. *J. Exp. Med.* **198**, 1361-1368.

Starr, T., Ng, T.W., Wehrly, T.D., Knodler, L.A. and Celli, J. (2008). *Brucella* intracellular replication requires trafficking through the late endosomal/lysosomal compartment. *Traffic* **9**, 678-694.

Steele-Mortimer, O., Méresse, S., Gorvel, J.P., Toh, B.H. and Finlay, B.B. (1999). Biogenesis of *Salmonella typhimurium*-containing vacuoles in epithelial cells involves interactions with the early endocytic pathway. *Cell Microbiol* **1**, 33-49.

Steele-Mortimer, O., St-Louis, M., Olivier, M. and Finlay, B.B. (2000). Vacuole acidification is not required for survival of *Salmonella enterica* serovar

typhimurium within cultured macrophages and epithelial cells. *Infect Immun* **68**, 5401-5404.

Steiner, O., Coisne, C., Engelhardt, B. and Lyck, R. (2011). Comparison of immortalized bEnd5 and primary mouse brain microvascular endothelial cells as *in vitro* blood-brain barrier models for the study of T cell extravasation. *J Cereb Blood Flow Metab* **31**, 315-327.

Stenmark, H. (2009). Rab GTPases as coordinators of vesicle traffic. *Nat Rev Mol Cell Biol* **10**, 513-525.

Stenmark, H., Parton, R.G., Steele-Mortimer, O., Lutcke, A., Gruenberg, J. and Zerial, M. (1994). Inhibition of rab5 GTPase activity stimulates membrane fusion in endocytosis. *EMBO J* **13**, 1287-1296.

Stins, M.F., Badger, J. and Kim, K.S. (2001). Bacterial invasion and transcytosis in transfected human brain microvascular endothelial cells. *Microb Pathog* **30**, 19-28.

Stins, M.F., Prasadarao, N.V., Ibric, L., Wass, C.A., Luckett, P. and Kim, K.S. (1994). Binding characteristics of S fimbriated *Escherichia coli* to isolated brain microvascular endothelial cells. *Am J Pathol* **145**, 1228-1236.

Stoll, B.J., Hansen, N., Fanaroff, A.A., Wright, L.L., Carlo, W.A., Ehrenkranz, R.A., Lemons, J.A., Donovan, E.F., Stark, A.R., Tyson, J.E., Oh, W., Bauer, C.R., Korones, S.B., Shankaran, S., Laptook, A.R., Stevenson, D.K., Papile, L.A. and Poole, W.K. (2002). Changes in pathogens causing early-onset sepsis in very-low-birth-weight infants. *N Engl J Med* **347**, 240-247.

Stowell, M.H., Marks, B., Wigge, P. and McMahon, H.T. (1999). Nucleotide-dependent conformational changes in dynamin: evidence for a mechanochemical molecular spring. *Nat Cell Biol* **1**, 27-32.

Sukumaran, S.K. and Prasadarao, N.V. (2002). Regulation of protein kinase C in *Escherichia coli* K1 invasion of human brain microvascular endothelial cells. *J. Biol. Chem.* **277**, 12253-12262.

Sukumaran, S.K. and Prasadarao, N.V. (2003). *Escherichia coli* K1 invasion increases human brain microvascular endothelial cell monolayer permeability by disassembling vascular-endothelial cadherins at tight junctions. *J Infect Dis* **188**, 1295-1309.

Sukumaran, S.K., Quon, M.J. and Prasadarao, N.V. (2002). *Escherichia coli* K1 internalization via caveolae requires caveolin-1 and protein kinase Cα interaction in human brain microvascular endothelial cells. *J. Biol. Chem.* **277**, 50716-50724.

Sukumaran, S.K., Shimada, H. and Prasadarao, N.V. (2003). Entry and intracellular replication of *Escherichia coli* K1 in macrophages require expression of outer membrane protein A. *Infect. Immun.* **71**, 5951-5961.

Sun, P., Yamamoto, H., Suetsugu, S., Miki, H., Takenawa, T. and Endo. T. (2003). Small GTPase Rah/Rab34 is associated with membrane ruffles and macropinosomes and promotes macropinosome formation. *J Biol Chem* **278**, 4063-4071.

Sundborger, A., Soderblom, C., Vorontsova, O., Evergren. E., Hinshaw, J.E. and Shupliakov, O. (2011). An endophilin-dynamin complex promotes budding of clathrin-coated vesicles during synaptic vesicle recycling. *J Cell Sci* **124**, 133-143.

Sverdlov, M., Shinin, V., Place, A.T., Castellon, M. and Minshall. R.D. (2009). Filamin A regulates caveolae internalization and trafficking in endothelial cells. *Mol Biol Cell* **20**, 4531-4540.

Sweitzer, S.M. and Hinshaw, J.E. (1998). Dynamin undergoes a GTP-dependent conformational change causing vesiculation. *Cell* **93**, 1021-1029.

Swerlick, R.A., Lee, K.H., Wick, T.M. and Lawley, T.J. (1992). Human dermal microvascular endothelial but not human umbilical vein endothelial cells express CD36 *in vivo* and *in vitro*. *J Immunol* **148**, 78-83.

Szmydynger-Chodobska, J., Pascale, C.L., Pfeffer. A.N., Coulter. C. and Chodobski, A. (2007). Expression of junctional proteins in choroid plexus epithelial cell lines: a comparative study. *Cerebrospinal Fluid Res* **4**, 11.

Talbert, A.W., Mwaniki, M., Mwarumba, S., Newton, C.R. and Berkley, J.A. (2010). Invasive bacterial infections in neonates and young infants born outside hospital admitted to a rural hospital in Kenya. *Pediatr Infect Dis J* **29**, 945-949.

Tanaka, K.A., Suzuki, K.G., Shirai, Y.M., Shibutani. S.T., Miyahara, M.S., Tsuboi, H., Yahara, M., Yoshimura, A., Mayor, S., Fujiwara, T.K. and Kusumi, A. (2010). Membrane molecules mobile even after chemical fixation. *Nat Methods* **7**, 865-866.

Tenenbaum, T., Papandreou, T., Gellrich, D., Friedrichs, U., Seibt, A., Adam, R. Wewer. C., Galla, H.J., Schwerk, C. and Schroten, H. (2009). Polar bacterial invasion and translocation of *Streptococcus suis* across the blood-cerebrospinal fluid barrier *in vitro*. *Cell Microbiol* **11**, 323-336.

Teng, C.H., Cai, M., Shin, S., Xie, Y., Kim, K.J., Khan. N.A., Di Cello, F. and Kim. K.S. (2005). *Escherichia coli* K1 RS218 interacts with human brain microvascular endothelial cells via type 1 fimbria bacteria in the fimbriated state. *Infect Immun* **73**, 2923-2931.

Thery, C., Ostrowski, M. and Segura, E. (2009). Membrane vesicles as conveyors of immune responses. *Nat Rev Immunol* **9,** 581-593.

Thomsen, P., Roepstorff, K., Stahlhut, M. and van Deurs, B. (2002). Caveolae are highly immobile plasma membrane microdomains, which are not involved in constitutive endocytic trafficking. *Mol Biol Cell* **13,** 238-250.

Tofte, R.W., Peterson, P.K., Kim, Y. and Quie, P.G. (1979). Opsonic activity of normal human cerebrospinal fluid for selected bacterial species. *Infect Immun* **26,** 1093-1098.

Torgersen, M.L., Skretting, G., van Deurs, B. and Sandvig, K. (2001). Internalization of cholera toxin by different endocytic mechanisms. *J Cell Sci* **114,** 3737-3747.

Tsien, R.Y. (1998). The green fluorescent protein. *Annu. Rev. Biochem.* **67,** 509-544.

Tuomanen, E.I., Saukkonen, K., Sande, S., Cioffe, C. and Wright, S.D. (1989). Reduction of inflammation, tissue damage, and mortality in bacterial meningitis in rabbits treated with monoclonal antibodies against adhesion-promoting receptors of leukocytes. *J Exp Med* **170,** 959-969.

Tweten, R.K. (2005). Cholesterol-dependent cytolysins, a family of versatile pore-forming toxins. *Infect Immun* **73,** 6199-6209.

Tzaban, S., Massol, R.H., Yen, E., Hamman, W., Frank, S.R., Lapierre, L.A., Hansen, S.H., Goldenring, J.R., Blumberg, R.S. and Lencer, W.I. (2009). The recycling and transcytotic pathways for IgG transport by FcRn are distinct and display an inherent polarity. *J. Cell Biol.* **185,** 673-684.

Uchiya, K., Barbieri, M.A., Funato, K., Shah, A.H., Stahl, P.D. and Groisman, E.A. (1999). A *Salmonella* virulence protein that inhibits cellular trafficking. *EMBO J* **18,** 3924-3933.

Uittenbogaard, A. and Smart, E.J. (2000). Palmitoylation of caveolin-1 is required for cholesterol binding, chaperone complex formation, and rapid transport of cholesterol to caveolae. *J Biol Chem* **275,** 25595-25599.

Ungewickell, E., Ungewickell, H., Holstein, S.E., Lindner, R., Prasad, K., Barouch, W., Martin, B., Greene, L.E. and Eisenberg, E. (1995). Role of auxilin in uncoating clathrin-coated vesicles. *Nature* **378,** 632-635.

Unhanand, M., Mustafa, M.M., McCracken, G.H., Jr. and Nelson, J.D. (1993). Gram-negative enteric bacillary meningitis: a twenty-one-year experience. *J Pediatr* **122,** 15-21.

Unsworth, K.E., Mazurkiewicz, P., Senf, F., Zettl, M., McNiven, M.A., Way, M. and Holden, D.W. (2007). Dynamin is required for F-actin assembly and pedestal

formation by enteropathogenic *Escherichia coli* (EPEC). *Cell Microbiol* **9**, 438-449.

Untucht, C., Rasch, J., Fuchs, E., Rohde, M., Bergmann, S. and Steinert, M. (2011). An optimized *in vitro* blood-brain barrier model reveals bidirectional transmigration of African trypanosome strains. *Microbiology* **157**, 2933-2941.

Urwyler, S., Nyfeler, Y., Ragaz, C., Lee, H., Mueller, L.N., Aebersold, R. and Hilbi, H. (2009). Proteome analysis of *Legionella* vacuoles purified by magnetic immunoseparation reveals secretory and endosomal GTPases. *Traffic* **10**, 76-87.

Valasek, M.A., Weng, J., Shaul, P.W., Anderson, R.G. and Repa, J.J. (2005). Caveolin-1 is not required for murine intestinal cholesterol transport. *J Biol Chem* **280**, 28103-28109.

Valdivia, R.H. and Falkow, S. (1996). Bacterial genetics by flow cytometry: rapid isolation of *Salmonella typhimurium* acid-inducible promoters by differential fluorescence induction. *Mol Microbiol* **22**, 367-378.

Van Engelenburg, S.B. and Palmer, A.E. (2010). Imaging type-III secretion reveals dynamics and spatial segregation of *Salmonella* effectors. *Nat Methods* **7**, 325-330.

Vanlandingham, P.A. and Ceresa, B.P. (2009). Rab7 regulates late endocytic trafficking downstream of multivesicular body biogenesis and cargo sequestration. *J Biol Chem* **284**, 12110-12124.

VanRheenen, S.M., Dumenil, G. and Isberg, R.R. (2004). *IcmF* and *DotU* are required for optimal effector translocation and trafficking of the *Legionella pneumophila* vacuole. *Infect. Immun.* **72**, 5972-5982.

Vassilieva, E.V., Ivanov, A.I. and Nusrat, A. (2009). Flotillin-1 stabilizes caveolin-1 in intestinal epithelial cells. *Biochem Biophys Res Commun* **379**, 460-465.

Veiga, E. and Cossart, P. (2005). *Listeria* hijacks the clathrin-dependent endocytic machinery to invade mammalian cells. *Nat Cell Biol* **7**, 894-900.

Veiga, E. and Cossart, P. (2006). The role of clathrin-dependent endocytosis in bacterial internalization. *Trends Cell Biol* **16**, 499-504.

Veiga, E., Guttman, J.A., Bonazzi, M., Boucrot, E., Toledo-Arana, A., Lin, A.E., Enninga, J., Pizarro-Cerda, J., Finlay, B.B., Kirchhausen, T. and Cossart, P. (2007). Invasive and adherent bacterial pathogens co-Opt host clathrin for infection. *Cell Host Microbe* **2**, 340-351.

Vimr, E.R. and Steenbergen, S.M. (2006). Mobile contingency locus controlling *Escherichia coli* K1 polysialic acid capsule acetylation. *Mol Microbiol* **60**, 828-837.

Volonte, D., Galbiati, F., Li, S., Nishiyama, K., Okamoto, T. and Lisanti. M.P. (1999). Flotillins/Cavatellins are differentially expressed in cells and tissues and form a hetero-oligomeric complex with caveolins *in vivo. J Biol Chem* **274**, 12702-12709.

Voth, D.E. and Heinzen, R.A. (2007). Lounging in a lysosome: the intracellular lifestyle of *Coxiella burnetii. Cell Microbiol* **9**, 829-840.

Waage, A., Halstensen, A., Shalaby, R., Brandtzaeg, P., Kierulf, P. and Espevik, T. (1989). Local production of tumor necrosis factor alpha, interleukin 1, and interleukin 6 in meningococcal meningitis. Relation to the inflammatory response. *J Exp Med* **170**, 1859-1867.

Wang, J., Gray-Owen, S.D., Knorre, A., Meyer, T.F. and Dehio, C. (1998). Opa binding to cellular CD66 receptors mediates the transcellular traversal of *Neisseria gonorrhoeae* across polarized T84 epithelial cell monolayers. *Mol Microbiol* **30**, 657-671.

Wang, J.A., Meyer, T.F. and Rudel, T. (2008). Cytoskeleton and motor proteins are required for the transcytosis of *Neisseria gonorrhoeae* through polarized epithelial cells. *Int J Med Microbiol* **298**, 209-221.

Wang, Y., Huang, S.H., Wass, C.A., Stins, M.F. and Kim, K.S. (1999). The gene locus *yijP* contributes to *Escherichia coli* K1 invasion of brain microvascular endothelial cells. *Infect Immun* **67**, 4751-4756.

Wang, Y., Wen, Z.G. and Kim, K.S. (2004). Role of S fimbriae in *Escherichia coli* K1 binding to brain microvascular endothelial cells *in vitro* and penetration into the central nervous system *in vivo. Microb Pathog* **37**, 287-293.

Ward, T.H. (2007). Trafficking through the early secretory pathway of mammalian cells. *Methods Mol Biol* **390**, 281-296.

Watson, R.O. and Galán, J.E. (2008). *Campylobacter jejuni* survives within epithelial cells by avoiding delivery to lysosomes. *PLoS Pathog* **4**, e14.

Weingart, C.L., Broitman-Maduro, G., Dean, G., Newman, S., Peppler, M. and Weiss, A.A. (1999). Fluorescent labels influence phagocytosis of *Bordetella pertussis* by human neutrophils. *Infect. Immun.* **67**, 4264-4267.

Weksler, B.B., Subileau, E.A., Perriere, N., Charneau, P., Holloway, K., Leveque, M., Tricoire-Leignel, H., Nicotra, A., Bourdoulous, S., Turowski, P., Male, D.K., Roux, F., Greenwood, J., Romero, I.A. and Couraud, P.O. (2005). Blood-brain barrier-specific properties of a human adult brain endothelial cell line. *FASEB J* **19**, 1872-1874.

Welch, R.A., Burland, V., Plunkett, G., 3rd, Redford, P., Roesch, P., Rasko, D., Buckles. E.L., Liou, S.R., Boutin, A., Hackett, J., Stroud, D., Mayhew. G.F., Rose. D.J.. Zhou, S., Schwartz, D.C., Perna, N.T., Mobley, H.L., Donnenberg, M.S. and Blattner, F.R. (2002). Extensive mosaic structure revealed by the complete genome sequence of uropathogenic *Escherichia coli*. *Proc Natl Acad Sci U S A* **99**, 17020-17024.

Wigge, P., Kohler, K., Vallis, Y., Doyle, C.A., Owen, D., Hunt, S.P. and McMahon, H.T. (1997). Amphiphysin heterodimers: potential role in clathrin-mediated endocytosis. *Mol Biol Cell* **8**, 2003-2015.

Wilfert, C.M. (1978). *E. coli* meningitis: K1 antigen and virulence. *Annu Rev Med* **29**, 129-136.

Willing, B.P., Russell, S.L. and Finlay, B.B. (2011). Shifting the balance: antibiotic effects on host-microbiota mutualism. *Nat Rev Microbiol* **9**, 233-243.

Wu, J.H., Chen, C.Y., Tsao, P.N., Hsieh, W.S. and Chou, H.C. (2009). Neonatal sepsis: a 6-year analysis in a neonatal care unit in Taiwan. *Pediatr Neonatol* **50**, 88-95.

Wynn, J.L. and Levy, O. (2010). Role of innate host defenses in susceptibility to early-onset neonatal sepsis. *Clin Perinatol* **37**, 307-337.

Xie, Y., Kolisnychenko, V., Paul-Satyaseela, M., Elliott, S., Parthasarathy, G., Yao, Y., Plunkett, G., 3rd, Blattner, F.R. and Kim, K.S. (2006). Identification and characterization of *Escherichia coli* RS218-derived islands in the pathogenesis of *E. coli* meningitis. *J Infect Dis* **194**, 358-364.

Yao, Q., Chen, J., Cao, H., Orth, J.D., McCaffery, J.M., Stan, R.V. and McNiven, M.A. (2005). Caveolin-1 interacts directly with dynamin-2. *J Mol Biol* **348**, 491-501.

Yao, Y., Xie, Y. and Kim, K.S. (2006). Genomic comparison of *Escherichia coli* K1 strains isolated from the cerebrospinal fluid of patients with meningitis. *Infect Immun* **74**, 2196-2206.

Yao, Y., Xie, Y., Perace, D., Zhong, Y., Lu, J., Tao, J., Guo, X. and Kim, K.S. (2009). The type III secretion system is involved in the invasion and intracellular survival of *Escherichia coli* K1 in human brain microvascular endothelial cells. *FEMS Microbiol Lett* **300**, 18-24.

Zaidi, A.K., Thaver, D., Ali, S.A. and Khan, T.A. (2009). Pathogens associated with sepsis in newborns and young infants in developing countries. *Pediatr Infect Dis J* **28**, S10-18.

Zelmer, A., Bowen, M., Jokilammi, A., Finne, J., Luzio, J.P. and Taylor, P.W. (2008). Differential expression of the polysialyl capsule during blood-to-brain transit of neuropathogenic *Escherichia coli* K1. *Microbiology* **154**, 2522-2532.

Zerial, M. and McBride, H. (2001). Rab proteins as membrane organizers. *Nat Rev Mol Cell Biol* **2**, 107-117.

Zhang, H., Mitin, A. and Vinogradov, S.V. (2009). Efficient transfection of blood-brain barrier endothelial cells by lipoplexes and polyplexes in the presence of nuclear targeting NLS-PEG-acridine conjugates. *Bioconjug Chem* **20**, 120-128.

Zhang, W.G., Khan, A.N., Kim, K.J., Stins, M. and Kim, K.S. (2002). Transforming growth factor-β increases *Escherichia coli* K1 adherence, invasion, and transcytosis in human brain microvascular endothelial cells. *Cell Tissue Res* **309**, 281-286.

Zheng, W. and Zhao, Q. (2002). Establishment and characterization of an immortalized Z310 choroidal epithelial cell line from murine choroid plexus. *Brain Res* **958**, 371-380.